Titre: Title:	Power Tracking Control of Heterogeneous Thermostatically Controlled Load Populations based on Fokker-Planck Equations
Auteur: Author:	Zhenhe Zhang
Date:	2025
Type:	Mémoire ou thèse / Dissertation or Thesis
Référence: Citation:	Zhang, Z. (2025). Power Tracking Control of Heterogeneous Thermostatically Controlled Load Populations based on Fokker-Planck Equations [Ph.D. thesis, Polytechnique Montréal]. PolyPublie. https://publications.polymtl.ca/68143/

URL de PolyPublie: PolyPublie URL:	https://publications.polymtl.ca/68143/
Directeurs de recherche: Advisors:	Guchuan Zhu
Programme: Program:	Génie électrique

POLYTECHNIQUE MONTRÉAL
affiliée à l'Université de Montréal

Power Tracking Control of Heterogeneous Thermostatically Controlled Load Populations based on Fokker-Planck Equations

ZHENHE ZHANG
Département de génie électrique

Thèse présentée en vue de l'obtention du diplôme de *Philosophiæ Doctor*
Génie électrique

Août 2025

POLYTECHNIQUE MONTRÉAL
affiliée à l'Université de Montréal

Cette thèse intitulée :

Power Tracking Control of Heterogeneous Thermostatically Controlled Load Populations based on Fokker-Planck Equations

présentée par **Zhenhe ZHANG**
en vue de l'obtention du diplôme de *Philosophiæ Doctor*
a été dûment acceptée par le jury d'examen constitué de :

Antoine LESAGE-LANDRY, président
Guchuan ZHU, membre et directeur de recherche
Shuang GAO, membre
Louis-A. DESSAINT, membre externe

DEDICATION

À tous les membres de ma famille,
vous êtes important pour moi...

ACKNOWLEDGEMENTS

First and foremost, I am deeply grateful to my supervisor, Professor Guchuan Zhu. He is always there to help me in my academic journey in École Polytechnique de Montreal. I am particularly appreciative of his patience on me, especially when we cannot get the anticipated experiment results.

I would also like to express my sincere gratitude to Prof. Antoine Lesage-Landry, Prof. Shuang Gao, and Prof. Louis-A. Dessaint, for their time, rigorous evaluation, and insightful comments to my thesis. Your expertise and constructive feedback have not only helped me improve the quality of my research but also broaden my academic understanding. I sincerely appreciate your patience, encouragement, and the thoughtful questions that made my defense an enriching experience.

Lastly, my profound appreciation goes to all my family members. Their roles are indispensable in my life and their love and support always keep me going.

RÉSUMÉ

Le réseau intelligent représente un progrès majeur par rapport au réseau conventionnel pour répondre aux préoccupations croissantes liées à l'efficacité énergétique et aux enjeux environnementaux. Avec des fonctionnalités clés telles que la communication bidirectionnelle et la surveillance en temps réel, la stabilité et la fiabilité du réseau sont considérablement améliorées. Les programmes de réponse à la demande, qui permettent aux consommateurs de jouer un rôle plus actif dans la gestion de leur consommation d'électricité, connaissent un engouement croissant ces dernières années. En tant que l'une des ressources DR les plus prometteuses, les charges contrôlées par thermostat (TCL) peuvent fournir des services auxiliaires flexibles au réseau grâce à leur inertie thermique et à leur large déploiement dans le réseau de distribution. Par conséquent, l'étude des techniques de contrôle d'une population de TCLs revêt un intérêt majeur, tant sur le plan théorique que pratique. Cette thèse vise à résoudre le problème de suivi de puissance pour une population de TCLs hétérogènes. Pour représenter avec précision le comportement thermodynamique, chaque charge est modélisée à l'aide de modèles de paramètres thermiques équivalents du premier ou du deuxième ordre, tandis que la dynamique macroscopique de la population est décrite par des équations de Fokker-Planck couplées ou leurs extensions d'ordre supérieur. Divers algorithmes de commande sont développés en s'appuyant sur la méthode de linéarisation entrée-sortie, accompagnés d'une analyse de stabilité rigoureuse du système en boucle fermée, incluant à la fois la dynamique de l'erreur de suivi et la dynamique interne à dimension infinie. Les algorithmes de commande proposés reposent uniquement sur des observations partielles de l'état de la population, indépendamment des paramètres du système, tout en offrant des performances accrues pour des ensembles de TCL à grande échelle et à très grande échelle. Pour alléger davantage le fardeau de communication, les techniques de commande déclenchée par événement sont adaptées dans le suivi de puissance. Les stratégies de commande déclenchée par événement statiques et dynamiques sont étudiées, chacune assurant la stabilité du système en boucle fermée tout en évitant l'apparition du phénomène de Zeno.

Cette thèse a contribué à approfondir la compréhension de la coordination de grandes populations de TCL pour améliorer leur performance dans les programmes de réponse à la demande au sein des réseaux intelligents. Nos résultats montrent que les méthodes de commande proposées sont hautement efficaces, en particulier pour les grandes populations hétérogènes de TCLs. Par ailleurs, les algorithmes de commande proposés démontrent une robustesse remarquable vis-à-vis de diverses perturbations fréquemment rencontrées en conditions réelles d'application.

ABSTRACT

The smart grid (SG) represents a major advancement over the conventional grid to meet the growing concern of energy efficiency and environmental challenges. With core features such as two-way communication and real-time monitoring, the stability and reliability of the grid is highly improved. Demand response (DR) programs, which empower energy consumers to take a more active role in managing their electricity usage, have grown increasingly popular in recent years. As one of the most promising DR resources, thermostatically controlled loads (TCLs) can provide flexible auxiliary services to the grid due to their thermal inertia and widespread presence across the distribution network. Therefore, it is of great theoretical and practical significance to study the control techniques for a population of TCLs. This dissertation aims at addressing the power tracking control problem for a popoulation of heterogeneours TCLs. To accurately capture the thermodynamic behavior, individual loads are modeled using first- or second-order equivalent thermal parameter (ETP) models, while the macroscopic dynamics of the population are described by coupled Fokker-Planck (CFP) equations or their higher-order extensions. Various control algorithms are developed based on the method of input–output linearization, accompanied by a rigorous stability analysis of the closed-loop system, including both the tracking error dynamics and the infinite-dimensional internal dynamics. The proposed control schemes use only partial observations of the state of the population, independent of system parameters, and exhibit enhanced performance for large-scale and ultra-large-scale ensembles of TCLs. To further alleviate communication burdens, event-triggerd control techniques are adapted in power tracking control. Both static and dynamic event-triggered control strategies are studied, each ensuring the closed-loop stability while preventing the occurrence of the Zeno phenomena.

This dissertation is expected to give a deeper understanding on coordinating large-scale TCL populations for their better performance in demand response programs within the smart grid. Our findings show that the proposed control methods are highly effective, particularly for large-scale heterogeneous TCL populations. Moreover, the proposed control schemes demonstrate robustness against a range of disturbances commonly encountered in real-world applications.

TABLE OF CONTENTS

LIST OF TABLES

LIST OF FIGURES

LIST OF SYMBOLS AND ABBREVIATIONS

AC	Air Conditioner
ADRC	Active Disturbance Rejection Control
AGC	Automatic Generation Control
AMI	Advanced Metering Infrastructure
ASMP	Ancillary Services Market Program
ATI	Average Triggering Interval
AVR	Automatic Voltage Regulation
BIBO	Bounded-Input, Bounded-Output
CFP	Coupled Fokker-Planck
CMP	Capacity Market Program
COP	Coefficient Of Performance
CPP	Critical Peak Pricing
DAU	Data Aggregator Unit
DBBP	Demand Bidding/Buyback Program
DER	Distributed Energy Resource
DG	Distribution Generation
DLC	Direct Load Control
DMS	Distribution Management System
DOE	Department Of Energy
DR	Demand Response
DSM	Demand Side Management
DSO	Distribution System Operator
EDRP	Emergency Demand Response Program
EE	Energy Efficiency
EKF	Extended Kalman Filter
EMS	Energy Management System
ESO	Extended State Observer
ESS	Electric Energy Storage
ESS	Energy Storage System
ETC	Event-Triggered Control
ETP	Equivalent Thermal Parameter
FACTS	Flexible AC Transmission System
FTISS	Finite-Time Input-to-state Stable

HEMS	Household Energy Management System
HVAC	Heating, Ventilation, And Air Conditioning
HVDC	High-Voltage Direct Current
IBR	Inclining Block Rate
IBVP	Initial-Boundary Value Problem
ICS	Interruptible/Curtailable Service
ICT	Information And Communications Technology
IEA	International Energy Agency
IRLS	Iteratively Reweighted Least Square
ISS	Input-to-State Stable
ISpS	Input-to-State Practically Stable
LADRC	Linear Active Disturbance Rejection Control
MG	Micro-Grid
MLE	Maximum Likelihood Estimator
MPC	Model Predictive Control
MVC	Minimum Variance Controller
NIST	National Institute Of Standards And Technology
ODE	Ordinary Differential Equation
OEB	Ontario Energy Board
OLS	Ordinary Least Square
OMS	Outage Management System
PAR	Peak-to-Average Ratio
PCC	Point Of Common Coupling
PDE	Partial Differential Equation
PDF	Probability Density Function
PHEV	Plug-In Hybrid Electric Vehicle
QoS	Quality Of Service
RES	Renewable Energy Resource
RMSE	Root-Mean-Square Error
RTP	Real-Time Pricing
SG	Smart Grid
SHS	Stochastic Hybrid System
SISO	Single-Input-Single-Output
SM	Smart Meter
STD	Standard Deviation
TCL	Thermostatically Controlled Load

TD	Tracking Differentiator
TOU	Time-Of-Use
ULO	Ultra-Low Overnight
VPP	Virtual Power Plant
WAMS	Wide Area Management System
ZOH	Zero-Order-Hold

LIST OF APPENDICES

CHAPTER 1 INTRODUCTION

1.1 General context of demand response in the smart grid

1.1.1 Conventional grid vs smart grid

The Smart Grid (SG) is a comprehensive concept that encompasses an extensive range of technologies, innovations, and solutions related to the power grid, all designed to accommodate the growing concern of energy efficiency and the pressing issue of climate change, see [8,12,16,43,86,153,197] etc. for an overview. The definition of it has been stated by many entities and researches, embodying the complexity and multiface of this concept. According to the International Energy Agency (IEA) [83],

> *A smart grid is an electricity network that uses digital and other advanced technologies to monitor and manage the transport of electricity from all generation sources to meet the varying electricity demands of end-users. Smart grids coordinate the needs and capabilities of all generators, grid operators, end-users and electricity market stakeholders to operate all parts of the system as efficiently as possible, minimising costs and environmental impacts while maximising system reliability, resilience, and stability.*

Some other definitions, such as the one provided by the U.S. Department of Energy (DOE) [195] or by the European Technology Platform (ETP) for the Electricity Networks of the Future [46], are also very common in the literature. Although general descriptions of this concept diverse, the core principles or features of the modernized power grid are commonly shared. Figure 1.1, adapted from [151], illustrates some predominant differences between the conventional grid and the smart grid infrastructure.

According to the National Institute of Standards and Technology (NIST) architecture [1,59], seven logical domains are included in the smart grid framework, which are, respectively, generation including distributed energy resources (DERs), transmission, distribution, customer, markets, operations, and service providers. In the following, some major differences of each domain are briefly summarized.

Engery generation In conventional power grids, the primary source of energy is dominated by few large power plants. While in contrast, the smart grid enables the integration of a higher percentage of DERs such as photovoltaic (PV) arrays, wind

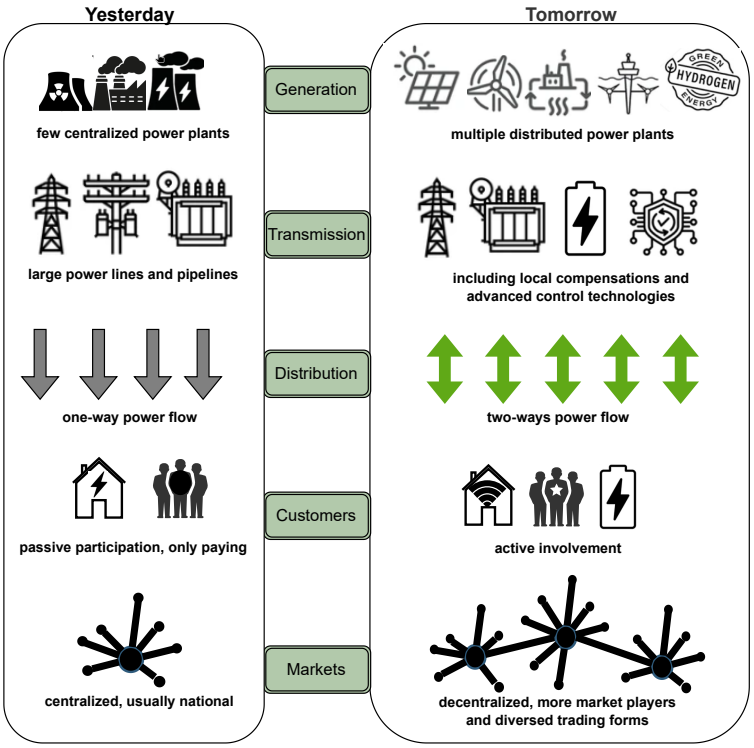

Figure 1.1 The differences between the conventional grid and the smart grid.

farms, geothermal and biomass energy sources, etc. Modern communication networks are deployed on the generation side to collect the real-time supply status.

Transmisson Smart transmission technologies, such as the high-voltage direct current (HVDC) and the Flexible AC Transmission Systems (FACTS) [105, 190], are used to transfer energies from the generation side to the distribution side through several substations. The direction and amount of power flows are monitored in real-time and a protection mechanism will be activated when transmission faults are detected.

Distribution The advanced metering infrastructure (AMI) systems, one of the core components in smart grid [88], are deployed at the distribution side, responsible for gathering and analyzing energy consumption information from a large number of customers. The smart meters (SMs) records the energy usages and the data aggregator units (DAUs) automatically read the data and forward it to the AMI system. Unlike in traditional power grids where the electricity only flows from the substations to customers, the smart grid allows two-way flow of electricity between substations and micro-grids (MGs). As aforementioned in the energy generation domain, there exist a lot of nondispatchable renewable energy resources (RESs) in the smart grid. The inter-

mittent behaviors of these generators will be timely observed and the supply-demand dismatches can be properly handled by the AMI system.

Customers Traditionally, the end-users are only passive customers, and the bills are generated based on their energy consumptions. In contrast, the smart grid empowers the customers with real-time access to their energy usage data and provides them with different demand response programs. The customers can be roughly categorized as industrial, commercial, and residential users. The household users can take an active role in the interactions with the power grid through their equipments such as heating, ventilation, and air conditioning (HVAC) devices or plug-in hybrid electric vehicles (PHEVs).

Markets The smart grid is a decentralized, open, and dynamic system that enables various electric suppliers and load-serving entities to exchange energies. Except for bulky generators and transmission system operators, distributed generators, demand response aggregators and energy storage providers all can compete for market share and revenue. The market platform provides improved flexibility, increased reliability and enhanced energy efficiency to the power grid.

Operations The smooth operation of the power system severely depends on advanced operation technologies, which include but not limit to Energy Management System (EMS), Automatic Generation Control (AGC), Distribution Management System (DMS), Automatic Voltage Regulation (AVR), Outage Management System (OMS), Wide Area Management System (WAMS), and Demand-side Management (DSM) [44, 49, 165, 194, 202]. With the help of various intelligent operation softwares, the real-time system awareness, intelligent energy distribution and automatic fault detection and correction etc. can be achieved.

Service providers Service providers offers various support for the business processes between power system producers, distributors, and customers. Some common services, like billing and account management, installation and management services, cyber security etc., are all available from utilities or third-party organizations.

It is remarkable that the seven domains are not independent, various interactions happen between them. Figure 1.2 shows the interoperability between them, illustrating both the communication and the energy flows inside the smart grid. The development and utilization of RESs is essential for ensuring a clean and low-carbon energy supply. Two main driven factors, i.e., the escalating energy demand and the concern on environmental impacts, are

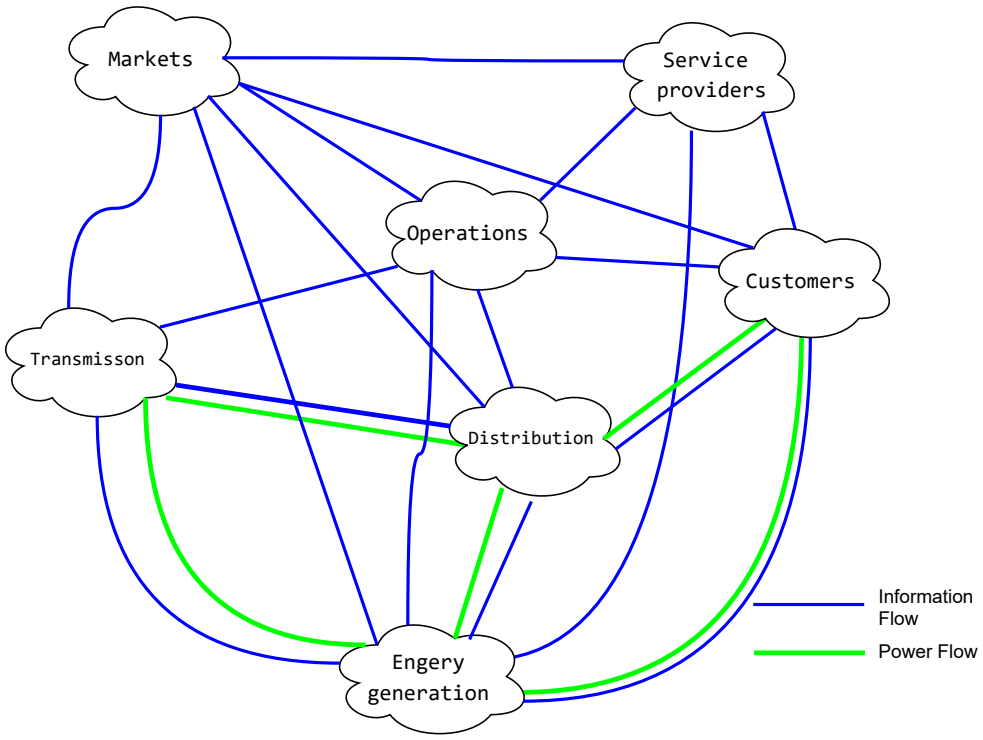

Figure 1.2 The smart grid architecture proposed by NIST.

the underlying reasons for the large-scale integration of RESs. Firstly, the ever-increasing energy demand is obvious. As the population size grows or more people move to the cities, more energy is required for powering houses, commercial buildings or industries. A rapid growing economy also required more energy investment, for example, PHEVs and data centers all consume a significant amount of electricity every day. Secondly, fossil fuel-based energy production generates massive amounts of greenhouse gas, which has a catastrophic impact on global climate, environment, and human health. Figure 1.3 shows the global investment on clean energies in the last decade. The data, with billion USD as units for the energy investment, is obtained from [84], while the value for year 2024 is an estimation. This graph indicates that developing clean energies is a global consensus, and now the investment on clean energies is almost twice as that on the fossil fuels. The penetration of RESs into the utility grid brings severe challenges to the stability, service quality, and reliability of the smart grid [7, 28, 141, 188]. Some renewable energy generators, such as wind turbines and solar photovoltaic (PV) systems, are heavily influenced by weather conditions, seasonal variations and geographical locations, thus the power output is highly unpredictable and has large fluctuations. The intermittent behavior increases the strain on the power grid, especially during periods of high demand. Some services traditionally provided by synchronous

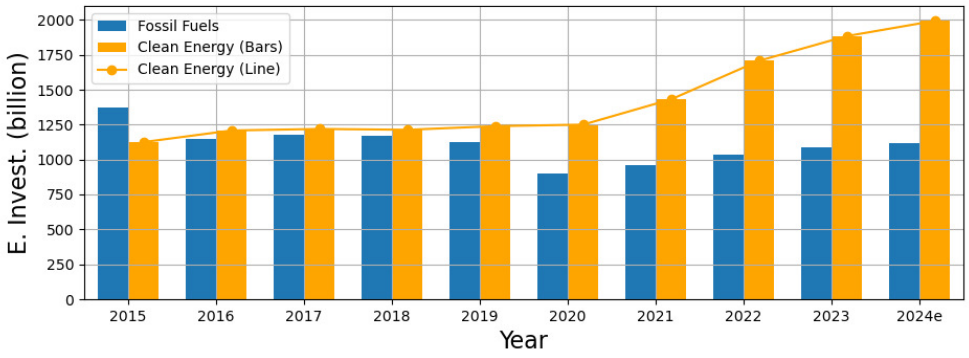

Figure 1.3 Global clean-energy investment in the last decade.

generators, such as load following, voltage and frequency stabilities, spinning reserve, etc., become more difficult when there are too much uncertainties introduced by RESs.

To effectively handle the issues arising from energy supply intermittency, it is essential to explore all available remedies and technologies, such as market competition, active energy storage, demand management, real-time forecasting etc., see [6,45,64,134,182] and references therein. As a cost-effective solution, demand-side management and demand response (DR) are introduced in the following.

1.1.2 Demand-side management

Demand-side management is not a new concept. A formal definition of DSM can be obtained from [60]:

> *Demand-side management is the planning, implementation, and monitoring of those utility activities designed to influence customer use of electricity in ways that will produce desired changes in the utility's load shape, i.e., changes in the time pattern and magnitude of a utility's load. (Gellings 1984-1988)*

Increasing supply by building new plants and transmission networks is costly, whose cost is usually passed to the customers meanwhile creating more pollutions. DSM, however, is a win-win-win for utilities, customers, and the planet. For the utilities, DSM is a cost-effective method for maintaining supply-demand balance and reducing peak-to-average power ratio (PAR), which significantly improves the efficiency and reliability of the grid. For the customers, the financial benefit, such as a lower electricity rate, is usually applied for reducing consumption or shifting electricity demand from on-peak to off-peak hours. For the planet, a

lower carbon footprint is achieved, which is essential for the global climate targets. Besides, less harmful pollutants are emitted, which is also indispensable to a sustainable future.

According to [15], there are three catagories for DSM, respectively Energy Efficiency (EE), Demand Response, and Distributed Energy Resources (DERs). EE refers to completing the same tasks with less power. DR programs adjust the load profile when the power grid is under stress, see the next subsection (subsection 1.1.3) for more details. DER refers to the decentralized power generation systems that connected to the grid at distribution level. It mainly consists of two subcategories, Distribution Generation (DG) and Electric Energy Storage (ESS).

DSM is not just a theoretical concept, it might happen in the daily routines of some Canadians. According to Ontario Energy Board (OEB), there are three types of electricity rates for residential customers to choose, respectively Time-of-Use (TOU), Ultra-Low Overnight (ULO) and Tiered prices. Table 1.1 shows the TOU rates for household users in Ontario, valid from November 2023 to October 2024. It is clear that the on-peak price are higher than those of mid-peak and off-peak periods. Therefore, if one person in Toronto uses TOU rates and tries to move his/her EV charging time or his/her washing and drying time from on-peak to off-peak periods, he/she is already participating in the demand-side management. For the tiered prices, it is similar to the domestic rates for household users in Quebec, as shown in Table 1.2, refer to rate D in [81]. According to Hydro-Quebec, if the daily consumption is less than 40 kW, the rate is billed at 6.704 ¢/kWh. Otherwise, a higher price of 10.342 ¢/kWh; is applied. Thus, if a person always tries to avoid using larger power consumption appliances, he/she is involved in the energy efficiency category of demand-side management.

Table 1.1 The TOU electricity prices in Ontario

TOU Period	Hours		TOU Prices (¢/kWh)
	Winter	Summer	
Off-peak	7 p.m. – 7 a.m.	7 p.m. – 7 a.m.	8.7
Mid-peak	11 a.m. – 5 p.m.	7 a.m. – 11 a.m. 5 p.m. – 7 p.m.	12.2
On-peak	7 a.m. – 11 a.m. 5 p.m. – 7 p.m.	11 a.m. – 5 p.m.	18.2

Table 1.2 The rate D prices in Quebec

Description		Prices ((¢/kWh))
system access charge		44.810
daily electricity consumption(kW)	[0,40]	6.704
	[40,65]	10.342

1.1.3 Demand response

Demand response is a subset of demand-side management, as claimed in subsection 1.1.2. After comparing existing definitions, the authors of [133] provide a relatively new definition of demand response:

> *Demand response is the actions of customer-sited energy resources, located downstream of metering points, to voluntarily, actively, and temporarily adjust their electricity production and/or consumption in response to signals (e.g., commands, prices, measurements).*

DR is a valuable tool for stabilizing the power grid in peak demand time or in emergencies. Figure 1.4 illustrates some common DR options. There are roughly two types of demand response programs, respectively price-based and incentive-based, based on how the load profile changes are brought about.

Price-based DR regulates the energy usage by changing price signals. Time-of-Use (TOU), a common strategy adopted in a lot of countries, charges the customers with different rates based on the consumption time of day or season. However, it uses a static price schedule, whose optimality is unclear and might cause a "rebound peak" after the namely on-peak period, see [3,155]. Real-time pricing (RTP) is a scheme that reflects the real-time wholesale price of electricity, usually fluctuates hourly based on advanced forecasting technologies. Critical peak pricing (CPP) entails using higher power chargers at a peak time. The difference between CPP and TOU is that TOU is designed for a medium and long-term, while CPP is usually applied for a short-term period, for example a few days in a year. Inclining block rate (IBR) is a scheme where customers pay higher prices if the total consumption exceeds a fixed threshold. It encourages end-users to use less energy and thus facilitates energy efficiency.

Incentive-based DR pays customers some monetary incentives in exchange for active responses from the DR events. Some common incentive-based options include direct load control (DLC), emergency demand response programs (EDRP), capacity market programs

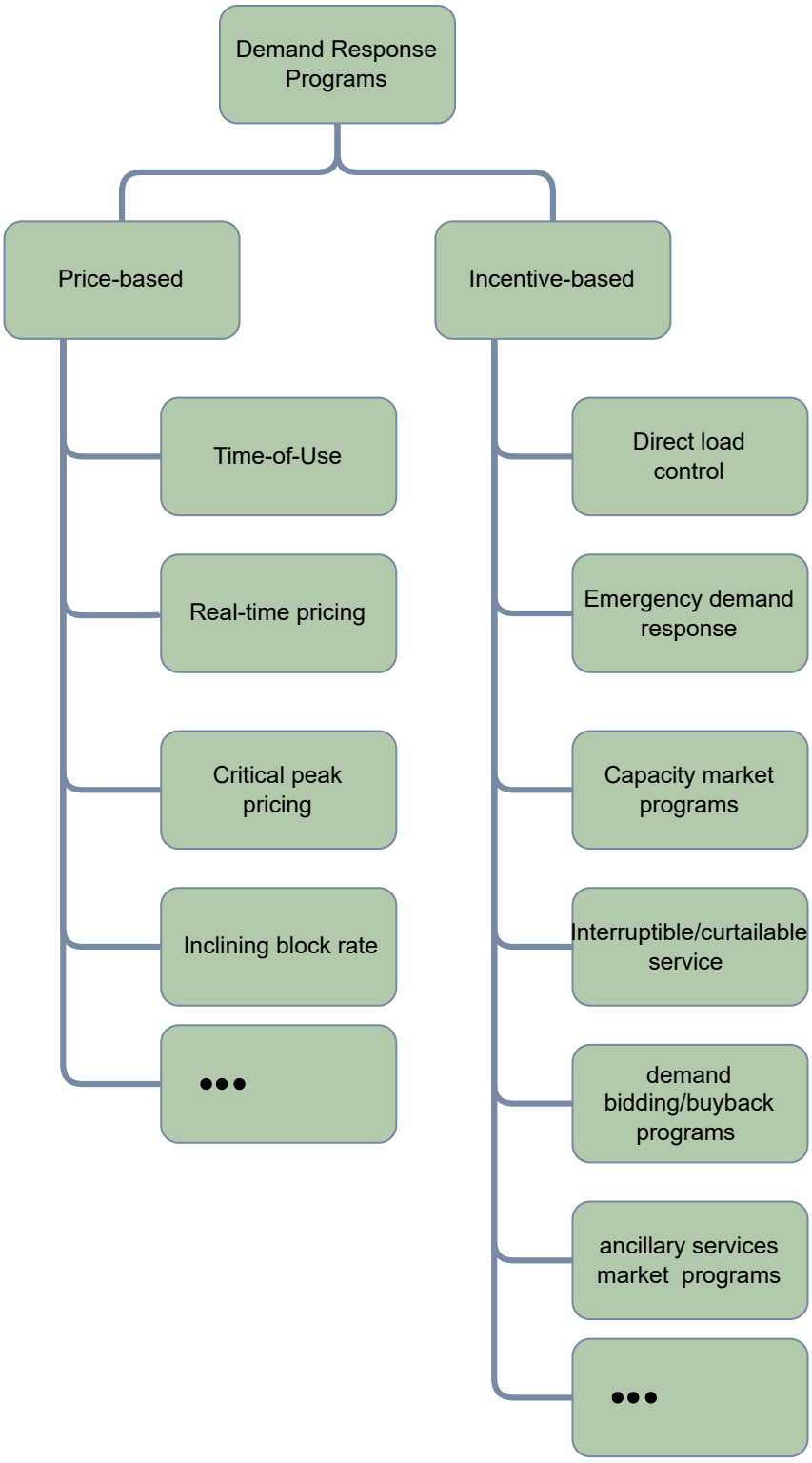

Figure 1.4 Classification of DR programs.

(CMP), interruptible/curtailable service (ICS), demand bidding/buyback programs (DBBP), ancillary services market programs (ASMP), etc. DLC grants the utilities or grid operators remotely regulate the appliances to fulfill demand and EDRP programs pays users for voluntarily decreasing power consumption in case of reserve shortfalls such as failure of generation units, extreme weather events etc. CMP requires a prespecified load reduction during system emergencies. ICS, which traditionally offers to larger industrial and commercial organizations, also requires a demand reduction at critical times. Unlike DLC and EDRP, CMP and ICS suffer penalties when fails to curtail. DBBP and ASMP are based on market clearing schemes, while DBBP is mainly offered to large market participants. The customers take a bid for curtailing at more suitable prices.

1.2 Thermostatically controlled loads for demand response

A thermostatically controlled load (TCL) is an electrical device that is designed by automatically heating or cooling a physical system so that the temperature is kept within a limited range or around a fixed set-point. For a TCL, such as an air conditioner, a heat pump, or a refrigerator, it is usually controlled by a bang-bang controller [104], where the control signal switches abruptly between two power states, ON and OFF respectively. The operations of TCLs all follow a similar manner. Without loss of generality, take a residential air conditioner (AC) as an example. When the temperature is above the deadband, the cooling device turns on, making the temperature drops. And when the temperature is below the deadband, the AC power turns off, and the temperature slowly increases. In the following, ACs are always used as the example for the analysis, and thus a TCL population has the same meaning of an AC population. However, the established work can be easily generalized to other types of cooling or heating devices whenever needed.

The most noticeable feature of a TCL is its high thermal inertia, which is defined as "*the capacity of a material to store heat and to delay its transmission*" [112]. Thus, temporary and short interruptions are allowed within a regular operating cycle with little or without compromise on the service quality. According to a study in UK, there is no significant difference on the human thermal comfort when the AC set-point increases from 22 °C to 24 °C, see [95, 170]. In fact, it is shown that the set-point of a TCL can be quite flexible between 19.5 °C and 25.5 °C without considering the thermal acceptability [214]. In summary, TCLs are ideal candidates for participating DR programs.

There are great potentials for populations of TCLs to participant in DR programs. Although a single TCL has limited impact on the whole grid, ensembles of a large number of TCLs, when managed in an orderly and controllable manner, can have a significant impact on the

entire power grid. According to the statistics, ACs account for around $30\% \sim 40\%$ of the total power consumption during the peak hours during summer in big cities of China, Spain, and India, see [39,75,204]. Thus, the potentials of TCLs need to be further explored and they can even act as a major role in responding to various demand response events. Many existing studies have shown that the population of TCLs can participate in tasks such as power balancing [77,93,124], energy arbitrage [26,129,152], frequency regulation [37,107,136,185], voltage adjustment [80,204,228], etc..

As one type of DERs, TCLs are usually geographically dispersed over a vast region. There are two closely-connected concepts aiming at aggregating such scattered resources, namely virtual power plant (VPP) and micro-grid (MG).

A VPP is a clustered, interconnected system which aggregates different types of DERs, aiming to provide affordable, secure, and flexible energy services similar to a conventional power plant. When distributed small-scale generators, energy storages or flexible loads are integrated into a VPP, they can be traded collectively in the energy market, where small individual asset is usually blocked by the minimum bid size. Figure 1.5, adopted from [156], shows the VPP communication model.

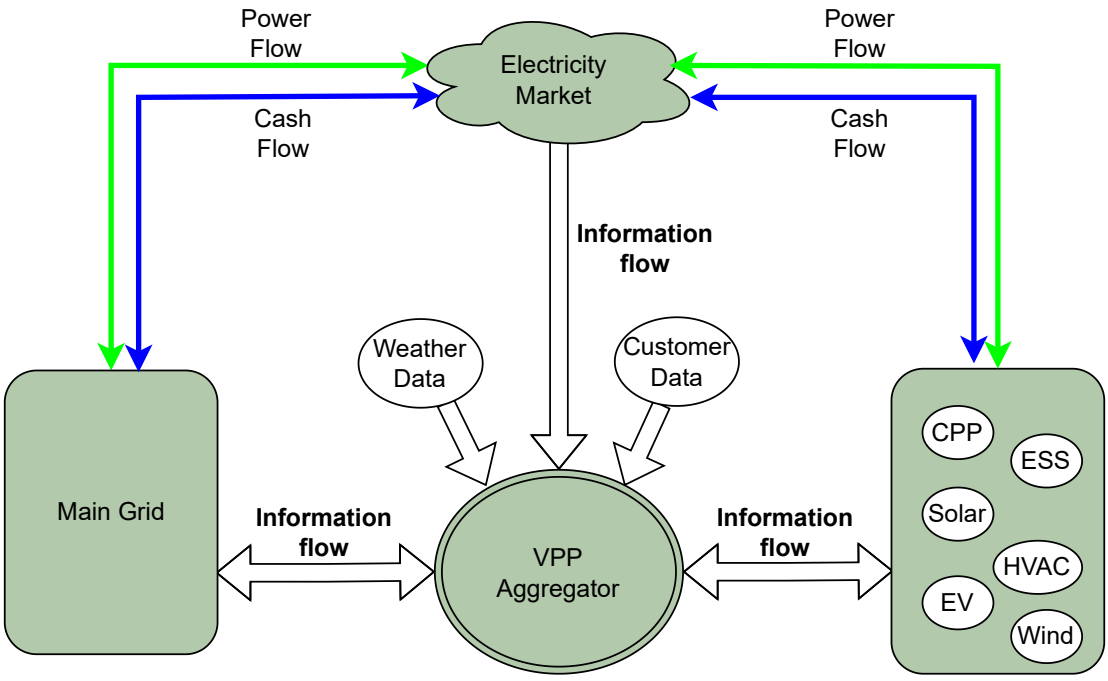

Figure 1.5 The VPP communication model.

A micro-grid is conceptualized as a group of interconnected DGs, DERs, and energy storage systems (ESSs) with clearly defined electrical boundaries that can be operated in grid-

connected mode or act in an islanded mode. According to [140, 157], there are four main components in a MG, respectively, distributed generators, local loads, ESS, and point of common coupling (PCC). An MG usually has a confined geographical limit, while the PCC controls the power exchange between the MG and the main utility grid. Figure 1.6 shows the typical architecture of a MG.

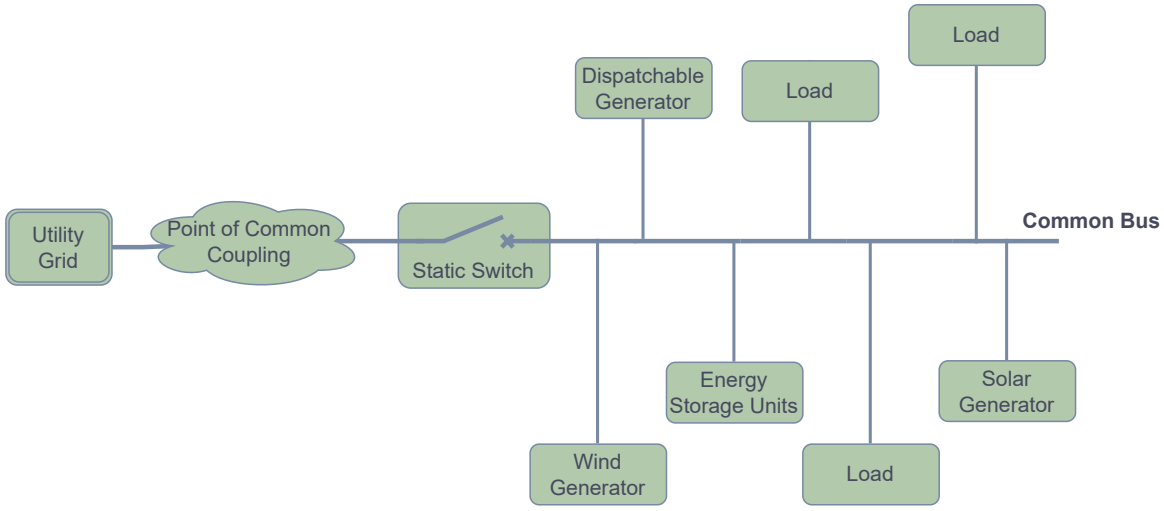

Figure 1.6 Schematic view of different components in a micro-grid.

Both VPP and MG involve the integration of DERs, and they offer different advantages and deficiencies. Some major differences are summarized in Table 1.3. These differences suggest that a MG focus more on end-user power supplies, while a VPP serves the interest of utility companies and puts more emphasis on the wholesale market.

In this work, the perspective of a distribution system operator (DSO) or a utility company is considered. The population size is assumed to be as large as possible. By doing so, we can better understand the dynamics of TCL populations at a larger scale and better harness the benefits of aggregating these loads. Thus, the scope of the current research is a VPP, not confined to a household energy management system (HEMS) or an MG with limited and usually fixed loads. At last, it is worthy pointing out that both VPPs and MGs are important in the context of the smart grid. The synergy between VPPs and MGs is at the forefront of research and revolutionizing the energy sector's landscape by providing reliable, efficient, and resilient grid services while facilitating the transition to a greener and more sustainable energy future.

Table 1.3 Major differences between a VPP and an MG

Description	VPP	MG
Connected the main grid	Always connected	Either connected mode or islanded mode
Energy storage system	May or may not have	Requires ESS
Grid contingency happens	Cannot deliver power	Can operate independently
Geographical area	wider area	limited
Technology dependencies	Mainly requires smart meters, information, and communications technologies (ICTs)	Mainly requires PCC, inverters, switches, etc.
Market	trade at the retailer and the wholesall market	retailer level, usually sell to local substations

1.3 Objective and contributions

With the development of many smart grid technologies, it requires that the demand-side takes an active role to avoid situations of power supply shortage or surplus. This dissertation focuses on designing control algorithms for heterogeneous TCL populations to fulfill the automatic power tracking tasks, especially in the context of demand response programs.

Heterogeneous TCL populations refer to ensembles of thermal devices of the same type (either cooling or heating), for example a group of ACs, with different thermal parameters. Note that even for two ACs manufactured with exactly the same technical specifications, they are still considered as two heterogeneous units due to different working environment. For example, they maybe working in two rooms with different sizes, building materials, or window-to-wall-ratios. Thus, heterogeneous populations, consisting of individuals with different thermal behaviors, are more common in real life and deserve to be better studied.

Heterogeneous TCL populations are well suitable for such kind of power tracking tasks, where some common load regulation tasks, such as peak clipping, valley filling, load shifting or flexible load shaping, can be easily achieved.

In this work, the method of input-output linearization is adopted in power tracking control. To develop effective control strategies, system performances, such as stability, robustness, etc., should be seriously considered. To this aim, we impose the finite-time input-to-state stability (FTISS) to the tracking error dynamics, which characterizes the desired performance

while ensuring the robustness of the system in the presence of modeling error, parametric uncertainties, and disturbances. Then, the active disturbance rejection control (ADRC) is utilized to improve the system performance. Furthermore, we employ event-triggered control strategies to reduce communication and computation burden, which is a critical issue in the implementation of large-scale TCL population control systems. The reference curves for power tracking control can be generated based on price changes in the market or intermittent behaviors from distributed generators. The property of the internal dynamics, which are also described by CFP equations, is rigorously analyzed to ensure the stability of the system in closed loop.

Specifically, the key findings are presented as follows:

- Based on the first-order equivalent thermal parameter (ETP[1]) model for thermal appliances and the coupled Fokker-Planck (CFP) model for aggregate population dynamics, a control framework which requires only partially observed states is proposed. The control scheme is in a composite form, where the auxiliary controller is quite flexible on its choices. It shows that the closed-loop system is FTISS when a sliding mode-like auxiliary controller is utilized. This finding fills the gap of designing control strategies with model-based methods, providing a feasible engineering solution for power regulations for a population of heterogeneous TCLs. The performance of the proposed control strategy is validated by investigating the power tracking effect in a simulator.

  The results of this work are published in *IEEE Access* in 2024 [220].

- Cost-effective event-triggered control strategies are developed. By seamlessly integrating with event-triggered mechanisms, the data transmission frequencies are significantly reduced. Both static and dynamic event-triggered methods are considered, and a rigorous theoretical analysis shows that their corresponding closed-loop systems are input-to-state practical stability (ISpS) and free from Zeno phenomena. The performances of the novel event-triggered control methods are quantitatively evaluated by numerical simulations. This work extends the proposed continuous-time control scheme [220] to the event-triggered control field, and demonstrates the applicability and potential for real-world applications.

  The results of this work are published in *IEEE Trans. Smart Grid* in 2024 [219].

- The second-order ETP model, compared with its first-order counterpart, is more accurate on describing the thermodynamics of a single TCL. When the individual TCL

[1]In this work, the abbreviation ETP is duplicated defined, but from now on, the ETP only stands for "the equivalent thermal parameter."

dynamics is of higher-order (≥ 2), the CFP model should also be generalized to high dimensional for the aggregate dynamics. The control laws in [220] and [219] are re-examined and modified to accommodate the high-dimensional scenario. Furthermore, incorporating the disturbance rejection control technique into the auxiliary controller significantly reduces the steady-state error, representing a notable improvement. This newly-introduced control scheme is evaluated by numerical simulations, and the results show an improved performance for the considered tracking problem.

The results of this work are reported in *IEEE Trans. Smart Grid* in 2025 (submitted).

1.4 Dissertation organization

The remainder of this thesis consists of 7 chapters, shown in Fig. 1.7, in addition to this chapter of introduction.

Chapter 2 establishes the scope of the research topic, and examines the existing literature related to this research work. The main focus is the coupled Fokker-Planck model, which is a partial differential equation (PDE) system commonly used for describing the aggregate dynamics of TCL populations. Moreover, some popular event-triggered control schemes are also reviewed, as this is an important step towards real-world applications, especially for resource-constrained systems. Compared with periodic control methods, the benefits in energy consumption and communication bandwidth usage often outweigh some possible performance degradations.

Chapter 3 presents some mathematical background knowledge, which serves as theoretical foundations for the subsequent controller design, stability analysis, and numerical implementations. On the other hand, some preliminary sensitivity analysis is conducted, which helps gaining insights into the qualitative responses of a TCL population. Chapter 3, together with Chapter 2, establishes the theoretical framework underpinning the research, providing details for tools such as the relevant models, hypotheses, stability analysis methods, simulation environment, etc., employed in Chapter 4, Chapter 5, and Chapter 6.

Chapter 4 presents a nonlinear controller which requires only partially observed states for the first-order TCL populations. A novel output function for the tracking problem is proposed, and the control scheme is derived based on a rigorous analysis on the tracking error dynamics. The closed-loop stability of the system is carefully checked to show the robustness of the proposed controller.

The research work in Chapter 5 and Chapter 6 is a direct extension of Chapter 4. Chapter 5 explores the integration of event-triggered mechanisms with the proposed control methods.

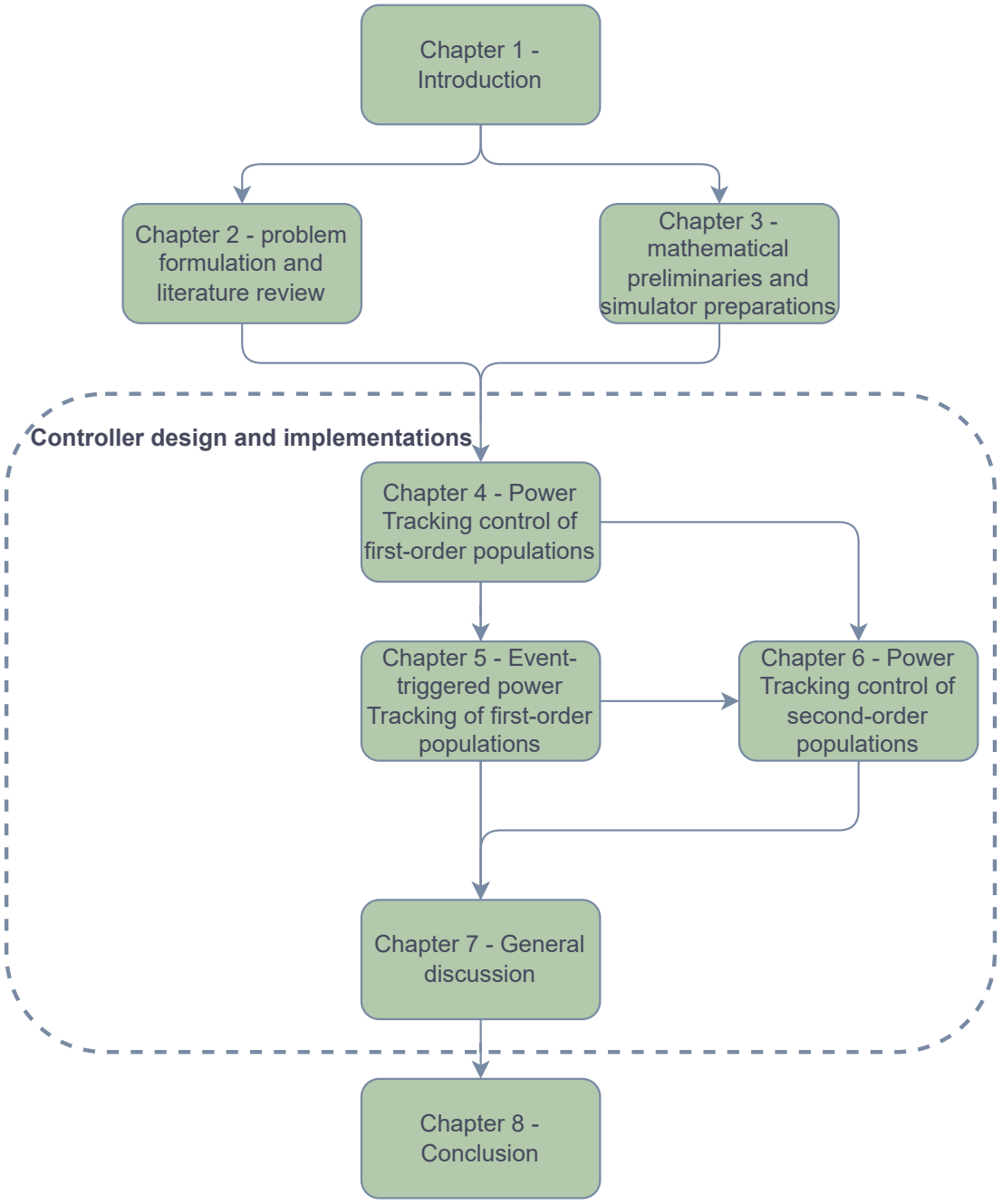

Figure 1.7 Flowchart of the dissertation structure.

For an event-triggered control method, it does not need to periodically broadcast the control signals to the whole population, which can significantly save the network communication resources. Both the static and dynamic event-triggered control strategies are explored in this part.

Chapter 6 generalize the work in Chapter 4 to higher-dimensional scenarios. A second-order ETP model is used for single TCL dynamics, and a generalized higher-dimensional coupled Fokker-Planck model is used for the aggregate dynamics. Compared with the first-order model, the second-order ETP model has enhanced accuracy on describing the thermodynamics by separating the mass and air temperatures. Another highlight is the adoption of linear active disturbance rejection control (LADRC) method as the auxiliary controller, and its effect on the the steady state errors is discreetly examined.

Chapter 7 highlights the intrinsic connections between the proposed control strategies. The underlying methodological relationship of the three control schemes developed in Chapter 4, Chapter 5 and Chapter 6 are re-examined.

Chapter 8 concludes the whole thesis, summarizing the key findings, considering limitations of the current work and suggesting possible avenues for future research.

CHAPTER 2 PROBLEM STATEMENT AND RELATED WORK

2.1 Scope of the dissertation

The coordination of a population of TCLs is a complex control problem, and there exist many control algorithms tailored for different tasks. In order to fulfill the objective of this dissertation, the scope of the solution should be well clarified. In the following, different aspects related to the design process are presented, which may help to clarify the capabilities of the proposed control algorithm.

2.1.1 Model-based or data-driven control strategies

For a large-scale population control prolbem, both model-based methods and data-driven methods [183, 187] are popular choices, and each group of methods has its advantages and limitations. In this work, we focus on model-based control methods for the power tracking task. The data-driven methods for TCL population control, see e.g. [34, 35, 168, 175], are out the scope of this work. Different with these data-driven methods, an aggregate model based on first principle is required before designing appropriate control strategies.

A few major factors need to take into consideration when characterizing the overall dynamics with an aggregate model. To begin, as aforementioned, the heterogeneity is quite common as the TCLs usually dispersed in a broad region with different working environments. Hence, there is a loss of fidelity in some works by assuming a collection of homogeneous loads. Here, homogeneity means that two TCLs will have identical temperature trajectories when starting with the same initial temperatures. It is shown in [20, 146] that the aggregate dynamics of a homogeneous population has a more fierce oscillation than its heterogeneous counterparts. Another factor to be mentioned is the time-varying external conditions, such as the outside temperatures, unexpected switching ONs/OFFs[1], locked-out time, communication delays, etc. They all have impacts on the aggregate dynamics to some extent, although not conducive to the controller design, should be taken into consideration. Finally, practical applications often requires the communication overheads as small as possible due to limited network bandwidth. To save the scarce communication resources, spatial and temporal measures can be explored. The conventional control signal transmission mechanism is time-triggered, i.e., the signals are generated and transmitted periodically with a prede-

[1] In this work, the word 'forced-switches' is used to refer to the state changes not happening on the deadband boundaries.

fined fixed-time interval. The huge amount of data can easily cause network congestion, and may block some more important data exchanges. Thus, event-triggered control mechanism should be given a priority to reduce the temporal redundancy. Another strategy can be used is only collecting partial information from the population. This can also largely relieve the communication burdens and simultaneously boost the privacy protections on the customers.

2.1.2 Centralized, decentralized, and distributed control

In general, control architectures can be broadly classified into three types: centralized, decentralized, and distributed, each with its own advantages and limitations. In a centralized control structure, all TCLs communicate directly with a central operator/power utility, which is responsible for monitoring and analyzing real-time data from the peripheral nodes and providing appropriate control signals. While in a distributed control scheme, each unit is independent with only possible communications with their neighbors, and there is no clusters of smaller "centralized" hubs which exists in a decentralized control structure. Figure 2.1 shows a schematic view of different control modes and Table 2.1 shows some major differences between different control patterns.

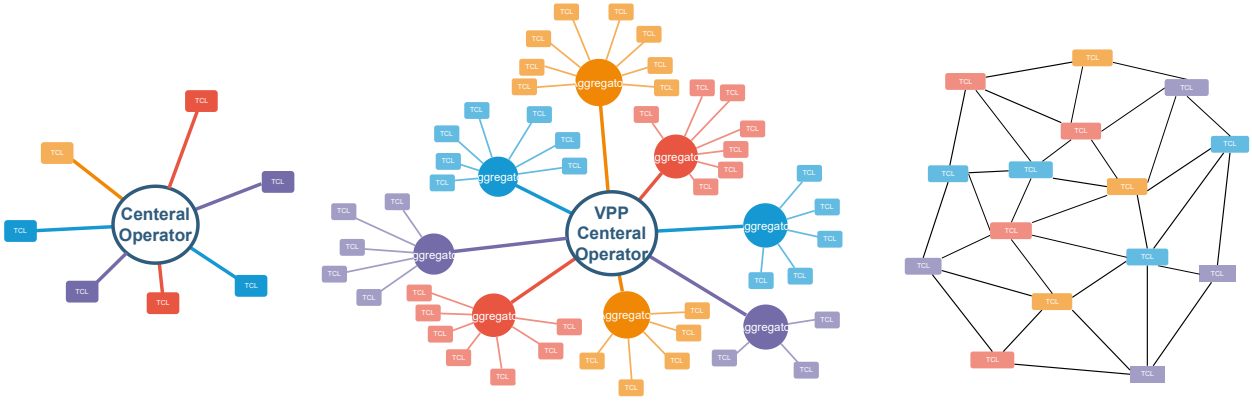

Figure 2.1 Different control architectures for TCL populations.

For decentralized control, the term "decentralized" may have two slightly ambiguous meanings:

1 In a VPP, the power utility usually divide the whole population into different subgroups, where TCLs with similar parameters are usually assigned into the same group. The operation workload is distributed to multiple sub-aggregators, and each of them can act as an independent central controller.

Table 2.1 Comparisons between centralized, decentralized, and distributed control schemes

	Centralized	Decentralized	Distributed
Deployment	easy	moderate	moderate
Fault Tolerance	low	moderate	high
Latency	low	moderate	high
Scalability	low	moderate	high
Maintenance	easy	moderate	hard

2 For each sub-aggregator, it broadcasts a common reference signal to all appliances, and each TCL controls its own power consumption with its local controller.

In this work, a decentralized control scheme with the second meaning is used, while the coordination problem between different sub-aggregators in the first meaning is out of the scope of this research. Thus, the focus is only part of the decentralized graph in Fig. 2.1. This control architecture is decentralized due to the fact that each individual unit is autonomous on its own behavior. This is also the same terminology used in [191, 192].

2.1.3 Model discretization or controller discretization

Modern controllers are usually implemented in digital platforms, thus, discrete-time controllers are commonly required as inputs. For a continuous-time system obtained from first principles or physical laws, there are two approaches to derive a corresponding digital controller. The first approach to achieve this is by discretizing the continuous-time plant and then design a discrete-time controller, while the second is by designing a continuous-time controller and then approximate it with a digital counterpart. The first approach is called model discretization, and the second one is called controller discretization. Figure 2.2 illustrates the two different routes for acquiring the final discrete-time controllers.

For a system described by partial differential equations (PDEs), discretization might not only happens in the time domain, but also in the the spatial domain. In the field of PDE controller design, two special terminologies, called “early-lumping” and “late-lumping”, are used to distinguish the model discretization and controller discretization strategies. “Early lumping” means approximating the PDE with a finite-dimensional, or lumped model before designing the controller, and “late-lumping” indicates designing a control scheme directly from the PDE model and then discretizing the controller for implementation purposes, refer to [137, Chapter 1] more details.

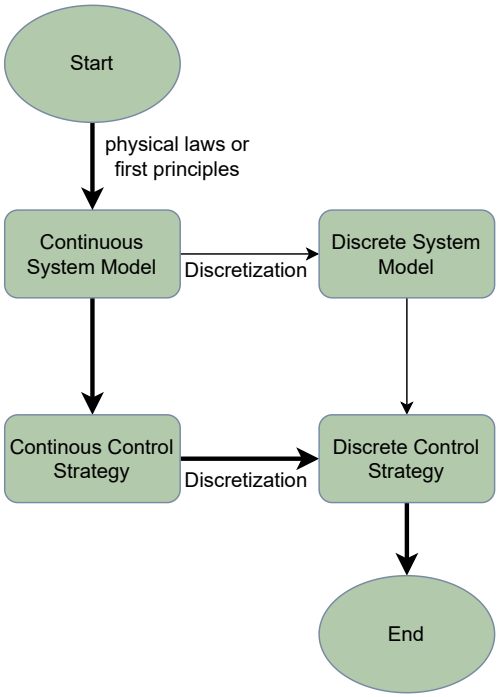

Figure 2.2 Different controller design approaches.

Both "early-lumping" and "late-lumping" have their particular advantages and disadvantages, as summarized in Table 2.2. Generally, "late-lumping" method can preserve the essential dynamics of the PDE, thus providing a higher model accuracy and more flexible controller design strategies. But this approach is often more mathematically involving, which requires more sophisticated deductions and computations. Some of the research works based on late-lumping approach can be found in observer design [127], fuzzy control schemes [162], or backstepping controller designs [13] etc. A loss of model accuracy usually happens when approximating the PDE dynamics with finite-dimensional equivalent models, which might only contain part of the information of the original PDE model. Furthermore, the space domain is usually divided by different binning or griding strategies, and choices of different bin sizes often results in models with different level of accuracy. Nevertheless, this approach allows leveraging classic control techniques, although they may suffer from the curse of dimensionality for applications in large-scale systems.

In this work, the controller discretization method is used. As we focus on PDE models in characterizing the population dynamics, controller discretization has the same meaning as late-lumping method here. Compared with model discretization method, the physical insight is well retained and the system stability and controller performance problems can be well dealt with [9, 143]. The design procedure is emphasize with bold lines in Fig. 2.2. Note that

Table 2.2 Comparisons of early-lumping and late-lumping schemes

	Early-lumping	Late-lumping
Model accuracy	low	high
Controller design	easy	difficult
Computational complexity	high	low
Implementation complexity	high	low

in Fig. 2.2, the two approaches both generate discrete-time control signals. However, it is worth mentioning that the aggregate models used in these two approaches are not appropriate for building simulation environments. To stay in closer line with practical applications, the simulation environment should be composed by individual units, and each of them owns individual dynamics. The population dynamics is the collective behavior of all TCLs, and the control signal should be broadcast to all members in the population. In this scenario, the aggregate models are only tools for analyzing the overall dynamics and for designing appropriate control schemes, and mismatches with the real world happen when used directly for the population dynamics.

The aggregate model used in this work is introduced in the following section, see Section 2.2. Some finite-dimensional state space models are also presented, as most finite-dimensional state space model can be treated as model discretization counterparts of the PDE system.

2.2 Literature review

2.2.1 Finite dimensional state space models

For the system dynamics, the key point is finding a way to characterize the evolution of probability distributions of the ONs and OFFs respectively. An intuitive method is to group the population into different temperature "bins", and check the number of TCLs in each temperature bin. By tracking over time, the evolution of the aggregate dynamics is vividly shown in the bins, and the aggregate power can be regulated by temperature priority control strategy, see [116–118, 198] and the references therein. Broadcasting ON and OFF signals based on a temperature priority list can achieve precise control to each individual TCL. However, this scheme requires huge communication resources and raises concerns on customer privacy leakage problems. Hence, decentralized control scheme based on the temperature set-point or forced-switching rate is a better choice for an extremely large population. Furthermore, it is better to acquire the transition probabilities from one state bin to other bins, then the ag-

gregate dynamics can be represented by a system of ordinary differential equations (ODEs), and many well-established control techniques for ODEs can be applied.

In [131], the extended Kalman filtering (EKF) technique is used to identify the state transition matrix, and a linear time-invariant (LTI) system is obtained for the heterogeneous populations. In [21], a bilinear state-space model with constant transition matrix is deduced by using a fixed transport rate. The authors of [36, 77] generalize the work of [21] to ODE systems with time-variant coefficient matrices. These ODE systems can be viewed as a form of simplified, lumped representation of a more complex underlying PDE model, where the spatial effects are averaged by a few bins. This connection is extremely obvious in [21], where the bilinear model is derived by the finite difference approximation of two coupled transport PDEs for homogeneous populations. In [178], a modified LTI model taking account of compressor delays is proposed and a probabilistic control strategy is provided. In [109], a distributed model predictive control (MPC) scheme is put forward by considering lockout time with an LTI state bins system. As the transport rate in each bin is different, non-uniform lengths for the state bins are more appropriate, refer to [177] for related works.

2.2.2 Coupled Fokker-Planck model for first-order TCL populations

The coupled Fokker-Planck model plays a primordial role in characterizing the aggregate dynamics of homogeneous TCL populations [126]. A first-order equivalent thermal parameter (ETP) model is used to describe the heat dynamics for an individual device. It is a lumped-parameter model widely used in the literature, among which a Wiener process is included to account for unexpected heat gains or losses, refer to [74, 115, 176] for more details. The aggregate model is obtained by investigating the evolution of probability densities of the TCL in the ON and OFF states, respectively. The stationary solution to the CFP is presented by Callaway in [24]. Additionally in this work, a linear ARMAX model (AutoRegressive Moving Average model with eXogenous inputs) is obtained through system identification technique, and a minimum variance controller (MVC) is designed, which is successfully used on tracking high-frequency power signals from wind farms. After introducing the set-point variation rate into the coupled PDEs, Bashash et al. [21] designed a sliding mode control method to regulate the aggregate powers. Note that in their work, there is no diffusion terms in the PDE system, as the noise process is not taken into account. Additionally, their design is based on model discretization method, where a bilinear state bin transition model is firstly derived before designing the controller. Hence, there is a close connection between CFP model and finite-dimensional state-space models. In [191, 192], after summing the two CFP equations, a linear controller is designed based on changing the average convection rate.

In [55], the effect of heterogeneity or other disturbances is incorporated in the CFP equations, and an model predictive control (MPC) method is presented.

Compared with finite dimensional state space models, the PDE paradigm provides a more generic framework for modeling the aggregate dynamics of TCL populations, which allows handling nonlinearity, time-varying operational conditions, and parametric uncertainties with often very simple control algorithms. There exist close connections between the CFP model and some commonly used state-space aggregate models. Many of the later can be treated as space-discretization implementations of the simplified CFP model. It has been shown that the finer the discretization, i.e., the more state bins, the more accuracy the aggregate dynamics, see [21, 131]. The original CFP model naturally contains more information than its discrete counterparts. However, a controller designed for a PDE system generally involves more complex mathematical analysis and is more challenging. Some of finite-dimensional aggregate models are already discussed in Section 2.2.1, and some more relevant works can be found in Markov chain model/state space transition model [36, 90, 109, 130, 131, 148, 163, 171, 177, 184], state queuing model [17, 19, 32, 116–118, 212], bilinear model [21, 77, 78, 198], duty cycle based model [68, 79, 122, 130, 132, 158, 159, 191, 192], etc.

For TCL population power consumption control, a thermostat set-point variation rate is broadcast to the population. Three types of signals are commonly used for controlling a population of TCLs, namely direct ON/OFF control, thermostat set-point control, and probability switching control. For direct ON/OFF control, the aggregator broadcasts switching-ON/OFF signals directly to the TCLs. For example, the authors in [115, 118, 172] control a population of TCLs based on a real-time temperature priority list. For thermostat set-point control, a set-point offset [184] or a set-point variation rate [21, 24] is broadcast to all the population members. For probability switching control, see e.g. [193, 215], a switching probability is broadcast to the population and each TCL reverses its states randomly with this probability. In general, the direct ON/OFF is quite efficient in reducing instantaneous power consumption, while thermostat set-point control is more suitable for load management purposes with a longer period [154, 198]. The probability switching control has a similar performance with set-point control, and both of them uses less communication resources compared to direct ON/OFF control.

2.2.3 Coupled Fokker-Planck model for higher order TCL populations

The dynamic models presented in Section 2.2.2 are all based on first-order ETP models. This approach simplifies the environment where the TCLs operate (e.g., residential houses or small commercial buildings) to a network of several nodes connected with equivalent thermal resis-

tances and capacitances. The nodes represent different parts of the building, such as walls, interior spaces, windows, etc. The heat flow and temperature changes in the house can be similarly analyzed as in an electrical circuit. The first-order ETP model only considers room air temperatures, while the second-order model considers both air and mass temperatures in the building. The later model tackles thermal behaviors in a building with a more refined approach, making it more accurate in capturing both steady-state and transient thermal dynamics, refer to [18, 89] for more details on the 2nd-order model. With enhanced accuracy, it is used in the Gridlab-d simulator for end-user modeling [27], and also used for demand response potential evaluations in [29, 115]. The authors of [14, 69] present more sophisticated 2nd-order thermal dynamics models by further considering the solar radiations. Models with order greater than 2 are also available, see [38, 102, 142, 150]. Generally, the more complicated or the higher order the model, the more accurate in predicting the temperature changes, but it also requires more complex circuit topologies and more computations. In Section 6.2, the CFP model is generalized to higher dimensional forms to present the dynamics of higher-order TCL populations. It focus on dealing with second-order populations. Eventually, the generalized CFP model can be extended to populations of order higher than 2.

Unlike first order populations, controlling a higher order population is not adequately studied in the literature. To characterize the aggregate load dynamics, the research work in [221] is reported in this dissertation. Similar to [126], the aggregate model is derived starting from a stochastic hybrid system (SHS) model, which includes both continuous and discrete behaviors in the mathematical expression. The existing CFP model can be treated as a 1D special case of the derived PDE system. However, this work only involves describing the overall dynamics, and no control laws is mentioned for the system. As for the space-discretization approximations of the underlying higher order CFP model, there already exist a few works on the second-order Markov chain model or the bilinear model. For example, [215, 216] deal with the Markov chain model, and it is observed that the more state bins, the more accurate for the model to capture the aggregate dynamics. Finally, MPC-based schemes are proposed for the second-order linear model in [108, 123], and for the bilinear model in [209].

2.2.4 Communication and computation burden reduction

Smart grid is changing the traditional power grid into a network-based distributed control system, realizing real-time system awareness, intelligent control, and self-healing. Thus, the communication and computation burden are crucially important, and it must be carefully considered for practical applications.

In the aforementioned literature in Section 2.2.2 and Section 2.2.3, it is supposed that the

control signals broadcast to the population periodically, which obviously generates great communication burdens. Moreover, a synchronized periodical data exchange is infeasible for nearly all the practical applications that involve communication networks spreading over a wide geographical region. Event-triggered control (ETC), which requires only to update the control signals when a certain triggering event occurs, can be exploited as an effective solution to alleviate the internet redundancy problem [72, 98, 139]. In the literature, threshold-based signals are one of the commonly used triggering conditions. Different types of threshold signals are available, including fixed threshold, relative threshold [186, 217], switching threshold [205], and dynamic threshold [52, 56, 160]. Among the aforementioned triggering mechanisms, dynamic threshold strategies have attracted much attention in recent years. Compared with static event-triggering schemes, auxiliary variables are additionally incorporated in the triggering threshold function, which can usually enlarge inter-event intervals and thus enable more flexible and effective resource utilization. Note that, to ensure the control performance, the closed-loop systems need to possess certain robust stability properties, in particular, they should be input-to-state stable (ISS) with respect to (w.r.t.) disturbances representing the effect of aperiodic sampling [56, 186]. Moreover, considering uncertainties in practical applications, a more realistic requirement is that the closed-loop system should be input-to-state practically stable (ISpS) w.r.t. the disturbances [62, 87]. It should be mentioned that the notion of ISS and its variations, including ISpS, play a vital role in robust control system design and analysis, allowing for characterizing the robust stability of a system w.r.t. disturbances induced by, e.g., external perturbations, modeling errors, and parametric uncertainties, as well as those introduced in control system implementations, such as measurement and actuation noises, sampling and quantization errors, and delays [138,181].

Real-time processing is another essential feature of smart grid. To guarantee a certain level of Quality of Service (QoS), TCL population control algorithms should not be time-consuming. However, a population with tens or hundreds of thousands of TCLs can be computational demanding [33, 38, 61, 82, 121, 135, 222]. Hence, low-complexity control laws that are insensitive to the population size should be well studied. Additionally, another method to reduce time cost is the use of only partially measured states. A higher response speed can be expected when the full state knowledge of the controlled system is not required. More importantly, only collecting partial information from the population can also significantly relieve the communication burden and simultaneously boost the privacy protections on the customers.

2.2.5 Concluding remarks

This chapter outlines the scope of the research problems of this thesis and presents a general review of related work in the literature. The effective operation and coordination of TCLs in a population is a challenging problem, and an accurate aggregate model is essential in capturing the evolution of the TCLs in ONs and OFFs states. In light of the review, PDE-based models provide spatial-temporal continuous descriptions on the distribution evolutions, capture subtle changes and dynamic behaviors of the population, and enable more in-depth analysis of the system responses. Many finite dimensional state space models can be treated as lumped counterparts of the PDE models by using "early-lumping" method. Some of them are only rough approximations of the underlying PDE model, while some useful information is either simplified or ignored. Therefore, the control strategies based on these lumped models might be not accurate and the stability results of the system cannot be guaranteed.

Some existing control algorithms derived from PDE models are reviewed in this part, highlighting aspects on which further exploration are still needed. Particularly, design of the system output function should account for both the ease of mathematical analysis and the clarity of physical interpretations while providing desired property for power control. Moreover, the control input, which is the change rate of the nominal temperature set-point, should not be too large, otherwise the aggregate power fluctuates fiercely and this might also cause uncomfortness to the customers. Thus, saturation functions should be introduced in the developed control strategies. Noting that the real-time information of the whole population is not available, as synchronized communication is impossible in a real-world scenario. Communication delays with various durations exist due to different communication technologies and geographical locations of the TCLs. Hence, decentralized control mode is a reasonable choice for the population. To reduce the communication burden, methods using partial measurements of the population or event-triggered control schemes can be considered. These motivations inspire the following research directions, which are further elaborated in the subsequent chapters.

CHAPTER 3 BASIC NOTATIONS, TOOLS, AND PRELIMINARIES

This chapter presents notions, tools, and mathematical preliminaries for controller design and stability analysis used in this thesis. Furthermore, the simulation environment is introduced and preliminary qualitative results are shown to illustrate the behavior of the considered problems.

3.1 Lyapunov stability theory

3.1.1 Lyapunov stability definitions

We first review some relevant notations and results on Lyapunov stability theory, refer to [92, 174, 189] for more details. Consider a time-varying system,

$$\dot{x} = f(t, x), \tag{3.1}$$

where $x \in \mathbb{D} \subset \mathbb{R}^n$ is the state variable, $f : \mathbb{R}_{\geq 0} \times \mathbb{D} \to \mathbb{R}^n$ is locally Lipschitz in x and piecewise continuous in t. Furthermore, assume that x_{eq} is the equilibrium point, i.e. $f(t, x_{\text{eq}}) \equiv 0$ for all $t \in [0, \infty)$.

Definition 3.1. ***Asymptotical stablility*** *The equilibrium x_{eq} is said to be Lyapunov stable at $t = t_0 \geq 0$ for the system* (3.1) *if*

$$\forall \varepsilon > 0, \exists \delta(\varepsilon, t_0) > 0, |x(t_0) - x_{eq}| < \delta \Rightarrow |x(t) - x_{eq}| < \varepsilon, \forall t \geq t_0.$$

It is uniformly Lyapunov stable if $\delta(\varepsilon, t_0)$ is independent of t_0, i.e.

$$\forall \varepsilon > 0, \exists \delta(\varepsilon) > 0, |x(t_0) - x_{eq}| < \delta \Rightarrow |x(t) - x_{eq}| < \varepsilon, \forall t \geq t_0.$$

It is attractive if

$$\exists c(t_0) > 0, \forall |x(t_0) - x_{eq}| < c(t_0) \Rightarrow \lim_{t \to +\infty} |x(t) - x_{eq}| = 0.$$

Or more precisely, $\exists c(t_0) > 0, \forall |x(t_0) - x_{eq}| < c(t_0)$, the following convergence result holds:

$$\forall \varepsilon > 0, \exists T(\varepsilon) > 0, \forall t \geq t_0 + T(\varepsilon), |x(t) - x_{eq}| < \varepsilon.$$

It is uniformly attractive if $c(t_0)$ is independent of t_0, i.e.

$$\exists c(t_0) > 0, \forall |x(t_0) - x_{eq}| < c \Rightarrow \lim_{t \to +\infty} |x(t) - x_{eq}| = 0.$$

It is asymptotically stable if it is both stable and attractive, i.e.

$$\forall \varepsilon, t_0 > 0, \exists \delta(\varepsilon, t_0) > 0, |x(t_0) - x_{eq}| < \delta \Rightarrow \lim_{t \to +\infty} |x(t) - x_{eq}| = 0.$$

Similarly, it is uniformly asymptotically stable if it is both uniformly stable and uniformly attractive,

$$\forall \varepsilon, t_0 > 0, \exists \delta > 0, |x(t_0) - x_{eq}| < \delta \Rightarrow \lim_{t \to +\infty} |x(t) - x_{eq}| = 0.$$

Remark 3.1. *Intuitively, an equilibrium is Lyapunov stable means that all solutions starting around the equilibrium stay in its neighborhood all the time. And the equilibrium is asymptotic stable means that all solutions starting near the equilibrium tend to it as $t \to \infty$.*

Note that the asymptotic stability (see Definition 3.1) does not quantify the rate of convergence. Hence, more specific definitions, such as exponential stability or finite-time stability, are required to be introduced.

Definition 3.2. ***Exponential stability*** *The equilibrium x_{eq} is exponentially stable if there exist constants $m, \alpha > 0$ and $\delta > 0$ such that for the system* (3.1)

$$\forall t \geq t_0, |x(t_0) - x_{eq}| \leq \delta \Rightarrow |x(t) - x_{eq}| < m e^{-\alpha(t - t_0)} |x(t_0) - x_{eq}|.$$

The largest constant α in the inequality is called the rate of convergence.

Comparison functions enable characterizing the stability properties of a dynamical system in a more natural and convenient manner. In the following, formal definitions of some commonly used comparison functions are introduced and then, an equivalent definition of Definition 3.1 is presented.

Definition 3.3. *A class $\mathcal{K}$ function is a function $\alpha : [0, a) \to \mathbb{R}_{\geq 0}, a > 0$ which is continuous, strictly increasing, and satisfies $\alpha(0) = 0$.*

Definition 3.4. *A class $\mathcal{K}_\infty$ function is a function $\alpha : \mathbb{R}_{\geq 0} \to \mathbb{R}_{\geq 0}$ which is continuous, strictly increasing, unbounded, and satisfies $\alpha(0) = 0$.*

Definition 3.5. *A class $\mathcal{L}$ function is a function $\alpha : \mathbb{R}_{\geq 0} \to \mathbb{R}_{\geq 0}$ which is continuous, strictly decreasing, and satisfies $\lim_{t\to\infty} \alpha(t) = 0$.*

Definition 3.6. *A class $\mathcal{KL}$ function is a continuous function $\beta : [0, a) \times \mathbb{R}_{\geq 0} \to \mathbb{R}_{\geq 0}$ which satisfies*

- *for each fixed s, $\beta(r, s)$ belongs to class $\mathcal{K}$;*
- *for each fixed r, $\beta(r, s)$ belongs to class $\mathcal{L}$.*

With the concepts of comparison functions, the stability properties of the system can be described in an equivalent manner as follows:

Lemma 3.1. *[189, Theorem 16.2] The equilibrium point x_{eq} is uniformly stable if and only if there exists a class $\mathcal{K}$ function α and a constant c, independent of t_0, such that for the system* (3.1)

$$|x(t)| < \alpha(|x(t_0)|), \forall t \geq t_0 \geq 0, \forall |x(t_0)| < c.$$

It is uniformly asymptotically stable if and only if there exists a class $\mathcal{KL}$ function α and a constant c, independent of t_0, such that

$$|x(t)| < \beta(|x(t_0)|, t - t_0), \forall t \geq t_0 \geq 0, \forall |x(t_0)| < c.$$

3.1.2 Finite time stability and ultimate boundedness

In the following, some Lyapunov theorems on time-varying systems are presented, and many of them can be found in the aforementioned textbooks [92, 174, 189].

Definition 3.7. ***Positive definite and positive semi-definite*** *A time-invariant function $W(x) : \mathbb{D} \to \mathbb{R}^n$ where $\mathbb{D} \subset \mathbb{R}^n$ is said to be positive definite if $W(0) = 0$, and $W(x) > 0, \forall x \neq 0$. It is radially unbounded if $W(x) \to \infty$ when $x \to \infty$. For a time-varying function $V(t, x)$, it is positive semi-definite if $V(t, x) \geq 0$. Moreover, it is positive definite if $V(t, x) \geq W_1(x)$ for some positive definite function $W_1(x)$, and it is radially unbounded is $W_1(x)$ is radially unbounded. It is decrescent if $V(t, x) \leq W_2(x)$ for some positive definite function $W_2(x)$.*

Negative definite and negative semi-definite functions can be defined in a similar manner; therefore, their definitions are omitted.

Theorem 3.1. *[92, Theorem 4.8] Consider the time-varying system $\dot{x} = f(t, x)$ in* (3.1)*. Let $V : \mathbb{R}_{\geq 0} \times \mathbb{D} \to \mathbb{R}$ be a continuously differentiable function (denoted as C^1 function hereafter). Suppose that*

$$V(t, x) \geq W_1(x),$$

and

$$\frac{\partial}{\partial t}V + \frac{\partial}{\partial x}f(t,x) \leq 0, \forall t \geq 0, \forall x \in \mathbb{D},$$

where $W_1(x)$ is a continuous positive definite function, then the origin is stable. If furthermore, $V(t,x)$ is decrescent with respect to a continuous positive definite function $W_2(x)$, i.e., $V(t,x) \leq W_2(x)$, then the origin is uniformly stable. Moreover, if there exists a continuous positive definite function $W_3(x)$, such that

$$\frac{\partial}{\partial t}V + \frac{\partial}{\partial x}f(t,x) \leq -W_3(x), \forall t \geq 0, \forall x \in \mathbb{D},$$

then, the origin is uniformly asymptotically stable. Replacing $W_i(x), i = 1,2,3$ with $k_i\|x\|^a$, where $k_i, i = 1,2,3$ and a are constants, the conditions for $V(t,x)$ become

$$k_1\|x\|^a \leq V(t,x) \leq k_2\|x\|^a,$$

and

$$\frac{\partial}{\partial t}V + \frac{\partial}{\partial x}f(t,x) \leq -k_3\|x\|^a, \forall t \geq 0, \forall x \in \mathbb{D},$$

then the origin is exponentially stable.

Definition 3.8. ***Finite-time stability*** *[65, Definition 3.1] Suppose $x = 0$ is an equilibrium of the system (3.1), i.e. $f(t,0) = 0$, $\forall t \geq 0$. The origin is said to be finite-time stable if it is Lyapunov stable and there exists some constant $T \in \mathbb{R}_{\geq 0}$ such that $\lim_{t\to T} x(t) = 0$. With the $\varepsilon - \delta$ language, it is:*

$$\forall \varepsilon, t_0 > 0, \exists \delta > 0, |x(t_0)| < \delta \Rightarrow \lim_{t\to T}|x(t)| = 0.$$

The function $T(x(t_0)) := \inf\{T : x(t) \equiv 0, \forall t \geq T\}$ is called the settling time function. The system (3.1) is uniformly finite-time stable if it is uniformly Lyapunov stable and there exists $T = T(x(t_0)) < \infty$ such that $\lim_{t\to T} x(t) = 0$.

Figure 3.1 shows a schematic graph on the differences between asymptotic stability, exponential stability, and finite-time stability. From a practical viewpoint, faster convergence speed is always perfered. In many dynamical systems, the settling time is commonly used as a performance specification.

Definition 3.9. *The solutions of the system $\dot{x} = f(t,x)$ are said to be uniformly bounded if $\exists c > 0$, independent of $t_0 \geq 0$, such that*

$$\forall a \in (0,c), \exists \alpha = f(a) > 0, \|x(t_0)\| \leq a \Rightarrow \|x(t)\| \leq \alpha, \forall t \geq t_0.$$

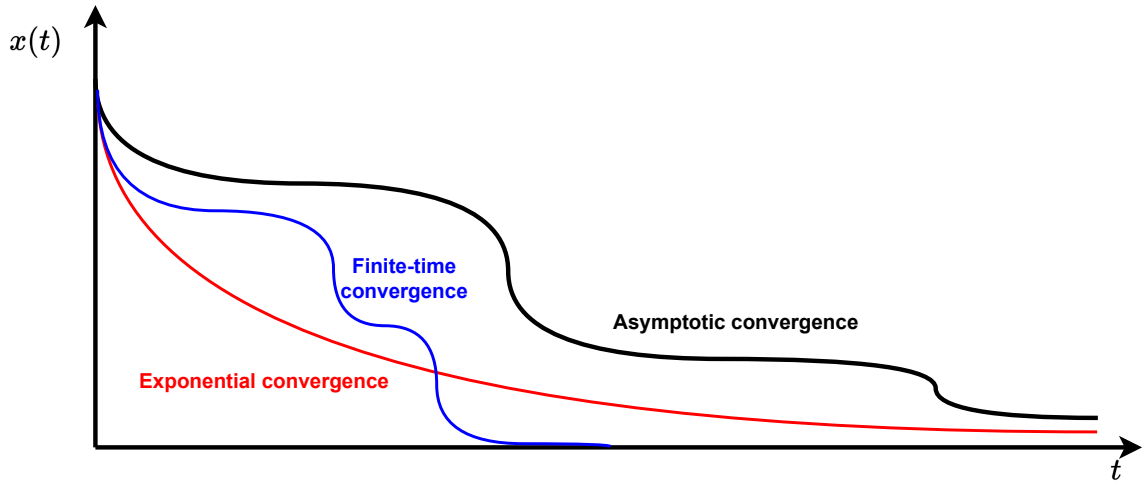

Figure 3.1 An illustration of different convergence patterns.

It is said to be uniformly ultimately bounded if $\exists b, c > 0$, *independent of* t_0, *such that*

$$\forall a \in (0, c), \exists T = T(a, b) > 0, \|x(t_0)\| \leq a \Rightarrow \|x(t)\| \leq b, \forall t \geq t_0 + T.$$

The concept of ultimate boundedness is useful in describing stability properties of perturbed systems. Consider a perturbed system

$$\dot{x} = f(t, x) + g(t, x), \tag{3.2}$$

where $x \in \mathbb{D} \subset \mathbb{R}^n$ is the state variable, $f : \mathbb{R}_{\geq 0} \times \mathbb{D} \to \mathbb{R}^n$ and $g : \mathbb{R}_{\geq 0} \times \mathbb{D} \to \mathbb{R}^n$ are locally Lipschitz in x and piecewise continuous in t. This system can be treated as a deviation of the nominal system (3.1). When the nominal system is exponentially stable and the perturbation term $g(t, x)$ is bounded, it can be shown that the solutions of the perturbed system is robust to the disturbances, see Theorem 3.2 for this property.

Theorem 3.2. *[92, Lemma 9.2] Suppose* $x = 0$ *is an exponentially stable point of the nominal system* (3.1), *and* $V(t, x)$ *is an associated Lyapunov function that satisfies*

$$c_1\|x\|^2 \leq V(t, x) \leq c_2\|x\|^2,$$

$$\frac{\partial}{\partial t}V + \frac{\partial}{\partial x}f(t, x) \leq -c_3\|x\|^2,$$

$$\|\frac{\partial}{\partial x}V\| \leq -c_3\|x\|^2, \forall t \geq 0, \forall x \in \mathbb{D},$$

where c_1, c_2, c_3, c_4 *are some positive constants, and* $\mathbb{D} := \{x \in \mathbb{R}^n | \|x\| < r\}$. *Furthermore, suppose that the perturbation term in system* (3.2) *is bounded, i.e.*

$$\|g(t,x)\| \leq \delta < \frac{c_3}{c_4}\sqrt{\frac{c_1}{c_2}}\theta r,$$

where $0 < \theta < 1$ *is a constant. Then, for all* $\|x(t_0)\| < \sqrt{\frac{c_1}{c_2}}r$, *the solution of the perturbed system* (3.2) *satisfies*

$$\|x(t)\| \leq ke^{-\gamma(t-t_0)}\|x(t_0)\|, \forall t_0 \leq t < t_0 + T$$

and

$$\|x(t)\| \leq b, \forall t \geq t_0 + T$$

for some finite time T, *where*

$$k = \sqrt{\frac{c_2}{c_1}}, \gamma = \frac{(1-\theta)c_3}{2c_2}, b = \frac{c_4}{c_3}\sqrt{\frac{c_2}{c_1}}\frac{\delta}{\theta}.$$

3.1.3 Input-to-state stability and generalizations

For a perturbed system under the form (3.2), if $g(t,x)$ depends only on t, then the perturbation term $g(t)$ can be visualized as a generalized input term, and then the system dynamics can be characterized by the notation of input-to-state stability. Consider a time-invariant system

$$\dot{x} = f(x,u), \tag{3.3}$$

where $x \in \mathbb{R}^n$ is the state variable, $u : \mathbb{R}_{\geq 0} \to \mathbb{R}^m$ is a bounded, piecewise continuous control input, and $f : \mathbb{R}^n \times \mathbb{R}^m \to \mathbb{R}^n$ is locally Lipschitz in x and u.

Definition 3.10. *The system* (3.3) *is input-to-state stable if there exists* $\beta \in \mathcal{KL}$ *and* $\gamma \in \mathcal{K}_\infty$ *such that for all* $x_0 \in \mathbb{R}^n$, *all admissible input* $u(t)$, *and all* $t \geq 0$,

$$|x(t)| \leq \beta(|x_0|, t) + \gamma(\|u\|_\infty). \tag{3.4}$$

Note that $\forall t \geq 0$, the solution $x(t)$ only depends on $u(s), 0 \leq s \leq t$. Thus, the second term in (3.4) is equivalent to

$$\gamma(\sup_{s\in[0,t]} \|u(s)\|).$$

In the following, we will not distinguish between these two formats. Furthermore, it is clear from (3.4) that the solution $x(t)$ is ultimately bounded by a class $\mathcal{K}$ function of $\|u\|_\infty$. When

$\|u\|_\infty$ is sufficiently small in magnitude, $x(t)$ converges asymptotically to the origin. The ISS-Lyapunov function is an important tool for the ISS assessment as described in the following theorems.

Definition 3.11. *[189, Definition 19.2] A continuously differentiable function $V : \mathbb{R}_{\geq 0} \times \mathbb{R}^n \to \mathbb{R}$ is called an ISS-Lyapunov function if there exist $\psi_1, \psi_2 \in \mathcal{K}_\infty, \chi \in \mathcal{K}$ and a continuous positive definite function W_3, such that*

$$\psi_1(\|x\|) \leq V(x) \leq \psi_2(x), \forall x \in R^n,$$

$$\|x\| \geq \chi(\|u\|) \Rightarrow \frac{\partial}{\partial x} V \cdot f(x,u) \leq -W_3(\|x\|),$$

where the function χ is called the Lyapunov gain.

Theorem 3.3. *[92, Theorem 3.1] A system $\dot{x} = f(t,x,u)$ is ISS if it admits a smooth ISS-Lyapunov function.*

For an autonomous system $\dot{x} = f(x,u)$, the condition in Theorem 3.3 is both necessary and sufficient.

The ISS concept bridges the gap between state-space methods and input-output methods, and it is widely used within the control community. It has a lot of generalizations, such as integral ISS, local ISS, incremental ISS, input-to-state dynamical stability (ISDS), input-to-state practical stability (ISpS), input-to-output stability (IOS), etc. In the following, notions of input-to-state practical stability (ISpS) and finite-time input-to-state stability are introduced.

Definition 3.12. *System* (3.3) *is input-to-state practically stable if there exists $\beta \in \mathcal{KL}$ and $\gamma \in \mathcal{K}_\infty$ and $d \in \mathbb{R}_{\geq 0}$ such that for all $x_0 \in \mathbb{R}^n$, all admissible input $u(t)$, and all $t \geq 0$, it holds*

$$|x(t)| \leq \beta(\|x_0\|, t) + \gamma(\|u\|_\infty) + d. \tag{3.5}$$

Note that in (3.5), the definition degenerates to the case of ISS if $d = 0$. Moreover, similar to the case in ISS, an ISpS-Lyapunov function can be parallelly defined.

Definition 3.13. *A continuously differentiable function $V : \mathbb{R}_{\geq 0} \times \mathbb{R}^n \to \mathbb{R}$ is called an ISS-Lyapunov function if there exist $\psi_1, \psi_2 \in \mathcal{K}_\infty, \chi \in \mathcal{K}$, a constant $c \in \mathbb{R}_{\geq 0}$, and a continuous positive definite function W_3, such that*

$$\begin{aligned} \psi_1(\|x\|) \leq V(x) \leq & \psi_2(x), \forall x \in R^n, \\ \|x\| \geq \max\{\chi(\|u\|), c\} \Rightarrow & \frac{\partial}{\partial x} V \cdot f(x,u) \leq -W_3(\|x\|). \end{aligned} \tag{3.6}$$

Note that $V(x)$ satisfying (3.6) with $c = 0$ is an ISS-Lyapunov function for system (3.3). Similarly, there exists an important relationship between the ISpS property and the ISpS-Lyapunov function, as described in Theorem 3.4.

Theorem 3.4. *[87, Proposition 2.1] System* (3.3) *is ISpS if and only if it admits an ISpS-Lyapunov function.*

Finite-time stability ensures that the controlled states can reach the equilibrium in finite time and exhibits strong robustness to uncertainties. Taking account of both ISS and finite-time stability properties, a new concept, finite-time input-to-state stability (FTISS), provides a refined characterization of the dynamical system.

Definition 3.14. *System* (3.3) *is finite-time input-to-state stable (with respect to $u(t)$) if for all $t_0 \geq 0$ and $x_0 = x(t_0)$, there exist $\gamma \in \mathcal{K}$, $\beta \in \mathcal{KL}$ such that*

$$\|x(t)\| \leq \beta(\|x_0\|, t - t_0) + \gamma(\|u\|_\infty),$$

and there exists a time constant $T = T(x_0)$ such that

$$\beta(\|x_0\|, t) \equiv 0, \forall t \geq t_0 + T.$$

A Lyapunov-like condition for FTISS is shown in Theorem 3.5.

Theorem 3.5. *[110, Lemma 1] Suppose $x = 0$ is an equilibrium of the dynamic system $\dot{x} = f(x, u)$. If there exists a Lyapunov function $V(x)$, three class $\mathcal{K}_\infty$ functions $\psi_1(x)$, $\psi_2(x)$ and $\psi_3(x)$, and two constants $\lambda > 0$ and $0 < \theta < 1$, such that $\forall x_0 \in \mathbb{R}^n$, all admissible input $u(t)$,*

$$\psi_1(x) \leq V(x) \leq \psi_2(x),$$

$$\dot{V}(x) \leq -2\lambda V^\theta(x) + \psi_3(\|u\|_\infty),$$

hold, then the closed-loop system is FTISS. Furthermore, the settling time is upper bounded by

$$T \leq \frac{V^{1-\theta}(\|x_0\|, t_0)}{\lambda(1-\theta)} + t_0.$$

Similar conclusions can also be drawn for input-to-state practically stable systems, refer to [231] for details.

3.2 Linear Active Disturbance Rejection Control

The active disturbance rejection control (ADRC) method, first proposed by Han [67], has attracted considerable attention in recent years. It is a practical adpative control method, and has been applied successully in a large variety of industrial fields, refer to [48, 100, 203, 207, 211, 226]. It consists mainly of three parts: a tracking differentiator (TD), an extended state observer (ESO), and an ESO-based feedback law. The TD focuses on the the reference signals, ensuring a smooth transition process while mitigating the noise amplification problem when using the conventional PID controller. The ESO is used to estimate the "total disturbance" in real time, including both unknown part of the system dynamics and uncertain external perturbations. With the information contained in the ESO, the feedback law neutralizes the negative effects of disturbances in real time, and transforms the closed-loop system into a nominal disturbance-free process. Linear ADRC (LADRC) is developped on the basis of ADRC method, where linear ESO and linear state feedback law are used. Compared with ADRC, LADRC uses less parameters, making the controller tuning process much simpler and easier to be deployed in practice. For more details on the parameter tuning process, see, e.g., [40, 70], and on the algorithm implementations, refere to [73, 229] etc.. With appropriately chosen hyperparameters, the LADRC algorithm provides a solution with disturbance rejection capabilities and often achieves satisfactory control performance.

In this work, the tracking error dynamics is a first-order model. Hence, for simplicity, the main emphasis is placed on the LADRC method for first-order plants.

Consider a first-order single-input-single-output (SISO) system

$$\dot{y}(t) = b_0 v(t) + f(t), \tag{3.7}$$

where $f(t)$ is the total disturbance, $v(t)$is the control input, $y(t)$ is the system output, b_0 is the known or unknown critical gain of the system. The total disturbance function $f(t)$ consists of both the unmeasured internal dynamics and the unexpected external disturbances, and its expression does not need to be explicitely known. Let $x_1(t) = y(t)$ be the system power output, $x_2(t) = f(t)$ be the extended state, and supppose that $f(t)$ is differentiable. Then, the SISO dynamics (3.7) can be rewritten as:

$$\begin{aligned} \dot{x} &= Ax + Bv(t) + E\dot{f}(t), \\ y &= Cx, \end{aligned} \tag{3.8}$$

where

$$x = \begin{bmatrix} x_1 \\ x_2 \end{bmatrix},\ A = \begin{bmatrix} 0 & 1 \\ 0 & 0 \end{bmatrix},\ B = \begin{bmatrix} b_0 \\ 0 \end{bmatrix},\ E = \begin{bmatrix} 0 \\ 1 \end{bmatrix},\ C = \begin{bmatrix} 1 & 0 \end{bmatrix}.$$

It is straightforward that the system (3.8) is observable. Thus the Luenberger observer is of the form:

$$\begin{aligned} \dot{\hat{x}} &= A\hat{x} + Bv(t) + L(y - \hat{y}), \\ \hat{y} &= C\hat{x}. \end{aligned} \tag{3.9}$$

where $\hat{x} = [\hat{x}_1, \hat{x}_2]^\top$ are the estimated states, and $L = [\beta_1, \beta_2]^\top$ are the observer gains. Let $e_i = x_i - \hat{x}_i, i = 1, 2$ be the state estimation errors. It follows by (3.8) and (3.9) that

$$\dot{e}(t) = (A - LC)e + E\dot{f}(t). \tag{3.10}$$

Note that

$$A - LC = \begin{bmatrix} -\beta_1 & 1 \\ -\beta_2 & 0 \end{bmatrix}.$$

and its characteristic equation is $s^2 + \beta_1 s + \beta_2 = 0$. Let

$$\beta_1 = 2\omega_o, \beta_2 = (\omega_o)^2,$$

where $\omega_o > 0$ is the observer bandwidth. Then $A - LC$ is exponentially stable. Furthermore, when $\dot{f}(t)$, the derivative of the total disturbance, is bounded, the observation errors become reasonably small within a finite time. Define the control input as:

$$v(t) = \frac{1}{b_0}(-k\hat{x}_1 - \hat{x}_2), \tag{3.11}$$

where k is the controller gain. Note that the controller gain and the observer bandwidth can be designed seperately according to the separation principle for linear systems. It follows that

$$\begin{aligned} \dot{x}_1 &= b_0 v(t) + x_2 \\ &= (-k\hat{x}_1 - \hat{x}_2) + x_2 \\ &= -kx_1 + k(x_1 - \hat{x}_1) + (x_2 - \hat{x}_2) \\ &= -kx_1 + ke_1 + e_2. \end{aligned}$$

Therefore, the convergence rate of $x_1(t)$ is determined by k, the controller gain, and a practical stability for the tracking can be achieved when the observation errors are constrained to a

small region. The tracking error of the extended state observer is not asymptotically stable. However, theoretical result shows that it is bounded when either the total disturbance or its derivative is bounded, see [51]. When the state feedback is also convergent, the closed-loop system is bounded-input, bounded-output (BIBO) stable, as described in Theorem 3.6.

Theorem 3.6. *For the SISO system* (3.8)*, the closed-loop system with the LADRC is BIBO stable if the state feedback law and the LESO are stable.*

The proof of Theorem 3.6 can also be generalized to higher-order sytems. The authors of [57, 208] present more elaborated stability analysis for these systems with generalized ESO.

3.3 Numerical estimations of function values

Consider a continuous function $f(x)$ whose analytical expression is unknown or very hard to be acquired. However, for any point inside the interval of interest, the integral results for some small narrow intervals are observable. The objective is to obtain a reliable estimation of the function value around a particular point x_0. In this work, three basic steps are used to obtain a relatively robust estimation of function values. First, a few small intervals with different sizes are seleted. Then, an array of function values are acquired by treating the function as contant in each interval. Finally, Huber's M-estimator is used to improve the estimation accuracy. A schematic graph is shown in Fig. 3.2 for the procedures. In the following, the method to obtain one estimation is explained, and Huber's M-estimation method is also briefly introduced.

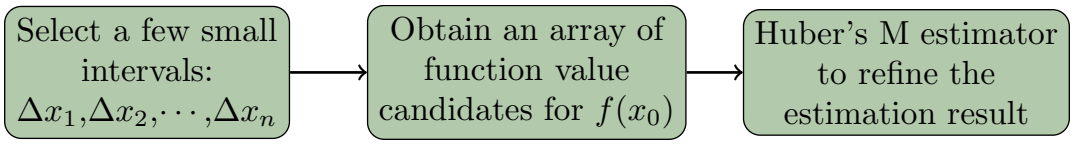

Figure 3.2 Basic steps for obtaining function value estimation.

3.3.1 Mid-point rule for one estimation

Let x_0 be the middle point of a small interval, and Δx be the length. If Δx is sufficiently small, and $f(x)$ changes relatively slowly in it, it is reasonable to treat it as constant. Let C_Δ denote the integral of $f(x)$ over the interval, i.e.

$$\int_{x_0-\frac{\Delta x}{2}}^{x_0+\frac{\Delta x}{2}} f(x)\,\mathrm{d}x = C_\Delta.$$

Because,

$$\int_{x_0-\frac{\Delta x}{2}}^{x_0+\frac{\Delta x}{2}} f(x)\,\mathrm{d}x \approx f(x_0)\Delta x,$$

it follows that

$$f(x_0) \approx \frac{C_\Delta}{\Delta x}.$$

This method is only a rough estimation, hence sometimes the error may be quite large. To improve the accurary, a straightforward method is to esimate multiple times with different intervals and to use the mean value as the final result. With a more elaborated manner, robust estimators, such as M estimators, S estimators, etc., can be introduced to get the final estimation. In this work, Huber's M estimator is used and the relevant background is briefly recalled in the next subsection.

3.3.2 Huber's M estimator

In statistics, Ordinary Least Squares (OLS) is a popular method for estimating unknown parameters in a regression model. It minimizes the squared sum of the differences between the observed values and the estimated output values. When the errors are normally distributed, the OLS estimator is also the maximum likelihood estimator (MLE). However, the OLS method is highly sensitive to outliers, thus leading to biased estimations. To overcome this issue, robust estimators are proposed [125, 128, 201], and many of them, for example M-estimators, S-estimators, MM estimators, least median square, etc., are frequently used in the literature.

The M-estimators are one type of the robust measures of location, where M stands for "maximum likelihood-type." In the robust M-estimators, a symmetric loss function of the residuals ρ is used, and the objective function is shown as follows:

$$\text{Minimize } \rho(r_i).$$

The loss function is appropriately chosen such that the impact of outliers is significantly reduced. Some common candidates for ρ are Huber's loss function, Hampel's loss function, Andrew's wave function, Tukey's Biweight function, etc., see [2, 41, 166]. The Huber's loss function is defined as:

$$H(x) := \begin{cases} \frac{1}{2}x^2, & |x| \le K, \\ K|x| - \frac{1}{2}K^2, & |x| > K, \end{cases} \tag{3.12}$$

where K is the bending constant to be tuned. For example, a 95% confidence interval of the estimation is obtaned when $K = 1.345$ and the residuals are normally distributed. Note that

Huber's loss function is quadratic for small values, but linear for large values. This character makes it quite resilent to outliers. The derivative of the loss function, also known as the distance function in some literature, is:

$$\Psi(x) = \begin{cases} x, & |x| \leq K, \\ K\text{sgn}(x), & |x| > K, \end{cases} \tag{3.13}$$

where $\text{sgn}(x)$ is the sign function. The weight function is defined as the fraction between $\Psi(x)$ and x:

$$W(x) := \begin{cases} 1, & |x| \leq K, \\ \dfrac{K}{|x|}, & |x| > K. \end{cases} \tag{3.14}$$

Suppose there exists a list of data points, $x_1, x_2, \ldots, x_n$,$n \in \mathbb{N}$, then Huber's M-estimator $x^\star$ is the weighted average of all the residuals:

$$x^\star := \frac{\sum_{i=0}^{n} w_i x_i}{\sum_{i=0}^{n} w_i}, \tag{3.15}$$

where $w_i = W(x_i - x^\star)$ is the weight for the corresponding data point.

The mathematical expression in (3.15) is in implicit form, as the weight w_i depends on the final M-estimator $x^\star$. Iteratively reweighted least squares (IRLS) algorithm can be applied to get a reliable estimation. The iterative formula is written as:

$$x_{k+1} = \frac{\sum_{i=0}^{n} W(x_i - x_k) x_i}{\sum_{i=0}^{n} W(x_i - x_k)}, k = 0, 1, \ldots. \tag{3.16}$$

The pseudocode in Algorithm 1 shows the basic steps for the iterative process.

Huber's M-estimator is a fairly simple strategy for estimating values. It is resistant to outliers, and the iterative algorithm is very easy to implement. However, the bending constant needs to be carefully chosen, and the maximum iteration of numbers and the convergence tolerance bound should also be reasonable values. In this work, the hyperparameters are empiracally determined, and more advanced estimation methods should be further explored.

Algorithm 1 Iteratively reweighted least squares for Huber's M-estimator

Input the dataset $x_1, x_2, \ldots, x_n$;
Initialize the relative tolerance ε, the maximum number of iterations $MaxIt$, the default threshold value $K = 1.345$;
Set the initial estimator θ_0 as the sample median;
$\theta_1 = \theta_0$;
for `k in 1:1:MaxIt` **do**
    Compute the residuals of the dataset;
    for `idx in 1:1:n` **do**
        if residuals[idx] == 0 **then**
            residuals[idx] = ε^3;
        end if
    end for
    Compute the weights for the dataset with (3.14);
    Compute θ_1 with (3.16) for the new weighted estimation;
    if $|\theta_1 - \theta_0| < \varepsilon$ **then**
        Break;
    end if
    $\theta_0 = \theta_1$;
end for
Output θ_1;

3.4 Numerical analysis of the aggregate dynamics

In this section, we present a numerical simulation study of a population of 1,000 ACs to evaluate the dynamics of the population.

3.4.1 Simulation setups

Table 3.1 lists some parameters and their default values used in the simulation. The thermal capacitances of the TCLs in the population follow the log-normal distribution with a mean value of 2 kWh/°C and a standard deviation of 0.2 kWh/°C. The thermal resistances of the TCLs also follow the log-normal distribution with a mean value of 0.5 °C/kW and a standard deviation of 0.2 °C/kW. The rated thermal powers are fixed as 14kW and the Coefficient of Performance (COP) is set to be 2.5 for all ACs. These values are similar to those listed in [24] and should be properly adjusted based on practical applications.

3.4.2 Step response of the aggregate dynamics

A set-point step response on the aggregate dynamics provides an intuitive understanding on the stability of a system. It provides information on how the system behaves when a step

Table 3.1 Simulation parameters and default values

Parameter	Description [unit]	Value
R	Equivalent thermal resistance[°C/kW]	LogN$(0.5, 0.4)$
C	Equivalent thermal capacitance[kW/°C]	LogN$(2, 2)$
P	Thermal power[kW]	14
η	Coefficient of Performance (COP)	2.5
$x_{\text{sp}}(0)$	Initial temperature set point[°C]	20
δ	Thermostat deadband width[°C]	0.5
p_f	Probability of forced switchings per hour	3
t_l	Lockout time of each unit [min]	5
t_d	Communication delays [sec]	LogN$(1, 0.2)$
Δt	Resolution of the simulator [sec]	30

change on the set-point is applied.

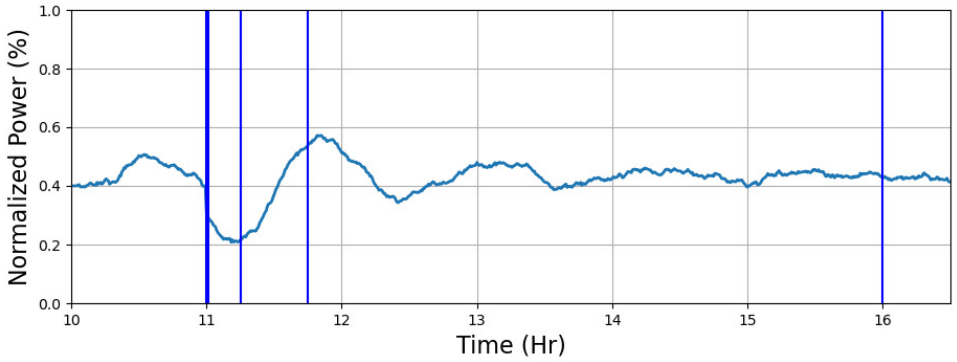

Figure 3.3 Aggregate power curve under sudden set-point change.

Figure 3.3 shows the aggregate power curve under approximate step change at 11:00am, where the aggregate power is normalized between 0 and 1 for better illustration. It is clear that there is a sudden power drop at 11:00am when a sudden set-point increase of 0.1 °C is introduced. The steady state aggregate power is before the set-point change is around 0.4, which means that there are around 40% percent of the ACs are in "ON" state. This steady value is determined by detailed population parameters. After the step stimulating input, the system presents more fierce oscillations in the next 1.5 hours before returning to steady state again.

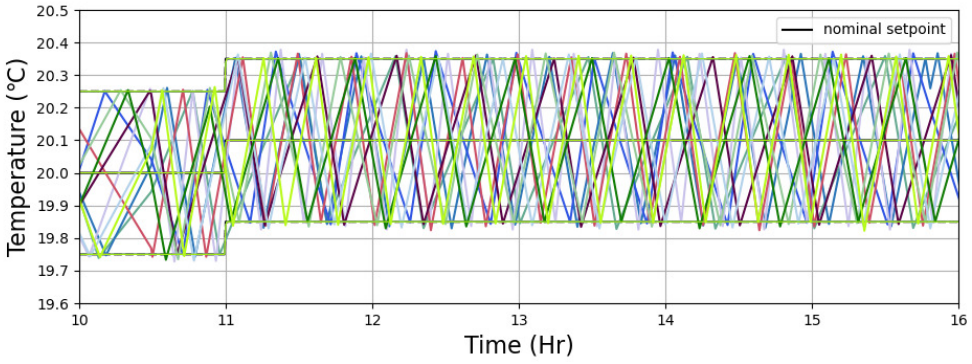

Figure 3.4 Temperature trajectories of the first 10 ACs.

Figure 3.4 shows the impact of step change on the population individuals, where the temperature trajectories of the firtst 10 ACs in the population are given. A nominal set-point change, which increases from 20 °C to 20.1 °C, is clearly seen at 11:00am on the image. Here, we call it "nominal" as the population is controlled in a decentralized manner, and each AC unit should determine its own set-point temperature after receiving the "nominal" set-point variation rate. The temperatures are increasing and decreasing with different velocities reflects that the population is heterogeneous. And the unnoraml temperatures outside the deadband maybe caused by locked-out mechanism in the population.

There are five particular time points to observe in Fig. 3.3, respectively, 11:00, 11:01, 11:25, 11:45 and 16:00. They are the time just before the set-point change, 1 minute after the set-point change, the approximate power valley moment, the approximate power peak moment and the new steady power moment after the step change. Five verticle lines are drawn on the graph to indicate their position. Figure 3.5a and 3.5b show the ON and OFF distributions at $t = 11:00^{-}$. Both of the histograms are almost uniformly distributed inside the deadband centering around 20 °C.

Figure 3.6a and 3.6b are the distributions at 11:01. The sudden set-point increasing behavior, which moves the nominal deadband a bit to the right, largely changes the landscape of the histograms. The AC units in "ON" states get a rapid reduction on its left side, while on the contrary, the AC units in "OFF" states rocket up on its left side. At this moment, the nominal center of the distributions is 20.1 °C. However, it is obvious that the two distributions are a bit left-skewed when using 20.1 °C as the center line. This means that the set-point change is a bit too sudden, and the system still needs a bit more time to settle down around the new nominal center.

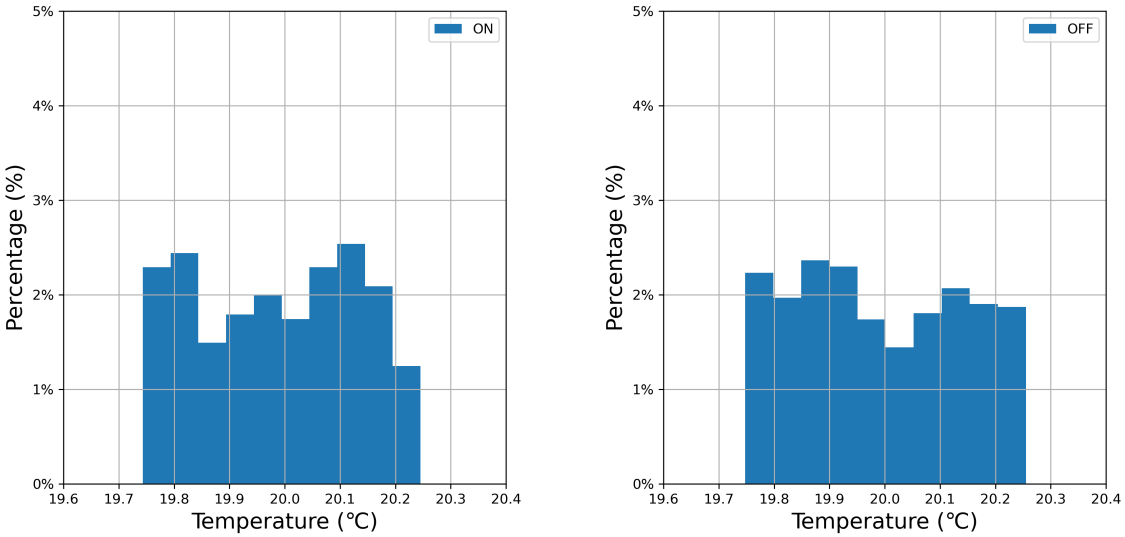

(a) (b)

Figure 3.5 $t = 11:00^{-}$ (a) ONs distribution; (b) OFFs distribution.

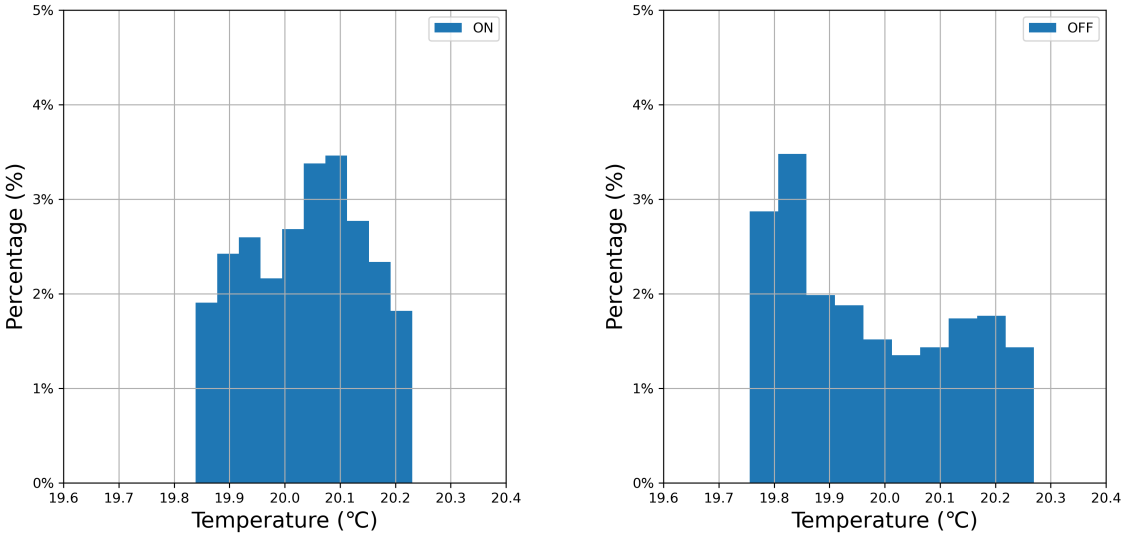

(a) (b)

Figure 3.6 $t = 11:01$ (a) ONs distribution; (b) OFFs distribution.

Figure 3.7a and 3.7b are the distributions at 11:25. It takes about 25 minutes for the aggregate power to reach the aggregate power valley. These two distributions are all centered around 20.1 °C. However, note that the ACs are not uniformly distributed, especially for those in "ON" states (see the image on the left side). This means that the system is still not in steady state, and more oscillations of the distributions are predictable.

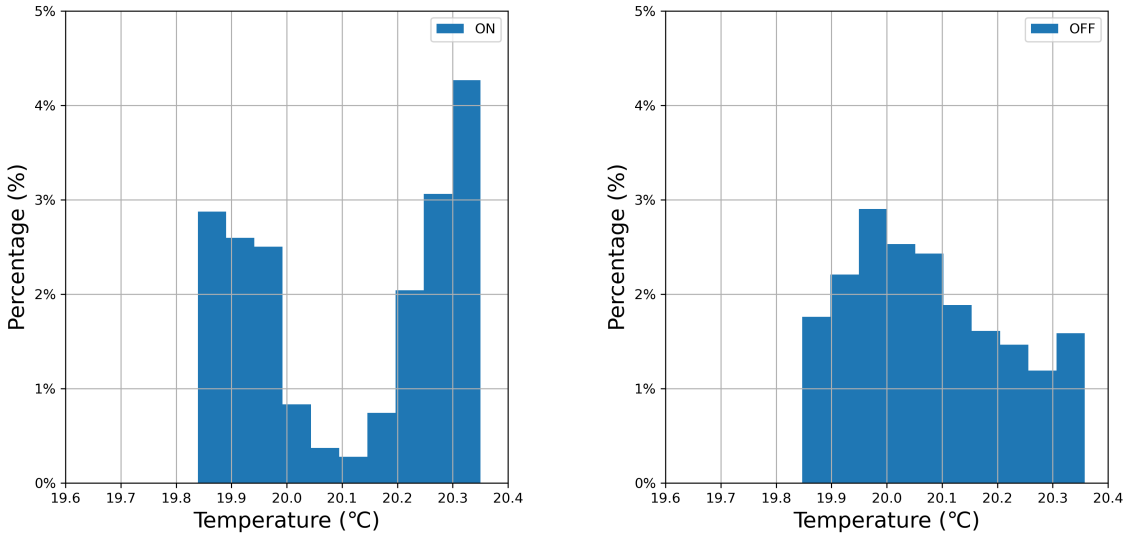

(a) (b)

Figure 3.7 t = 11:25 (a) ONs distribution; (b) OFFs distribution.

Figure 3.8a and 3.8b are histograms for almost the power peak moment. Compared with Fig. 3.7a, there are more ACs in "ON" state in Fig. 3.8a, thus, the aggregate power is larger. On the other hand, similar as those at 11:25, the histograms are also not uniformly distributed. This suggests that future fluctuations are to be expected.

Figure 3.9a and 3.9b present histograms in the new steady state. Both of the distributions are centering around 20.1 °C, and they become almost uniform distributed again.

The simulation result shows that sudden changes on the set-point temperature cause large oscillations on the system. In fact, the larger the set-point changes, the more fierce the oscillations are, as shown in Fig. 3.10. Thus, large instant changes should be carefully avoided and the set-point variation rate should be constraint when designing a controller.

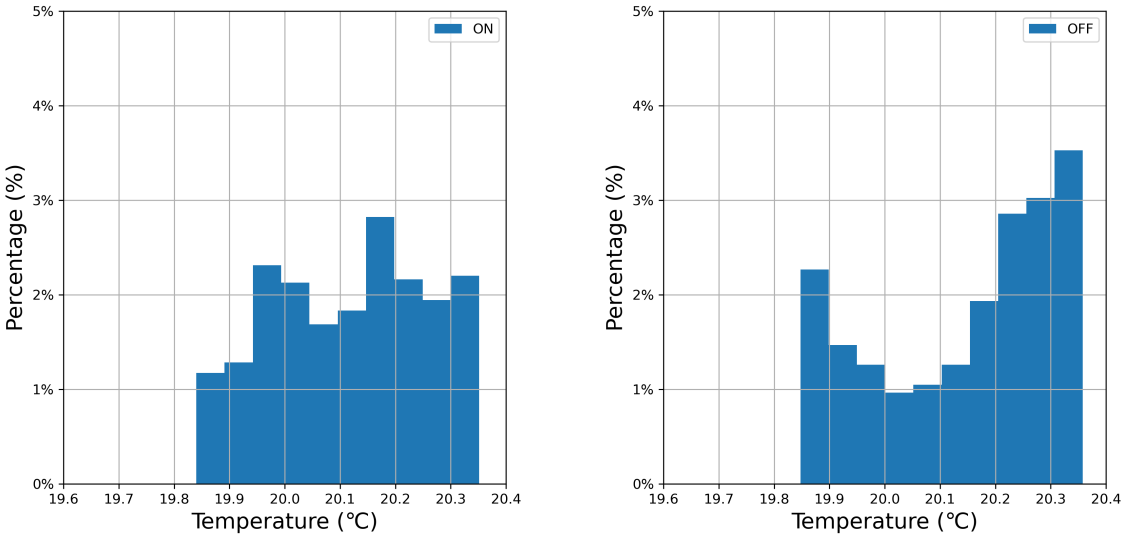

(a) (b)

Figure 3.8 t = 11:45 (a) ONs distribution; (b) OFFs distribution.

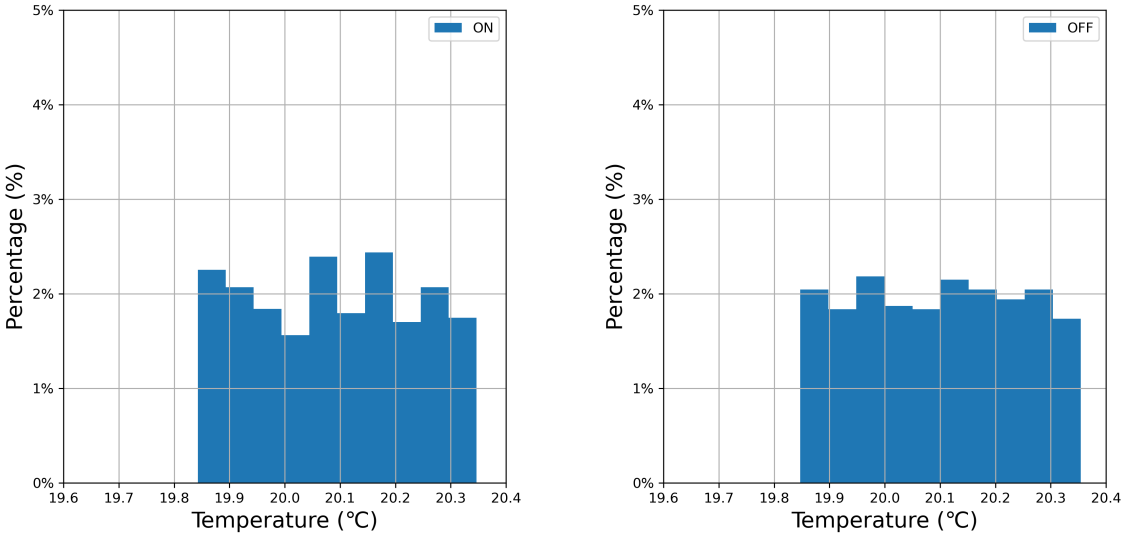

(a) (b)

Figure 3.9 t = 16:00 (a) ONs distribution; (b) OFFs distribution.

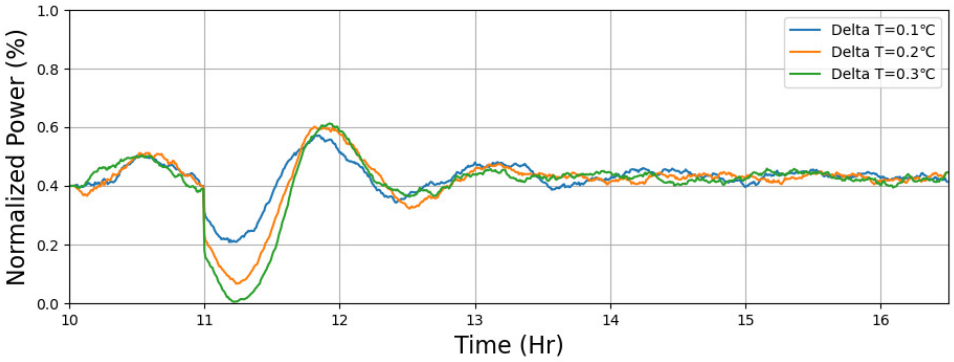

Figure 3.10 The impact of different set-point offset.

CHAPTER 4 ARTICLE 1: POWER TRACKING CONTROL OF HETEROGENEOUS POPULATIONS OF THERMOSTATICALLY CONTROLLED LOADS WITH PARTIALLY MEASURED STATES

Zhenhe Zhang, Jun Zheng, Guchuan Zhu
Published in: IEEE Access
Publication date: April 22, 2024

Abstract

This paper presents a new aggregate power tracking control scheme for populations of thermostatically controlled loads (TCLs). The control design is performed in the framework of partial differential equations (PDEs) based on a late-lumping procedure without truncating the infinite-dimensional model describing the dynamics of the TCL population. An input-output linearization control scheme, which is independent of system parameters and uses only partial state measurement, is derived, and a sliding mode-like control is applied to achieve finite-time input-to-state stability for tracking error dynamics. Such a control strategy can ensure robust performance in the presence of modeling uncertainties, while considerably reducing the communication burden in large-scale distributed systems similar to that considered in the present work. A rigorous analysis of the closed-loop stability of the underlying PDE system was conducted, which guarantees the validity of the developed control scheme. Simulation studies were performed while considering two TCL populations with a significant difference in their size, and the results show that the developed control scheme performs well in both cases, thereby confirming the effectiveness of the proposed solution.

keywords Aggregate power tracking control, finite-time input-to-state stability, input-output linearization, partial differential equations, thermostatically controlled loads.

4.1 Introduction

In the context of today's smart grids, it is widely recognized that demand response (DR) programs have great potentials in dealing with ongoing demands, while enhancing the energy efficiency and resilience of the power grid [53, 66, 173, 230]. As a promising demand-response enabled resource, thermostatically controlled loads (TCLs), such as air conditioners (ACs), space heating devices, refrigerators, and water heaters, are attracting increasing attention. Although a single TCL unit has very limited power regulation capability, ensembles of a

large number of TCLs, when managed in an orderly and controllable manner, can have a significant impact on the entire power grid [169, 179, 199, 222]. It has been shown that a large TCL population can be managed to support demand response tasks, including peak load shaving and load following [33, 77, 159, 206], and to provide ancillary services, such as primary or secondary frequency controls [131, 136, 200, 215].

The present work focuses on load tracking control, which allows the aggregate power of a TCL population to follow a desired consumption profile. The control design is based on a model of the dynamics of the TCL population described by partial differential equations (PDEs). Specifically, we consider a set of TCLs in which the dynamics of every individual device are modeled by a lumped stochastic hybrid system (SHS) operated through thermostat-based deadband control. The aggregate dynamics of such a TCL population can be modeled by two coupled Fokker-Planck equations (see, e.g, [24, 36, 126, 221]) describing the evolution of the probability distribution of TCLs in the ON and OFF states over the temperature. Note that the same form of PDE-based models can also be derived by assuming that the dynamics of individual TCLs are described by deterministic systems while considering population heterogeneity [21, 54, 146]. Compared with finite-dimensional state-space models, such as state-bins [108, 123, 171, 178, 216] or state queues [94, 117, 198], the PDE paradigm provides a more generic framework for modeling the aggregate dynamics of TCL populations, which allows handling nonlinearity, time-varying operational conditions, and parametric uncertainties with often very simple control algorithms. However, the PDE control system design procedure generally involves more complex mathematical analysis and is more challenging.

It is known that the total power consumption of a TCL population can be manipulated by changing the temperature set-point, moving the deadband, or interfering with the probability distributions of the TCLs via forced switches (see, e.g., [21, 24, 123, 193, 215]). Because a TCL population usually contains a large number of units that may spread over a large geographical area, only decentralized or distributed schemes are applicable. In fact, a remarkable amount of work on the control of TCL populations has been reported in the literature, and the majority of the proposed solutions are based on lumped models by applying optimization theory and optimal control techniques, in particular model predictive control (see, e.g, [21, 108, 117, 120, 123, 131, 164, 171, 178, 193, 198, 215, 216, 223]). It should be noted that, owing the nature of the considered problem, control schemes requiring the state measurement of the entire population in real-time are practically infeasible (see, e.g., [196] and the references therein). This problem can be addressed using state observers [131, 144]. Nevertheless, it is still very challenging to assess the performance of model-based state estimation algorithms because it depends heavily on the accuracy of the system parameters.

The load tracking control algorithm developed in the present work is a decentralized scheme in which the rates for set-point temperature adjustment generated by a central unit are broadcast to the TCLs over the population. Emphasis is placed on solving issues arising in practical applications, particularly communication restrictions and modeling uncertainties for large-scale TCL populations. The control system design is carried out in the framework of PDE-based modeling and control techniques. It should be noted that the two basic paradigms in PDE control system design and implementation, namely early-lumping and late-lumping procedures, have all been applied to the control of the coupled Fokker-Planck equations associated with TCL populations. The early-lumping method discretizes the underlying PDEs to obtain a lumped model, and then applies the techniques for finite-dimensional control system design [21, 24, 54, 146, 193]. In contrast, with the late-lumping method, the controller is designed using the PDE model and then discretized for implementation [55, 223]. A significant advantage of the late-lumping method is that it can preserve the essential properties of the PDE model and no approximation is required in the control design.

In this paper, we developed a new control algorithm based on the input-output linearization technique, which results in a system composed of finite-dimensional input-output dynamics and infinite-dimensional internal dynamics. The control design amounts then to finding a robust closed-loop control law that stabilizes the finite-dimensional input-output dynamics while guaranteeing the stability of the infinite-dimensional internal dynamics. Specifically:

- A new system output for power tracking control is proposed, guaranteeing the controllability of the input-output dynamics.
- An input-output linearization control law, which is independent of system parameters, e.g., the diffusion coefficient, while requiring only knowledge of the states of TCLs near the deadband boundaries, is derived.
- To tackle modeling uncertainties while making the control scheme computationally tractable, a sliding mode-like tracking control scheme that can achieve finite-time input-to-state stability (FTISS) [76, 114], is designed.
- The non-negativeness of the solution to the Fokker-Planck equations under the developed control law and other properties required to ensure closed-loop stability are rigorously validated.

The main contribution of the present work lies in the simplicity, scalability, and applicability of the control strategy developed under a generic framework. In addition, it is worth noting

that compared to the existing TCL control techniques, the developed control algorithm requires only measuring the state of the TCLs near the end-points of the deadband. Because the cyclic rate of the TCLs is much slower than the controller sampling rate, the communication burden can be significantly reduced. Obviously, it is very difficult for state feedback control schemes based on lumped aggregate models to achieve such features, which is critical for practical implementations.

The remainder of this paper is organized as follows. Section 4.2 introduces the notations used in the study and preliminaries on FTISS. Section 4.3 presents the first-order equivalent thermal parameter (ETP) model for a single TCL unit and the coupled Fokker-Planck model for the aggregate dynamics of the TCL population. Section 4.4 presents the power tracking control design and closed-loop stability analysis. The results of simulation study for validating the developed control strategy are reported in Section 4.5, followed by concluding remarks in Section 4.6. Finally, the proof of one of the main theoretical results is presented in the appendix.

4.2 Notations and preliminaries

4.2.1 Notations

Let $\mathbb{R} := (-\infty, +\infty)$, $\mathbb{R}_{\geq 0} := [0, +\infty)$, $\mathbb{R}_{>0} := (0, +\infty)$, and $\mathbb{R}_{\leq 0} := (-\infty, 0]$. Denote by $\partial_s f$ the derivative of the function f w.r.t. argument s. Note that, for notation simplicity, we may omit the arguments of functions if there is no ambiguity.

By convention, we denote by $|\cdot|$ the module of a function. For positive integers m, n and a given (open or closed) domain $\Omega \subset \mathbb{R}^n$, let $L^\infty(\Omega; \mathbb{R}^m) := \{\phi : \Omega \to \mathbb{R}^m |\ \phi \text{ is measurable in } \Omega \text{ and satisfies ess sup}_{s\in\Omega}|\phi(s)| < +\infty\}$. For $\phi \in L^\infty(\Omega; \mathbb{R}^m)$, the norm of ϕ is defined by $\|\phi\|_{L^\infty(\Omega)} := \text{ess sup}_{s\in\Omega}|\phi(s)|$. Let $L^\infty_{\text{loc}}(\Omega; \mathbb{R}^m) := \{\phi : \Omega \to \mathbb{R}^m |\ \phi \in L^\infty(\Omega'; \mathbb{R}^m) \text{ for any } \Omega' \subsetneqq \Omega\}$

For given (open or closed) domains $\Omega_1, \Omega_2 \subset \mathbb{R}^n$ and $\Omega_3 \subset \mathbb{R}$, let $C(\Omega_1; \Omega_3) := C^0(\Omega_1; \Omega_3) := \{\phi : \Omega_1 \to \Omega_3 |\ \phi \text{ is continuous w.r.t. its all augments in } \Omega_1\}$. For positive integers i, j, let $C^i(\Omega_1; \Omega_3) := \{\phi : \Omega_1 \to \Omega_3 |\ \phi \text{ has continuous derivatives up to order } i \text{ w.r.t. its all augments in } \Omega_1\}$, and $C^{i,j}(\Omega_1 \times \Omega_2; \Omega_3) := \{\phi : \Omega_1 \times \Omega_2 \to \Omega_3 |\ \phi \text{ has continuous derivatives up to order } i \text{ w.r.t. its augments in } \Omega_1 \text{ and up to order } j \text{ w.r.t. its augments in } \Omega_2\}$. In particular, if $\Omega_3 = \mathbb{R}$, we denote $C(\Omega_1) := C^0(\Omega_1; \mathbb{R})$ and $C^i(\Omega_1) := C^i(\Omega_1; \mathbb{R})$ for $i > 0$.

As in [114] and [92], we define the following sets of comparison functions. Let $\mathcal{K} := \{\vartheta : \mathbb{R}_{\geq 0} \to \mathbb{R}_{\geq 0} |\ \vartheta(0) = 0, \vartheta \text{ is continuous, strictly increasing}\}$; $\mathcal{L} := \{\vartheta : \mathbb{R}_{\geq 0} \to \mathbb{R}_{\geq 0} |\ \vartheta \text{ is continuous, strictly decreasing, } \lim_{s\to+\infty} \vartheta(s) = 0\}$; $\mathcal{KL} := \{\beta : \mathbb{R}_{\geq 0} \times \mathbb{R}_{\geq 0} \to \mathbb{R}_{\geq 0} |\ \beta(\cdot, t) \in$

$\mathcal{K}, \forall t \in \mathbb{R}_{\geq 0}$, and $\beta(s,\cdot) \in \mathcal{L}, \forall s \in \mathbb{R}_{>0}\}$; $\mathcal{K}_\infty := \{\vartheta : \mathbb{R}_{\geq 0} \to \mathbb{R}_{\geq 0} |\ \vartheta \in \mathcal{K}$ and $\lim_{s\to+\infty} \vartheta(s) = +\infty\}$; $\mathcal{GKL} := \{\beta : \mathbb{R}_{\geq 0} \times \mathbb{R}_{\geq 0} \to \mathbb{R}_{\geq 0} |\ \beta(\cdot, 0) \in \mathcal{K}$, and for each fixed $s \in \mathbb{R}_{>0}$ there exists $\widetilde{T}(s) \in \mathbb{R}_{\geq 0}$ such that $\beta(s,t) = 0$ for all $t \geq \widetilde{T}(s)\}$.

4.2.2 Finite-time input-to-state stability of finite dimensional systems

Consider the following nonlinear system

$$\dot{z}(t) = f(z(t), d(t)), \quad \forall t \in \mathbb{R}_{\geq 0}, \tag{4.1a}$$

$$z(0) = z_0, \tag{4.1b}$$

where $z := [z_1, z_2, ..., z_n]^\top \in \mathbb{R}^n$ is the state, $z_0 \in \mathbb{R}^n$ is the initial datum, $d \in \mathcal{D} := L^\infty_{\text{loc}}(\mathbb{R}_{\geq 0}; \mathbb{R}^m)$ is the input (disturbance) to the system, $f : \mathbb{R}^n \times \mathbb{R}^m \to \mathbb{R}^n$ is a nonlinear function that is continuous w.r.t. (z, d), ensures the forward existence of the system solutions, at least locally, and satisfies $f(0,0) = 0$, and $m \geq 1$ and $n \geq 1$ are integers.

Definition 4.1. *System* (4.1) *is said to be finite-time input-to-state stable (FTISS) if there exist functions $\vartheta \in \mathcal{K}$ and $\beta \in \mathcal{GKL}$ such that for any $x_0 \in \mathbb{R}^n$ and $d \in \mathcal{D}$ its trajectory satisfies*

$$|z(t)| \leq \beta(|z_0|, t) + \vartheta(\|d\|_{L^\infty(0,t)}), \quad \forall t \in \mathbb{R}_{\geq 0}. \tag{4.2}$$

Remark 4.1. *Note that FTISS is defined in a similar way to the definition of input-to-state stability (ISS) in [92, Chapter 4] via the norm of d over the interval $(0,t)$ rather than $(0,+\infty)$. Thus, the FTISS presented here is a refined notion of the one introduced in [76, 114], where the second term in the right-hand side of* (4.2) *is under the form $\vartheta(\|d\|_{L^\infty(0,+\infty)})$, which describes the influence of the global bounds of d instead of the bounds of d over the finite time interval $(0,t)$.*

Definition 4.2. *A continuously differentiable function $V : \mathbb{R}^n \to \mathbb{R}_{\geq 0}$ is said to be an FTISS Lyapunov function for system* (4.1) *if there exist functions $\mu_1, \mu_2 \in \mathcal{K}_\infty$, $\chi \in \mathcal{K}$ and constants $c > 0$ and $\theta \in (0,1)$ such that for all $x \in \mathbb{R}^n$ and all $d \in \mathcal{D}$ it holds that*

$$\mu_1(|x|) \leq V(x) \leq \mu_2(|x|),$$
$$|z| \geq \chi(|d|) \Rightarrow DV(z) \cdot f(z,d) \leq -cV^\theta(z),$$

where $DV(z) := \left[\frac{\partial V}{\partial z_1}, \ldots, \frac{\partial V}{\partial z_n}\right]$.

The following Lyapunov-like lemma gives a sufficient condition for the FTISS.

Lemma 4.1. *System* (4.1) *is FTISS if it admits a finite-time ISS Lyapunov function.*

Proof. Setting $\mathcal{V} := \{z | V(z) \leq \mu_2(\chi(|d|))\}$ in the proof of [76, Theorem 1(a)], the lemma statement follows immediately. □

4.3 Mathematical model and problem specification

4.3.1 Dynamics of individual TCLs

In the present work, we focus on modeling the population of residential air conditioners (ACs). While, its extension to other cooling and heating devices is straightforward. We consider the case where all ACs are operated by thermostats and hence, every AC switches between the ON and OFF states whenever it reaches the prescribed lower or upper temperature bounds. For simplicity, we ignore the solar irradiation and internal heat gains and assume that the ACs operate at a fixed frequency. Then, the dynamics of the indoor temperature, denoted by $x(t)$, can be expressed by the following SHS (see, e.g., [24, 126, 193]):

$$\mathrm{d}x(t) = \frac{1}{CR}\left(x_a(t) - x(t) - s(t)RP\right)\mathrm{d}t + \sigma\,\mathrm{d}w(t), \tag{4.3}$$

where $x_a(t)$ is the ambient temperature, R, C, and P are the thermal resistance, capacitance, and power, respectively, and $s(t)$ is the switching signal. In (4.3), $w(t)$ is a standard Wiener process, which, along with the parameter σ, represents modeling uncertainties, such as unaccounted heat loss or heat gain, parameter variations, and disturbances.

For a thermostat-controlled AC, the switching signal $s(t)$ takes a binary value from $\{0, 1\}$, representing the OFF and ON states, respectively. Figure 4.1 illustrates one possible trajectory of an AC described by (4.3), where the temperature moves back-and-forth in a fixed-width region. Meanwhile, forced switches, denoted by $r(t)$, may also occur in the process. Let $r(t) = 1$ represent the occurrence of switching and 0 otherwise and suppose that $\underline{x}$ and $\overline{x}$ are the lower and upper temperature bounds, respectively. Then, the switching signal $s(t)$ for an AC can be expressed as

$$s(t) = \begin{cases} 1, & \text{if } x \geq \overline{x}; \\ 0, & \text{if } x \leq \underline{x}; \\ (s(t^-) \wedge r(t)) + (s(t^-) \vee r(t)), & \text{otherwise}; \end{cases}$$

where "+" is the one-bit binary addition with overflow. In addition, the notations $(\cdot)^-$ and $(\cdot)^+$ denote the left and right limits of the scalar variable, respectively. Note that different

actions, such as random switches to avoid power demand oscillations due to synchronization within a TCL population, mechanisms for blocking the switches to protect the ACs, etc., can be integrated in the design of forced switching schemes.

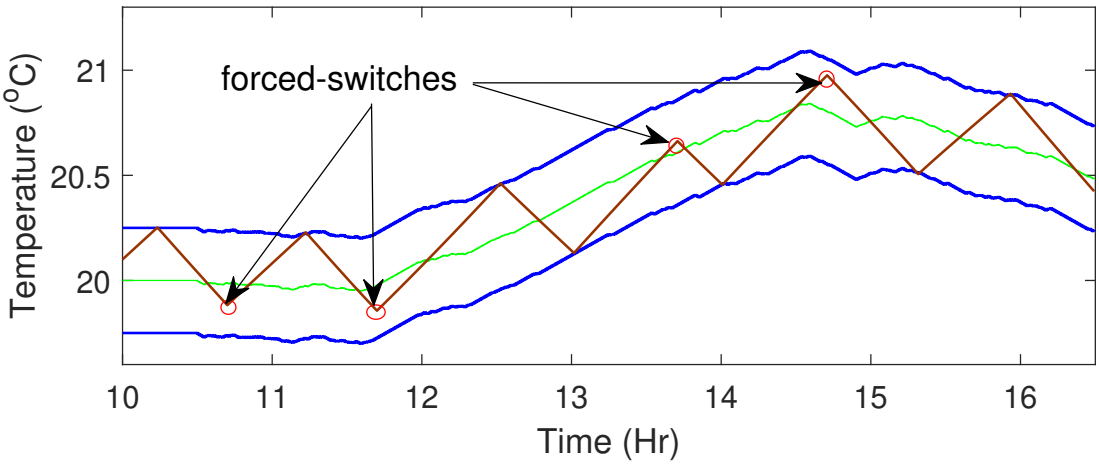

Figure 4.1 Hybrid thermostat-based deadband control scheme.

4.3.2 Dynamics of aggregate TCL population

As mentioned previously, the dynamics of an aggregate TCL population can be characterized by the evolution of the distributions of the TCLs over temperature. When the number of TCLs in the population tends to be infinite, this population can be modeled as a continuum whose temperature distribution is governed by the coupled Fokker-Planck equations [24, 54, 126, 146]. Specifically, we denote by $f_1(x,t)$ and $f_0(x,t)$ the probability density functions (PDFs) of the TCLs in the ON and OFF states at temperature x and time t, respectively. As illustrated in Fig. 4.2, we assume that all the loads are confined in a fixed temperature range (x_L, x_H) along all possible operations, where x_L and x_H are constants, which is a reasonable assumption for practical application. Moreover, owing to the nature of thermostat-based control, there must be that $f_1(x,t) = 0$ for all $x \leq \underline{x}$ and $t \in \mathbb{R}_{>0}$, and that $f_0(x,t) = 0$ for all $x \geq \overline{x}$ and $t \in \mathbb{R}_{>0}$. Therefore, we can divide the range (x_L, x_H) into three segments:

$$I_a := (x_L, \underline{x}), I_b := (\underline{x}, \overline{x}), I_c := (\overline{x}, x_H),$$

which will be used in the upcoming study.

Suppose that the dynamics of each load in the TCL population are described by (4.3). Let

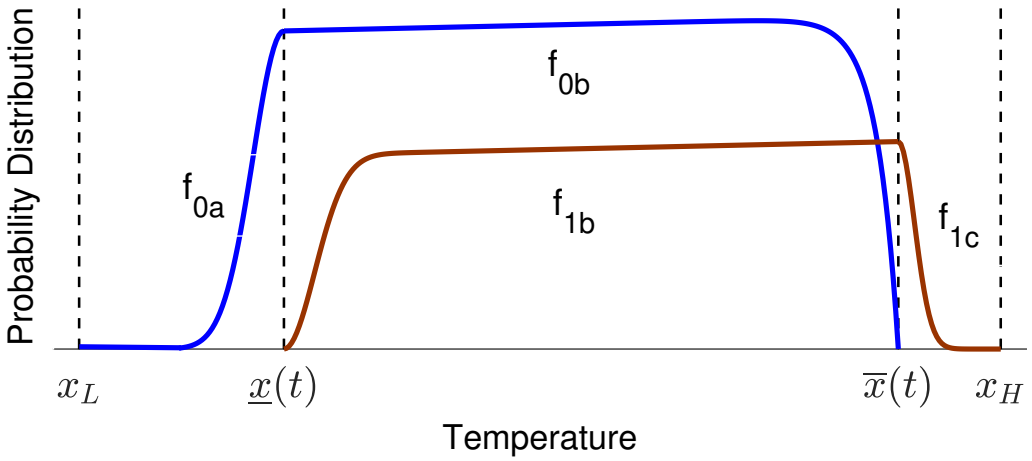

Figure 4.2 Illustration of probability density functions of a TCL population at a given time.

further

$$\alpha_0(x,t) := \frac{1}{CR}\left(x_a(t) - x\right),$$
$$\alpha_1(x,t) := \frac{1}{CR}\left(x_a(t) - x - RP\right).$$

The evolutions of $f_0(x,t)$ and $f_1(x,t)$ are governed by the following coupled Fokker-Planck equations [24, 126, 193]:

$$\partial_t f_0 = \partial_x\left(\frac{\sigma^2}{2}\partial_x f_0 - (\alpha_0 - u) f_0\right) \text{ in } I_a \times \mathbb{R}_{>0}, \tag{4.4a}$$
$$\partial_t f_0 = \partial_x\left(\frac{\sigma^2}{2}\partial_x f_0 - (\alpha_0 - u) f_0\right) - g(f_0, f_1) \text{ in } I_b \times \mathbb{R}_{>0}, \tag{4.4b}$$
$$\partial_t f_1 = \partial_x\left(\frac{\sigma^2}{2}\partial_x f_1 - (\alpha_1 - u) f_1\right) + g(f_0, f_1) \text{ in } I_b \times \mathbb{R}_{>0}, \tag{4.4c}$$
$$\partial_t f_1 = \partial_x\left(\frac{\sigma^2}{2}\partial_x f_1 - (\alpha_1 - u) f_1\right) \text{ in } I_c \times \mathbb{R}_{>0}, \tag{4.4d}$$

where $g(f_0, f_1)$ represents the net probability flux due to the switches which only occur over the segment I_b, that is, the so-called forced switches. Hence, the signs of $g(f_0, f_1)$ in (4.4b) and (4.4c) should be opposite to each other, which implies a mass conservation property as claimed in Theorem 4.3 in Section 4.4.3. Note that (4.4b) and (4.4c) have a general form compared to that given in [193] (see (19a) and (19b) of that paper), where an explicitly linear function $g(f_0, f_1)$ was used to model a switching rate control scheme.

Following [193], we introduce the notation of probability flows $\mathcal{F}_i$. When there is no additional flux from the forced switches, i.e., $g = 0$, $\mathcal{F}_i$ is the integral of the probability fluxes $\partial_t f_i$ over the temperature (x-) coordinate:

$$\mathcal{F}_i(x,t) := \frac{\sigma^2}{2}\partial_x f_i(x,t) - (\alpha_i(x,t) - u(t))f_i(x,t), i = 0, 1.$$

The boundary conditions can then be written as

$$\begin{aligned}
\mathcal{F}_0(x_L^+, t) =& 0, \quad \forall t \in \mathbb{R}_{>0}, && \text{(4.5a)}\\
\mathcal{F}_0(\underline{x}^-, t) =& \mathcal{F}_0(\underline{x}^+, t) + \mathcal{F}_1(\underline{x}^+, t), \quad \forall t \in \mathbb{R}_{>0}, && \text{(4.5b)}\\
f_0(\underline{x}^-, t) =& f_0(\underline{x}^+, t), \quad \forall t \in \mathbb{R}_{>0}, && \text{(4.5c)}\\
f_0(\overline{x}^-, t) =& 0, \quad \forall t \in \mathbb{R}_{>0}, && \text{(4.5d)}\\
f_1(\underline{x}^+, t) =& 0, \quad \forall t \in \mathbb{R}_{>0}, && \text{(4.5e)}\\
f_1(\overline{x}^-, t) =& f_1(\overline{x}^+, t), \quad \forall t \in \mathbb{R}_{>0}, && \text{(4.5f)}\\
\mathcal{F}_1(\overline{x}^+, t) =& \mathcal{F}_0(\overline{x}^-, t) + \mathcal{F}_1(\overline{x}^-, t), \quad \forall t \in \mathbb{R}_{>0}, && \text{(4.5g)}\\
\mathcal{F}_1(x_H^-, t) =& 0, \quad \forall t \in \mathbb{R}_{>0}, && \text{(4.5h)}\\
\mathcal{F}_0(\underline{x}^-, t) >& \mathcal{F}_0(\underline{x}^+, t), \quad \forall t \in \mathbb{R}_{>0}, && \text{(4.5i)}\\
\mathcal{F}_1(\overline{x}^+, t) <& \mathcal{F}_1(\overline{x}^-, t), \quad \forall t \in \mathbb{R}_{>0}. && \text{(4.5j)}
\end{aligned}$$

The initial data of f_0 and f_1 defined over $\overline{I}_{a0} := [x_L, \underline{x}(0)], \overline{I}_{b0} := [\underline{x}(0), \overline{x}(0)]$, and $\overline{I}_{c0} := [\overline{x}(0), x_H]$ are given by

$$\begin{aligned}
f_0(0,x) =& f_0^{a0}(x), \quad \forall x \in \overline{I}_{a0}, && \text{(4.6a)}\\
f_0(0,x) =& f_0^{b0}(x), \quad \forall x \in \overline{I}_{b0}, && \text{(4.6b)}\\
f_1(0,x) =& f_1^{b0}(x), \quad \forall x \in \overline{I}_{b0}, && \text{(4.6c)}\\
f_1(0,x) =& f_1^{c0}(x), \quad \forall x \in \overline{I}_{c0}. && \text{(4.6d)}
\end{aligned}$$

Note that the integration of $f_1(x,t)$ with respect to x is the proportion of the ACs in ON state in the population. Thus, the total power demand of the TCL population at time $t \in \mathbb{R}_{\geq 0}$ is given by

$$y_{\text{total}}(t) := \frac{P}{\eta}\int_{\underline{x}(t)}^{x_H} f_1(x,t)\,\mathrm{d}x, \tag{4.7}$$

where η is the load efficiency coefficient, which indicates the effectiveness of a device at transferring heat versus the amount of electrical power it consumes.

Remark 4.2. *We provide remarks on the boundary conditions presented in* (4.5).

(i) For continuous functions α_0, α_1*, and* u*, the boundary conditions in* (4.5) *are equivalent to:*

$$\frac{\sigma^2}{2}\partial_x f_0(x_L^+, t) = (\alpha_0(x_L^+, t) - u(t)) f_0(x_L^+, t), \tag{4.8a}$$

$$\partial_x f_0(\underline{x}^-, t) = \partial_x f_0(\underline{x}^+, t) + \partial_x f_1(\underline{x}^+, t), \tag{4.8b}$$

$$f_0(\underline{x}^-, t) = f_0(\underline{x}^+, t), \tag{4.8c}$$

$$f_0(\overline{x}, t) = 0, \tag{4.8d}$$

$$f_1(\underline{x}, t) = 0, \tag{4.8e}$$

$$f_1(\overline{x}^-, t) = f_1(\overline{x}^+, t), \tag{4.8f}$$

$$\partial_x f_1(\overline{x}^+, t) = \partial_x f_0(\overline{x}^-, t) + \partial_x f_1(\overline{x}^-, t), \tag{4.8g}$$

$$\frac{\sigma^2}{2}\partial_x f_1(x_H^-, t) = (\alpha_1(x_H^-, t) - u(t)) f_1(x_H^-, t), \tag{4.8h}$$

$$\partial_x f_1(\underline{x}^+, t) > 0, \tag{4.8i}$$

$$\partial_x f_0(\overline{x}^-, t) < 0. \tag{4.8j}$$

(ii) It is worth noting that this set of boundary conditions ((4.5) *or* (4.8)*), with possible variations, is commonly used in the literature [24, 126, 193], which captures the basic properties of the considered problem, for example, impenetrable wall reflections (*(4.8a) *and* (4.8h)*), absorbing actions due to thermostat switching (*(4.8d)*) and* (4.8e)*), and probability conservation at the boundaries of the deadband (*(4.8b) *and* (4.8g)*). Note that because of the absorbing property and the continuity of the PDFs on the boundaries of the deadband, the conditions* (4.8b) *and* (4.8g) *remain the same as those originally derived in [126], even though the considered problem in the present work contains control actions.*

4.3.3 Problem statement and basic assumptions

In this work, we study the dynamics described by the PDE model (4.4) under the boundary and initial conditions (4.5) and (4.6). Based on (4.7), a new output function will be defined and specified in Section 4.4. With these dynamics, a continuous time controller that considers the convergence time and robustness is designed to stabilize the tracking process.

In the sequel, we assume that $x_a \in C(\mathbb{R}_{\geq 0})$ $\underline{x}, \overline{x} \in C^1(\mathbb{R}_{\geq 0}; \mathbb{R}_{>0})$, and denote

$$\begin{aligned} S_{ab} := &\left(C^{2,1}(I_a \times \mathbb{R}_{>0}) \cap C(\overline{I}_a \times \mathbb{R}_{\geq 0})\right) \\ &\cup \left(C^{2,1}(I_b \times \mathbb{R}_{>0}) \cap C(\overline{I}_b \times \mathbb{R}_{\geq 0})\right), \\ S_{bc} := &\left(C^{2,1}(I_b \times \mathbb{R}_{>0}) \cap C(\overline{I}_b \times \mathbb{R}_{\geq 0})\right) \\ &\cup \left(C^{2,1}(I_c \times \mathbb{R}_{>0}) \cap C(\overline{I}_c \times \mathbb{R}_{\geq 0})\right). \end{aligned}$$

Based on the physical properties of the problem, we impose the following structural conditions and basic assumptions on the solution and control for the system:

• The function of net probability flux g belongs to $C^1(\mathbb{R}^2; \mathbb{R})$ and satisfies

(G1) $g(0, \tau) \leq 0$ for all $\tau \in \mathbb{R}$;

(G2) $g(s, 0) \geq 0$ for all $s \in \mathbb{R}$;

(G3) $|g_s(s, \tau)| + |g_\tau(s, \tau)| \leq 1$ for all $(s, \tau) \in \mathbb{R}^2$.

• The pair of solution (f_0, f_1) and the control u satisfy

(U) $u \in C(\mathbb{R}_{\geq 0}; \mathbb{R})$ such that $\dot{\underline{x}} = \dot{\overline{x}} = u$ in $\mathbb{R}_{\geq 0}$;

(F1) $f_0^{a0} \in C(\overline{I}_{a0}; \mathbb{R}_{\geq 0})$, $f_0^{b0} \in C(\overline{I}_{b0}; \mathbb{R}_{\geq 0})$, $f_1^{b0} \in C(\overline{I}_{b0}; \mathbb{R}_{\geq 0})$, $f_1^{c0} \in C(\overline{I}_{c0}; \mathbb{R}_{\geq 0})$;

(F2) $f_0 \in S_{ab}$ and has derivatives $\partial_x f_0(x_L^+, t)$, $\partial_x f_0(\underline{x}^\pm, t)$, and $\partial_x f_0(\overline{x}^-, t)$ for any fixed $t \in \mathbb{R}_{>0}$;

(F3) $f_1 \in S_{bc}$ and has derivatives $\partial_x f_1(x_H^-, t)$, $\partial_x f_1(\overline{x}^\pm, t)$, and $\partial_x f_1(\underline{x}^+, t)$ for any fixed $t \in \mathbb{R}_{>0}$.

Remark 4.3. *It should be mentioned that for $f_0 = 0$ (or $f_1 = 0$), condition (G1) (or (G2)) guarantees $-g(f_0, f_1) \geq 0$ (or $g(f_0, f_1) \geq 0$) in* (4.4b) *(or* (4.4c)*) . This indicates that forced switching, which generates additional fluxes, is only possible from the f_1 system into the f_0 system when f_0 is zero.*

Condition (G3) indicates that the change in the probability density of the additional flux cannot be too fast for practical applications. This is in accordance with the suggestion provided in [193].

Condition (F1) indicates that the initial data are assumed to be nonnegative and continuous over the given domains. Conditions (F2) and (F3) describe the regularity of the solutions at the endpoints of the given domains at any time t.

4.4 Control design and stability analysis

In this section, we design a feedback control law to ensure that the output of the system (4.4)-(4.6) tracks a reference power curve, and assess the stability of the error dynamics in the framework of FTISS theory. Moreover, we study the mass conservation and non-negativeness properties of the solutions to the considered system, which allows further clarification of the physical meanings of the mathematical model.

4.4.1 Control design

The control objective is to drive the power consumption of the population to track the desired regulation signal. To this end, we choose an output of the power tracking control scheme as

$$y(t) := y_{\text{total}}(t) + \frac{P}{\eta}\int_{\overline{x}(t)}^{x_H} f_1(x,t)\,\mathrm{d}x - \frac{P}{\eta}\int_{x_L}^{\underline{x}(t)} f_0(x,t)\,\mathrm{d}x, \quad t \in \mathbb{R}_{\geq 0}. \tag{4.9}$$

It is worth noting that, as the probability flows of f_0 and f_1 always move towards the deadband, $y(t)$ defined in (4.9) converges to the aggregated power demand $y_{\text{total}}(t)$ in the steady state. The motivation to add two extra terms to $y_{\text{total}}(t)$ is to ensure the controllability of the input-output dynamics.

The regulation of power consumption of the TCL population is achieved by moving the mass of the temperature distribution, and the control signal is chosen to be the set-point temperature variation rate $\dot{x}_{\text{sp}}$, which may induce a change in the probability flux [24, 221]. As we consider a control scheme with a fixed deadband width, denoted by δ_0, we have $\overline{x} = x_{\text{sp}} - \frac{\delta_0}{2}$, $\underline{x} = x_{\text{sp}} + \frac{\delta_0}{2}$. Thus, the actual control signal is given by $u(t) := \dot{x}_{\text{sp}} = \dot{\underline{x}} = \dot{\overline{x}}$.

Let $y_d : \mathbb{R}_{\geq 0} \to \mathbb{R}$ be the desired power profile, which is sufficiently smooth, and define the power tracking error as

$$e(t) := y(t) - y_d(t).$$

In what follows, we introduce a nonlinear control law and derive the corresponding tracking error dynamics.

Theorem 4.1. *Consider the system given in* (4.4) *and* (4.9) *under the boundary conditions in* (4.5) *(or equivalently* (4.8)*). Let the control input be defined as*

$$u(t) := \frac{k|e(t)|^{\gamma}\text{sgn}(e(t)) + \Phi(t)}{2\left(f_1(\overline{x},t) + f_0(\underline{x},t)\right)}, \tag{4.10}$$

where $k \in \mathbb{R}_{>0}$ *and* $\gamma \in (0,1)$ *are constants,* $\mathrm{sgn}(e)$ *is the sign function defined by*

$$\mathrm{sgn}(e) := \begin{cases} -1, & e < 0, \\ 0, & e = 0, \\ 1, & e > 0, \end{cases}$$

and

$$\Phi(t) := -\frac{\eta}{P}\dot{y}_d(t). \tag{4.11}$$

Then, the power tracking error dynamics are given by

$$\dot{e}(t) = -\frac{P}{\eta}k|e(t)|^{\gamma}\mathrm{sgn}(e(t)) + \Gamma(t), \tag{4.12}$$

where

$$\begin{aligned}\Gamma(t) :=& \frac{P}{\eta}\left(\alpha_1(\overline{x},t)f_1(\overline{x},t) + \alpha_0(\underline{x},t)f_0(\underline{x},t)\right) - \frac{\sigma^2 P}{2\eta}\left(\partial_x f_1(\underline{x}^+,t) + \partial_x f_1(\overline{x}^+,t)\right) \\ & - \frac{\sigma^2 P}{2\eta}\left(\partial_x f_0(\underline{x}^-,t) + \partial_x f_0(\overline{x}^-,t)\right) + \frac{P}{\eta}\int_{\underline{x}(t)}^{\overline{x}(t)} g(f_0,f_1)\,\mathrm{d}x. \end{aligned} \tag{4.13}$$

Remark 4.4. $\Gamma(t)$ *defined in* (4.13) *captures the terms depending on the diffusion coefficient or requiring instantaneous state measurements and will be treated as a disturbance thereafter. Moreover, the control law given in* (4.10) *involves only the measurement of the states (probability distributions* f_0 *and* f_1*) on the end-points of the deadband (*$\underline{x}$ *and* $\overline{x}$*), which results in a control scheme with significantly reduced communication burden compared to control schemes that require full-state measurements.*

Proof of Theorem 4.1. Note that

$$\begin{aligned}\dot{e}(t) &= \dot{y}(t) - \dot{y}_d(t) \\ &= \frac{\mathrm{d}}{\mathrm{d}t}\left(\frac{P}{\eta}\int_{\underline{x}(t)}^{x_H} f_1(x,t)\,\mathrm{d}x + \frac{P}{\eta}\int_{\overline{x}(t)}^{x_H} f_1(x,t)\,\mathrm{d}x - \frac{P}{\eta}\int_{x_L}^{\underline{x}(t)} f_0(x,t)\,\mathrm{d}x\right) - \dot{y}_d(t) \\ &= \frac{P}{\eta}\frac{\mathrm{d}}{\mathrm{d}t}\int_{\underline{x}(t)}^{x_H} f_1(x,t)\,\mathrm{d}x + \frac{P}{\eta}\frac{\mathrm{d}}{\mathrm{d}t}\int_{\overline{x}(t)}^{x_H} f_1(x,t)\,\mathrm{d}x - \frac{P}{\eta}\frac{\mathrm{d}}{\mathrm{d}t}\int_{x_L}^{\underline{x}(t)} f_0(x,t)\,\mathrm{d}x - \dot{y}_d(t).\end{aligned}$$

Hence, we decompose the whole computation process into three steps.

Step 1: Compute $\frac{\mathrm{d}}{\mathrm{d}t}\int_{\overline{x}(t)}^{x_H} f_1(x,t)\,\mathrm{d}x$. It follows immediately from Leibniz's integral rule and

(4.4d) that

$$\begin{aligned}
&\frac{\mathrm{d}}{\mathrm{d}t}\int_{\overline{x}(t)}^{x_H} f_1(x,t)\,\mathrm{d}x\\
=&0-\dot{\overline{x}}(t)f_1(\overline{x},t)+\int_{\overline{x}(t)}^{x_H}\partial_t f_1(x,t)\,\mathrm{d}x\\
=&-u(t)f_1(\overline{x},t)+\int_{\overline{x}(t)}^{x_H}\partial_x\left(\frac{\sigma^2}{2}\partial_x f_1(x,t)-(\alpha_1(x,t)-u(t))f_1(x,t)\right)\mathrm{d}x\\
=&-u(t)f_1(\overline{x},t)+\left(\frac{\sigma^2}{2}\partial_x f_1(x_H^-,t)-(\alpha_1(x_H^-,t)-u(t))f_1(x_H^-,t)\right)\\
&-\left(\frac{\sigma^2}{2}\partial_x f_1(\overline{x}^+,t)-(\alpha_1(\overline{x},t)-u(t))f_1(\overline{x},t)\right).
\end{aligned}$$

Using boundary condition (4.8h), it follows that

$$\frac{\mathrm{d}}{\mathrm{d}t}\int_{\overline{x}(t)}^{x_H} f_1(x,t)\,\mathrm{d}x=-2u(t)f_1(\overline{x},t)-\frac{\sigma^2}{2}\partial_x f_1(\overline{x}^+,t)+\alpha_1(\overline{x},t)f_1(\overline{x},t). \tag{4.14}$$

Step 2: Compute $\frac{\mathrm{d}}{\mathrm{d}t}\int_{\underline{x}(t)}^{x_H} f_1(x,t)\,\mathrm{d}x$. Since

$$\frac{\mathrm{d}}{\mathrm{d}t}\int_{\underline{x}(t)}^{x_H} f_1(x,t)\,\mathrm{d}x=\frac{\mathrm{d}}{\mathrm{d}t}\int_{\underline{x}(t)}^{\overline{x}(t)} f_1(x,t)\,\mathrm{d}x+\frac{\mathrm{d}}{\mathrm{d}t}\int_{\overline{x}(t)}^{x_H} f_1(x,t)\,\mathrm{d}x,$$

and $\frac{\mathrm{d}}{\mathrm{d}t}\int_{\overline{x}}^{x_H} f_1(x,t)\,\mathrm{d}x$ is given by (4.14), we only need to compute $\frac{\mathrm{d}}{\mathrm{d}t}\int_{\underline{x}(t)}^{\overline{x}(t)} f_1(x,t)\,\mathrm{d}x$. It follows from (4.4c) and (4.8e) that

$$\begin{aligned}
\frac{\mathrm{d}}{\mathrm{d}t}\int_{\underline{x}(t)}^{\overline{x}(t)} f_1(x,t)\,\mathrm{d}x=&u(t)f_1(\overline{x},t)+\int_{\underline{x}(t)}^{\overline{x}(t)} g(f_0,f_1)\,\mathrm{d}x\\
&+\int_{\underline{x}(t)}^{\overline{x}(t)}\partial_x\left(\frac{\sigma^2}{2}\partial_x f_1(x,t)-(\alpha_1(x,t)-u(t))f_1(x,t)\right)\mathrm{d}x\\
=&u(t)f_1(\overline{x},t)+\int_{\underline{x}(t)}^{\overline{x}(t)} g(f_0,f_1)\,\mathrm{d}x\\
&+\left(\frac{\sigma^2}{2}\partial_x f_1(\overline{x}^-,t)-(\alpha_1(\overline{x}^-,t)-u(t))f_1(\overline{x}^-,t)\right)\\
&-\left(\frac{\sigma^2}{2}\partial_x f_1(\underline{x}^+,t)-(\alpha_1(\underline{x}^+,t)-u(t))f_1(\underline{x}^+,t)\right)\\
=&u(t)f_1(\overline{x},t)+\frac{\sigma^2}{2}\partial_x f_1(\overline{x}^-,t)-(\alpha_1(\overline{x},t)-u(t))f_1(\overline{x},t)\\
&-\frac{\sigma^2}{2}\partial_x f_1(\underline{x}^+,t)+\int_{\underline{x}(t)}^{\overline{x}(t)} g(f_0,f_1)\,\mathrm{d}x
\end{aligned}$$

$$
\begin{aligned}
=&2u(t)f_1(\overline{x},t)+\frac{\sigma^2}{2}\partial_x f_1(\overline{x}^-,t)-\alpha_1(\overline{x},t)f_1(\overline{x},t)\\
&-\frac{\sigma^2}{2}\partial_x f_1(\underline{x}^+,t)+\int_{\underline{x}(t)}^{\overline{x}(t)} g(f_0,f_1)\,\mathrm{d}x. \qquad (4.15)
\end{aligned}
$$

Combining (4.14) and (4.15) we obtain by (4.8h)

$$
\frac{\mathrm{d}}{\mathrm{d}t}\int_{\underline{x}(t)}^{x_H} f_1(x,t)\,\mathrm{d}x=-\frac{\sigma^2}{2}\partial_x f_1(\underline{x}^+,t)-\frac{\sigma^2}{2}\partial_x f_0(\overline{x}^-,t)+\int_{\underline{x}(t)}^{\overline{x}(t)} g(f_0,f_1)\,\mathrm{d}x. \qquad (4.16)
$$

Step 3: Compute $\frac{\mathrm{d}}{\mathrm{d}t}\int_{x_L}^{\underline{x}(t)} f_0(x,t)\,\mathrm{d}x$. According to (4.4a) and (4.8a), we have

$$
\begin{aligned}
\frac{\mathrm{d}}{\mathrm{d}t}\int_{x_L}^{\underline{x}(t)} f_0(x,t)\,\mathrm{d}x=&u(t)f_0(\underline{x},t)+\int_{x_L}^{\underline{x}(t)}\partial_t f_0(x,t)\,\mathrm{d}x\\
=&u(t)f_0(\underline{x},t)+\int_{x_L}^{\underline{x}(t)}\partial_x\left(\frac{\sigma^2}{2}\partial_x f_0-(\alpha_0-u)f_0\right)\mathrm{d}x\\
=&u(t)f_0(\underline{x},t)+\left(\frac{\sigma^2}{2}\partial_x f_0(\underline{x}^-,t)-(\alpha_0(\underline{x},t)-u(t))f_0(\underline{x},t)\right)\\
&-\left(\frac{\sigma^2}{2}\partial_x f_0(x_L^+,t)-(\alpha_0(x_L^+,t)-u(t))f_0(x_L^+,t)\right)\\
=&2u(t)f_0(\underline{x},t)+\frac{\sigma^2}{2}\partial_x f_0(\underline{x}^-,t)-\alpha_0(\underline{x},t)f_0(\underline{x},t). \qquad (4.17)
\end{aligned}
$$

Finally, by combining (4.14), (4.16), and (4.17), we obtain:

$$
\begin{aligned}
\dot{e}(t)=&\frac{P}{\eta}\left(-\frac{\sigma^2}{2}\partial_x f_1(\underline{x}^+,t)-\frac{\sigma^2}{2}\partial_x f_0(\overline{x}^-,t)\right)\\
&+\frac{P}{\eta}\left(-2u(t)f_1(\overline{x},t)-\frac{\sigma^2}{2}\partial_x f_1(\overline{x}^+,t)+\alpha_1(\overline{x},t)f_1(\overline{x},t)\right)\\
&-\frac{P}{\eta}\left(2u(t)f_0(\underline{x},t)+\frac{\sigma^2}{2}\partial_x f_0(\underline{x}^-,t)-\alpha_0(\underline{x},t)f_0(\underline{x},t)\right)\\
&-\dot{y}_d(t)+\frac{P}{\eta}\int_{\underline{x}(t)}^{\overline{x}(t)} g(f_0,f_1)\,\mathrm{d}x\\
=&-\frac{2P}{\eta}u(t)\left(f_1(\overline{x},t)+f_0(\underline{x},t)\right)-\frac{\sigma^2 P}{2\eta}\partial_x f_1(\underline{x}^+,t)\\
&-\frac{\sigma^2 P}{2\eta}\partial_x f_1(\overline{x}^+,t)-\frac{\sigma^2 P}{2\eta}\partial_x f_0(\underline{x}^-,t)\\
&-\frac{\sigma^2 P}{2\eta}\partial_x f_0(\overline{x}^-,t)+\frac{P}{\eta}\int_{\underline{x}(t)}^{\overline{x}(t)} g(f_0,f_1)\,\mathrm{d}x\\
&+\frac{P}{\eta}\alpha_1(\overline{x},t)f_1(\overline{x},t)+\frac{P}{\eta}\alpha_0(\underline{x},t)f_0(\underline{x},t)-\dot{y}_d(t).
\end{aligned}
$$

The error dynamics can then be expressed as

$$\dot{e}(t) = -\frac{2P}{\eta}u(t)\left(f_1(\overline{x},t) + f_0(\underline{x},t)\right) + \frac{P}{\eta}\Phi(t) + \Gamma(t).$$

Let

$$u(t) := \frac{v(t) + \Phi(t)}{2\left(f_1(\overline{x},t) + f_0(\underline{x},t)\right)},$$

where $v(t)$ is an auxiliary control input, then

$$\dot{e}(t) = -\frac{P}{\eta}v(t) + \Gamma(t). \tag{4.18}$$

Considering an auxiliary control of the form:

$$v(t) := k|e(t)|^{\gamma}\mathrm{sgn}(e(t)), \tag{4.19}$$

the tracking error dynamics in the closed loop are then given by (4.12). □

Remark 4.5. *Note that for the given initial data (see (F1)), it can be shown that the term* $f_1(\overline{x},t) + f_0(\underline{x},t)$ *is strictly positive (see Theorem 4.4 (iii) in Section 4.4.2). Therefore, the control signal* u*, given in* (4.10) *is well-defined. In addition,* u *is continuous due to the fact that* $\gamma \in (0,1)$ *and the assumptions on the continuity of* $\dot{y}_d(t)$ *and* $f_1(\overline{x},t) + f_0(\underline{x},t)$ *(see (F2) and (F3)). It is also worth noting that, as* $f_1(\overline{x},t)$ *and* $f_0(\underline{x},t)$ *describe the probability density of TCLs in the ON and OFF states at the prescribed upper and lower temperature boundaries* $\overline{x}$ *and* $\underline{x}$*, respectively, it is impossible in practice that* $f_1(\overline{x},t) + f_0(\underline{x},t) \to 0$ *as* $t \to +\infty$*.*

Figure 4.3 shows the schematic diagram of an implementation of the proposed power tracking control for a TCL population on a digital platform. Note that each TCL is configured with a zero-order-hold (ZOH), which allows keeping the control signal to be a constant in every controller execution period. Furthermore, a numerical approximation method, which uses only partially observed states, is used to compute the values of $f_1(\overline{x}(t_k),t_k)$ and $f_0(\underline{x}(t_k),t_k)$ in $u(t_k)$ at the control center.

4.4.2 Finite-time input-to-state stability of the tracking error dynamics

In this section, we assess the robust stability of the tracking error dynamics in the sense of FTISS, with Γ as the input (disturbance). One of the main properties of the closed-loop system is stated below.

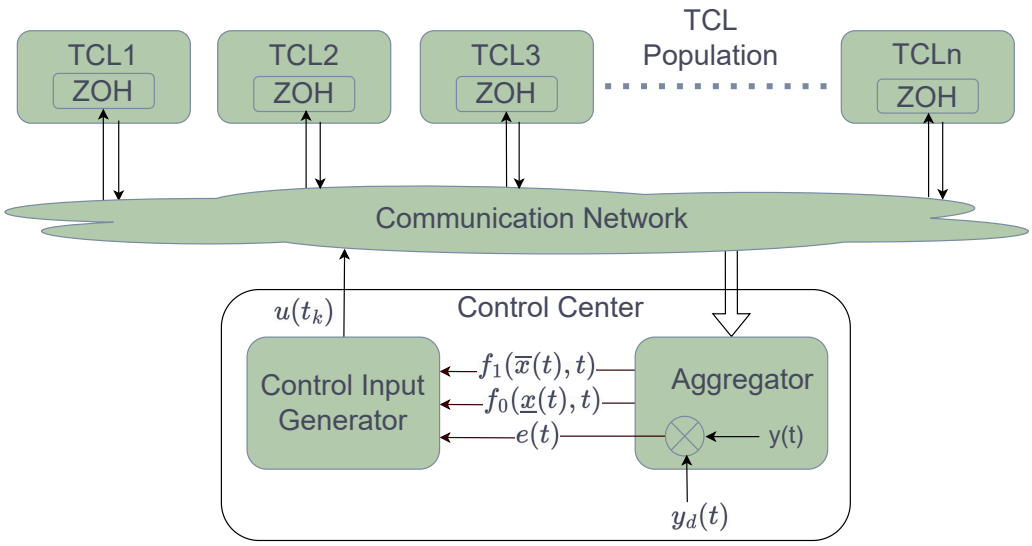

Figure 4.3 Schematics diagram of power tracking control of a TCL population.

Theorem 4.2. *The power tracking error dynamics* (4.12) *under the control law given in* (4.10) *are FTISS w.r.t.* $\Gamma(t)$ *for any* $\gamma \in (0,1)$.

Proof. Consider a Lyapunov candidate of the form $V(e) = \frac{1}{2}e^2$. The time derivative of V along the trajectory of the tracking error dynamics (4.12) is given by:

$$\begin{aligned}
\dot{V} &= e\dot{e} \\
&= e\left(-\frac{P}{\eta}k|e|^{\gamma}\mathrm{sgn}(e) + \Gamma\right) \\
&= -\frac{P}{\eta}k|e|^{1+\gamma} + e\Gamma \\
&= -\frac{P}{\eta}k\left(\sqrt{2V}\right)^{1+\gamma} + e\Gamma \\
&= -\frac{P}{\eta}k\left(2V\right)^{\frac{1+\gamma}{2}} + e\Gamma,
\end{aligned}$$

which implies that

$$DV(e)\cdot f(e,\Gamma) \leq -\frac{P}{\eta}k(2V)^{\frac{1+\gamma}{2}} + |e||\Gamma| \tag{4.20}$$

with $f(e,\Gamma) := -\frac{P}{\eta}k|e(t)|^{\gamma}\mathrm{sgn}(e(t)) + \Gamma(t)$.

Let $C_0 \in (0,k)$ be a constant. Then, for any $|e| \geq \left(\frac{\eta}{PC_0}|\Gamma|\right)^{\frac{1}{\gamma}}$, i.e., $|\Gamma| \leq \frac{P}{\eta}C_0|e|^{\gamma}$, we deduce

by (4.20) that

$$\begin{aligned} DV(e)\cdot f(e,\Gamma) &\le -\frac{P}{\eta}k(2V)^{\frac{1+\gamma}{2}} + \frac{P}{\eta}C_0|e|^{1+\gamma} \\ &= -\frac{P}{\eta}k(2V)^{\frac{1+\gamma}{2}} + \frac{P}{\eta}C_0(2V)^{\frac{1+\gamma}{2}} \\ &= -\frac{P}{\eta}(k-C_0)2^{\frac{1+\gamma}{2}}V^{\frac{1+\gamma}{2}}. \end{aligned}$$

Note that $\frac{P}{\eta}(k-C_0)2^{\frac{1+\gamma}{2}} > 0$, $\frac{1+\gamma}{2} \in (\frac{1}{2}, 1)$, and that $\chi(s) := (\frac{\eta}{PC_0}s)^{\frac{1}{\gamma}}$ is a $\mathcal{K}$-function w.r.t. $s \in \mathbb{R}_{\ge 0}$. The FTISS of system (4.12) is then guaranteed by Lemma 4.1. □

4.4.3 Properties of the governing PDEs

In practice, we can assume that the number of TCLs in a population remains unchanged within a specific DR control period. Therefore, the mass conservation property of the solutions to the system (4.4)-(4.6) should be verified under the imposed boundary conditions, thereby conforming the compliance of the mathematical model with the imposed condition. Moreover, non-negativeness of the solutions is also required.

Theorem 4.3 (Mass conservation property)**.** *The solution to the initial-boundary value problem (IBVP)* (4.4)-(4.6) *is conservative in the sense that*

$$\int_{x_L}^{\overline{x}(t)} f_0(x,t)\,\mathrm{d}x + \int_{\underline{x}(t)}^{x_H} f_1(x,t)\,\mathrm{d}x = 1 \quad \forall t \in \mathbb{R}_{\ge 0}, \tag{4.21}$$

provided that

$$\int_{x_L}^{\underline{x}(0)} f_0^{a0}(x)\,\mathrm{d}x + \int_{\underline{x}(0)}^{\overline{x}(0)} f_0^{b0}(x)\,\mathrm{d}x + \int_{\underline{x}(0)}^{\overline{x}(0)} f_1^{b0}(x)\,\mathrm{d}x + \int_{\overline{x}(0)}^{x_H} f_1^{c0}(x)\,\mathrm{d}x = 1. \tag{4.22}$$

Proof. Using (4.4a), (4.4b), (4.8a), (4.8b), and (4.8d), and noting (U) and (F2), we have

$$\begin{aligned} \frac{\mathrm{d}}{\mathrm{d}t}\left(\int_{x_L}^{\overline{x}(t)} f_0(x,t)\,\mathrm{d}x\right) =& \frac{\mathrm{d}}{\mathrm{d}t}\left(\int_{x_L}^{\underline{x}(t)} f_0(x,t)\,\mathrm{d}x + \int_{\underline{x}(t)}^{\overline{x}(t)} f_0(x,t)\,\mathrm{d}x\right) \\ =& \int_{x_L}^{\underline{x}(t)} \partial_t f_0(x,t)\,\mathrm{d}x + f_0(\underline{x}(t),t)\dot{\underline{x}}(t) + \int_{\underline{x}(t)}^{\overline{x}(t)} \partial_t f_0(x,t)\,\mathrm{d}x \\ &+ f_0(\overline{x}(t),t)\dot{\overline{x}}(t) - f_0(\underline{x}(t),t)\dot{\underline{x}}(t) \\ =& \int_{x_L}^{\underline{x}(t)} \partial_x\left(\frac{\sigma^2}{2}\partial_x f_0(x,t) - (\alpha_0(x,t)-u(t))f_0(x,t)\right)\mathrm{d}x \end{aligned} \tag{4.23}$$

$$
\begin{aligned}
&+\int_{\underline{x}(t)}^{\overline{x}(t)}\partial_x\left(\frac{\sigma^2}{2}\partial_x f_0(x,t)-(\alpha_0(x,t)-u(t))f_0(x,t)\right)\mathrm{d}x\\
&-\int_{\underline{x}(t)}^{\overline{x}(t)} g(f_0,f_1)\,\mathrm{d}x\\
=&\left(\frac{\sigma^2}{2}\partial_x f_0(x,t)-(\alpha_0(x,t)-u(t))f_0(x,t)\right)\Big|_{x_L^+}^{\underline{x}^-(t)}\\
&+\left(\frac{\sigma^2}{2}\partial_x f_0(x,t)-(\alpha_0(x,t)-u(t))f_0(x,t)\right)\Big|_{\underline{x}^+(t)}^{\overline{x}^-(t)}\\
&-\int_{\underline{x}(t)}^{\overline{x}(t)} g(f_0,f_1)\,\mathrm{d}x\\
=&\frac{\sigma^2}{2}\partial_x f_0(\underline{x}^-(t),t)-(\alpha_0(\underline{x}(t))-u(t))f_0(\underline{x}(t),t)-0\\
&+\frac{\sigma^2}{2}\partial_x f_0(\overline{x}^-(t),t)-(\alpha_0(\overline{x}(t))-u(t))f_0(\overline{x}(t),t)\\
&-\left(\frac{\sigma^2}{2}\partial_x f_0(\underline{x}^+(t),t)-(\alpha_0(\underline{x}(t))-u(t))f_0(\underline{x}(t),t)\right)\\
&-\int_{\underline{x}(t)}^{\overline{x}(t)} g(f_0,f_1)\,\mathrm{d}x\\
=&\frac{\sigma^2}{2}(\partial_x f_0(\underline{x}^-(t),t)-\partial_x f_0(\underline{x}^+(t),t))\\
&+\frac{\sigma^2}{2}\partial_x f_0(\overline{x}^-(t),t)-\int_{\underline{x}(t)}^{\overline{x}(t)} g(f_0,f_1)\,\mathrm{d}x\\
=&\frac{\sigma^2}{2}\partial_x f_1(\underline{x}^+,t)+\frac{\sigma^2}{2}\partial_x f_0(\overline{x}^-(t),t)-\int_{\underline{x}(t)}^{\overline{x}(t)} g(f_0,f_1)\,\mathrm{d}x.
\end{aligned}
$$

Similarly, we infer from (4.4c), (4.4d), (4.8e), (4.8g), (4.8h), (U), and (F3) that

$$
\begin{aligned}
&\frac{\mathrm{d}}{\mathrm{d}t}\left(\int_{\underline{x}(t)}^{x_H} f_1(x,t)\,\mathrm{d}x\right)\\
=&\frac{\mathrm{d}}{\mathrm{d}t}\left(\int_{\underline{x}(t)}^{\overline{x}(t)} f_1(x,t)\,\mathrm{d}x+\int_{\overline{x}(t)}^{x_H} f_1(x,t)\,\mathrm{d}x\right)\\
=&-\frac{\sigma^2}{2}\partial_x f_1(\underline{x}^+,t)-\frac{\sigma^2}{2}\partial_x f_0(\overline{x}^-(t),t)+\int_{\underline{x}(t)}^{\overline{x}(t)} g(f_0,f_1)\,\mathrm{d}x.
\end{aligned}
\tag{4.24}
$$

By (4.23) and (4.24), we obtain

$$
\frac{\mathrm{d}}{\mathrm{d}t}\left(\int_{x_L}^{\overline{x}(t)} f_0(x,t)\,\mathrm{d}x+\int_{\underline{x}(t)}^{x_H} f_1(x,t)\,\mathrm{d}x\right)=0\quad\forall t\in\mathbb{R}_{\geq 0},
$$

which along with (4.22) implies (4.21). □

Theorem 4.4 (Non-negativeness)**.** *The following statements hold true for the solution to IBVP* (4.4)-(4.6)*:*

(i) $f_0(x,t) \geq 0$ *for all* $x \in [x_L, \overline{x}(t)]$ *and all* $t \in \mathbb{R}_{\geq 0}$*;*

(ii) $f_1(x,t) \geq 0$ *for all* $x \in [\underline{x}(t), x_H]$ *and all* $t \in \mathbb{R}_{\geq 0}$*;*

(iii) $f_0(\underline{x}(t),t) + f_1(\overline{x}(t),t) > 0$ *for all* $t \in \mathbb{R}_{>0}$*.*

The proof of this theorem is provided in Appendix 4.7.

4.5 Simulation study

In this section, we present the results obtained in simulation study to demonstrate the effectiveness of the proposed control scheme. Note that the control law given in (4.10) is derived from the coupled Fokker-Planck equations, which assume a population of an infinite number of TCLs. Therefore, the larger the population size, the more accurate the PDE model. Consequently, a better performance can be expected for populations with larger numbers. To illustrate this property, we consider in the simulation two heterogeneous populations, with 1,000 and 100,000 TCLs respectively. To quantitatively evaluate the control performance, root-mean-square error (RMSE) is used to measure the average tracking errors.

4.5.1 Simulation setup

A numerical simulation is conducted to validate the proposed control scheme and evaluate its performance. Table 4.1 lists the physical parameters of the AC units utilized in the simulation, which are the same as those in [24]. The thermal capacitances of the TCLs in the population follow the log-normal distribution with a mean value of 10 kWh/°C and a standard deviation of 2 kWh/°C. The thermal resistances of the TCLs also follow the log-normal distribution with a mean value of 2 °C/kW and a standard deviation of 0.4 °C/kW. This results in a heterogeneity described by σ in the Fokker-Planck equations (4.4) [24, 145]. Nevertheless, as mentioned in Remark 4.4, the implementation of the proposed robust control scheme is independent of the value of σ. In our experiment, the initial temperatures of the AC units are uniformly distributed around the initial set-point $x_{\text{sp}}^0 = 20$°C over the deadband, and initially 40% of the AC units are set randomly in the ON-state. This setting causes the population to begin running from an almost steady state.

The disturbances brought into the system come mainly from the following three sources. First, all AC units operate under the same varying outside temperature, as depicted in

Table 4.1 Simulation parameter

Parameter	Description (Unit)	Value
R	average thermal resistance (°C/kW)	2
C	average thermal capacitance (kWh/°C)	10
P	electric power (kW)	14
η	load efficiency	2.5
x_{sp}^0	initial temperature set-point (°C)	20
δ	temperature deadband width (°C)	0.5
p_f	forced switch probability per hour (%)	3
t_{ci}	control interval (second)	30
t_{lock}	locked time of each TCL (minute)	6

Fig. 4.4, which rises from 30°C at 11:30 to 23°C at 12:30 and then drops back from 14:30 to 15:30. Second, a forced random switch mechanism is added to desynchronize AC operations. The number of forced interrupts per hour can be adjusted through the hyper-parameter p_f. Moreover, a safe border distance of 5% of the deadband width is incorporated to prevent forced switches from happening when an AC is around $\overline{x}(t)$ and in "ON" state or around $\underline{x}(t)$ and in "OFF" state. Finally, because frequent switching leads to reduced energy efficiency and more rapid compressor wear out, a lockout time, t_{lock}, is included for each AC. Thus, an AC unit remains inactive to the control signals when it is locked.

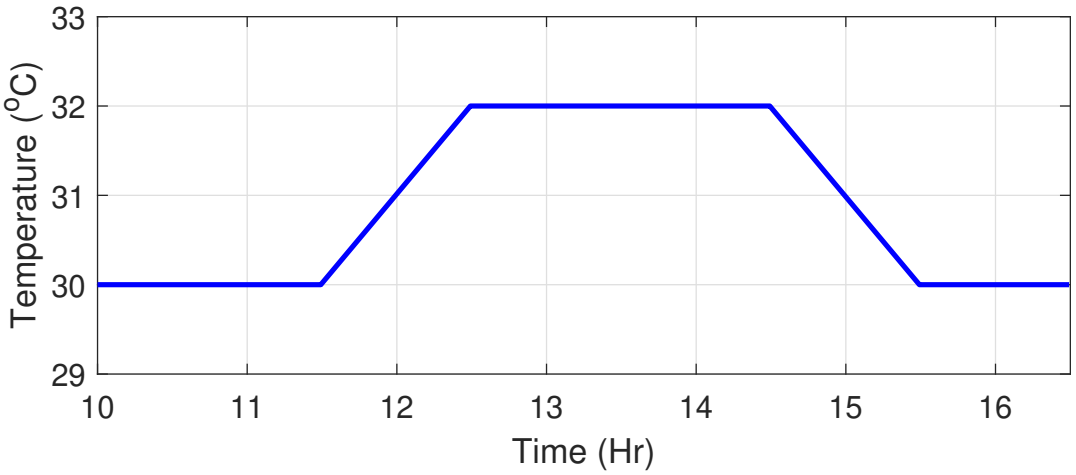

Figure 4.4 Ambient temperature.

The reference power is a predefined curve, as shown in Fig. 4.5, which is chosen arbitrarily. From 10:30 to 11:30, the normalized desired power is maintained constant at 0.4. From 11:30 to 12:00, the reference power drops to 0.2 and keeps constant for the following two and a half hours. From 14:30, the desired power rises to 0.5 in 30 minutes and remains constant until

16:30. During the rising and dropping phases, the desired power is specified by a smooth polynomial with the endpoint constraints given below:

$$y_d(t) = (y_d(t_f) - y_d(t_i))\,\tau^5(t) \sum_{l=0}^{4} a_l \tau^l(t), t \in [t_i, t_f], \tag{4.25}$$

$$\dot{y}_d(t_i) = \dot{y}_d(t_f) = \ddot{y}_d(t_i) = \ddot{y}_d(t_i) = \dddot{y}_d(t_i) = \dddot{y}_d(t_f) = 0, \tag{4.26}$$

where t_i and t_f are, respectively, the starting and ending times, and $\tau(t) := (t - t_i)/(t_f - t_i)$. By a direct computation, the coefficients can be determined as follows:

$$a_0 = 126,\ a_1 = 420,\ a_2 = 540,\ a_3 = 315, \text{ and } a_4 = 70.$$

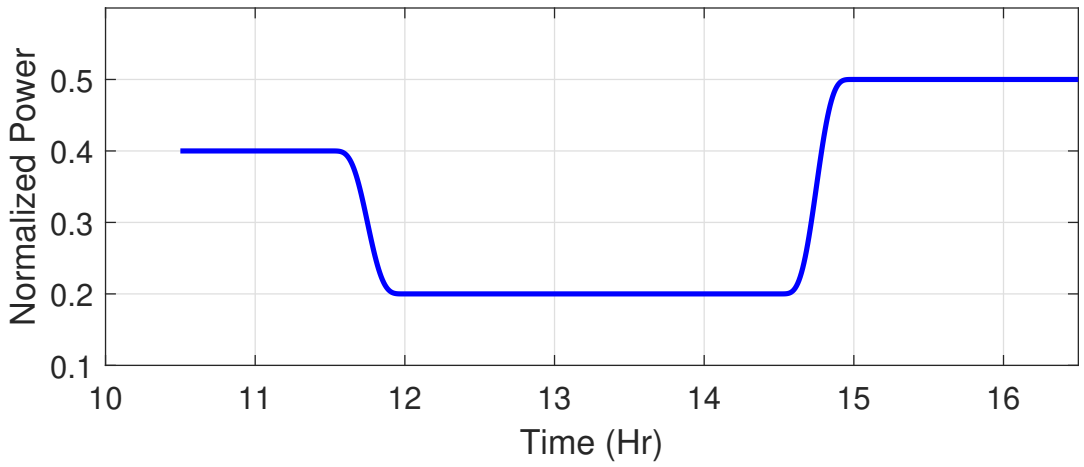

Figure 4.5 Desired power profile.

In the simulation, the control signal is updated every 30 seconds (t_{ci} in Table 4.1). The control signal that every AC receives is the set-point variation rate. To compute the denominator of the controller given in (4.10), a mid-point rectangular method with a temperature bin width δ_x is used to estimate $f_1(\overline{x}(t_k), t_k)$ and $f_0(\underline{x}(t_k), t_k)$. The percentage of ACs falling in the rectangular region is used as $f_1(\overline{x}(t_k), t_k) \times \delta_x$ or $f_0(\underline{x}(t_k), t_k) \times \delta_x$. In general, δ_x should not be too large because the underlying system has complex nonlinear dynamics. On the other hand, considering the limited number of ACs involved in the simulation, the bin width δ_x should not be too small, which may introduce larger biases. In our implementation, histogram bin widths of 0.008°C, 0.004°C, and 0.002°C are used, which are reasonable and provide reliable estimations of $f_1(\overline{x}(t_k), t_k)$ and $f_0(\underline{x}(t_k), t_k)$. Note that the mid-point rule

only requires partially observed states of the population distributions, which is a great relief of the communication burden.

4.5.2 Numerical results and analysis

First, we present the test results for the population with 1,000 TCLs. The control cycle lasts for 6 hours, from 10:30 to 16:30. The test is performed continuously for 10 episodes, and the tracking performance is measured by the RMSE, as reported in Table 4.2. In the test, the controller parameters in (4.10) are set to be $k = 8$ and $\gamma = 0.5$, respectively. The final result shows that the mean RMSE for this setting is 0.896%, and the standard deviation (STD) of the RMSEs is 0.040%.

Table 4.2 Tracking performance of 10 episodes for the population with 1,000 TCLs

Episode	1	2	3	4	5
RMSE (%)	0.948	0.923	0.844	0.834	0.935
Episode	6	7	8	9	10
RMSE (%)	0.880	0.923	0.890	0.925	0.861

Figure 4.6 shows a sample of the control results corresponding to the episode with an RMSE of 0.948%. It can be seen from Fig. 4.6a that the proposed control strategy is effective. The temperature evolution of 10 randomly selected ACs in the population is presented in Fig. 4.6b. It can be observed that all of them, unless forced switches occur, operate smoothly inside the deadband between the turning-on and turning-off points. Figure 4.6c shows the control signal generated during this episode. During the first 30 minutes (from 10:00 to 10:30), the controller is inactive, and the system operates in an open-loop mode. The control loop is closed at 10:30. It can be observed that the amplitude of the control signal may vary importantly in transient state or when the reference power raises or drops rapidly.

When the number of ACs increases, the model of the coupled Fokker-Planck equations becomes more accurate. To evaluate the effectiveness of the proposed control strategy, tracking control performance is examined for a population of 100,000 ACs. The RMSE values for 10 continuous tests are shown in Table 4.3, which gives a mean RMSE of 0.497% and an STD of 0.004%. In this test, $k = 15$ and $\gamma = 0.5$ are used. Figure 4.7 illustrates one of the control samples corresponding to the episode with an RMSE of 0.505%. The normalized power consumption is shown in Fig. 4.7a, and the temperature evolutions of 10 ACs are shown in Fig. 4.7b. The control signal is shown in Fig. 4.7c.

The results of the comparative study show clearly that the tracking control system performs

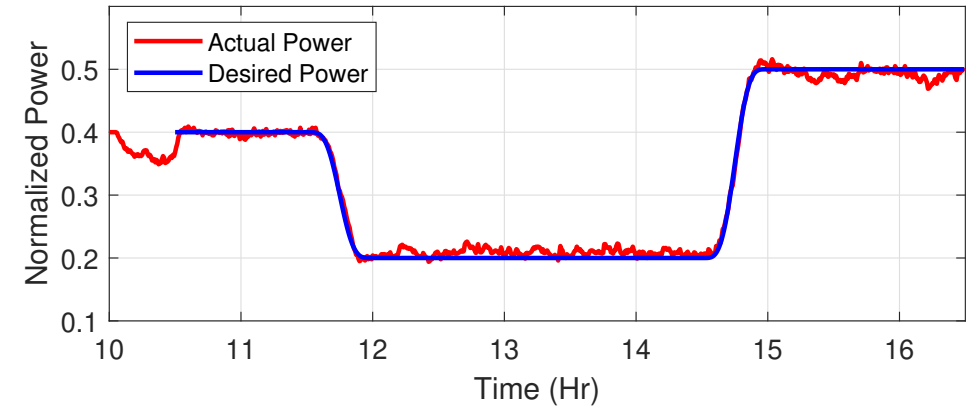

(a)

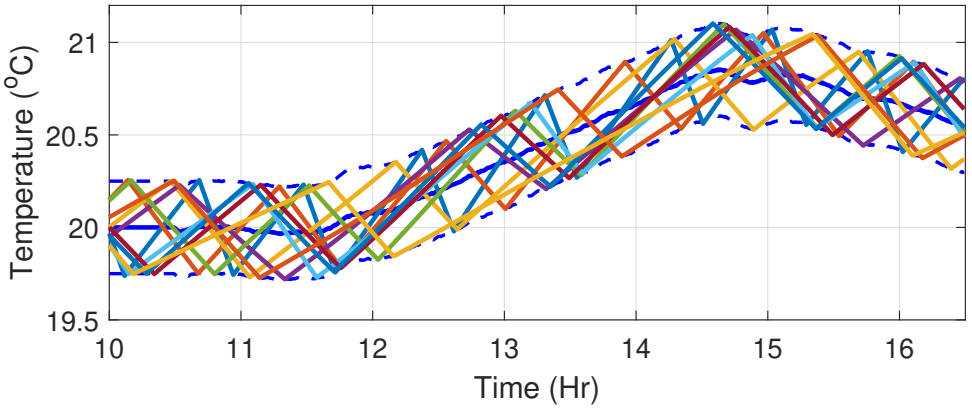

(b)

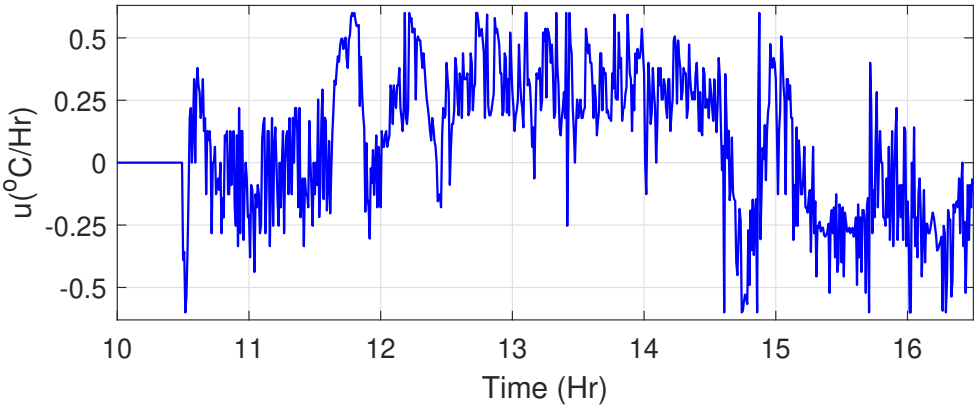

(c)

Figure 4.6 Control performance for a population of 1,000 TCLs: (a) tracking performance; (b) temperature trajectories of 10 ACs; (c) set-point variation rate.

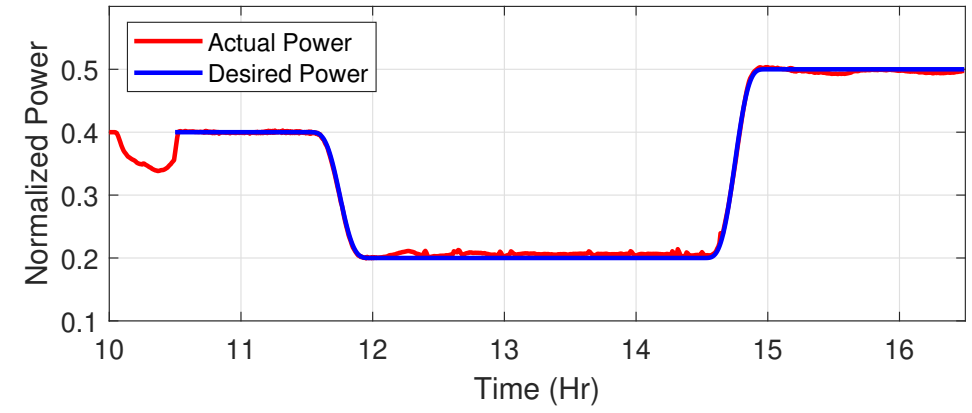

(a)

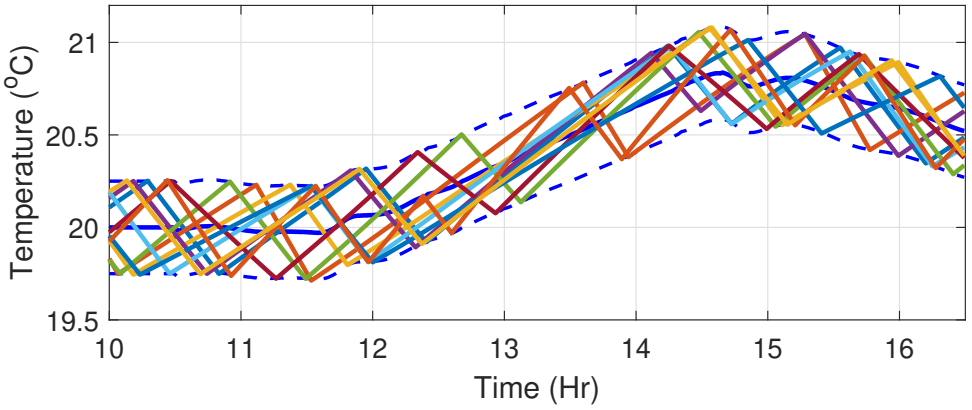

(b)

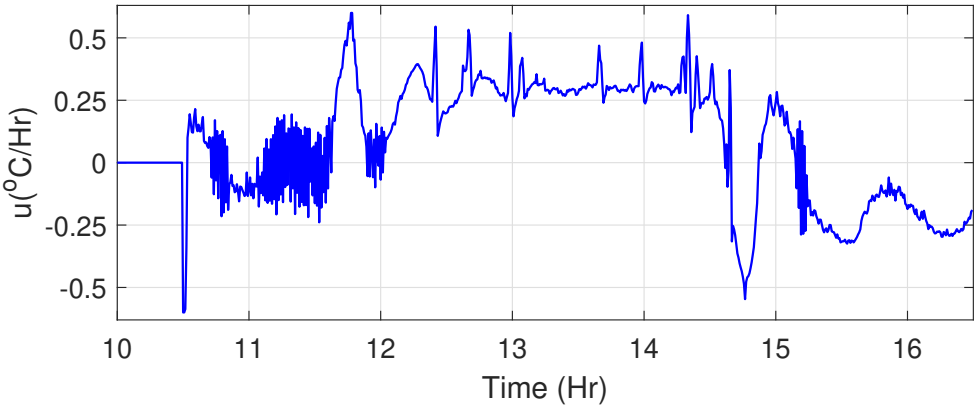

(c)

Figure 4.7 Control performance for a population of 100,000 TCLs: (a) tracking performance; (b) temperature trajectories of 10 ACs; (c) set-point variation rate.

Table 4.3 Tracking performance of 10 episodes for the population with 100,000 TCLs

Episode	1	2	3	4	5
RMSE (%)	0.505	0.500	0.496	0.491	0.490
Episode	6	7	8	9	10
RMSE (%)	0.497	0.499	0.495	0.498	0.500

better for the population of larger size with smaller RMSE, smoother power trajectory, and less "noisy" control signals. This is consistent with the nature of the PDE model on which the proposed control scheme is based. Nevertheless, the performance is not significantly degraded for a population with a significantly smaller size. This demonstrates the robustness and potential applicability of the developed control strategy to practical systems.

4.6 Conclusion

In this work, we have developed a strategy for power tracking control of heterogeneous TCL populations based on a PDE model. It is shown that the proposed control scheme can ensure a robust performance in the presence of modeling uncertainties in the sense of FTISS and requires measuring the states of the system only on the end-points of the deadband. The simulation results provided encouraging evidence that the proposed control approach is highly effective. However, great challenges still exist for deploying this control scheme for real world applications. Particularly, the Fokker-Planck equations can only describe TCL populations with a limited heterogeneity and hence, they cannot capture populations involving different type of devices or systems. Moreover, power tracking is only a task in demand response programs. Therefore, coordinating with other systems in the grid, such as distributed power generation [232] and energy storage [5], or other demand-response tasks, such as frequency regulation or transaction controls [82, 101, 103, 149, 210], is still a challenging problem. These issues will be considered in our future work.

4.7 Appendix: Proof of Theorem 4.4

We first prove statement (i). Given any $T > 0$, it suffices to show that $f_0 \geq 0$ over $[x_L, \overline{x}(t)] \times [0, T]$ for all $t \in [0, T]$.

Indeed, the transformations of variable $y := \frac{x - x_L}{\overline{x} - x_L} := \frac{x - x_L}{h}$ and $f_0(x, t) = f_0(yh + x_L, t) :=$

$\tilde{f}_0(y,t)$ yield

$$\begin{aligned}
\partial_x f_0 &= \frac{1}{h}\partial_y \tilde{f}_0, \\
\partial_{xx} f_0 &= \frac{1}{h^2}\partial_{yy}\tilde{f}_0, \partial_t f_0 \\
&= \partial_t \tilde{f}_0 + \partial_y \tilde{f}_0 \frac{\partial y}{\partial t} \\
&= \partial_t \tilde{f}_0 - (x - x_L)\frac{\dot{\bar{x}}}{h^2}\partial_y \tilde{f}_0 \\
&= \partial_t \tilde{f}_0 - \frac{1}{h} yu \partial_y \tilde{f}_0.
\end{aligned}$$

Note that

$$x \in [x_L, \underline{x}] \Leftrightarrow y \in [0,1], 0 < \delta_0 \leq h(t) \leq x_H - x_L, \forall t \in [0,T].$$

The PDEs (4.4a) and (4.4b) are equivalent to

$$\partial_t \tilde{f}_0 - \frac{1}{h}\left(\frac{\sigma^2}{2h}\partial_{yy}\tilde{f}_0 + ((1+y)u - \tilde{\alpha}_0)\,\partial_y \tilde{f}_0 - \tilde{\alpha}_{0y}\tilde{f}_0\right) = 0, \quad \forall y \in (0, z(t)), \forall t \in (0,T], \tag{4.27a}$$

$$\partial_t \tilde{f}_0 - g(\tilde{f}_0, \tilde{f}_1) - \frac{1}{h}\left(\frac{\sigma^2}{2h}\partial_{yy}\tilde{f}_0 + ((1+y)u - \tilde{\alpha}_0)\,\partial_y \tilde{f}_0 - \tilde{\alpha}_{0y}\tilde{f}_0\right) = 0, \quad \forall y \in (z(t), 1), \forall t \in (0,T], \tag{4.27b}$$

respectively, where $\tilde{\alpha}_0(y,t) := \alpha_0(yh(t) + x_L, t)$, $f_1(x,t) = f_1(yh + x_L, t) := \tilde{f}_1(y,t)$, and $z(t) := 1 - \frac{\delta_0}{h(t)}$.

Note that (4.8) is equivalent to (4.5), and (4.8a), (4.8b), and (4.8d) become

$$\frac{\sigma^2}{2}\partial_y \tilde{f}_0(0^+, t) - (\tilde{\alpha}_0(0^+, t) - u(t))h(t)\tilde{f}_0(0^+, t) = 0, \ \forall t \in (0,T], \tag{4.28a}$$

$$\partial_y \tilde{f}_0\left(z^-(t), t\right) - \partial_y \tilde{f}_0\left(z^+(t), t\right) = \sigma_0(t), \ \forall t \in (0,T], \tag{4.28b}$$

$$\tilde{f}_0(1^-, t) = 0 \ \forall t \in (0,T], \tag{4.28c}$$

where, for the given solution f_1, $\sigma_0(t) := \frac{\sigma^2}{2}\partial_x f_1(\underline{x}^+(t), t)$ is a well-defined function w.r.t. t, and $\sigma_0(t) > 0$ for all $t \in [0,T]$ owing to (F3) and (4.8i).

The initial data of $\tilde{f}_0$ over the domain $[0, z(t)]$ and $[z(t), 1]$ are given by

$$\tilde{f}_0^{a0}(y) := f_0^{a0}(yh(0) + x_L) \geq 0,$$

and

$$\tilde{f}_0^{b0}(y) := f_0^{b0}(yh(0) + x_L) \geq 0,$$

respectively.

Let $\phi(y) := e^{m(y-\frac{1}{2})^2}$ and $\tilde{f}_0 := \phi e^{\gamma t}\hat{f}_0$ with $m > 0$ and $\gamma > 0$ being constants that will be chosen later. Then (4.27) and (4.28) lead to

$$\partial_t \hat{f}_0 - \frac{\sigma^2}{2h^2}\partial_{yy}\hat{f}_0 + \mathcal{B}(y,t)\partial_y \hat{f}_0 + \mathcal{C}(y,t)\hat{f}_0 = 0, \quad \forall y \in (0, z(t)), \forall t \in (0,T], \tag{4.29a}$$

$$\partial_t \hat{f}_0 - \frac{\sigma^2}{2h^2}\partial_{yy}\hat{f}_0 + \mathcal{B}(y,t)\partial_y \hat{f}_0 + \mathcal{C}(y,t)\hat{f}_0 + \frac{e^{-\gamma t}}{\phi(y)} g(\tilde{f}_0, \tilde{f}_1) = 0,$$
$$\forall y \in (z(t), 1), \forall t \in (0,T], \tag{4.29b}$$

$$\frac{\sigma^2}{2}\partial_y \hat{f}_0(0^+, t) - k(t)\hat{f}_0(0^+, t) = 0, \quad \forall t \in (0,T], \tag{4.29c}$$

$$\partial_y \hat{f}_0\left(z^-(t), t\right) - \partial_y \hat{f}_0\left(z^+(t), t\right) = \hat{\sigma}_0(t), \quad \forall t \in (0,T], \tag{4.29d}$$

$$\hat{f}_0(1^-, t) = 0, \quad \forall t \in (0,T], \tag{4.29e}$$

where

$$\begin{aligned}
\mathcal{B}(y,t) :=& -\frac{1}{h}\left(\frac{\sigma^2}{2h}\frac{2\partial_y \phi}{\phi} + (1+y)u - \tilde{\alpha}_0\right), \\
\mathcal{C}(y,t) :=& \frac{1}{h}\left(\gamma - \frac{\sigma^2}{2h}\frac{\partial_{yy}\phi}{\phi} - \frac{\partial_y \phi}{\phi}\left((1+y)u - \tilde{\alpha}_0\right) + \tilde{\alpha}_{0y}\right), \\
k(t) :=& \frac{m\sigma^2}{2} + (\tilde{\alpha}_0(0^+, t) - u(t))h(t), \\
\hat{\sigma}_0(t) :=& \frac{e^{-\gamma t}}{\phi(1)}\sigma_0(t).
\end{aligned}$$

The initial data for the $\hat{f}_0$-system over the domain $[0, z(t)]$ and $[z(t), 1]$ are given by

$$\hat{f}_0^{a0}(y) := \frac{\tilde{f}_0^{a0}(y)}{\phi(y)} \geq 0 \quad \text{and} \quad \hat{f}_0^{b0}(y) := \frac{\tilde{f}_0^{b0}(y)}{\phi(y)} \geq 0, \tag{4.30}$$

respectively.

Note that $u, \tilde{\alpha}_0$, and $\tilde{\alpha}_{0y}$ are continuous in $[0,1] \times [0,T]$. Letting first m and then γ be

sufficiently large, there must be positive constants k_0 and c_0 such that

$$k(t) \geq k_0, \forall t \in (0, T], \tag{4.31}$$
$$\mathcal{C}(y,t) - 1 \geq c_0, \forall (y,t) \in (0,1) \times (0,T]. \tag{4.32}$$

To prove the non-negativeness property of f_0, it suffices to show that $\hat{f}_0 \geq 0$ in $[0,1] \times [0,T]$. We now proceed with the proof by contradiction. Assume that there exists a point $(y_0, t_0) \in [0,1] \times [0,T]$ such that

$$\hat{f}_0(y_0, t_0) = \min_{(y,t) \in [0,1] \times [0,T]} \hat{f}_0(y,t) < 0.$$

Considering (4.29e) and (4.30), we have $y_0 \neq 1$ and $t_0 \in (0,T]$.

Case 1: $y_0 \in (0, z(t_0))$. At point (y_0, t_0), it holds that

$$\partial_t \hat{f}_0(y_0,t_0) \leq 0, \partial_y \hat{f}_0(y_0,t_0) = 0, \partial_{yy} \hat{f}_0(y_0,t_0) \geq 0.$$

Then (4.29a) and (4.32) imply that

$$\begin{aligned} 0 > (c_0 + 1)\, \hat{f}_0(y_0,t_0) \geq{}& \partial_t \hat{f}_0(y_0,t_0) - \frac{\sigma^2}{2h^2(t_0)} \partial_{yy} \hat{f}_0(y_0,t_0) \\ &+ \mathcal{B}(y_0,t_0) \partial_y \hat{f}_0(y_0,t_0) + \mathcal{C}(y_0,t_0) \hat{f}_0(y_0,t_0) \\ ={}& 0, \end{aligned}$$

which leads to a contradiction.

Case 2: $y_0 \in (z(t_0), 1)$. At the point (y_0, t_0), it also holds that

$$\partial_t \hat{f}_0(y_0,t_0) \leq 0, \partial_y \hat{f}_0(y_0,t_0) = 0, \partial_{yy} \hat{f}_0(y_0,t_0) \geq 0.$$

In addition, using the Mean Value Theorem, (G1), and (G2), we obtain:

$$\begin{aligned} & g(\tilde{f}_0(y_0,t_0), \tilde{f}_1(y_0,t_0)) \\ ={}& g(0, \tilde{f}_1(y_0,t_0)) + \tilde{f}_0(y_0,t_0) g_s(s, \tilde{f}_1(y_0,t_0))|_{s=\xi} \\ \leq{}& |\tilde{f}_0(y_0,t_0)|, \end{aligned}$$

where ξ is between 0 and $\tilde{f}_0(y_0,t_0)$.

It follows that

$$\frac{e^{-\gamma t_0}}{\phi(y_0)} g(\tilde{f}_0(y_0,t_0), \tilde{f}_1(y_0,t_0)) \leq |\tilde{f}_0(y_0,t_0)| \frac{e^{-\gamma t_0}}{\phi(y_0)} = -\hat{f}_0(y_0,t_0). \tag{4.33}$$

From (4.29b), (4.32), and (4.33), we obtain:

$$\begin{aligned}
0 >& c_0 \hat{f}_0(y_0,t_0) \\
\geq& \left(\mathcal{C}(y_0,t_0) - 1\right) \hat{f}_0(y_0,t_0) \\
\geq& \mathcal{C}(y_0,t_0)\hat{f}_0(y_0,t_0) + \frac{e^{-\gamma t_0}}{\phi(y_0)} g(\tilde{f}_0(y_0,t_0), \tilde{f}_1(y_0,t_0)) \\
\geq& \partial_t \hat{f}_0(y_0,t_0) - \frac{\sigma^2}{2h^2(t_0)} \partial_{yy}\hat{f}_0(y_0,t_0) + \frac{e^{-\gamma t_0}}{\phi(y_0)} g(\tilde{f}_0(y_0,t_0), \tilde{f}_1(y_0,t_0)) \\
&+ \mathcal{B}(y_0,t_0)\partial_y \hat{f}_0(y_0,t_0) + \mathcal{C}(y_0,t_0)\hat{f}_0(y_0,t_0) \\
=& 0,
\end{aligned}$$

which leads to a contradiction.

Case 3: $y_0 = 0$. It follows that $\partial_y \hat{f}_0(0^+,t_0) \geq 0$, which, along with (4.29c) and (4.31), yields

$$0 < -k_0 \hat{f}_0(0^+,t_0) \leq -k(t_0)\hat{f}_0(0^+,t_0) \leq \frac{\sigma^2}{2}\partial_t \hat{f}_0(0^+,t) - k(t_0)\hat{f}_0(0^+,t) = 0.$$

We get a contradiction.

Case 4: $y_0 = 1$. It follows that $\partial_y \hat{f}_0(1^+,t_0) \leq 0$, which along with (4.29c) and (4.31) yields

$$0 < -k_0 \hat{f}_0(0^+,t_0) \leq -k(t_0)\hat{f}_0(0^+,t_0) \leq \frac{\sigma^2}{2}\partial_y \hat{f}_0(0^+,t) - k(t_0)\hat{f}_0(0^+,t) = 0.$$

We get a contradiction.

Case 5: $y_0 = z(t_0)$. It follows that $\partial_y \hat{f}_0(z^-(t_0),t_0) \leq 0$ and $\partial_y \hat{f}_0(z^+(t_0),t_0) \geq 0$, which along with (4.29d) and $\hat{\sigma}_0(t) > 0$ yields

$$0 \geq \partial_y \hat{f}_0(z^-(t_0),t_0) - \partial_y \hat{f}_0(z^+(t_0),t_0) = \hat{\sigma}_0(t_0) > 0,$$

leading to a contradiction.

Because we always obtain a contradiction in each case, we have shown that $\hat{f}_0 \geq 0$ over the domain $[0,1] \times [0,T]$, which implies the non-negativeness property of f_0 over the domain $[x_L, \overline{x}(t)] \times [0,T]$ for all $t \in [0,T]$ and all $T \in \mathbb{R}_{>0}$.

Because the proof of statement (ii) can proceed in the same way as above, we omit the details

of the proof.

Finally, suppose that statement (iii) fails to be true; then, for any given $T \in \mathbb{R}_{>0}$ there must be a $t_0 \in (0, T]$ such that

$$f_0(\underline{x}(t_0), t_0) + f_1(\overline{x}(t_0), t_0) = 0,$$

which, along with the non-negativeness property of f_0 and f_1, implies that f_0 and f_1 attain their minima at $(\underline{x}(t_0), t_0)$ and $(\overline{x}(t_0), t_0)$, respectively. Then, using the same argument as that in *Case 5*, we obtain a contradiction. Therefore, statement (iii) holds true.

CHAPTER 5 ARTICLE 2: EVENT-TRIGGERED POWER TRACKING CONTROL OF HETEROGENEOUS TCL POPULATIONS

Zhenhe Zhang, Jun Zheng, Guchuan Zhu
Published in: IEEE Transactions on Smart Grid
Publication date: January 09, 2024

Abstract

This paper presents a study on event-triggered power tracking control of heterogeneous thermostatically controlled load (TCL) populations. The developed schemes are based on continuous-time tracking control of TCL populations of which the aggregated dynamics are described by coupled Fokker-Planck equations. Two event-triggering mechanisms, namely static and dynamic event-triggered control strategies, are proposed, which can guarantee the input-to-state practical stability (ISpS) of the tracking error dynamics while excluding Zeno phenomenon. A simulation study is conducted, and the obtained results show that the developed control strategies can significantly reduce the communication burden while still offering a satisfactory control performance.
keywords heterogeneous thermostatically controlled loads, coupled Fokker-Planck equations, event-triggered control, input-to-state practical stability.

5.1 Introduction

Demand response (DR) programs, together with flourishing smart-grid technologies, are creating more sustainable, resilient, and efficient power systems. The paradigm of DR allows the consumers to be actively engaged into power consumption management, offering cost-effective solutions for eliminating electricity supply-demand discrepancies. It is noted that there exist a great variety of DR programs [66, 173, 196, 213]. The focus of the present work is placed on managing populations of thermostatically controlled loads (TCLs), such as air conditioning units, refrigerators, heat pumps, etc., as demand-response resources capable of providing ancillary services, including peak-load shaving, load shifting, frequency regulation, etc., see, e.g., [38, 58, 120, 124, 129, 161, 191]. In this context, a heterogeneous TCL population refers to an ensemble of thermal devices of the same type with potentially different parameters [21, 24, 55, 116, 117, 126, 178, 193, 198, 215, 224].

As a promising distributed DR resource, TCLs are usually geographically spread over a wide

area and are connected via communication networks for information exchange. Based on the information flow in the population, there are roughly three control paradigms, i.e., centralized control, decentralized control, and distributed control. In this work, a decentralized control strategy is adopted, where a central unit, also called an aggregator, is responsible of managing the power consumption of the TCL population by controlling the temperature set-point. Concerning the control design for a TCL population, some popular aggregated models are proposed to characterize the underlying dynamics, including coupled Fokker-Planck (CFP) equation models [21, 24, 55, 126, 193, 224], state-bins models [178, 215], state-queuing models [116, 117, 198] and so on. It should be noted that in the existing literature, the controllers designed based on these models are of continuous time and will use periodically sampled data in their implementation. Therefore, the control signals need to be broadcast to the entire population periodically.

Obviously, continuously or periodically delivering control signals generates heavy communication burdens. Moreover, a synchronized periodical data exchange is infeasible for nearly all the practical applications that involve communication networks spread over a wide geographical region. Event-triggered control (ETC), which requires only to update the control signals when a certain triggering event occurs, is then developed as a solution to overcome this difficulty [72, 98, 139]. In the literature, threshold-based signals are one of the commonly used triggering conditions. Different types of threshold signals are available, including fixed threshold, relative threshold [186, 217], switching threshold [205], and dynamic threshold [52,56,160]. Among the aforementioned triggering mechanisms, dynamic threshold strategies have attracted much attention in recent years. Compared with static event-triggering schemes, auxiliary variables are additionally incorporated in the triggering threshold function, which can usually enlarge inter-event intervals and thus enable more flexible and effective resource utilization. Note that, to ensure the control performance, the closed-loop systems need to possess certain robust stability properties, in particular, they should be input-to-state stable (ISS) with respect to (w.r.t.) disturbances representing the effect of aperiodic sampling [56, 186]. Moreover, considering uncertainties in practical applications, a more realistic requirement is that the closed-loop system should be input-to-state practically stable (ISpS) w.r.t. the disturbances [87, 181]. It should be mentioned that the notion of ISS and its variations, including ISpS, play a vital role in robust control system design and analysis, allowing for characterizing the robust stability of a system w.r.t. disturbances induced by, e.g., external perturbations, modeling errors, and parametric uncertainties, as well as those introduced in control system implementations, such as measurement and actuation noises, sampling and quantization errors, and delays [138, 180].

The aim of this work is to develop ETC schemes for power tracking of heterogeneous TCL

populations. To this goal, we adopt the emulation approach. Specifically, we choose first a modified version of the continuous-time control scheme presented in [220]. Then, a static event-triggering mechanism, which combines fixed threshold and relative threshold signals, is proposed. We show that the ISpS of the closed-loop system with this triggering scheme can be achieved and the Zeno phenomenon is excluded from this triggering scheme. Furthermore, a dynamic event-triggering strategy, derived from the static one, is developed. The closed-loop stability and enlarged inter-execution time properties are investigated. Finally, numerical simulation is conducted to evaluate the proposed event-trigged control schemes. It should be noted that although it has been shown in the recent literature that event-triggered paradigm is beneficial to different problems in power systems control, see, e.g., [30,31,85,106,111,218], to the best of authors' knowledge, the present work is the first attempt to apply this method to the control of TCL populations for power tracking.

The main contributions of this work can be summarized as follows:

- An input-output linearization control law, which requires only partial measurement of the system state on the end-points of the temperature deadband, has been developed for power tracking control of heterogeneous TCL populations described by CFP equations.
- Two ETC schemes (static and dynamic) have been proposed, which allow for a further reduction of communication burdens.
- It is shown that the proposed ETC schemes can guarantee a robust stability, in the sense of ISpS, of the tracking error dynamics w.r.t. the effect of aperiodic sampling and in the presence of different types of disturbances, and the avoidance of the Zeno phenomenon related to the ETC schemes has been assessed rigorously.
- The stability of the closed-loop system including infinite-dimensional internal dynamics has been verified, and the validity and the effectiveness of the proposed control schemes have been confirmed by a comparative simulation study.

The remainder of the paper is organized as follows. In Section 5.2, some notations and terminologies are introduced. Section 5.3 recalls the CFP model for heterogeneous TCL populations and the continuous-time tracking control law presented in [220]. Then, a static ETC scheme based on the proposed controller is derived, and its closed-loop stability and Zeno-behavior free properties are analyzed in Section 5.4. A dynamic triggering scheme is developed by composing a new auxiliary variable in Section 5.5. A simulation study is carried out in Section 5.6 to validate the developed control schemes. Finally, concluding remarks are outlined in Section 5.7.

5.2 Notations and preliminaries

Let $\mathbb{R} := (-\infty, +\infty)$, $\mathbb{R}_{\geq 0} := [0, +\infty)$, $\mathbb{R}_{>0} := (0, +\infty)$, and $\mathbb{R}_{\leq 0} := (-\infty, 0]$. Let $\mathbb{N}$ denote the set of non-negative integers.

By convention, let $\|x\|$ be the Euclidean norm of a vector $x \in \mathbb{R}^n (n \geq 1)$. In particular, let $|x| := \|x\|$ for $x \in \mathbb{R}$.

For a function $f : \mathbb{R}_{\geq 0} \to \mathbb{R}$, we denote by $f(t^+)$, or respectively $f(t^-)$, the limit of $f(s)$ when s tends to t from the right, or respectively from the left.

For given (open or closed) domains $\Omega_1, \Omega_2 \subset \mathbb{R}^n (n \geq 1)$ and $\Omega_3 \subset \mathbb{R}$, let $C(\Omega_1; \Omega_3) := C^0(\Omega_1; \Omega_3) := \{\phi : \Omega_1 \to \Omega_3 |\ \phi$ is continuous w.r.t. all its augments in $\Omega_1\}$. For positive integers i, j, let $C^i(\Omega_1; \Omega_3) := \{\phi : \Omega_1 \to \Omega_3 |\ \phi$ has continuous derivatives up to order i w.r.t. its all augments in $\Omega_1\}$, and $C^{i,j}(\Omega_1 \times \Omega_2; \Omega_3) := \{\phi : \Omega_1 \times \Omega_2 \to \Omega_3 |\ \phi$ has continuous derivatives up to order i w.r.t. its augments in Ω_1 and up to order j w.r.t. its augments in $\Omega_2\}$. In particular, if $\Omega_3 = \mathbb{R}$, we denote $C(\Omega_1) := C^0(\Omega_1; \mathbb{R})$ and $C^i(\Omega_1) := C^i(\Omega_1; \mathbb{R})$ for $i \geq 1$.

As in [92] and [91], for some $a \in \mathbb{R}_{>0}$, a function $\alpha : [0, a) \to R_{\geq 0}$ is said to be in class $\mathcal{K}$ ($\alpha \in \mathcal{K}$) if α is continuous, strictly increasing and $\alpha(0) = 0$. If, in addition, $a = +\infty$ and $\alpha(r) \to +\infty$ as $r \to +\infty$, α is said to be in class $\mathcal{K}_\infty$. A continuous function $\beta : [0, a) \times \mathbb{R}_{\geq 0} \to \mathbb{R}_{\geq 0}$ is said to be in class $\mathcal{KL}$ ($\beta \in \mathcal{KL}$) if $\beta(\cdot, s) \in \mathcal{K}$ for each fixed $s \in \mathbb{R}_{\geq 0}$, $\beta(r, \cdot)$ is strictly decreasing and $\beta(r, s) \to 0$ as $s \to +\infty$ for each fixed $r \in \mathbb{R}_{>0}$.

Definition 5.1. *([87]) Consider a system*

$$\dot{x} = f(x, u), \tag{5.1}$$

where $x \in \mathbb{R}^n$, $u \in \mathbb{R}^m$, $f : \mathbb{R}^n \times \mathbb{R}^m \to \mathbb{R}^n$ is locally Lipschitz continuous, and $m, n \geq 1$. System (5.1) *is said to be input-to-state practically stable (ISpS) w.r.t. u if there exist $\beta \in \mathcal{KL}, \gamma \in \mathcal{K}$, and $d \in \mathbb{R}_{\geq 0}$ such that for any initial data $x(0)$ and any continuous input u, the following inequality holds:*

$$\|x(t)\| \leq \beta(\|x(0)\|, t) + \gamma\left(\sup_{s \in (0,t)} \|u(s)\|\right) + d, \forall t \in \mathbb{R}_{\geq 0}. \tag{5.2}$$

Moreover, if (5.2) *holds for $d = 0$, then System* (5.1) *is said to be input-to-state stable (ISS).*

Definition 5.2. *A function $V \in C^1(\mathbb{R}^n; \mathbb{R}_{\geq 0})$ is called an ISpS-Lyapunov function for* (5.1) *if:*

(i) there exist functions $\psi_1, \psi_2 \in \mathcal{K}_\infty$ *such that*

$$\psi_1(\|x\|) \leq V(x) \leq \psi_2(\|x\|), \forall x \in \mathbb{R}^n;$$

(ii) there exist a function $\chi \in \mathcal{K}$*, a constant* $c \in \mathbb{R}_{\geq 0}$*, and a positive definite function* α *such that*

$$\|x\| \geq \max\{\chi(\|u\|), c\} \Rightarrow \nabla V(x) \cdot f(x,u) \leq -\alpha(\|x\|), \tag{5.3}$$

where $\nabla V(x)$ *is the gradient of* $V(x)$*, i.e.,* $\nabla V(x) := \left(\frac{\partial V(x)}{\partial x_1}, \frac{\partial V(x)}{\partial x_2}, ..., \frac{\partial V(x)}{\partial x_n}\right)$.

Note that $V(x)$ satisfying (5.3) with $c = 0$ is an ISS-Lyapunov function for system (5.1). An important relationship between the ISpS (respectively ISS) and the existence of an ISpS (respectively ISS) Lyapunov function for system (5.1) is given below (see, e.g., [181]).

Lemma 5.1. *System* (5.1) *is ISpS (respectively ISS) if and only if it admits an ISpS (respectively ISS) Lyapunov function.*

5.3 Dynamic model of TCL populations and power tracking control

5.3.1 Dynamics of a single TCL

In this work, we consider a population of residential air conditioners (ACs) represented by the first-order equivalent thermal parameter (ETP) model [176]. Suppose that $x_i(t)$ and $x_i^a(t)$ are the temperature and ambient temperature for the i-th AC, respectively, and $s_i(t)$ is its thermostat state with a value of 1 for the ON-state and 0 for the OFF-state. Then, the dynamics of the indoor temperature can be described by the following stochastic hybrid system (SHS) [24, 126, 221]:

$$\mathrm{d}x_i(t) = \frac{1}{C_i R_i}\left(x_i^a(t) - x_i(t) - s_i(t) R_i P_i\right)\mathrm{d}t + \sigma\,\mathrm{d}w_i(t), \tag{5.4}$$

where C_i, R_i, and P_i are thermal capacitance, resistance, and cooling power, respectively, w_i is assumed to be a standard Wiener process, and σ is the variance parameter that takes account of uncertain modeling errors. Let $x_{sp,i}(t)$ be the set-point temperature of the i-th device and δ be a prescribed deadband width. The lower and upper temperature boundary can be respectively written as

$$\underline{x}(t) = x_{sp,i}(t) - \frac{\delta}{2}, \overline{x}(t) = x_{sp,i}(t) + \frac{\delta}{2}.$$

Then, the thermostat state in (5.4) is given by [224]

$$s_i(t) = \begin{cases} 1, & \text{if } x_i(t) \geq \overline{x}(t); \\ 0, & \text{if } x_i(t) \leq \underline{x}(t); \\ (s_i(t^-) \wedge r_i(t)) + (s_i(t^-) \vee r_i(t)), & \text{otherwise;} \end{cases} \tag{5.5}$$

where "+" is the one-bit binary addition with overflow, $r_i(t)$ is the forced switching signal. Note that the boolean-valued variable $s_i(t)$ will be opposite to $s_i(t^-)$ when the forced-switch occurs. For example, if $s_i(t^-) = 0$ and $r_i(t) = 1$, then $s_i(t) = 0 \wedge 1 + 0 \vee 1 = 0 + 1 = 1$. Note also that the generalized deadband control given in (5.5) is indeed of event-triggering nature.

5.3.2 Coupled Fokker-Planck equations for the aggregated dynamics of the population

Consider a large group of ACs, whose dynamics are described by (5.4) and (5.5). Let $f_1(x,t)$ and $f_0(x,t)$ be the probability densities for the loads in the ON and OFF states, respectively. It is shown that the aggregated dynamics of the population can be modeled by a system of coupled Fokker-Planck equations given below [24, 124, 126]:

$$\partial_t f_0 = \partial_x \left(\frac{\sigma^2}{2} \partial_x f_0 - (\alpha_0 - u) f_0 \right), \tag{5.6a}$$

$$\partial_t f_1 = \partial_x \left(\frac{\sigma^2}{2} \partial_x f_1 - (\alpha_1 - u) f_1 \right), \tag{5.6b}$$

where $u(t) := \dot{\underline{x}} = \dot{\overline{x}}$ is the control input to be designed later, and

$$\alpha_1(x,t) := \frac{1}{CR} \left(x^a(t) - x - RP \right),$$
$$\alpha_0(x,t) := \frac{1}{CR} \left(x^a(t) - x \right),$$

where R, C and P are average values of thermal capacitance, resistance, and cooling power of the population, respectively, and $x^a(t)$ is the time-varying ambient temperature.

In practical application scenarios, the operation of all the ACs is confined to a fixed temperature range (x_L, x_H) for all $t \in [t_0, T]$, where x_L ad x_H are, respectively, lower and upper temperature boundaries for the ACs, and t_0 and T are the starting and ending time instants. Then, f_0 and f_1 are confined in a fixed temperature range (x_L, x_H) along all possible operations, as illustrated in Fig. 5.1. Moreover, for heterogeneous TCL populations, we introduce $g(f_0, f_1)$ to represent modeling errors, such as forced switchings [193, 220]. Then, the

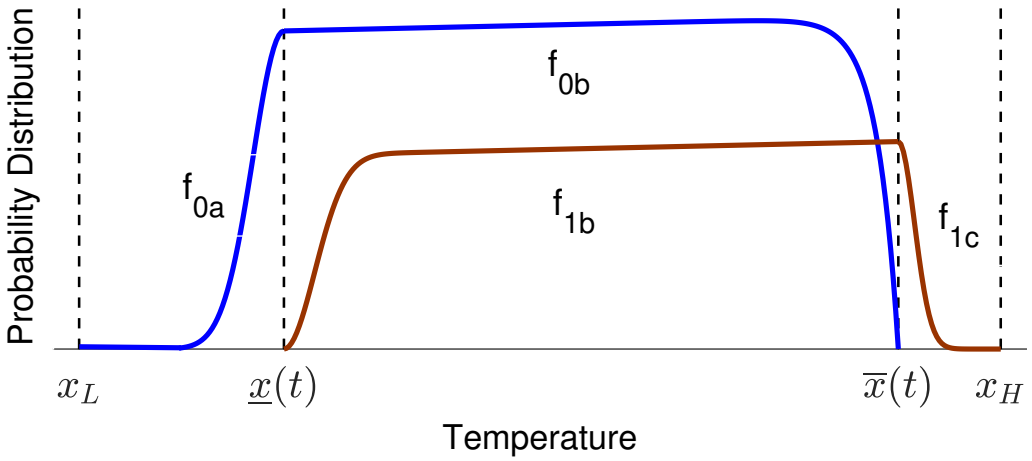

Figure 5.1 Illustration of probability density functions of a TCL population at a given time.

dynamics of the population are described by [24, 193, 220]

$$\partial_t f_0 = \partial_x \left(\frac{\sigma^2}{2} \partial_x f_0 - (\alpha_0 - u) f_0 \right) - g(f_0, f_1), \quad \forall (x,t) \in (x_L, \overline{x}) \times [t_0, T], \tag{5.7a}$$

$$\partial_t f_1 = \partial_x \left(\frac{\sigma^2}{2} \partial_x f_1 - (\alpha_1 - u) f_1 \right) + g(f_0, f_1), \quad \forall (x,t) \in (\underline{x}, x_H) \times [t_0, T]. \tag{5.7b}$$

Moreover,based on the conservative property of the number of the TCLs switching between ON and OFF states, $g \in C(\mathbb{R}^2; \mathbb{R})$ should satisfy that

$$\begin{aligned} g(0,\tau) \leq & 0 \leq g(s,0), \forall (s,\tau) \in \mathbb{R}^2, \\ |g(s,\tau)| \leq & \min\{|s|, |\tau|\}, \forall (s,\tau) \in \mathbb{R}^2, \end{aligned}$$

and that

$$g(f_0(x,t), f_1(x,t)) \equiv 0$$

for $(x,t) \in (x_L, \underline{x}) \times [t_0, T]$ or $(\overline{x}, x_H) \times [t_0, T]$. The boundary conditions for the CFP equations are given by

$$\partial_x f_1(\overline{x}^+, t) = \partial_x f_0(\overline{x}^-, t) + \partial_x f_1(\overline{x}^-, t), \tag{5.8a}$$

$$\partial_x f_0(\underline{x}^-, t) = \partial_x f_0(\underline{x}^+, t) + \partial_x f_1(\underline{x}^+, t), \tag{5.8b}$$

$$f_0(\overline{x}, t) = 0, \tag{5.8c}$$

$$f_1(\underline{x}, t) = 0, \tag{5.8d}$$

$$f_0(\underline{x}^-,t) = f_0(\underline{x}^+,t), \tag{5.8e}$$

$$f_1(\overline{x}^-,t) = f_1(\overline{x}^+,t), \tag{5.8f}$$

$$\frac{\sigma^2}{2}\partial_x f_0(x_L^+,t) = (\alpha_0(x_L^+,t)-u(t))f_0(x_L^+,t), \tag{5.8g}$$

$$\frac{\sigma^2}{2}\partial_x f_1(x_H^-,t) = (\alpha_1(x_H^-,t)-u(t))f_1(x_H^-,t), \tag{5.8h}$$

$$\partial_x f_1(\underline{x}^+,t) > 0, \tag{5.8i}$$

$$\partial_x f_0(\overline{x}^-,t) < 0. \tag{5.8j}$$

As indicated in [220], (5.8a)-(5.8h) are conservation of probability conditions, among which (5.8c) and (5.8d) are absorbing conditions, (5.8e) and (5.8f) are continuity conditions, and (5.8g) and (5.8h) capture the properties of impenetrable wall reflections. The conditions (5.8i) and (5.8j) capture the properties of probability flows defined via the integral of $\partial_t f_i$ over the temperature coordinate when no additional flux is involved due to the forced switches.

5.3.3 Continuous-time tracking control law

As $f_1(x,t)$ is the probability density function of TCLs in the ON-state, the aggregated power of a TCL population with the same power consumption P is given by [21,24,55,193,215,224]:

$$y_{\text{total}}(t) := \frac{P}{\eta}\int_{\underline{x}(t)}^{x_H} f_1(x,t)\,\mathrm{d}x, \quad \forall t \in [t_0,T], \tag{5.9}$$

where $\eta > 1$ is the load efficiency of the cooling devices. To ensure a required controllability of the input-output dynamics, we use an output function as follows:

$$y(t) := y_{\text{total}}(t) + \frac{P}{\eta}\int_{\overline{x}(t)}^{x_H} f_1(x,t)\,\mathrm{d}x - \frac{P}{\eta}\int_{x_L}^{\underline{x}(t)} f_0(x,t)\,\mathrm{d}x, \quad t \in [t_0,T]. \tag{5.10}$$

Suppose that $y_d(t) \in C^1(\mathbb{R}_{\geq 0};\mathbb{R})$ is the desired power consumption profile in responding to DR control signals from the power network for, e.g., peak-load shaving or load shifting, and denote by $e(t)$ the tracking error, i.e.

$$e(t) := y(t) - y_d(t). \tag{5.11}$$

Based on (5.7), (5.9), (5.10), (5.11), and the boundary conditions (5.8), the tracking error dynamics can be expressed by:

$$\dot{e}(t) = -\frac{2P}{\eta}u(t)\left(f_1(\overline{x},t) + f_0(\underline{x},t)\right) + \frac{P}{\eta}\Phi(t) + \Gamma(t), \tag{5.12}$$

where

$$\Phi(t) := -\frac{\eta}{P}\dot{y}_d(t),$$

and

$$\begin{aligned}\Gamma(t) :=& \alpha_1(\overline{x},t)f_1(\overline{x},t) + \alpha_0(\underline{x},t)f_0(\underline{x},t) - \frac{\sigma^2 P}{2\eta}\partial_x f_1(\underline{x}^+,t) \\ &- \frac{\sigma^2 P}{2\eta}\partial_x f_1(\overline{x}^+,t) - \frac{\sigma^2 P}{2\eta}\partial_x f_0(\underline{x}^-,t) - \frac{\sigma^2 P}{2\eta}\partial_x f_0(\overline{x}^-,t) \\ &+ \frac{P}{\eta}\int_{\underline{x}(t)}^{\overline{x}(t)} g(f_0,f_1)\,\mathrm{d}x. \end{aligned} \tag{5.13}$$

Thus, with the following nonlinear control:

$$u(t) = \frac{ke(t) + \Phi(t)}{2\left(f_1(\overline{x},t) + f_0(\underline{x},t)\right)}, \tag{5.14}$$

the tracking error dynamics (5.12) become

$$\dot{e}(t) = -\frac{P}{\eta}ke(t) + \Gamma(t). \tag{5.15}$$

Note that the control law (5.14) only requires partial state information at the endpoints of the deadband. Compared with the control methods requiring full state measurements, the communication burden can be significantly reduced. Moreover, this control law is independent of σ in the Fokker-Planck equations, which is considered as a parametric uncertainty captured by $\Gamma(t)$. The reason to treat σ as an unknown parameter is mainly due to the fact that it is not physically measurable and its estimation may be very complex and infeasible for practical applications (see, e.g., [145]). Denote

$$\begin{aligned} I_{lm} :=& \left(C^{2,1}((x_L,\underline{x})\times(t_0,T)) \cap C([x_L,\underline{x}]\times[t_0,T])\right) \\ &\cup \left(C^{2,1}((\underline{x},\overline{x})\times(t_0,T)) \cap C([\underline{x},\overline{x}]\times[t_0,T])\right), \\ I_{mh} :=& \left(C^{2,1}((\underline{x},\overline{x})\times(t_0,T)) \cap C([\underline{x},\overline{x}]\times[t_0,T])\right) \\ &\cup \left(C^{2,1}((\overline{x},x_H)\times(t_0,T)) \cap C([\overline{x},x_H]\times[t_0,T])\right). \end{aligned}$$

In the sequel, we always assume that the ambient temperature $x^a \in C([t_0,T];\mathbb{R}_{\geq 0})$ and $\underline{x},\overline{x} \in C^1([t_0,T];[x_L,x_H])$. Moreover, under the control law (5.14), we assume that the solution (f_0,f_1) to the system (5.7) admits the following regularity properties:

(i) $f_0 \in I_{lm}$ and has derivatives $\partial_x f_0(x_L^+, t)$, $\partial_x f_0(\underline{x}^{\pm}, t)$, and $\partial_x f_0(\overline{x}^-, t)$ for any fixed $t \in [t_0, T]$;

(ii) $f_1 \in I_{mh}$ and has derivatives $\partial_x f_1(x_H^-, t)$, $\partial_x f_1(\overline{x}^{\pm}, t)$, and $\partial_x f_1(\underline{x}^+, t)$ for any fixed $t \in [t_0, T]$;

(iii) $\partial_x f_1(\underline{x}^+(t), t)$, $\partial_x f_1(\overline{x}^+(t), t)$, $\partial_x f_0(\underline{x}^-(t), t)$, and $\partial_x f_0(\overline{x}^-(t), t)$ are continuous w.r.t. $t \in [t_0, T]$.

Note that under these conditions, $\Gamma(t)$ given by (5.13) is continuous, and hence $e(t)$ governed by (5.15) is continuously differentiable. In addition, given nonnegative initial data (f_0^0, f_1^0), with slight modifications of the proof of Proposition 4.3 in [220], it can be shown that

$$\begin{aligned} f_0(x,t) \geq & 0, \forall x \in [x_L, \overline{x}], t \in [t_0, T], \\ f_1(x,t) \geq & 0, \forall x \in [\underline{x}, x_H], t \in [t_0, T], \\ f_0(\underline{x}(t), t) + f_1(\overline{x}(t), t) > & 0, \forall t \in [t_0, T], \end{aligned}$$

among which the last property guarantees that the control signal u defined by (5.14) is well-defined.

It is also worth mentioning that the system is conservative in the following sense (see [220, Proposition 4.2]):

$$\int_{x_L}^{\overline{x}(t)} f_0(x,t)\,\mathrm{d}x + \int_{\underline{x}(t)}^{x_H} f_1(x,t)\,\mathrm{d}x = 1, \ \forall t \in (t_0, T],$$

provided

$$\int_{x_L}^{\overline{x}(t_0)} f_0^0(x)\,\mathrm{d}x + \int_{\underline{x}(t_0)}^{x_H} f_1^0(x)\,\mathrm{d}x = 1.$$

5.4 A static event-triggered tracking control scheme

5.4.1 Error dynamics with event-triggered tracking control

For an emulation-based ETC, the control inputs generated by (5.14) are updated only at discrete time instants. Therefore,

$$u(t) = u(t_i) = \frac{k e(t_i) + \Phi(t_i)}{2\left(f_1(\overline{x}(t_i), t_i) + f_0(\underline{x}(t_i), t_i)\right)}, \quad t \in [t_i, t_{i+1}), i \in \mathbb{S}, \tag{5.16}$$

where $\mathbb{S}$ is a subset of $\mathbb{N}$. Figure 5.2 shows the schematic diagram for power tracking control of a TCL population. The solid line in the figure shows that the signals are continuously or periodically monitored, while the dashed line indicates that the signals are sent aperiodically. Note that each TCL is configured with a zero-order-hold (ZOH), which allows keeping the control signal to be a constant in each inter-execution interval. Furthermore, note that the data transmission from the TCLs to the aggregator are also aperiodic. It is mainly because first, a numerical approximation method is used to compute the values of $f_1(\overline{x}(t), t)$ and $f_0(\underline{x}(t), t)$ [220]. Thus, only a portion of TCLs need to report their states to the aggregator when their temperatures are around the deadband endpoints. In addition, when the system is running in a steady regime, each TCL needs only to send a signal to the aggregator when it changes its state at the endpoints. The aggregator continuously collects information on $e(t), f_1(\overline{x}(t), t)$, and $f_0(\underline{x}(t), t)$. Nevertheless, the controller will not update until the next triggering event occurs.

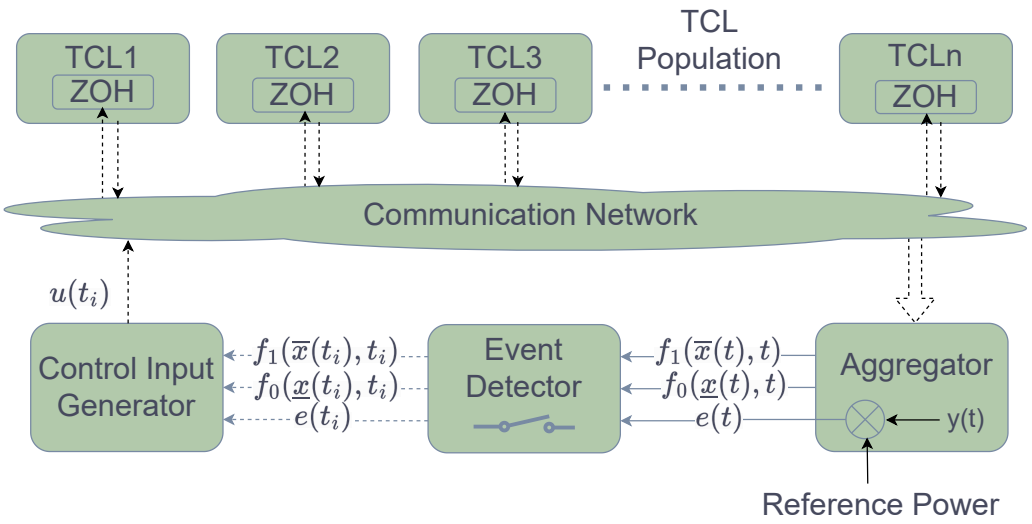

Figure 5.2 Schematics of event-triggered power tracking control of a TCL population.

Define

$$\tilde{e}(t) := e(t_i) - e(t), \tag{5.17}$$

and let $\tilde{u}(t) := u(t_i) - u(t)$. Then

$$\begin{aligned}\dot{e}(t) &= -\frac{2P}{\eta} u(t_i) \left(f_1(\overline{x}, t) + f_0(\underline{x}, t)\right) + \frac{P}{\eta}\Phi(t) + \Gamma(t) \\ &= -\frac{2P}{\eta} \left(u(t) + \tilde{u}(t)\right) \left(f_1(\overline{x}, t) + f_0(\underline{x}, t)\right) + \frac{P}{\eta}\Phi(t) + \Gamma(t)\end{aligned}$$

$$
\begin{aligned}
&= -\frac{P}{\eta}ke(t) + \Gamma(t) - \frac{2P}{\eta}\tilde{u}(t)\left(f_1(\overline{x},t) + f_0(\underline{x},t)\right) \\
&= -\frac{P}{\eta}ke(t) + \Gamma(t) \\
&\quad - \frac{P}{\eta}\frac{f_1(\overline{x},t) + f_0(\underline{x},t)}{f_1(\overline{x}(t_i),t_i) + f_0(\underline{x}(t_i),t_i)}(ke(t_i) + \Phi(t_i)) + \frac{P}{\eta}(ke(t) + \Phi(t)).
\end{aligned}
$$

Let

$$
p(t) := \frac{f_1(\overline{x},t) + f_0(\underline{x},t)}{f_1(\overline{x}(t_i),t_i) + f_0(\underline{x}(t_i),t_i)}.
$$

Then, $\forall t \in [t_i, t_{i+1})$, it follows

$$
\begin{aligned}
\dot{e}(t) &= -\frac{P}{\eta}ke(t) + \Gamma(t) - \frac{P}{\eta}\left(p(t)ke(t_i) - ke(t)\right) - \frac{P}{\eta}\left(p(t)\Phi(t_i) - \Phi(t)\right) \\
&= -\frac{P}{\eta}ke(t) + \Gamma(t) - \frac{P}{\eta}\left(ke(t_i) - ke(t)\right) \\
&\quad - \frac{P}{\eta}(p(t)-1)ke(t_i) - \frac{P}{\eta}\left(p(t)\Phi(t_i) - \Phi(t)\right) \\
&= -\frac{P}{\eta}ke(t) - \frac{P}{\eta}k\tilde{e}(t) + \Gamma(t) - \frac{P}{\eta}(p(t)-1)ke(t_i) - \frac{P}{\eta}\left(p(t)\Phi(t_i) - \Phi(t)\right).
\end{aligned}
$$

Therefore, the tracking error dynamics under an ETC scheme can be written as

$$
\dot{e}(t) = -\frac{P}{\eta}ke(t) - \frac{P}{\eta}k\tilde{e}(t) + \overline{\Gamma}(t), \tag{5.18}
$$

where

$$
\overline{\Gamma}(t) := \Gamma(t) - \frac{P}{\eta}(p(t)-1)ke(t_i) - \frac{P}{\eta}\left(p(t)\Phi(t_i) - \Phi(t)\right).
$$

5.4.2 Design of static event-triggering condition

Note that the tracking error dynamics in (5.18) are not only influenced by $e(t)$ and $\tilde{e}(t)$, but also by $\overline{\Gamma}(t)$. Therefore, we introduce a constant positive offset, ϵ, on the basis of the triggering condition proposed in [186]. The triggering condition is designed as:

$$
\begin{cases}
t_0 = 0, \\
t_{i+1} = \inf\left\{t > t_i : |e(t_i) - e(t)| \geq \max\{k'|e(t)|, \epsilon\}\right\},
\end{cases} \tag{5.19}
$$

where $\epsilon > 0$ is a pre-defined threshold, and $k' \in (0,1)$ is a hyper-parameter. Figure 5.3 shows the flowchart for implementing such an ETC scheme, where Δt is a constant sampling

period. Note that the system needs to compute and broadcast $u(t_i)$ only when the triggering event in (5.19) occurs.

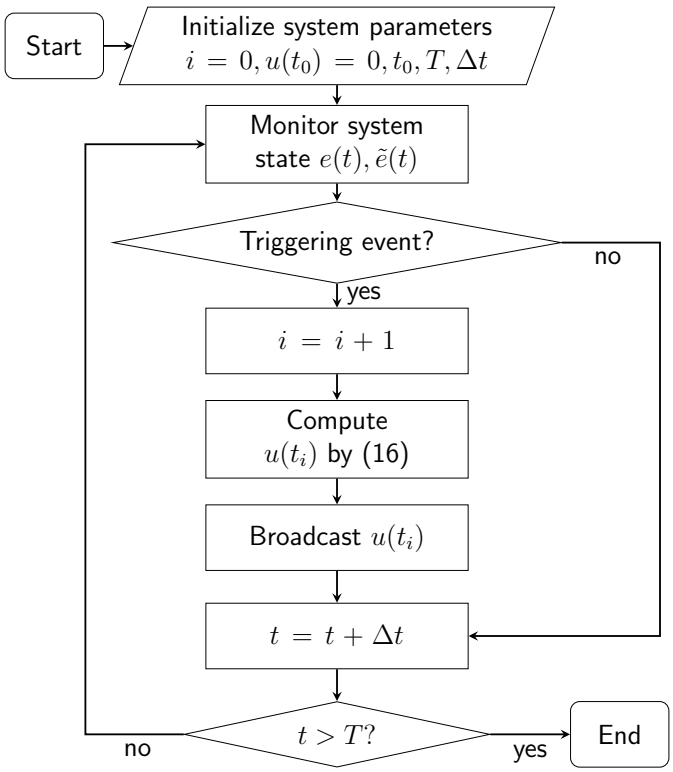

Figure 5.3 Flowchart for static ETC algorithm.

In what follows, we show that the closed-loop system with the proposed ETC scheme is ISpS. Specifically, we have:

Theorem 5.1. *Under the event triggering condition* (5.19)*, the tracking error dynamics governed by* (5.18) *are ISpS w.r.t.* $\overline{\Gamma}(t)$.

Proof. Let $V(e) := \frac{1}{2}e^2$. Then

$$\begin{aligned}\dot{V}(e) =& e(t)\dot{e}(t)\\ =& -\frac{P}{\eta}ke^2(t) - \frac{P}{\eta}ke(t)\tilde{e}(t) + e(t)\overline{\Gamma}(t)\\ \leq& -\frac{P}{\eta}ke^2(t) + \frac{P}{\eta}k|e(t)||\tilde{e}(t)| + |e(t)||\overline{\Gamma}(t)|. \end{aligned} \tag{5.20}$$

With the proposed triggering condition (5.19), it follows that

$$|\tilde{e}(t)| \leq \max\{k'|e(t)|, \epsilon\}, \forall t \in [t_0, T].$$

Thus,

$$|e(t)||\tilde{e}(t)| \leq |e(t)| \max\{k'|e(t)|, \epsilon\}, \forall t \in [t_0, T]. \tag{5.21}$$

Note that

$$|e(t)| \max\{k'|e(t)|, \epsilon\} = k'|e(t)|^2 < 2k'V(e) + \frac{\epsilon^2}{k'}$$

when $k'|e(t)| \geq \epsilon$, and

$$|e(t)| \max\{k'|e(t)|, \epsilon\} = \epsilon|e(t)| < \frac{\epsilon^2}{k'} \leq 2k'V(e) + \frac{\epsilon^2}{k'}$$

when $k'|e(t)| < \epsilon$. Hence, it always holds that

$$|e(t)| \max\{k'|e(t)|, \epsilon\} < 2k'V(e) + \frac{\epsilon^2}{k'}. \tag{5.22}$$

Using the inequalities in (5.20), (5.21), and (5.22), we have

$$\begin{aligned}\dot{V}(e) \leq & -\frac{P}{\eta}2kV(e) + 2\frac{P}{\eta}kk'V(e) + \frac{P}{\eta}\frac{k\epsilon^2}{k'} + |e(t)||\overline{\Gamma}(t)| \\ = & \frac{P}{\eta}(-2k + 2kk')V(e) + \frac{P}{\eta}\frac{k\epsilon^2}{k'} + |e(t)||\overline{\Gamma}(t)|.\end{aligned}$$

Define $\chi(s) := 2k_1\frac{\eta}{P}s$ for $s \in \mathbb{R}_{\geq 0}$. It is clear that $\chi \in \mathcal{K}$. Let $c := \sqrt{2\frac{k_2 k}{k'}}\epsilon$ with $k_1, k_2 \in \mathbb{R}_{>0}$. Note that as $-2k + 2kk' = -2k(1 - k') < 0$, we can always find k_1, k_2 such that

$$-2k + 2kk' + \frac{1}{k_1} + \frac{1}{k_2} < 0.$$

Consequently, for all $t \in [t_0, T]$, we have

$$\dot{V}(e) \leq \frac{P}{\eta}\left(-2k + 2kk' + \frac{1}{k_1} + \frac{1}{k_2}\right)V(e),$$

as long as

$$|e(t)| \geq \max\{\chi(|\overline{\Gamma}(t)|, c)\}.$$

Thus, $V(e)$ is an ISpS-Lyapunov function for the error dynamics (5.18). By Lemma 5.1, the system (5.18) is ISpS w.r.t. $\overline{\Gamma}(t)$. □

For an ETC scheme, the inter-sampling intervals should be lower bounded by a positive number τ_0, i.e., $t_{i+1} - t_i > \tau_0 > 0$ for all $i \in \mathbb{S}$. Otherwise, Zeno behavior might happen, that

is, an infinite number of triggerings take place in a finite amount of time. In the following, we show that our triggering condition excludes Zeno behavior.

Theorem 5.2. *The dynamic system* (5.18) *under the execution rule given in* (5.19) *is Zeno-free.*

Proof. Let $t_i \leq t < t_{i+1}, i \in \mathbb{S}$. Note that

$$\begin{aligned}|e(t_i) - e(t)| =& \left| \int_{t_i}^{t} \dot{e}(t) \mathrm{d}t \right| \\ =& \left| \int_{t_i}^{t} \left(-\frac{P}{\eta} k e(t) - k \frac{P}{\eta} \tilde{e}(t) + \overline{\Gamma}(t) \right) \mathrm{d}t \right| \\ \leq& \frac{P}{\eta} k \int_{t_i}^{t} |e(t)| \mathrm{d}t + \frac{P}{\eta} k \int_{t_i}^{t} |\tilde{e}(t)| \mathrm{d}t + \int_{t_i}^{t} |\overline{\Gamma}(t)| \mathrm{d}t.\end{aligned}$$

First, because $e(t)$ is continuous in $[t_i, t_{i+1}]$, $\sup_{t_i \leq t < t_{i+1}} |e(t)|$ is finite. Then, it follows that

$$\sup_{t_i \leq t < t_{i+1}} |\tilde{e}(t)| \leq \max \left\{ k' \sup_{t_i \leq t < t_{i+1}} |e(t)|, \epsilon \right\} \leq k' \sup_{t_i \leq t < t_{i+1}} |e(t)| + \epsilon.$$

Furthermore, as $\overline{\Gamma}(t)$ is bounded in $[t_0, T]$, $\sup_{t_i \leq t < t_{i+1}} |\overline{\Gamma}(t)|$ is finite. Therefore, for all $t \in [t_i, t_{i+1})$, it follows that

$$|e(t_i) - e(t)| \leq \left(\frac{P}{\eta} k \sup_{t_i \leq t < t_{i+1}} |e(t)| + \frac{P}{\eta} k k' \sup_{t_i \leq t < t_{i+1}} |e(t)| + \frac{P}{\eta} k \epsilon + \sup_{t_i \leq t < t_{i+1}} |\overline{\Gamma}(t)| \right) (t - t_i).$$

Particularly, we have

$$|e(t_i) - e(t_{i+1})| \leq \left(\frac{P}{\eta} k (1 + k') C_e(i) + \frac{P}{\eta} k \epsilon + C_{\overline{\Gamma}}(i) \right) \Delta t_i, \tag{5.23}$$

where $C_e(i) := \sup_{t_i \leq t < t_{i+1}} |e(t)|$, $C_{\overline{\Gamma}}(i) := \sup_{t_i \leq t < t_{i+1}} |\overline{\Gamma}(t)|$, and $\Delta t_i := t_{i+1} - t_i$.

On the other hand, according to the event triggering condition, we have

$$|e(t_i) - e(t_{i+1})| \geq \max\{k' |e(t_{i+1})|, \epsilon\} \geq \epsilon. \tag{5.24}$$

Define

$$C_e := \max_{t_0 \leq t \leq T} |e(t)| \quad \text{and} \quad C_{\overline{\Gamma}} := \max_{t_0 \leq t \leq T} |\overline{\Gamma}(t)|,$$

then

$$C_e(i) \leq C_e \quad \text{and} \quad C_\Gamma(i) \leq C_{\overline{\Gamma}}, \quad \forall i \in \mathbb{S}. \tag{5.25}$$

By the inequalities in (5.23), (5.24), and (5.25), we have

$$\begin{aligned}\Delta t_i \geq & \frac{\epsilon}{\frac{P}{\eta}k(1+k')C_e(i) + \frac{P}{\eta}k\epsilon + C_{\overline{\Gamma}}(i)} \\ \geq & \frac{\epsilon}{\frac{P}{\eta}k(1+k')C_e + \frac{P}{\eta}k\epsilon + C_{\overline{\Gamma}}} \\ > & 0, \forall i \in \mathbb{S}.\end{aligned}$$

Thus, the Zeno behavior is excluded for all $t \in [t_0, T]$. □

5.5 A dynamic event-triggered tracking control scheme

Dynamic event-triggering mechanisms can be seen as filtered versions of static schemes. Besides some available system information (such as state or output), an internal dynamic variable is also included in the triggering condition. Hence, the triggering events can be dynamically adjusted at different times. With some elaborated properties of the auxiliary dynamic variable (such as nonnegativity), a dynamic event triggering scheme can extend the triggering intervals and thus further reduce the consumption of network resources.

In this section, a dynamic ETC scheme is designed based on the static scheme (5.19), and then the closed-loop stability of the system under this control scheme is assessed.

5.5.1 A dynamic execution rule

Note that the static triggering condition (5.19) can be equivalently written as:

$$\begin{cases} t_0 = 0, \\ t_{i+1} = \inf\left\{t > t_i : \max\left\{k'^2|e(t)|^2, \epsilon^2\right\} \leq |\tilde{e}(t)|^2\right\}. \end{cases} \tag{5.26}$$

Based on (5.26), we propose the following dynamic triggering condition:

$$\begin{cases} t_0 = 0, \\ t_{i+1} = \inf\{t > t_i : 2\rho(t) + \theta k\left(\max\left\{k'^2|e(t)|^2, \epsilon^2\right\} - |\tilde{e}(t)|^2\right) \leq 0\}, \end{cases} \tag{5.27}$$

where $\theta \in \mathbb{R}_{\geq 0}$ is a hyper-parameter, $\rho(t)$ is an internal dynamic variable satisfying

$$\dot{\rho}(t) = -\alpha(\rho(t)) + \frac{k}{2}\left(\max\left\{k'^2|e(t)|^2, \epsilon^2\right\} - |\tilde{e}(t)|^2\right) \tag{5.28}$$

with α being a Lipschitz continuous function and belonging to $\mathcal{K}_\infty$, and $\rho(t_0) := \rho_0 \in \mathbb{R}_{\geq 0}$.

Note that when θ tends to $+\infty$, the dynamic triggering scheme falls down to the static one. It is clear that $\rho(t)$ can be seen as a filtered value of $\max\{k'^2|e(t)|^2, \epsilon^2\} - |\tilde{e}(t)|^2$. Furthermore, it admits a special property, that is, it is always nonnegative, as stated below.

Lemma 5.2. *Suppose that α is a locally Lipschitz continuous function and belongs to $\mathcal{K}_\infty$. Let $e(t), \tilde{e}(t)$, and $\rho(t)$ be given by* (5.18), (5.17), *and* (5.28), *respectively. Then, $\rho(t) \geq 0$ for all $t \in [t_0, T]$.*

Proof. Based on the triggering condition given in (5.27), it always holds that

$$\rho(t) + \frac{\theta k}{2}\left(\max\left\{k'^2|e(t)|^2, \epsilon^2\right\} - |\tilde{e}(t)|^2\right) \geq 0.$$

If $\theta = 0$, the result is trivial. If $\theta > 0$, it follows that

$$\frac{k}{2}\max\left\{k'^2|e(t)|^2, \epsilon^2\right\} - |\tilde{e}(t)|^2 \geq -\frac{1}{\theta}\rho(t).$$

Thus, by the internal variable dynamics (5.28), it yields

$$\dot{\rho}(t) \geq -\alpha(\rho(t)) - \frac{1}{\theta}\rho(t).$$

According to the comparison lemma for ordinary differential equations, $\rho(t) \geq 0$ for all $t \in [t_0, T]$. □

In what follows, we show that the closed-loop system is still ISpS under this dynamic triggering condition.

Theorem 5.3. *There exists a function α, which is locally Lipschitz continuous and belongs to $\mathcal{K}_\infty$, such that the system given by* (5.18) *and* (5.28) *is ISpS under the dynamic triggering scheme* (5.27).

Proof. Let $W(t) := V(e(t)) + \rho(t)$ with $V(e(t)) := \frac{1}{2}|e(t)|^2$. For all $t \in [t_0, T]$, we have

$$\begin{aligned}
\frac{\mathrm{d}}{\mathrm{d}t}W(t) =& e(t)\left(-\frac{P}{\eta}ke(t) - \frac{P}{\eta}k\tilde{e}(t) + \overline{\Gamma}(t)\right) + \dot{\rho}(t) \\
\leq& -\frac{P}{\eta}2kV(e(t)) + \frac{P}{\eta}k|e(t)||\tilde{e}(t)| + |e(t)||\overline{\Gamma}(t)| + \dot{\rho}(t) \\
\leq& -\frac{P}{\eta}2kV(e(t)) + \frac{P}{\eta}\frac{k}{2}\left(|e(t)|^2 + |\tilde{e}(t)|^2\right) \\
&+ \frac{\varsigma}{2}|e(t)|^2 + \frac{1}{2\varsigma}|\overline{\Gamma}(t)|^2 + \dot{\rho}(t) \quad (\varsigma \in \mathbb{R}_{>0}) \\
=& -\left(\frac{P}{\eta}k - \varsigma\right)V(e(t)) + \frac{1}{2\varsigma}|\overline{\Gamma}(t)|^2 - \alpha(\rho(t)) \\
&+ \frac{P}{\eta}\frac{k}{2}\max\left\{k'^2|e(t)|^2, \epsilon^2\right\} \quad \text{(by (5.28))} \\
\leq& -\frac{P}{\eta}\left(k - kk'^2 - \frac{\eta}{P}\varsigma\right)V(e(t)) + \frac{P}{\eta}\frac{k}{2}\epsilon^2 + \frac{1}{2\varsigma}|\overline{\Gamma}(t)|^2 - \alpha(\rho(t)).
\end{aligned}$$

Choose $\varsigma \in \mathbb{R}_{>0}$ and $\alpha \in \mathcal{K}_\infty$ such that

$$\begin{aligned}
\lambda_d &:= k - kk'^2 - \frac{\eta}{P}\varsigma > 0, \\
\alpha(s) &\geq \frac{P}{\eta}\lambda_d s, \forall s \in \mathbb{R}_{\geq 0},
\end{aligned}$$

then,

$$\frac{\mathrm{d}}{\mathrm{d}t}W(t) \leq -\frac{P}{\eta}\lambda_d W(t) + \frac{1}{2\varsigma}|\overline{\Gamma}(t)|^2 + \frac{P}{\eta}\frac{k}{2}\epsilon^2, \forall t \in [t_0, T].$$

By the comparison lemma, we obtain

$$\begin{aligned}
W(t) \leq& e^{-\frac{P}{\eta}\lambda_d(t-t_0)}W(t_0) + \int_{t_0}^{t} e^{-\frac{P}{\eta}\lambda_d(t-s)}\left(\frac{1}{2\varsigma}|\overline{\Gamma}(s)|^2 + \frac{P}{\eta}\frac{k}{2}\epsilon^2\right)\mathrm{d}s \\
\leq& e^{-\frac{P}{\eta}\lambda_d(t-t_0)}W(t_0) + \left(\frac{1}{2\varsigma}\max_{t\in[t_0,T]}|\overline{\Gamma}(s)|^2 + \frac{P}{\eta}\frac{k}{2}\epsilon^2\right)\int_{t_0}^{t} e^{-\frac{P}{\eta}\lambda_d(t-s)}\,\mathrm{d}s
\end{aligned}$$

Because

$$\int_{t_0}^{t} e^{-\frac{P}{\eta}\lambda_d(t-s)}\,\mathrm{d}s = \frac{\eta}{P}\lambda_d - \frac{\eta}{P}\lambda_d e^{\frac{P}{\eta\lambda_d}(t_0-t)} \leq \frac{\eta}{P}\lambda_d,$$

it follows that for all $t > t_0$:

$$W(e(t)) \leq e^{-\frac{P}{\eta}\lambda_d(t-t_0)}W(t_0) + \frac{\eta}{2\varsigma P\lambda_d}\max_{s\in[t_0,t]}|\overline{\Gamma}(s)|^2 + \frac{k}{2\lambda_d}\epsilon^2. \tag{5.29}$$

By Lemma 5.2, it always holds that

$$V(e(t)) \leq W(e(t)),\ \forall t > t_0. \tag{5.30}$$

Therefore, by (5.29), (5.30), and Definition 5.1, we can conclude that the tracking error dynamics (5.18) under the dynamic triggering condition (5.27) are ISpS. □

In the following theorem, we show that the next execution time for a given state under the dynamic event triggering condition (5.27) cannot be smaller than that of the static triggering condition (5.19).

Theorem 5.4. *Suppose that $t > t_i$ and the next execution time for static and dynamic events are t^s_{i+1} and t^d_{i+1}, respectively. Then, $t^d_{i+1} \geq t^s_{i+1}$.*

Proof. (Proof by contradiction). If $t^d_{i+1} < t^s_{i+1}$, then based on the static execution rule (5.26), we must have

$$\max\left\{k'^2\left|e\left(t^d_{i+1}\right)\right|^2, \epsilon^2\right\} - \left|\tilde{e}\left(t^d_{i+1}\right)\right|^2 > 0. \tag{5.31}$$

Case 1: $\theta > 0$. By the dynamic triggering rule (5.27), we have

$$2\rho\left(t^d_{i+1}\right) + \theta k\left(\max\left\{k'^2\left|e\left(t^d_{i+1}\right)\right|^2, \epsilon^2\right\} - \left|\tilde{e}\left(t^d_{i+1}\right)\right|^2\right) \leq 0.$$

Since $\rho(t) \geq 0$ always holds true, then

$$\max\left\{k'^2\left|e\left(t^d_{i+1}\right)\right|^2, \epsilon^2\right\} - \left|\tilde{e}\left(t^d_{i+1}\right)\right|^2 \leq 0,$$

which is a contradiction to (5.31).
Case 2: $\theta = 0$. By the dynamic triggering condition (5.27) and Lemma 5.2, we have

$$\rho\left(t^d_{i+1}\right) = 0.$$

From the dynamics of $\rho(t)$ in (5.28), it follows that

$$0 \geq \dot{\rho}\left(t^d_{i+1}\right) = \frac{1}{2}\max\left\{k'^2\left|e\left(t^d_{i+1}\right)\right|^2, \epsilon^2\right\} - \frac{1}{2}\left|\tilde{e}\left(t^d_{i+1}\right)\right|^2,$$

which is also a contradiction to (5.31). □

Remark 5.1. *Theorem 5.4 is a property on one sampling interval with the same starting state for static and dynamic triggering schemes given in* (5.19) *and* (5.27)*, respectively. The other inter-execution intervals may vary depending on the starting states. Nevertheless, we can*

conclude from this theorem that the minimum inter-execution time for the dynamic triggering scheme is larger than that of the static one. Thus, the Zeno behavior will also be excluded from the proposed dynamic triggering scheme.

5.5.2 An implementation of the dynamic triggering scheme

In our experiment, we set $\alpha(\rho(t)) = \lambda_\alpha \rho(t)$ with $\lambda_\alpha \in \mathbb{R}_{>0}$. Let

$$f(t) := \frac{k}{2}\left(\max\left\{k'^2|e(t)|^2, \epsilon^2\right\} - |\tilde{e}(t)|^2\right).$$

Then, the solution to the internal dynamics (5.28) is

$$\rho(t) = e^{-\lambda_\alpha(t-t_0)}\rho(t_0) + e^{-\lambda_\alpha(t-t_0)}\int_{t_0}^{t} e^{\lambda_\alpha(s-t_0)} f(s)\,\mathrm{d}s. \tag{5.32}$$

Based on (5.32), for $n \in \mathbb{N}$, the values of $\rho(t_n)$ can then be computed with numerical integration methods. In a digital-controlled platform, the signals are usually sampled at evenly spaced time intervals. An algorithm to compute $\rho(t_n)$ with a fixed time interval Δt is shown in Algorithm 2. In the 6th line of the algorithm, we compute the integration by using the

Algorithm 2 Pseudo code for computing $\rho(t_n)$ in the dynamic triggering scheme.

1: **Initialize:**
   $\theta, \lambda_\alpha, \rho(t_0), \Delta t$, `sum` $= 0$, `n` $= 0$, `eps=1e-8`
2: **while** $t_n \leq T$ **do**
3: `f[n]` $= \frac{k}{2} \cdot (\max\{k'^2|e(t_n)|^2, \epsilon^2\} - |\tilde{e}(t_n)|^2)$
4: `Sum` $= e^{-\lambda_\alpha(t_n - t_0)} \cdot \rho(t_0)$
5: **for** `idx in 1:1:n` **do**
6: `sum` $=$ `sum` $+ e^{-\lambda_\alpha(n-idx)\Delta t} \cdot$ `f[n]` $\cdot \Delta t$
7: **end for**
8: $\rho(t_n) = \max\{$`sum,eps`$\}$
9: $f(t_n) =$ `f[n]`
10: **if** $\rho(t_n) + \theta f(t_n) \leq 0$ **then**
11: `Update the control signal`
12: **end if**
13: $t_n = t_n + \Delta t$
14: **end while**

right-endpoint rectangular method, which gets an approximative value based on the definition of Riemann integral; see [25, 167]. It is noted that although theoretically $\rho(t_n)$ should always be nonnegative as given in Lemma 5.2, this may not be true with the numerical computation. Thus, in the 8th line, we use a very tiny positive number `eps` as a lower bound for

guaranteeing the nonnegativity of $\rho(t_n)$. This will affect the numerical precision. Whereas, the use of higher sampling rates or periodic event-triggered methods [71] may lighten its negative effect.

Note that compared with the static ETC scheme (5.19), only the triggering condition and the function $\rho(t)$ need to be changed in the dynamic event triggering condition (5.27). Thus, the flowchart of the dynamic ETC scheme is similar to that shown in Fig. 5.3 by incorporating Algorithm 2.

5.6 Experimental validation

In this section, we perform numerical simulations to evaluate the performance of the developed ETC schemes. The simulation is conducted on a workstation with four Intel Xeon W3550 CPUs with 16 GB RAM running at 3.07 GHz. The operating system is Arch Linux 6. Python programming language is used to implement the simulation.

5.6.1 Simulation setup

In the simulation study, we consider a population of heterogeneous ACs, each of them is governed by the first-order ETP model with randomly generated thermal parameters [24, 55, 145, 224]. Note that the controller is designed by using the CFP model that is of infinite dimension. To assess the validity and the performance of the developed control strategy, we consider a population with a modest number of only 5,000 ACs. Eventually, as the CFP model becomes more accurate as the number of TCLs increases, we can reasonably expect a better performance when the proposed control scheme is applied to populations of larger sizes. The parameters used in the simulation are summarized in Table 5.1. The thermal capacitances of the TCLs in the population follow the log-normal distribution with a mean value of 10 kWh/°C and a standard deviation of 2 kWh/°C. The thermal resistances of the TCLs also follow the log-normal distribution with a mean value of 2 °C/kW and a standard deviation of 0.4 °C/kW. This results in a heterogeneity described by σ in the Fokker-Planck equations (5.6) [24, 145, 224]. Nevertheless, as mentioned earlier, the implementation of the proposed robust control scheme is independent of the value of σ. The sampling interval, t_c, in the simulation is set to be 30 seconds, as listed in Table 5.1, which can be adjusted based on specific applications. To update control signals with (5.14) or (5.16), the values of $f_1(\overline{x}, t)$ and $f_0(\underline{x}, t)$ are required. The midpoint rule with a temperature bin width denoted by δ_x is used. Note that the bin width should not be too large, as the solutions to the CFP model are nonlinear functions. It should not be too small, because the number of ACs in

the simulation is limited, which may cause biases. In the implementation, three bin widths, 0.08, 0.04, and 0.02, are used to obtain initial estimations. Then, the average value of these initial estimations is used in the controller.

Three types of disturbances, corresponding to the dynamical model (5.4), are added in the simulation. First, a local forced switch process, which allows for alternating the state of each TCL, is introduced. The probability of switching rate is set to be 3% per hour. Second, random communication delays following a log-normal distribution are added for each AC. Based on the research of [147], the average value of the delay is set to be 1 second, the standard deviation is 0.2 seconds, and the maximum delay is limited to 2 seconds. In this setting, no significant effect on the set-point change for each AC unit was observed. Finally, a lockout time, t_l, is included, allowing for mitigating the impact of frequent switchings of the compressor.

Table 5.1 Parameters used in the simulation.

Parameters	**Values**
R: average thermal resistance	2 °C/kW
C: average thermal capacitance	10 kWh/°C
P: electric power	14 kW
η: load efficiency	2.5
θ_{sp}: intial set point	20 °C
δ: deadband width	0.5 °C
t_c: control interval length	30 seconds
δ_x: initial histogram bin width	0.02 °C
p: forced switch probability per hour	3%
t_d: average network delays	1 second
t_l: lockout time of each TCL	6 minutes

In the initialization phase, the temperature of ACs is uniformly distributed over a deadband centered at 20 °C, and 40% of the ACs are randomly set to the ON-state. In the control execution phase, the data transmitted from TCLs are collected with a frame of 30 seconds. For the implementation of the continuous-time controller (5.14), the control signal is sampled periodically. While the static triggering scheme (5.19) and the dynamic triggering scheme (5.27) are updated aperiodically.

In the experiment, we consider the same scenario studied in [220]. Specifically, the control cycle is 6 hours, from 10:30 to 16:30. The population shares a common ambient temperature curve, as shown in Fig. 5.4. Furthermore, we use a predefined power profile, shown in Fig. 5.5, as the reference for tracking control. In the first hour, the desired (normalized)

power is maintained constant at 0.4. Then, it drops to 0.2 in half an hour and maintains constant for the next 2.5 hours until 14:30. Starting from 14:30, it rises to 0.5 in the next 30 minutes and stays constant until the end of the control cycle. During the rising and dropping phases, the desired power curve is specified by a smooth polynomial of the form:

$$y_d(t) := (y_d(t_f) - y_d(t_i))\,\tau^5(t) \sum_{l=0}^{4} a_l \tau^l(t), t \in [t_i, t_f], \tag{5.33}$$

where t_i and t_f are, respectively, the starting and ending times, and $\tau(t) := (t - t_i)/(t_f - t_i)$. By setting

$$\dot{y}_d(t_i) = \dot{y}_d(t_f) = \ddot{y}_d(t_i) = \ddot{y}_d(t_i) = \dddot{y}_d(t_i) = \dddot{y}_d(t_f) = 0,$$

the coefficients of the polynomial (5.33) are given by [99]:

$$a_0 = 126,\ a_1 = 420,\ a_2 = 540,\ a_3 = 315, \text{ and } a_4 = 70.$$

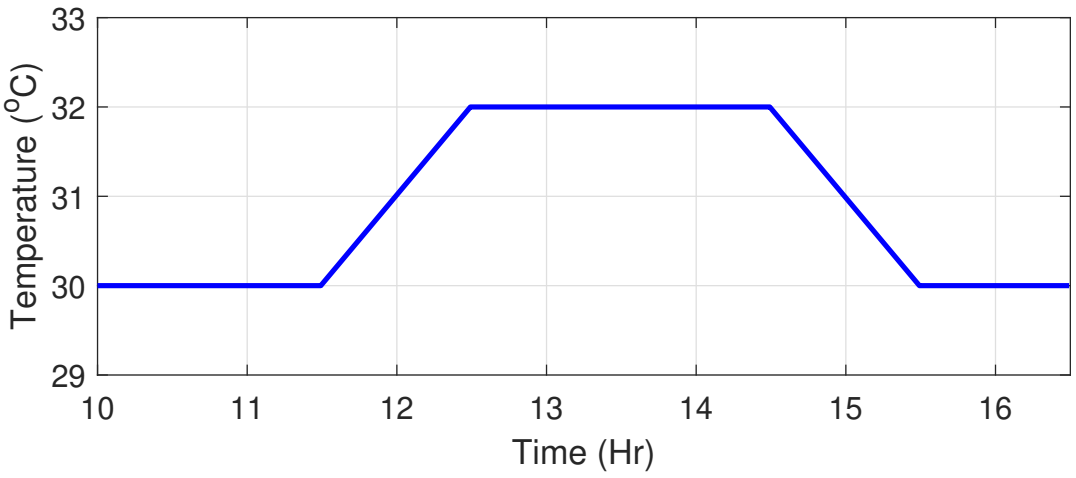

Figure 5.4 Ambient temperature.

5.6.2 Results of static ETC

We start the experiment by examining the continuous-time control scheme (5.14). The sampling interval of the periodic control scheme is set to be 30 seconds (t_c in Table 4.1). During the test, the parameters k and γ in (5.14) are chosen to be $k = 8$ and $\gamma = 0.5$. The

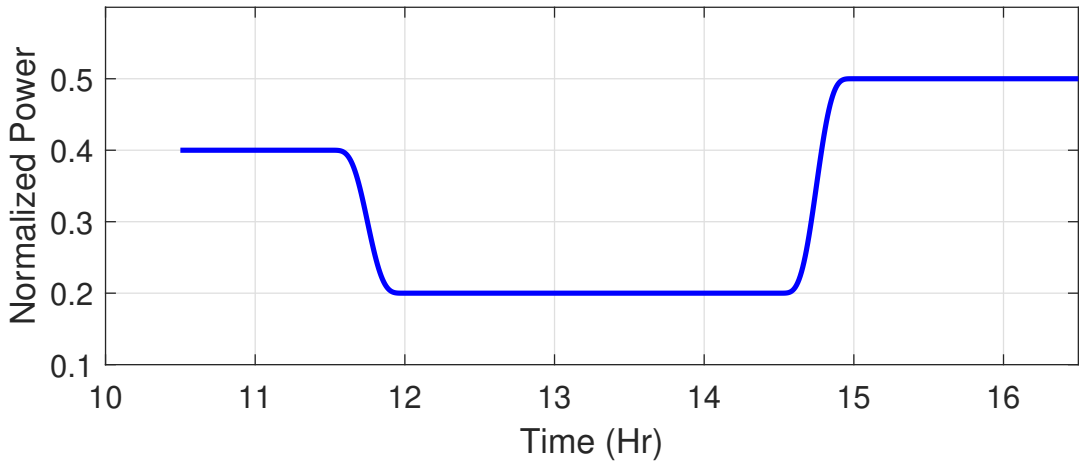

Figure 5.5 Desired power profile.

same values are used in the ETC schemes. The tracking performance is indicated by the rooted-mean-squared errors (RMSEs) of the normalized power. Table 5.2 shows the RMSEs of 5 continuously tested episodes with an average value of RMSEs of 1.068%. This set of data will be used as a baseline to evaluate the performance of the static ETC scheme (5.19) and the dynamic ETC scheme (5.27).

Table 5.2 Tracking performance of 5 episodes with periodic control strategy.

Episode	1	2	3	4	5
RMSE (%)	1.018	1.074	1.056	1.115	1.075

For the static ETC scheme (5.19), different choices of k' and ϵ are examined. Each configuration is successively tested 5 times, and the average triggering intervals (ATIs) and the average rooted-mean-squared errors (ARs) are recorded, as summarized in Table 5.3. The units for ATIs and ARs are second and kW, respectively.

For the average event-triggering intervals (ATIs), the trend w.r.t. the controller parameter variations is apparent. Specifically, for a fixed k', the ATIs increase as ϵ increases. When ϵ is fixed, the triggering intervals also increase as k' increases. The average RMSEs (ARs) share the same trend as the ATI, increasing slightly when either k' or ϵ increases. The best AR is achieved with $k' = 0.1$ and $\epsilon = 0.001$, and the worst case is the one with $k' = 0.5$ and $\epsilon = 0.005$. Figure 5.6 illustrates one tracking control execution sample with $k' = 0.1$ and $\epsilon = 0.001$ and another one with $k' = 0.5$ and $\epsilon = 0.005$. For ease of comparison, the results of a periodic control sample with an RMSE of 1.018% are also displayed. In this test, the

Table 5.3 Comparison of the static ETC for different k' and ϵ.

ATI/AR k' / ϵ	0.1	0.3	0.5
0.001	85.0 / 1.252	130.2 / 1.415	161.7 / 1.528
0.002	108.1 / 1.284	142.7 / 1.385	178.4 / 1.507
0.003	132.4 / 1.299	162.3 / 1.440	200.4 / 1.530
0.004	162.2 / 1.360	187.3 / 1.475	206.9 / 1.505
0.005	183.4 / 1.402	201.9 / 1.436	219.7 / 1.524

ATI with $k' = 0.1$ and $\epsilon = 0.001$ is 89.3 seconds and the RMSE is 1.364%. For the sample with $k' = 0.5$ and $\epsilon = 0.005$, the ATI is 237.4 seconds and the RMSE is 1.484%. Compared with the periodic control scheme, the average control update intervals of the ETC scheme increase by $3 \sim 7$ times while the performance remains similar.

5.6.3 Results of dynamic ETC

For the dynamic ETC scheme (5.27), we set $k' = 0.1$, $\epsilon = 0.003$, $\rho(t_0) = 1$, and $\alpha(\rho) = -10\rho$ (k' and ϵ are randomly chosen from Table 5.3, and $\rho(t_0)$ and $\alpha(\rho)$ can be adjusted based on specific applications). The effect of different choices of θ is reported in Table 5.4. It can be observed that first, the ATI decreases when θ increases. Hence, the value of θ is inversely proportional to the inter-execution interval. Moreover, the averages of RMSEs (ARs) are also inversely proportional to the values of θ. They drop slightly while θ increases. This trend, as shown in Table 5.4, is different from that in Table 5.3, which is always proportional to k' or ϵ. Finally, although the inter-execution interval keeps decreasing, it is always larger than 132.4 seconds in the static ETC scheme. This observation complies with the claim of Theorem 5.4. Nevertheless, more appropriate values of k', ϵ, and θ should be determined based on the requirements of practical applications.

Table 5.4 Average triggering intervals (ATI) for different values of θ.

θ	0.1	1	5
ATI/AR	171.7 / 1.523	162.2 / 1.401	154.4 / 1.429
θ	10	50	100
ATI/AR	153.4 / 1.339	148.6 / 1.353	145.2 / 1.323

Figure 5.7 shows two samples of the system using the dynamic ETC scheme with $\theta = 0.1$ and $\theta = 100$. The same periodic control result shown in Fig. 5.6 is also depicted for comparison.

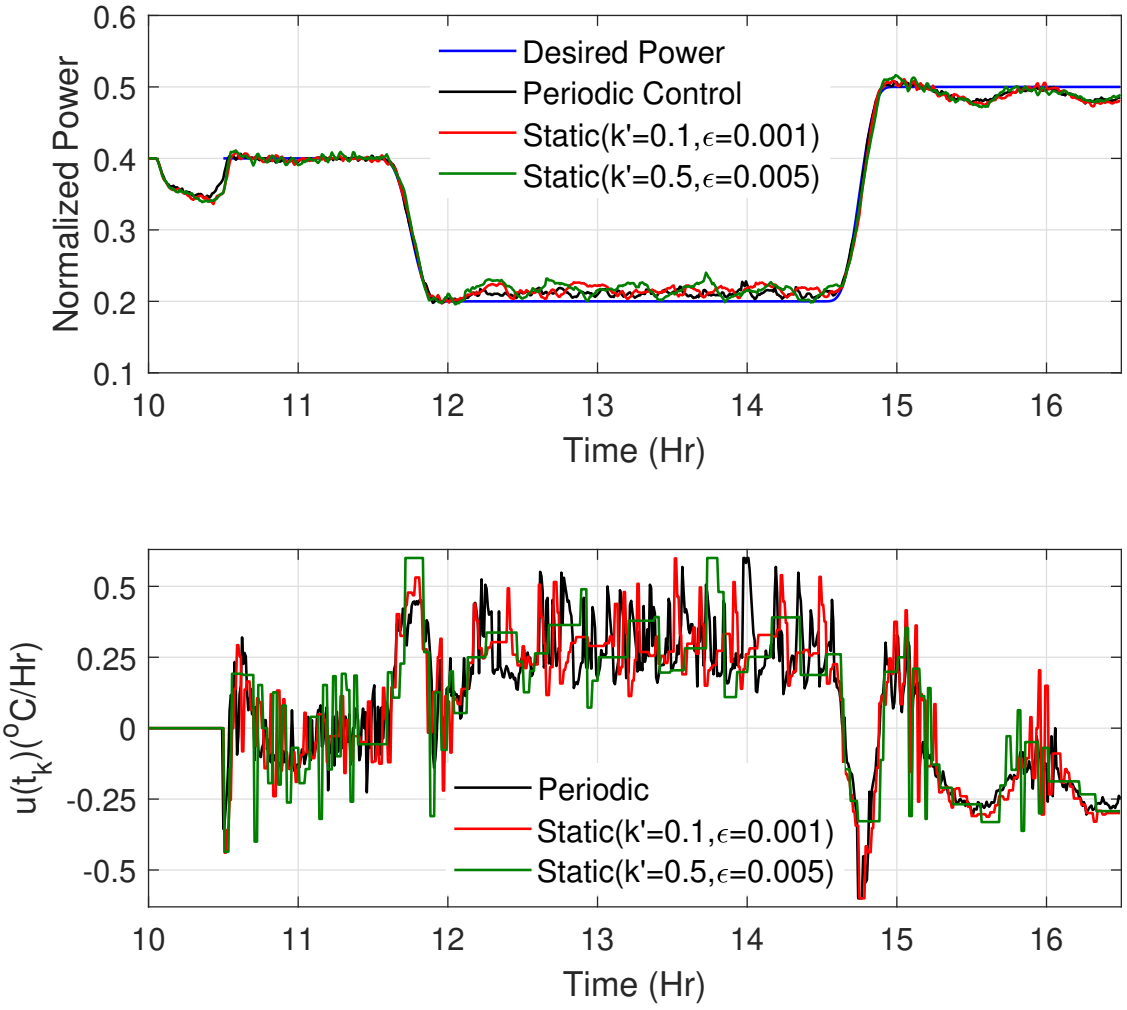

Figure 5.6 Static triggering scheme. Top: tracking performance; bottom: set-point variation rate.

For the dynamic ETC with $\theta = 0.1$, the ATI is 170.1 seconds and the RMSE is 1.491%. For the dynamic ETC with $\theta = 100$, the ATI is 145.0 seconds and the RMSE is 1.389%. It is evident that the tracking performance remains similar, while the dynamic triggering schemes can significantly reduce the control update frequencies.

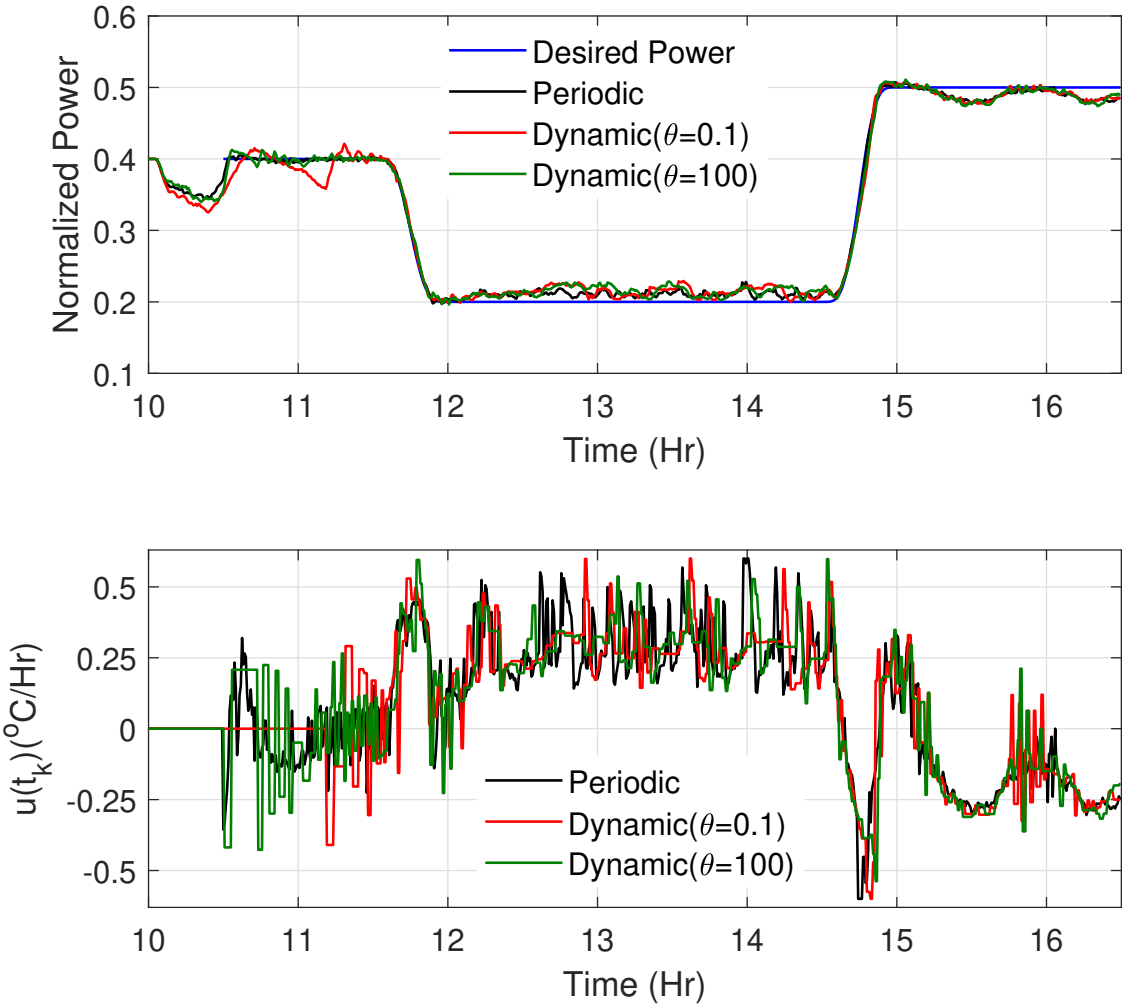

Figure 5.7 Dynamic triggering scheme. Top: tracking performance; bottom: set-point variation rate.

To better visualize the effect of ETC, we show in Fig. 5.8 the distribution of execution intervals of the static ETC and the dynamic ETC. The static ETC result is a sample with $k = 0.1, \epsilon = 0.003$, and the dynamic ETC result is a sample with $k = 0.1$, $\epsilon = 0.003$, and $\theta = 0.1$. It is clear that the mass of the execution interval distribution is concentrated around $120 \sim 140$ seconds, which are $3 \sim 5$ times larger than the sampling period. Moreover, the distribution of execution intervals for the dynamic ETC scheme tends to have more occurrence on the right side, thereby representing a higher mean inter-execution gap compared to the

static ETC scheme.

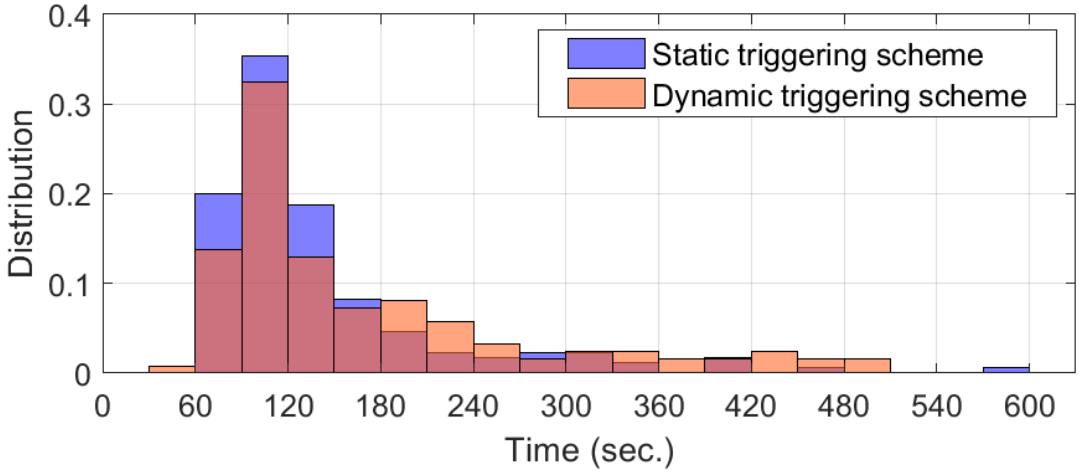

Figure 5.8 Inter-execution time distributions of static and dynamic ETC schemes.

5.7 Conclusion

This paper presented the development, implementation, and validation of static and dynamic ETC schemes for power tracking control of TCL populations for which the aggregate dynamics are described by coupled Fokker-Planck equations. The control design is based on the emulation approach, which is widely adopted in the development of ETC. The basic properties for ETC systems, in particular the closed-loop stability with aperiodic control updates and the avoidance of Zeno phenomenon have been rigorously analyzed, which ensures that the proposed control strategies are well-behaved. A simulation study has been carried out, and the results indicate that both static and dynamic ETC schemes perform well and are effective in extending the control execution interval compared to the original continuous-time control scheme, thereby allowing for relaxing the capacity constraint on the underlying communication infrastructure for supporting the DR programs, which is indeed one of the most important considerations for real-time implementations. The realization of the present work is an encouraging attempt, which represents a step forward towards practical applications of numerous recently developed techniques for power systems control in the context of the smart grid.

CHAPTER 6 ARTICLE 3: POWER TRACKING CONTROL OF SECOND-ORDER HETEROGENEOUS TCL POPULATIONS

Zhenhe Zhang, Guchuan Zhu
Published in: IEEE Transactions on Smart Grid
Submission date: June 21, 2025

Abstract

This paper addresses the modeling and control of heterogeneous thermostatically controlled load (TCL) populations, which is an important issue for demand response programs in the context of smart grid technologies. Specifically, we consider in the present work the problem of power consumption control of 2nd-order TCL populations whose dynamics are described by higher-order coupled Fokker-Planck (CFP) equations. Based on this model, a nonlinear power tracking control scheme with partially observed states is developed. For further performance improvement, an active disturbance rejection control is employed, which allows for the power tracking error to converge to a small bounded region even in the presence of various types of disturbances, including communication delays, lockout effect, varying ambient temperatures, etc.. A numerical simulation study is conducted to demonstrate the effectiveness and the performance of the proposed control scheme.

keywords Power tracking control, heterogeneous thermostatically controlled loads, higher-order coupled Fokker-Planck equations, linear active disturbance rejection control.

6.1 Introduction

In light of the rapidly increasing energy demand and the surging integration of intermittent renewable energy sources, demand-side management (DSM) has gained momentum in maintaining the reliability and efficiency of the modern smart grid, see, e.g., [11, 113]. Many demand response programs, either price-based or incentive-based, play a pivotal role in maintaining the supply-demand balances. By leveraging the collective behaviors of consumers, power consumption burdens can be shifted from on-peak to off-peak hours. It is known that thermostatically controlled loads (TCLs), such as air conditioners, heat pumps, water heaters, refrigerators, etc., represent an important proportion of the total energy consumption and are usually tolerated to small fluctuations inside the comfort zone. These characteristics make TCLs suitable for power regulation tasks, such as peak shaving or valley filling, for

responding to demand response events [38, 58, 120].

The present work deals with power tracking problems for heterogeneous TCL populations based on the decentralized control paradigm [191, 192], which can make the aggregate power of the population to follow desired consumption profiles. Specifically, we consider a heterogenous population with its TCLs described by the second-order equivalent thermal parameter (ETP) model. In such a control system, each unit in the population is operated by a thermostat, taking independent actions in responding to a common control signal from the control center. It is also supposed that communication delays exist in signal transmission within the population, and forced switching between ON and OFF states is also allowed.

The considered control scheme falls into the category of model-based control methods, where the coupled Fokker-Planck (CFP) model originally introduced in [126] plays an essential role in characterizing the aggregate dynamics of the TCL populations. It is noted that by continuously adjusting the nominal set-point temperatures, Callaway [24] has successfully used this model on tracking high-frequency power signals generated from wind farms. After introducing the set-point variation rate into the coupled PDEs, Bashash et al. [21] designed a sliding mode control scheme to regulate the aggregate powers. In [55], an model predictive control (MPC) method is proposed while including the effect of heterogeneity into the CFP equations. In [219, 220], another continuous controller and its event-triggered schemes are considered for load following tasks. However, all the aforementioned PDE models are derived from a simplified first-order ETP model for individual loads. It has been shown that a second-order ETP model, which considers both indoor air temperature and mass temperature, is more accurate for describing the underlying steady and transient thermal dynamics (see, e.g., [115, 215]). Hence, the corresponding CFP model should also be generalized for describing the aggregate dynamics of higher-dimensional TCL populations. It should also be noted that there exists also a rich literature on finite-dimensional models of aggregate TCL dynamics, such as state-bins model [21, 77, 108, 178, 215], state-queueing model [17, 116], etc., and most of them can be derived from the CFP model by discretizing the temperature variables over the space.

Real-time processing is one of the essential considerations in order to guarantee a certain level of quality of service (QoS). However, controlling a population composed of tens or hundreds of thousands of TCLs can be computationally demanding [61, 222]. Therefore, low-complexity control algorithms that are insensitive to the population size should be well studied. For this reason, control schemes without using full state knowledge of the system are highly preferred. More importantly, only collecting partial state information from the population can also significantly relieve communication burdens and simultaneously boost

the privacy protections on the customers.

The present work is a further improvement of [219] by using second-order models for individual loads and a higher-dimensional CFP model for the aggregate dynamics while considering various disturbances which may occur in practical applications. Particularly, disturbance rejection control, such as active disturbance rejection control (ADRC) or linear ADRC (LADRC) [4, 63, 67, 73], are incorporated into the control scheme. The main contributions of this paper include:

- an improved aggregate model, which slightly modifies the work in [221] and deals with higher-order thermal dynamics, is introduced;
- a nonlinear power tracking control law based on the method of input-output linearization while requiring only partially observed states of the population is developed;
- an improved auxiliary controller scheme by utilizing LADRC is proposed, which can significantly suppress the steady state error due to diverse disturbances;
- the robust stability of the closed-loop system in the sense of input-to-state stability (ISS) is assessed.

The remainder of the paper is organized as follows. Section 6.2 presents the dynamical model of the system, including both the second-order ETP model for individual thermal loads and the generalized CFP model for the population. Section 6.3 puts forward the control law design for power tracking and assess the closed-loop stability of the system. In Section 6.4, simulation results are presented, showing that the proposed control law performs well for larger-scale TCL populations. Section 6.5 concludes the work by providing discussions on its limitation and potential future improvements.

6.2 Mathematical model for TCL populations

In this section, we investigate the thermodynamics of a single TCL unit and explore the aggregate dynamics of a large population. The single TCL dynamics is described by the second-order ETP model, and the aggregated dynamics of TCL populations is characterized by generalized coupled Fokker-Planck equations. Residential air conditioners (ACs) are considered in the following study. Nevertheless, the established model can be easily generalized to other types of cooling or heating devices.

6.2.1 Second order ETP model for a single TCL

The ETP model is widely used to describe household thermal dynamics, where the parameters in a heat transfer process are analogized to circuit parameters such as voltages, currents, capacitances, resistances, and so on. For the second-order ETP model, the temperature evolution process inside a room can be equivalently represented by the electrical schematic shown in Fig. 6.1. Compared with the first-order ETP model [24, 224], this model further takes mass temperature, equivalent mass capacitance, and equivalent mass resistance into consideration, resulting in an enhanced accuracy.

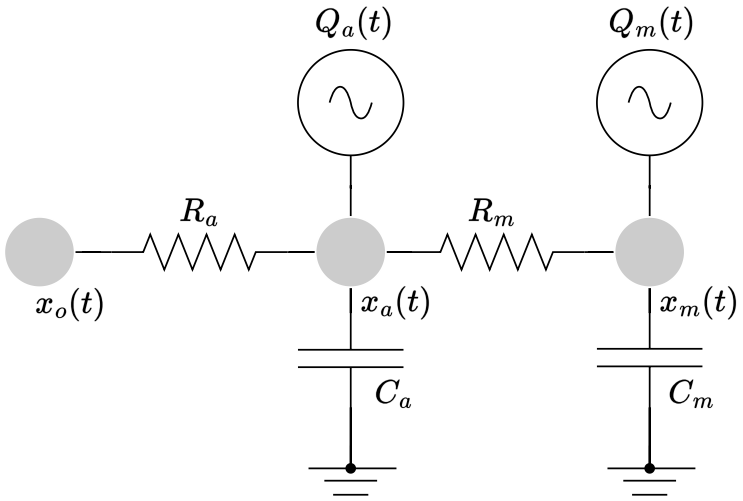

Figure 6.1 The circuit diagram for the second-order ETP model.

Denote by $x_a(t)$ and $x_m(t)$ the indoor air and the mass temperatures, respectively. For notational simplicity, we may omit the time variable if no ambiguities occur. Then, for the air temperature node and the mass node in Fig 6.1, it yields:

$$\begin{aligned} C_a\dot{x}_a &= \frac{x_m - x_a}{R_m} + \frac{x_o - x_a}{R_a} + Q_a, \\ C_m\dot{x}_m &= \frac{x_a - x_m}{R_m} + Q_m, \end{aligned} \tag{6.1}$$

where C_a, R_a, C_m, and R_m are equivalent capacitances and resistances of air and mass respectively, Q_a and Q_m represent the heat gain to the interior air and mass, and x_o denotes the outside temperature. Suppose that the heat gain directly added onto the bulk of mass, Q_m, is insignificant, and the heat gain on the interior air is approximately written as:

$$Q_a = s(t)\eta P, \tag{6.2}$$

where P is the rated power of the cooling device, η is the coefficient of performance (COP), and $s(t)$ is the thermostat operating state of the unit. The state transition law of $s(t)$ is defined as:

$$s(t) = \begin{cases} 1, & \text{if } x_a(t) \geq \overline{x}_a(t); \\ 0, & \text{if } x_a(t) \leq \underline{x}_a(t); \\ s(t^-), & \text{otherwise,} \end{cases} \tag{6.3}$$

where $\underline{x}_a(t) = x^a_{sp}(t) - \frac{\delta_a}{2}$ and $\overline{x}_a(t) = x^a_{sp}(t) + \frac{\delta_a}{2}$ are the lower and upper boundaries with $x^a_{sp}(t)$ being the set-point temperature, and δ_a being a constant dead-band width, and (t^-) means approaching t from the left side.

The hybrid model defined by (6.1), (6.2), and (6.3) captures the temperature variations in a room. It reveals the temperature changing pattern of a local area where the TCL is located, reflecting the relationship between indoor mass or air temperatures, power consumption, and outside weather profile. In a more compact form while considering the disturbances, the dynamic model of a TCL can be equivalently written as:

$$\mathrm{d}x = (Ax + B_0 - s(t)B_1)\,\mathrm{d}t + \sigma\,\mathrm{d}W, \tag{6.4}$$

where $x := \begin{bmatrix} x_a, x_m \end{bmatrix}^\top$,

$$A := \begin{bmatrix} -\dfrac{1}{C_a}\left(\dfrac{1}{R_a} + \dfrac{1}{R_m}\right) & \dfrac{1}{C_a R_m} \\ \dfrac{1}{C_m R_m} & -\dfrac{1}{C_m R_m} \end{bmatrix}, \tag{6.5}$$

$$B_0 := \begin{bmatrix} \dfrac{1}{C_a R_a} x_o \\ 0 \end{bmatrix}, \tag{6.6}$$

$$B_1 := \begin{bmatrix} \dfrac{1}{C_a}\eta P \\ 0 \end{bmatrix}, \tag{6.7}$$

W is a Wiener process on 2D space, and σ is a constant measuring the standard deviation of uncounted heat sources or sinks.

Remark 6.1. *In* (6.3)*, the values of* $s(t)$*, either 0 or 1, are determined only by* $x_a(t)$*,* $\overline{x}_a(t)$*, and* $\underline{x}_a(t)$*. For notational simplicity, we will use hereafter* $x_{sp}(t), \delta, \overline{x}(t)$*, and* $\underline{x}(t)$ *in the replace of* $x^a_{sp}(t), \delta_a, \overline{x}_a(t)$*, and* $\underline{x}_a(t)$*, respectively. For a more generic switching scheme depending also on the value of mass temperature, a more elaborated research is needed (see, e.g., [221]).*

6.2.2 Aggregate dynamics of TCL populations

In this work, a generalized CFP model on second-order/higher-order hybrid-state dynamics is used to describe the aggregate dynamics (see, e.g., [221]).

Consider the tracking process in $[t_0, T]$, where t_0 is the starting point and T is the ending moment satisfying $0 \leq t_0 < T < \infty$. For the space variables, divide the region $\mathbb{R}^2$ into three parts with two air temperature boundaries, denoted by Ω_a, Ω_b, and Ω_c, respectively:

$$\begin{aligned}
\Omega_a &:= \left\{ (x_a, x_m) \in \mathbb{R}^2 : x_a < x_{sp} - \frac{\delta}{2} \right\}, \\
\Omega_b &:= \left\{ (x_a, x_m) \in \mathbb{R}^2 : x_{sp} - \frac{\delta}{2} < x_a < x_{sp} + \frac{\delta}{2} \right\}, \\
\Omega_c &:= \left\{ (x_a, x_m) \in \mathbb{R}^2 : x_a(t) > x_{sp} + \frac{\delta}{2} \right\}.
\end{aligned}$$

Let $f_{0a}(x,t)$ and $f_{0b}(x,t)$ be the probability density function (PDF) for the ACs in OFF ($s = 0$) states in region Ω_a and Ω_b respectively, and accordingly $f_{1b}(x,t)$ and $f_{1c}(x,t)$ be the PDFs in ON ($s = 1$) states in region Ω_b and Ω_c respectively. Note that there is no need to consider $f_{0c}(x,t)$ and $f_{1a}(x,t)$, as they are always zero for all $t \in [t_0, T]$. Assume that $f_{0a}(x,t), f_{0b}(x,t), f_{1b}(x,t)$, and $f_{1c}(x,t)$ are $C^{2,1}$ in each region, where $C^{2,1}$ denotes the class of functions having 2nd order continuous partial derivatives with respect to x and 1st order continuous derivative with respect to t. Furthermore, assume that all the above functions have uniformly continuous partial derivatives of order up to 2 on bounded subsets in each region. Then, for a population of higher-order heterogenous ACs, the aggregated dynamics of the population satisfy the following coupled Fokker-Planck equations:

$$\frac{\partial}{\partial t} f_{0a}(x,t) + \nabla \cdot \Big((\alpha_0(x,t) - U(t)) f_{0a}(x,t) \Big) - \frac{\sigma^2}{2} \Delta f_{0a}(x,t) = 0, \tag{6.8a}$$

$$\frac{\partial}{\partial t} f_{0b}(x,t) + \nabla \cdot \Big((\alpha_0(x,t) - U(t)) f_{0b}(x,t) \Big) - \frac{\sigma^2}{2} \Delta f_{0b}(x,t) = 0, \tag{6.8b}$$

$$\frac{\partial}{\partial t} f_{1b}(x,t) + \nabla \cdot \Big((\alpha_1(x,t) - U(t)) f_{1b}(x,t) \Big) - \frac{\sigma^2}{2} \Delta f_{1b}(x,t) = 0, \tag{6.8c}$$

$$\frac{\partial}{\partial t} f_{1c}(x,t) + \nabla \cdot \Big((\alpha_1(x,t) - U(t)) f_{1c}(x,t) \Big) - \frac{\sigma^2}{2} \Delta f_{1c}(x,t) = 0. \tag{6.8d}$$

where $\nabla = (\frac{\partial}{\partial x_a}, \frac{\partial}{\partial x_m})$ is the gradient operator, $\Delta = \frac{\partial^2}{\partial x_a^2} + \frac{\partial^2}{\partial x_m^2}$ is the Laplacian operator,

$U(t) := [u(t), 0]^\top$ is the control input, and

$$\alpha_1(x,t) := Ax + B_0,$$
$$\alpha_0(x,t) := Ax + B_0 - B_1,$$

with A, B_0, and B_1 defined in (6.5), (6.6), and (6.7). For (6.8), as the probability flux of entering and leaving the deadband bounds should be equal, the conservation conditions are:

$$\frac{\partial}{\partial x_a} f_{0a}(\underline{x}^-, x_m, t) - \frac{\partial}{\partial x_a} f_{0b}(\underline{x}^+, x_m, t) - \frac{\partial}{\partial x_a} f_{1b}(\underline{x}^+, x_m, t) = 0, \tag{6.9a}$$
$$\frac{\partial}{\partial x_a} f_{1c}(\overline{x}^+, x_m, t) - \frac{\partial}{\partial x_a} f_{1b}(\overline{x}^-, x_m, t) - \frac{\partial}{\partial x_a} f_{0b}(\overline{x}^-, x_m, t) = 0, \tag{6.9b}$$
$$\forall x_m \in \mathbb{R}, t \in [t_0, T],$$

where $(\cdot)^-$ and $(\cdot)^+$ denote the left and right limit of the variable. The absorbing condition is:

$$f_{0b}(\overline{x}, x_m, t) = f_{1b}(\underline{x}, x_m, t) = 0, \tag{6.10a}$$
$$\frac{\partial}{\partial x_a} f_{0b}(\overline{x}^-, x_m, t) > 0, \frac{\partial}{\partial x_a} f_{1b}(\underline{x}^+, x_m, t) > 0, \tag{6.10b}$$
$$\forall x_m (\in \mathbb{R}, t \in [t_0, T].$$

And the natural boundary conditions are:

$$f_{0a}(-\infty, x_m, t) = f_{1c}(+\infty, x_m, t) = 0. \tag{6.11a}$$
$$\frac{\partial}{\partial x_a} f_{0a}(-\infty, x_m, t) = \frac{\partial}{\partial x_a} f_{1c}(+\infty, x_m, t) = 0. \tag{6.11b}$$
$$f_{0a}(x_a, \pm\infty, t) = f_{0b}(x_a, \pm\infty, t) = 0, \tag{6.11c}$$
$$f_{1b}(x_a, \pm\infty, t) = f_{1c}(x_a, \pm\infty, t) = 0. \tag{6.11d}$$
$$\frac{\partial}{\partial x_m} f_{0a}(x_a, \pm\infty, t) = \frac{\partial}{\partial x_m} f_{0b}(x_a, \pm\infty, t) = 0, \tag{6.11e}$$
$$\frac{\partial}{\partial x_m} f_{1b}(x_a, \pm\infty, t) = \frac{\partial}{\partial x_m} f_{1c}(x_a, \pm\infty, t) = 0. \tag{6.11f}$$

Additionally, at the lower and upper bounds of the deadband, the continuity conditions need

to be respected:

$$f_{0a}(\underline{x}, x_m, t) = f_{0b}(\underline{x}, x_m, t), \tag{6.12a}$$
$$f_{1b}(\overline{x}, x_m, t) = f_{1c}(\overline{x}, x_m, t), \tag{6.12b}$$
$$\forall x_m \in \mathbb{R}, t \in [t_0, T].$$

Finally, the total mass probability should be unity, that is:

$$\int_{-\infty}^{+\infty}\int_{-\infty}^{+\infty} f_{0a}\mathrm{d}x_m\mathrm{d}x_a + \int_{-\infty}^{+\infty}\int_{-\infty}^{+\infty}(f_{0b}+f_{1b})\mathrm{d}x_m\mathrm{d}x_a + \int_{-\infty}^{+\infty}\int_{-\infty}^{+\infty} f_{1c}\mathrm{d}x_m\mathrm{d}x_a = 1. \tag{6.13}$$

In summary, (6.8), along with its boundaries conditions (6.9), (6.10), (6.11), (6.12), and (6.13), describes the overall dynamics for populations with higher-order load dynamics, which will be the basis for designing effective control schemes in the following Section 6.3.

Remark 6.2. *In this work, we assume that the control input* $u(t) = \dot{x}_{sp} = \dot{\overline{x}} = \dot{\underline{x}}$ *is always continuous, or equivalently,* $x_{sp}, \overline{x}, \underline{x} \in C^1([t_0, T], \mathbb{R})$*. For piece-wise continuous control inputs, random jump terms would be included in the dynamics in* (6.8)*, see [221] for more details. Additionally, certain smoothness conditions on the initial distributions are also set as default, otherwise, the solutions to* (6.8) *can only hold in a weak sense. These issues are beyond the scope of this work.*

6.3 Power tracking controller design and closed-loop stability

6.3.1 Input-output dynamics

By the dynamics in (6.8), the aggregate power at time $t \in [t_0, T]$ should be:

$$y_p = \frac{P}{\eta}\int_{\underline{x}}^{\overline{x}}\int_{-\infty}^{+\infty} f_{1b}(x_a, x_m, t)\mathrm{d}x_m\mathrm{d}x_a + \frac{P}{\eta}\int_{\overline{x}}^{+\infty}\int_{-\infty}^{+\infty} f_{1c}(x_a, x_m, t)\mathrm{d}x_m\mathrm{d}x_a.$$

However, to guarantee the input-output controllability, a slightly modified version of the output function is used, shown as follows:

$$\begin{aligned} y =& \frac{P}{\eta}\int_{\underline{x}}^{\overline{x}}\int_{-\infty}^{+\infty} f_{1b}(x_a, x_m, t)\mathrm{d}x_m\mathrm{d}x_a + 2\frac{P}{\eta}\int_{\overline{x}}^{+\infty}\int_{-\infty}^{+\infty} f_{1c}(x_a, x_m, t)\mathrm{d}x_m\mathrm{d}x_a \\ & - \frac{P}{\eta}\int_{-\infty}^{\underline{x}}\int_{-\infty}^{+\infty} f_{0a}(x_a, x_m, t)\mathrm{d}x_m\mathrm{d}x_a. \end{aligned} \tag{6.14}$$

Note that in steady state, there will be no ACs in Ω_a and Ω_c, thus $y = y_p$ holds. Suppose $y_d \in C^1([t_0, T], \mathbb{R}_{\geq 0})$, where $\mathbb{R}_{\geq 0} := [0, \infty)$, is the reference power curve. Then, the tracking

error is written as:

$$e = y_d - y. \tag{6.15}$$

The main objective is to find a control law $u(t) = \dot{x}_{sp}(t) = \dot{\overline{x}} = \dot{\underline{x}}$ such that the tracking error (6.15) tends to zero. To this aim, we compute the derivative of $e(t)$ first. The computation process is similar to that in [219], and the final error dynamics is written as:

$$\dot{e} = \dot{y}_d + 2\frac{P}{\eta}u(t)\left(\int_{-\infty}^{+\infty} f_{1c}|_{\overline{x}}\,\mathrm{d}x_m + \int_{-\infty}^{+\infty} f_{0a}|_{\underline{x}}\,\mathrm{d}x_m\right) + \Gamma(t). \tag{6.16}$$

where

$$\begin{aligned}\Gamma(t) := &-\frac{P}{\eta}\int_{-\infty}^{+\infty}(\alpha_1 f_{1c})\,|_{\overline{x}}\mathrm{d}x_m - \frac{P}{\eta}\int_{-\infty}^{+\infty}(\alpha_0 f_{0a})\,|_{\underline{x}}\mathrm{d}x_m \\ &+ \frac{P\sigma^2}{2\eta}\int_{-\infty}^{+\infty}\left[\left(\frac{\partial}{\partial x_a}f_{1c}\right)|_{\overline{x}^+}\mathrm{d}x_m + \left(\frac{\partial}{\partial x_a}f_{0b}\right)|_{\overline{x}^-}\right. \\ &\left.+\left(\frac{\partial}{\partial x_a}f_{1b}\right)|_{\underline{x}^+} + \left(\frac{\partial}{\partial x_a}f_{0a}\right)|_{\underline{x}^-}\right]\mathrm{d}x.\end{aligned} \tag{6.17}$$

Note that in (6.16) and (6.17), notations similar as $f_{0a}|_{\underline{x}} := f_{0a}(\underline{x}, x_m, t)$ are applied for notational simplicity. Define

$$u(t) := \frac{\eta}{2P}\frac{v(t) - \dot{y}_d}{\int_{-\infty}^{+\infty} f_{1c}|_{\overline{x}}\mathrm{d}x_m + \int_{-\infty}^{+\infty} f_{0a}|_{\underline{x}}\mathrm{d}x_m}, \tag{6.18}$$

where $v(t)$ is an auxiliary control to be determined, then the tracking error dynamics become:

$$\dot{e} = v(t) + \Gamma(t). \tag{6.19}$$

With the boundary conditions given in (6.9), (6.10), (6.11), (6.12), and the probability conservation property (6.13), it can be shown that, similar to the proof given in [220], the denominator in the controller (6.18) is always positive in $[t_0, T]$, for all $0 \leq t_0 < T < \infty$ under appropriate initial conditions. Suppose that the auxiliary controller $v(t)$ and the derivative of the reference power curve $\dot{y}_d$ are bounded, then the control signal generated by (6.20) is always bounded. Thus, the existence and uniqueness of the solutions to the CFP system (6.8) is always guaranteed (see [10, 22, 96, 97]).

The control scheme (6.18) is in an ideal form without constraints on the maximum temperature offsets. Furthermore, note that the denominator in (6.18) requires analytical solution of the PDE system, which is hard to obtain. Hence, approximation techniques, such as numerical estimations, need to be exploited for efficient controller implementation. Finally, the auxiliary control, $v(t)$, is also undetermined and it is expected to have the ability to reject

disturbances. In the following, we tackle these issues by incorporating saturation function in the control law, using mid-point rule for numerical estimations, and introducing LADRC in the auxiliary controller to counteract unknown and unmodeled disturbances.

6.3.2 Introducing saturation control

In practical application scenarios, drastic temperature fluctuations may introduce instabilities to power systems and can cause discomfort to residents. Hence, the set-point temperature offset per hour should be appropriately constrained. For this reason, a saturation function with a constant limit M is added to (6.18), leading to a saturated control:

$$\mathrm{sat}(u(t)) = \begin{cases} M, & \text{when} \quad u(t) > M, \\ u(t), & \text{when} \quad |u(t)| \leq M, \\ -M, & \text{when} \quad u(t) < -M, \end{cases} \tag{6.20}$$

where M is the maximum changing velocity at time t or the maximum temperature set-point offset per hour. Let $\delta u(t)$ denote the difference between $\mathrm{sat}(u(t))$ and $u(t)$, i.e.,

$$\delta u(t) := \mathrm{sat}(u(t)) - u(t),$$

then, the error dynamics (6.16) become:

$$\begin{aligned} \dot{e}(t) =& \dot{y}_d(t) + 2\frac{P}{\eta}\mathrm{sat}(u(t)) \left(\int_{-\infty}^{+\infty} f_{1c}|_{\overline{x}} \, \mathrm{d}x_m + \int_{-\infty}^{+\infty} f_{0a}|_{\underline{x}} \, \mathrm{d}x_m \right) + \Gamma(t) \\ =& \dot{y}_d(t) + 2\frac{P}{\eta}u(t) \left(\int_{-\infty}^{+\infty} f_{1c}|_{\overline{x}} \, \mathrm{d}x_m + \int_{-\infty}^{+\infty} f_{0a}|_{\underline{x}} \, \mathrm{d}x_m \right) \\ & + \Gamma(t) + 2\frac{P}{\eta}\delta u(t) \left(\int_{-\infty}^{+\infty} f_{1c}|_{\overline{x}} \, \mathrm{d}x_m + \int_{-\infty}^{+\infty} f_{0a}|_{\underline{x}} \, \mathrm{d}x_m \right) \\ =& v(t) + \tilde{\Gamma}(t), \end{aligned} \tag{6.21}$$

where

$$\tilde{\Gamma}(t) := \Gamma(t) + 2\frac{P}{\eta}\delta u(t) \left(\int_{-\infty}^{+\infty} f_{1c}|_{\overline{x}} \mathrm{d}x_m + \int_{-\infty}^{+\infty} f_{0a}|_{\underline{x}} \mathrm{d}x_m \right). \tag{6.22}$$

In (6.18) and (6.20), the auxiliary control signal $v(t)$ is undetermined, and there exist various choices. In [220] and [219], a proportional auxiliary controller and a slide mode-like version are respectively utilized for power tracking control of the first-order TCL populations. In the following, the proportional auxiliary controller continues to be used and acts as a baseline for control performance verification of the second-order populations. An upgraded version

combined with LADRC is proposed to counteract the disturbances due to unmeasurable and unmodeled dynamics.

6.3.3 Proportional auxiliary controller

When $v(t) = -ke(t)$, where k is the proportional gain, the tracking dynamics in (6.19) for the second-order populations become:

$$\dot{e} = -ke + \Gamma(t). \tag{6.23}$$

For (6.23), the equilibrium solution is $e_{\text{eq}}(t) = \frac{1}{k}\Gamma(t)$. Note that $\Gamma(t)$ is a bounded function in $[t_0, T]$, i.e., there exists a positive constant C_Γ such that $\Gamma(t) \leq C_\Gamma, \forall t \in [t_0, T]$. Thus, the tracking error will always converge to a bounded interval $[-\frac{1}{k}C_\Gamma, \frac{1}{k}C_\Gamma]$ despite the uncertain initial conditions or small disturbances. In the context of the input-to-state stability (ISS), this stability property is characterized by the following theorem.

Theorem 6.1. *Consider the system* (6.8) *with the output defined in* (6.14)*. Suppose that the control law is given by* (6.18) *with proportional auxiliary controller* $v(t) = -ke(t)$*. Then, the tracking error dynamics given in* (6.19) *are ISS with respect to* $\Gamma(t)$*.*

Proof. For the unforced dynamics $\dot{e} = -ke$, the origin is globally asymptotically stable for any $k > 0$. Chose a Lyapunov function candidate of the form $V(e) = \frac{1}{2}e^2(t)$, which is positive-definite and radically unbounded. Furthermore, letting θ be a constant with $0 < \theta < 1$, then we have

$$\begin{aligned}
\dot{V}(e) &= e\dot{e} \\
&= -ke^2 + e\Gamma(t) \\
&\leq -ke^2 + |e(t)||\Gamma(t)| \\
&= -(1-\theta)ke^2 - \theta ke^2 + |e||\Gamma(t)|.
\end{aligned}$$

Then,

$$\dot{V}(e) \leq -(1-\theta)ke^2$$

provided that

$$-\theta ke^2 + |e||\Gamma(t)| \leq 0,$$

and the latter inequality is satisfied if

$$|e| \geq \frac{1}{\theta k}|\Gamma(t)|.$$

Defining a Lyapunov gain function $\chi(r) = \frac{1}{\theta k}r$, then $\dot{V}(e) \leq -(1-\theta)ke^2(t)$ for all $|e(t)| \geq$

$\chi(|\Gamma(t)|)$. Because there exists a smooth ISS-Lyapunov function $V(e)$, the system is ISS with respect to $\Gamma(t)$, see [92, 181]. □

The stability result given in Theorem 6.1 is under the assumption that the control input takes the form of (6.20). After introducing the saturation function, the error dynamics change to (6.21), and a similar stability result still holds, as shown in Theorem 6.2.

Theorem 6.2. *Consider the system* (6.8) *with the output defined in* (6.14). *Suppose that the control law is given by* (6.18) *and* (6.20) *with proportional auxiliary controller* $v(t) = -ke(t)$. *Then, the tracking error dynamics given in* (6.21) *are ISS with respect to* $\tilde{\Gamma}(t)$.

The proof Theorem 6.2 can be proceeded in a similar way as the proof of Theorem 6.1 and hence, it is omitted.

6.3.4 LADRC auxiliary controller

It should be noted that there may be steady-state errors with the proportional auxiliary controller. Moreover, modeling errors due to unaccounted heat loss or gain should also be well compensated in the control process. In what follows, LADRC method is employed to suppress these effects. LADRC is a model-free control technique which is developed on the basis of ADRC method and can effectively counteract the negative impacts of internal disturbances or other unconsidered dynamics. With an appropriate tuning, this control algorithm can achieve satisfactory control effects in many practical applications (see, e.g., [70, 73]).

Note that in the considered problem, although the value of $\tilde{\Gamma}(t)$ in (6.21) is not available or very hard to measure, all its information is hidden in the error dynamics. Therefore, $\tilde{\Gamma}(t)$ can be treated as an extended state, and the negative effects can be actively compensated by inject the estimate of disturbances obtained by an observer to the controller. Specifically, let $x_1 = e$ and x_2 be the total disturbance (including $\tilde{\Gamma}(t)$) of the system. Then, it follows that

$$\dot{x}_1 = v(t) + x_2. \tag{6.24}$$

Let $\hat{x}_1$ and $\hat{x}_2$ be the estimates of x_1 and x_2, respectively. Then, an extended observer for state and disturbance estimation can be chosen as:

$$\begin{aligned} \dot{\hat{x}}_1 &= \beta_1(e - \hat{x}_1) + v(t) + \hat{x}_2, \\ \dot{\hat{x}}_2 &= \beta_2(e - \hat{x}_1), \end{aligned} \tag{6.25}$$

where $\beta_1 > 0$ and $\beta_2 > 0$ are the observer gains. By the LADRC algorithm, the linear

feedback control is designed as:

$$v(t) = -k\hat{x}_1 - \hat{x}_2. \tag{6.26}$$

It follows that

$$\begin{aligned}\dot{x}_1 &= (-k\hat{x}_1 - \hat{x}_2) + x_2 \\ &= -kx_1 + k(x_1 - \hat{x}_1) + (x_2 - \hat{x}_2) \\ &= -kx_1 + ke_1 + e_2.\end{aligned} \tag{6.27}$$

Suppose $\omega_c > 0$ and $\omega_o > 0$ are the auxiliary controller bandwidth and observer bandwidth, respectively, and let $k = \omega_c$, $\beta_1 = 2\omega_o$, $\beta_2 = \omega_o^2$. By the separation principle for linear control systems, ω_c and ω_o can be designed separately with their values tuned based on the applications. When the observer errors are sufficiently small, the power tracking error, i.e., e, drops to 0 quickly.

Note that from (6.24) to (6.27), the negative effect of $x_1(t)$ (including $\tilde{\Gamma}(t)$) can be greatly constrained by incorporating $\hat{x}_2$ in the control scheme. Thus, a better performance with the new auxiliary controller can be expected. Comparative studies are conducted in Section 6.4 to illustrate the performance of the two auxiliary controllers.

Remark 6.3. *It can be shown that the observation errors for $\hat{x}_1$ and $\hat{x}_2$ are small when $\dot{x}_2$ is bounded (see, e.g., [40, 57, 225, 227]). However, this conclusion is only piecewisely valid in the considered problem. Suppose that there is no modeling error in the system, then $\dot{x}_2 = \dot{\tilde{\Gamma}}(t)$ always holds. However, it should be noted that the saturation function included in $\tilde{\Gamma}(t)$ in* (6.22) *is not differentiable when saturation happens. Thus, with appropriately tuned parameters, $\hat{x}_1$ and $\hat{x}_2$ will only approach to e and $\tilde{\Gamma}(t)$ piecewisely in $t \in [t_0, T]$, $0 \leq t_0 < T < \infty$.*

6.3.5 Numerical implementation of the control scheme

To implement the proposed controller in (6.18) and (6.20), a significant challenge still exists. Note that in the denominator of (6.18), the internal states, $\int_{-\infty}^{+\infty} f_{0a}|_{\underline{x}} \mathrm{d}x_m$ and $\int_{-\infty}^{+\infty} f_{1c}|_{\overline{x}} \mathrm{d}x_m$, are required in the computation. Because the accurate state values are not accessible, two numerical estimations based on midpoint rule are introduced to obtain their practical approximations. In the following, we assume that the controller is implemented on a digital platform, and the control signals are generated and broadcast periodically to the population.

Specifically, consider the region $\Omega_{\underline{x}} := [\underline{x} - \frac{\Delta x_a}{2}, \underline{x} + \frac{\Delta x_a}{2}] \times \mathbb{R}$ with an air temperature bin width Δx_a. Let N be the size of the AC population and n_1 denotes the number of ACs in

$\Omega_{\underline{x}}$ at time $t_i, i \in \mathbb{N}$. We have then

$$\int_{\underline{x}-\frac{\Delta x_a}{2}}^{\underline{x}+\frac{\Delta x_a}{2}} \int_{-\infty}^{+\infty} f_{0a}(x_a, x_m, t_i)\mathrm{d}x_m\mathrm{d}x_a \approx \frac{n_1}{N}.$$

By the mid-point rule w.r.t. the air temperature variable x_a, we have

$$\int_{-\infty}^{+\infty} f_1(\underline{x}, x_m, t_i)\mathrm{d}x_m \approx \frac{n_1}{N\Delta x_a}.$$

Then, a reasonable estimate of $\int_{-\infty}^{+\infty} f_{0a}|_{\underline{x}}\mathrm{d}x_m$ is:

$$\widehat{E}_{\underline{x}} := \frac{n_1}{N\Delta x_a}. \tag{6.28}$$

Similarly, letting n_2 be the number of ACs in the region $\Omega_{\overline{x}} := [\overline{x} - \frac{\Delta x_a}{2}, \overline{x} + \frac{\Delta x_a}{2}] \times \mathbb{R}$ at time t_i, the estimate of $\int_{-\infty}^{+\infty} f_{1c}|_{\overline{x}}\mathrm{d}x_m$ is:

$$\widehat{E}_{\overline{x}} := \frac{n_2}{N\Delta x}. \tag{6.29}$$

Note that in (6.28) and (6.29), only partially observed states are collected for the computation, which will considerably relieve the communication burden. According to (6.28) and (6.29), the controller and the saturation control in (6.18) and (6.20) change to

$$\widehat{u}(t_i) := \frac{\eta}{2P}\frac{v(t_i) - \dot{y}_d(t_i)}{\widehat{E}_{\underline{x}} + \widehat{E}_{\overline{x}}}, \tag{6.30}$$

and

$$\mathrm{sat}(\widehat{u}(t_i)) = \begin{cases} M, & \text{when} \quad \widehat{u}(t_i) > M, \\ \widehat{u}(t_i), & \text{when} \quad |\widehat{u}(t_i)| \leq M, \\ -M, & \text{when} \quad \widehat{u}(t_i) < -M, \end{cases} \tag{6.31}$$

respectively.

When the LADRC algorithm is used as the auxiliary control scheme, the negative effects of the total disturbance, including $\tilde{\Gamma}(t_i)$, quantization noise, etc., will be timely compensated. Figure 6.2 shows the controller implementation process in a practical scenario, where the shadowed region highlights the computation procedure for the LADRC auxiliary controller.

6.4 Simulation study

In this section, we investigate the effectiveness of the proposed control strategy for power tracking control by numerical simulations. Note that the control strategy is designed based

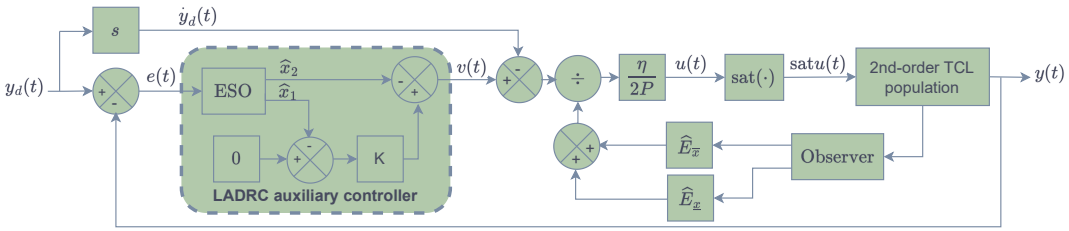

Figure 6.2 Block diagram for the controller implementation.

on the coupled Fokker-Planck model, which is derived by assuming an infinite collections of TCLs. Therefore, the more TCLs in the population, the more accurate the aggregate model. Accordingly, the proposed control scheme is supposed to have a better performance when the population size increases. To verify this claim, comparative results with two different population sizes containing, respectively, 1,000 and 100,000 TLCs are tested in Subsection 6.4.2 and 6.4.3. Furthermore, the control effects with the proportional auxiliary controller and the LADRC auxiliary controller are tested for the purpose of comparison. A concise analysis is reported at the end of this section.

6.4.1 Simulation setups

Table 6.1 lists some parameters and their default values used in the simulation. The air and mass thermal resistances of the population follow log-normal distributions, with mean values of 2 °C/kW,1 °C/kW and standard deviations (STDs) of 0.4 °C/kW, 0.2 °C/kW, respectively. Similarly, the air and mass thermal capacitances are also log-normally distributed, with mean values as 3.6 kW/°C, 4.3 kW/°C, and STDs as 0.72 kW/°C and 0.86 kW/°C, respectively. The rated thermal power is fixed as 2kW and the coefficient of performance (COP) is set to be 3 for all the TCLs. These values are justified in [18, 123] and should be properly adjusted based on practical applications.

Various types of perturbations are also considered in the simulation. A forced switching mechanism, which mimics unpredictable switchings in the population, is incorporated in the simulated operation. For each AC unit, the probability of forced switching ONs/OFFs per hour is 3%. Furthermore, a lockout mechanism is also introduced, as excessive switchings accelerates wear and tear on the compressors. In our setting, only forced switchings can break the lockout effect, otherwise each AC keeps its ON/OFF state unchanged for at least 5 minutes after the last alternation. During the locked time, the set-point temperature keeps updating. Whereas, the AC unit ignores the temperature changing signal. Finally, communication delays are also taken into account since individuals in the population usually

Table 6.1 Simulation parameters and default values

Parameter	Description [unit]	Value
R_a	Equivalent indoor air thermal resistance[°C/kW]	LogN$(2, 0.4)$
R_m	Equivalent building mass thermal resistance[°C/kW]	LogN$(1, 0.2)$
C_a	Equivalent indoor air thermal capacitance[kW/°C]	LogN$(3.6, 0.72)$
C_m	Equivalent building mass thermal capacitance[kW/°C]	LogN$(4.3, 0.86)$
P	Thermal power[kW]	2
η	Coefficient of Performance (COP)	3
x_{sp} or x_{sp}^{a}	Initial temperature set point[°C]	20
δ or δ_a	Thermostat deadband width[°C]	0.5
p_f	Probability of forced switchings per hour	3
t_l	Lockout time of each unit [min]	5
t_d	Communication delays [sec]	LogN$(1, 0.2)$
Δt	Resolution of the simulator [sec]	30

spread over a wide region. In the experiment, each AC unit is randomly assigned with a constant delay, drawing from a log-normal distribution with a mean value of 1 second and an STD of 0.2 second.

We examine the aggregate power of the population for 6.5 hours, starting at 10:00 and ending at 16:30. The system operates in an open-loop mode in the first half an hour while the closed-loop control is activated in the following 6 hours. During this period, the outside temperature is time-varying, as shown in Fig. 6.3a. The desired normalized power curve is shown in Fig. 6.3b, which is determined by the following polynomial [99]:

$$y_d(t) := (y_d(t_f) - y_d(t_i))\,\tau^5(t) \sum_{l=0}^{4} a_l \tau^l(t), t \in [t_i, t_f],$$

where t_i and t_f are the beginning and ending points, $\tau(t) := (t - t_i)/(t_f - t_i)$, and $a_0 = 126$, $a_1 = 420$, $a_2 = 540$, $a_3 = 315$, and $a_4 = 70$.

The sampling resolution in the simulation, Δt, is set to 30 seconds. The control signal is computed and broadcast at every sampling instant. The values of $\int_{\infty}^{\infty} f_0(\underline{x}, x_m, t)\mathrm{d}x_m$ and $\int_{\infty}^{\infty} f_1(\overline{x}, x_m, t)\mathrm{d}x_m$ are estimated by the midpoint rule [23] with respect to the x_a-coordinate. The average estimation of three bin widths, 0.008, 0.004 and 0.002 °C, respectively, are used

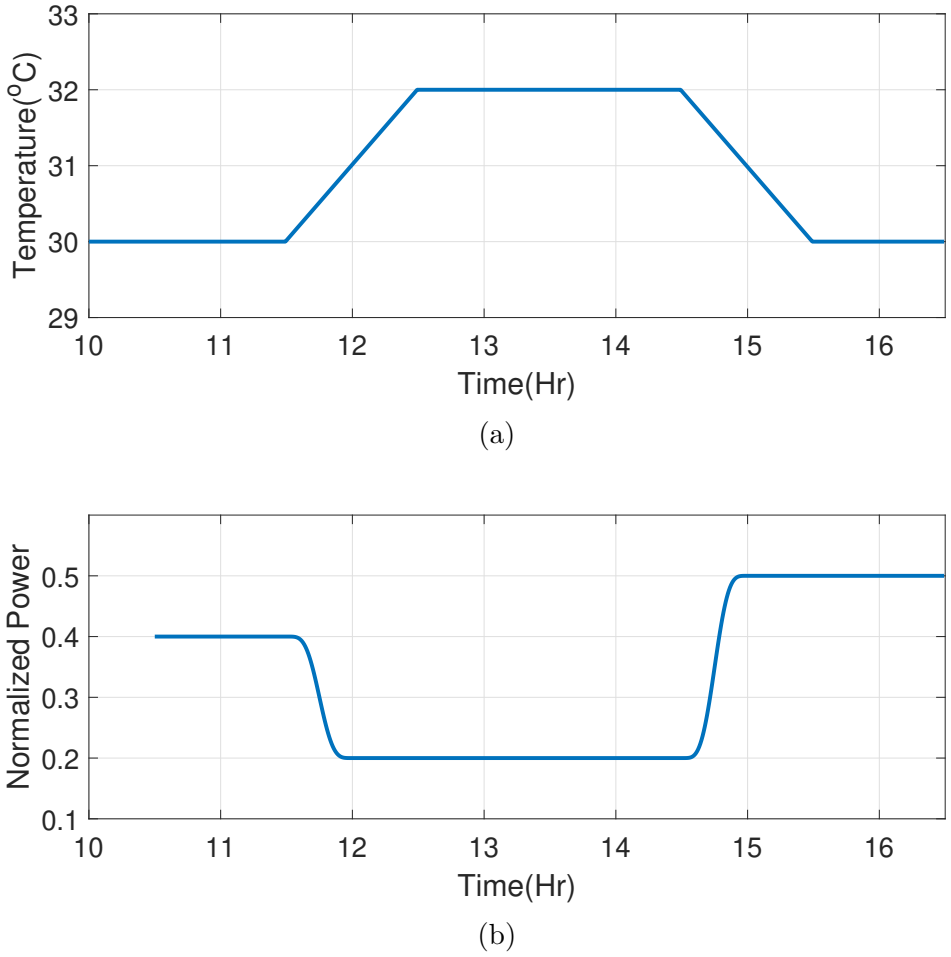

Figure 6.3 Ambient temperature and desired power curve (a) ambient temperature curve; (b) desired power profile.

to reduce random errors and improve the reliability. The computation time of the control signal, usually less than 0.01 millisecond, is ignored in the simulation, as it is very small compared to the communication delays and sampling intervals.

6.4.2 Numerical results for 1000 ACs

In the simulation, $k = 100$ is used for the proportional auxiliary controller, and $k_p = 50$, $l_1 = 100$, and $l_2 = 2500$ are used for the LADRC auxiliary controller. The numerical results are summarized in Table 6.2, where the RMSE values are multiplied by 100 for the ease of readability. The mean values for proportional (RMSE-P) and LADRC auxiliary controller (RMSE-L) are 1.158% and 0.751%, respectively, and the STDs are 0.012% and 0.035%. The data show that the controllers performance well, as the mean values are quite small (all below 2%) and the STDs are also not significant.

Table 6.2 Power tracking results for 1000 ACs

Episode	1	2	3	4	5
RMSE-P(%)	1.151	1.169	1.141	1.158	1.155
RMSE-L(%)	0.700	0.754	0.745	0.813	0.755
Episode	6	7	8	9	10
RMSE-P(%)	1.171	1.174	1.166	1.147	1.147
RMSE-L(%)	0.769	0.745	0.706	0.794	0.730

For a better visualization, the time evaluation of the data in Episode 1 in Table 6.2 with LADRC auxiliary controller is shown in Fig. 6.4. The tracking effect is illustrated in Fig. 6.4a, whereas the results with proportional controller is shown as a baseline. The tracking errors between the actual and the desired powers are shown in Fig. 6.4b, and Fig. 6.4c presents the changing velocities broadcasted to the population. In this tracking process, the RMSE is 0.700% and the tracking errors belong in $[-0.021\%, 0.023\%]$. Note that in Fig. 6.4c, the changing velocities are constrained to be within $[-1, 1]$. Thus, the maximal set-point temperature offset cannot exceed $1\,^{\circ}\mathrm{C}$ per hour. In fact, the set-point temperature for this episode is in the rang $[20\,^{\circ}\mathrm{C}, 21.82\,^{\circ}\mathrm{C}]$ all along 6.5 hours.

In the simulation, communication delays and lockout time are also considered. Figure 6.5 shows the temperature profiles and action curves for the first and second AC units in the population. Note that the mass temperature changes are slower than that for the air temperature, while the later ones move back and forth inside a fixed deadband region. Another remarkable point is that the actions are hardly distinguishable to the one shown in Fig. 6.4c, which is the "ideal" action profile without delays or any other disruptions.

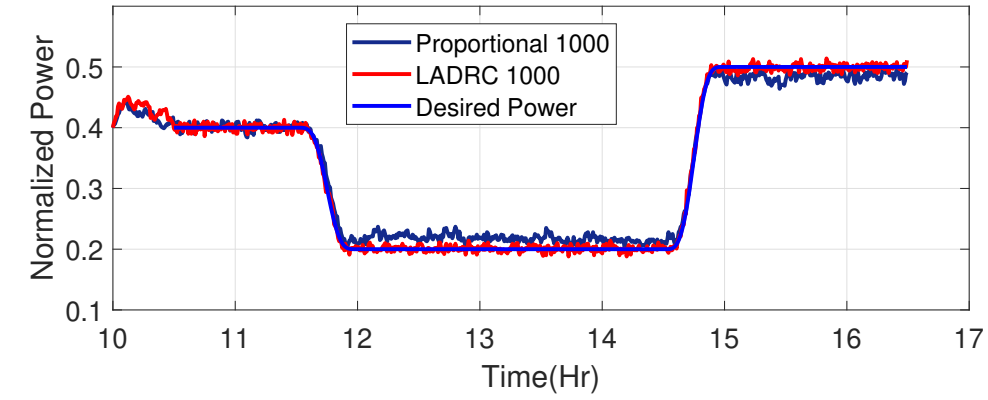

(a)

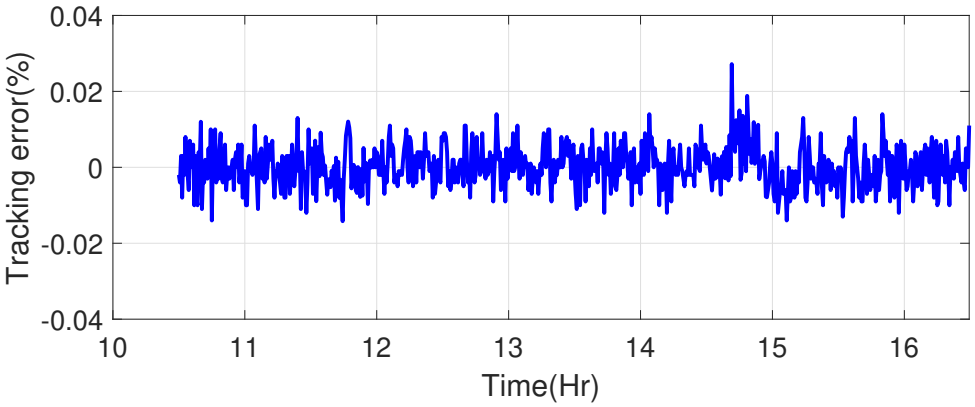

(b)

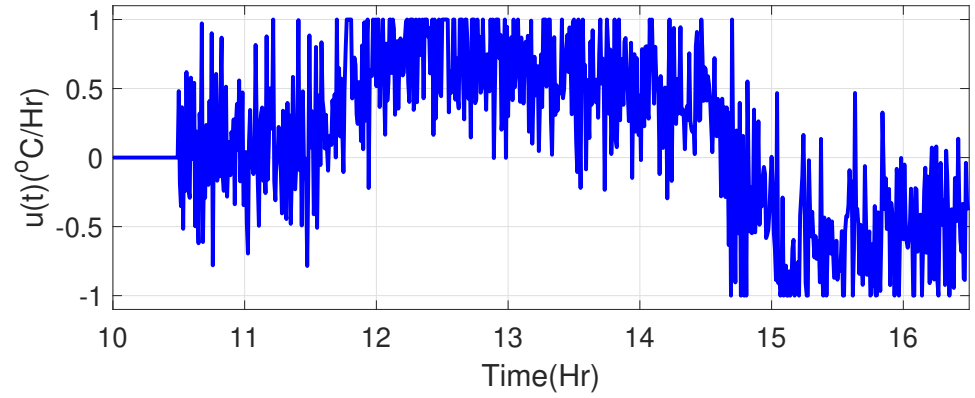

(c)

Figure 6.4 Control performance for a population of 1000 ACs: (a) tracking curve; (b) tracking errors; (c) set-point variation rate.

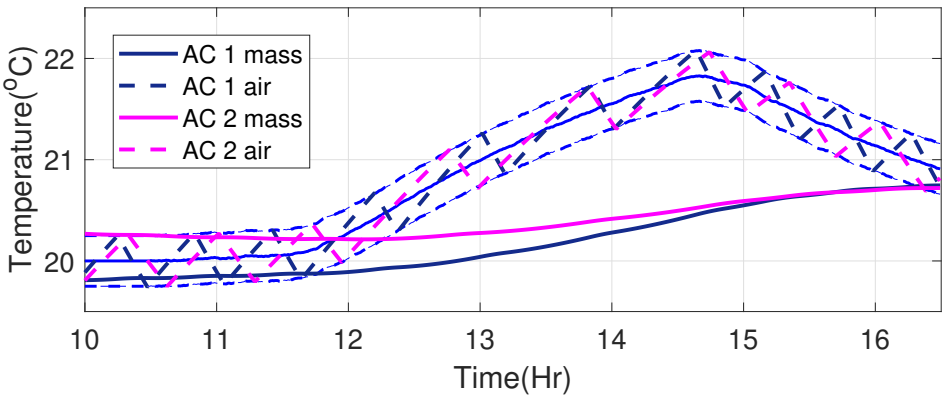

(a)

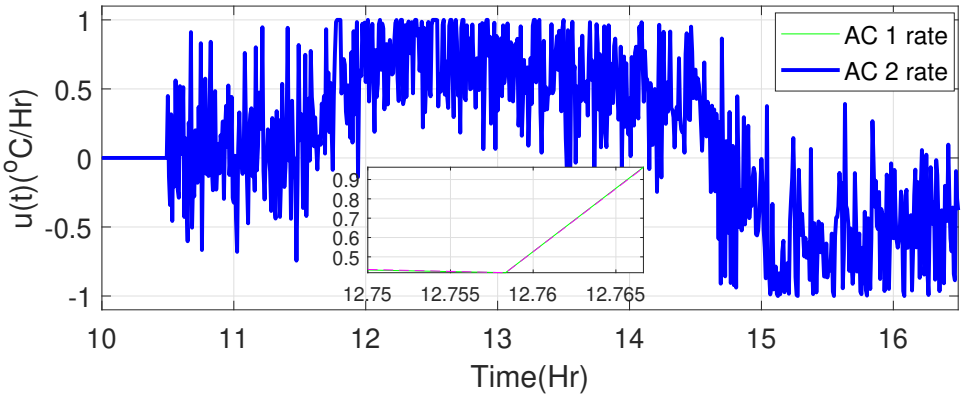

(b)

Figure 6.5 Trajectories and actions of No. 1 and No. 2 AC in the population of 1,000 ACs (a) air and mass temperature trajectories; (b) independent set-point changing velocities.

6.4.3 Numerical results for 100,000 ACs

For a population of 100,000 ACs, power tracking control is also tested for 10 times successively. The final results are listed by order in Table 6.3. The mean RMSE-Ps and RMSE-Ls are 1.050% and 0.295%, respectively, and the STDs are 0.006% and 0.007%.

Table 6.3 Power tracking results for 100,000 ACs

Episode	1	2	3	4	5
RMSE-P(%)	1.045	1.052	1.047	1.046	1.056
RMSE-L(%)	0.294	0.304	0.293	0.305	0.293
Episode	6	7	8	9	10
RMSE-P(%)	1.060	1.044	1.046	1.047	1.061
RMSE-L(%)	0.287	0.294	0.302	0.297	0.283

Similar as in the previous subsection, the first tracking episode is used to demonstrate the control effect. Figure 6.6 shows the power tracking curve, the tracking-error sequence, and the broadcasted control signals. Meanwhile, Fig. 6.7 shows the temperature profiles and control actions for the first two AC units in the population.

6.4.4 Results analysis

The results in Table 6.2 and Table 6.3 are very promising. It can be seen that LADRC performs better than the proportional control, as the mean RMSE is smaller while the standard deviations are almost the same. Another remarkable point is that the LADRC auxiliary controller uses a smaller proportional gain k_p while having a better performance than the proportional controller. By Theorem 6.1 and 6.2, larger proportional gains should be used to narrow down the convergence zone bounds. However, larger gains may induce chattering phenomena. Hence, LADRC auxiliary controller can act as a remedy for avoid using large proportional gains. Finally, the results also show that the proposed control law indeed performs better on larger size populations, when compared either by RMSE-Ps or RMSE-Ls. The average RMSE becomes smaller, demonstrating that the actual power consumption is getting closer to the reference one. Meanwhile, the STD becomes smaller, showing that the control effects are more stable under the same varying outside temperatures and a same level of disturbances.

Finally, another noticeable feature in tracking control is the fast response property of the proposed control scheme. When the reference power drops rapidly during 11:30 am$\sim$12:00 pm or increases dramatically during 14:30 pm$\sim$15:00 pm, the tracking control still performers well, as shown in Fig. 6.4a and Fig. 6.6a. This observation shows that the designed control

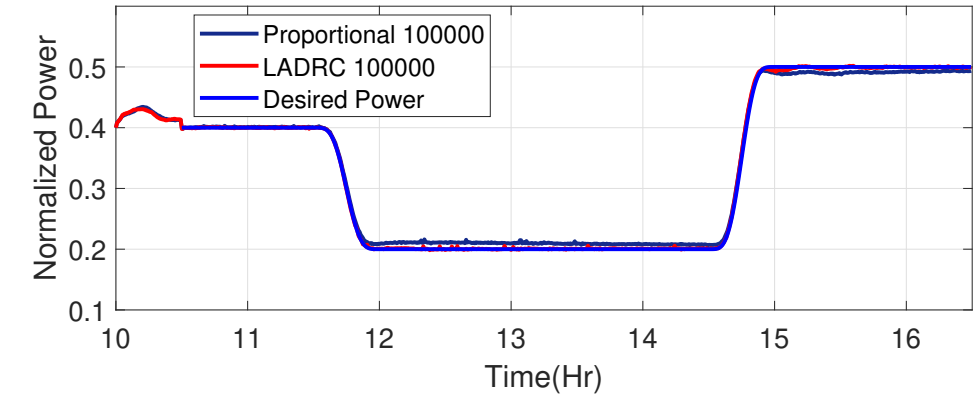

(a)

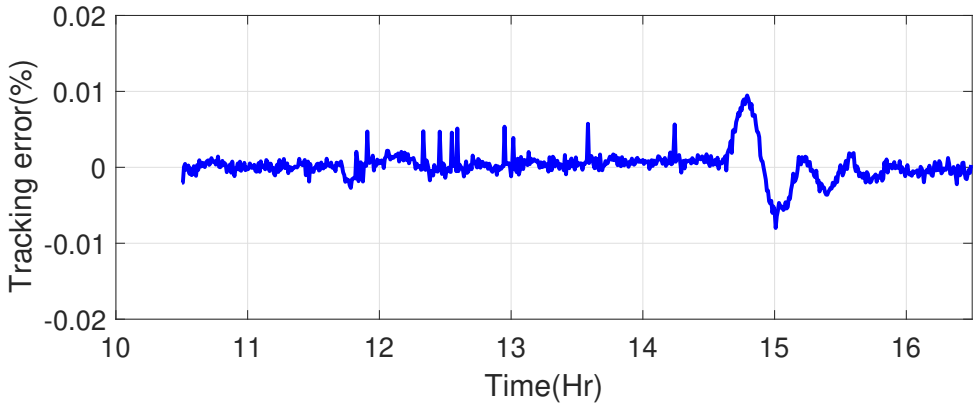

(b)

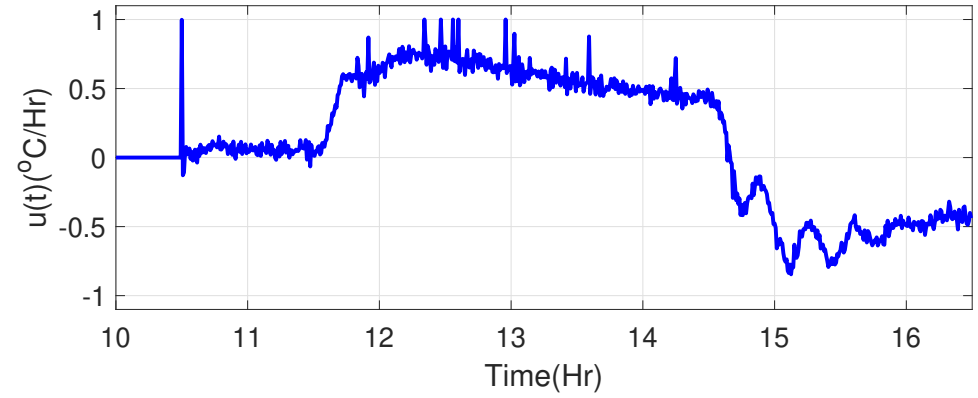

(c)

Figure 6.6 Control performance for a population of 100,000 ACs: (a) tracking curve; (b) tracking errors; (c) set-point variation rate.

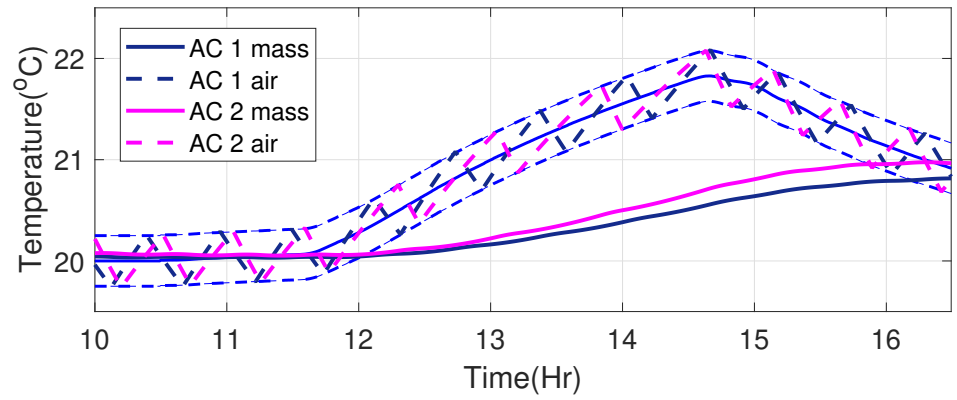

(a)

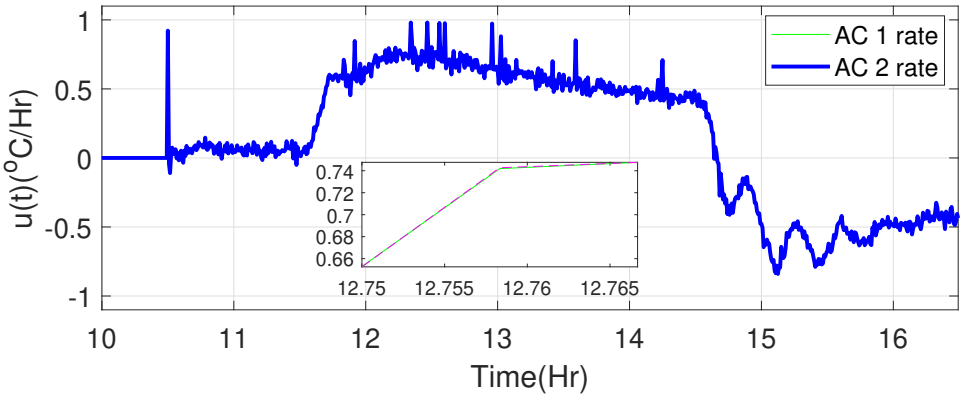

(b)

Figure 6.7 Trajectories and actions of No. 1 and No. 2 AC in the population of 100,000 ACs (a) air and mass temperature trajectories; (b) independent set-point changing velocities.

law, which has a negligible computational complexity, is even suitable for participating in real time electricity markets or taking active part in time urgent frequency regulation tasks.

6.5 Conclusion

Power tracking control of the second-order heterogeneous TCL populations is investigated in the context of smart grid. A novel nonlinear control strategy, which requires only partially observed states is designed based on the input-output dynamics of the system. Specifically, a generalized CFP model is introduced to characterize the aggregate dynamics of the TCL population when the dynamics of individual TCLs are described by a hybrid 2nd order ETP model. Then, a nonlinear control scheme with saturation and disturbance rejection capability is designed. The stability of the closed-loop system has been analyzed, and the tracking performance is validated by numerical simulations. The obtained results demonstrate that the proposed control method has great potential for real-world applications, where the environments are usually with parameter uncertainties or disruptions. It should be noted that the considered aggregate model deals with TCL populations of the same type, requiring that the power of each unit is approximately the same. Therefore, different types of heating or cooling devices need to be treated as separate groups. The cooperation problem between different groups, or more generally with other types of appliances, such as distributed generators, energy storage devices in the micro-grids, is a research topic worthy exploring [42, 50, 119].

CHAPTER 7 GENERAL DISCUSSION

As the conventional grid transitions to a more intelligent and efficient smart grid network, thermostatically controlled loads (TCLs) are emerging as one type of flexible loads that offer an important demand response (DR) capability, thereby ensuring improved reliability, enhanced sustainability and better customer service. Their ability to adjust power consumptions in response to rapidly changing supply-demand mismatches makes them more valuable in demand response programs. The focus of this thesis is the regulation of aggregate power consumptions of heterogeneous TCL populations, with the rate of change in set-point temperatures as control input. By employing a model-based approach, effective control strategies for regulating the collective power consumptions are presented. The coupled Fokker-Planck (CFP) model is used to characterize the evolution of the distribution of TCLs in ON and OFF states of the population. Compared with finite-dimensional lumped models, the PDE paradigm provides a more generic framework and a higher model accuracy, thus facilitating more flexible control designs.

A well-designed output function is crucial for achieving desired system responses, and its design should take account of both mathematical validity and physical meaningfulness. By mathematical validity, it means that for a tracking control problem, the input-output dynamics of the system should be controllable, ensuring that external inputs has the ability to drive the aggregate power to the desired value. Particularly, it is essential to ensure that the system is computationally tractable and free of singularity points in the derivative of the output function. Otherwise, it hinders the analysis of the tracking error dynamics and thereby preventing the development of effective control strategies. By physical meaningfulness, it means that the system output should have practical meanings for the problem. Inspired by the results obtained in a preliminary Monte-Carlo simulation on the aggregate dynamics of TCL populations presented in Chapter 3, the work in Chapter 4 solves this tricky problem by proposing a new output function, which is equivalent to the real aggregate power demand in steady state. In fact, according to our simulation, there are only a small fraction of TCLs outside the deadband in transient state, and almost no TCLs remain outside the deadband in steady state. This observation supports the validity of the proposed output scheme.

Chapter 4 proposed a nonlinear control scheme based on the method of input-output linearization which guarantees a robust performance. As a standard component in validating tracking control schemes, the stability of the closed-loop system involving infinite-dimensional internal dynamics has been assessed by a rigorous analysis. The work of Chapter 4 paves the path for

further investigations. Among which, Chapter 5 addresses the challenging problem of further minimizing communication burden that may occur in larger-scale TCL populations. For a network-controlled system, communication burden is a critical obstacle for real-world implementations. By using event-triggered control techniques, the convergence of the tracking error is re-examined, and the proposed triggering conditions can also make sure that no Zeno phenomena will occur. This work broadens the applicability and scalability of the proposed control strategies for practical, real-life systems. Chapter 6 extends the considered problem to higher-dimensional systems by using second order ETP model aiming at an enhanced accuracy on the thermodynamics of a single TCL. The second order ETP model will result in a generalized PDE dynamics with higher-dimensional spaces, and controller re-design is inevitable. First, a minor variation on the system output function, which preserves the mathematical validity and physical meaning, is proposed. Then, in parallel, a new type of control law is derived under this modification with a similar computational procedure. Further, by incorporating saturation and disturbance rejection abilities with a linear ADRC scheme, this control strategy also exhibits enhanced robustness with respect to different disturbances.

In summary, this thesis is motivated by the application of advanced control theory and techniques to a significant problem in the rapidly evolving field of the smart grid, where advancements can have substantial impacts from engineering, academic, and economic, perspectives. The research comprises a series of studies, each focusing on a specific problem encountered in practical applications, all of which are closely connected by a strong methodological foundation. The work of this thesis is grounded in rigorous theoretical analysis, complemented by validation through numerical simulations. Despite the mathematical challenges inherent in analyzing and designing PDE control systems, the achievements of this thesis demonstrate the promise and potential of applying advanced control theory and techniques to practical problems across diverse fields.

CHAPTER 8 CONCLUSION

8.1 Summary of research work

TCLs, as promising flexible loads, present great potential to help maintain the reliability and stability of the future smart grid. This thesis presents an in-depth investigation of the power tracking control problem using heterogeneous TCL populations as demand response resources. In this work, advanced modeling methods are introduced and novel control strategies are proposed for coordinating large or ultra-large scale heterogeneous populations.

Chapter 2 is the problem formulation and in-depth literature review part, right after the research background shown in Chapter 1. The research scope is clarified in this part, and some existing models and control strategies are meticulously examined.

Chapter 3 details some mathematical preliminaries of the thesis, including theoretical tools for controller design, stability analysis, and numerical implementations. Furthermore, a Monte-Carlo simulation on a TCL population is conducted, which helps to gain better intuitive understandings of the aggregate dynamics of the system.

Chapter 4 proposes a nonlinear control scheme by investigating the power tracking error dynamics. An novel system output function is proposed by integrating the distribution functions of the TCLs, on the premise that the evolution of the population is characterized by the CFP model. Under the framework of input-output linearization, multiple candidates of the auxiliary controller can be considered. A sliding model mode-like auxiliary control is selected, and it is then shown that the overall system is finite-time input-to-state stable. The feasibility and effectiveness of the proposed control scheme are validated by numerical simulations. Furthermore, it has also been shown that this method performs better on larger size populations. This finding is consistent with the underlying model we used in control design, where an infinite collection of TCLs is assumed for the coupled Fokker-Planck model.

Chapter 5 tackles the problem related to the communication burden by integrating event-triggered mechanisms with a control scheme based on the one proposed in Chapter 4. Both the static and dynamic triggering conditions are studied. It is shown that the closed-loop system is input-to-state practical stable with either the static or dynamic triggering approaches, and no Zeno phenomena happen for both cases. The simulation results show that the communication burden can be tremendously reduced, whereas the tracking performances are within tolerable degradation.

The work of Chapter 6 is built on top of that in Chapter 4. A second-order ETP model is

utilized in the place of the original first-order model. This model involves the mass and air temperatures, which takes account of equivalent mass and air capacitances, and equivalent mass and air resistances into consideration, leading to enhanced accuracy. Accordingly, a higher-dimensional coupled Fokker-Planck model is used to describe the aggregate dynamics. Furthermore, an LADCR method is introduced as the auxiliary controller, which reduces the steady state error and shows better performance than the proportional auxiliary controller.

8.2 Limitations and future research prospects

The proposed control strategies in this dissertation demonstrate excellent performance in a simulation environment, and the obtained results indicate the feasibility and effectiveness of coordinating large scale TCLs for demand response programs. Due to limited time and research facilities, many issues are remaining to be explored in the future. Some of them are shown as follows:

- In this work, the TCLs in a population are considered as fixed power. However, this might not be true in reality. For example, most of the modern air conditioners are variable-speed, thus their power consumptions change according to different interior or exterior conditions. Furthermore, most modern air conditioners are accompanied by many auxiliary functions, which makes its dynamics more challenging for prediction. The power fluctuations will certainly cause trouble for us to calculate the population aggregate power.

- The reference power data used in this work are designed from subjective experience, only for demonstration purpose. Actually, the reference curve should be provided by a utility company, which could be generated by complex optimization or predictive algorithms. Therefore, the derivative of the curve should be considered at higher layers in a complete demand response control framework.

- It is observed that a better performance is achieved with LADRC auxiliary controller when compared with proportional auxiliary controller. It will be of interest to integrate this control scheme with event-triggered control schemes. Note that the LADRC method needs continuous observations on the tracking error and the total disturbance, while the event-triggered control method naturally rejects periodically broadcast control signals. A control strategy which can exploit the advantages of both control schemes is a great extension of the current work.

- The thermal comfortness is not considered in the current work. We try to accom-

plish the demand response task as soon as possible, and the negative effects caused by rapid temperature variations are not considered. In fact, in real-life environments, temperatures should be kept inside a comfort zone that the customers prefer as much as possible. Smoothly slowing down the regulation process based on customer comfortness should be further explored in the future.

REFERENCES

[1] B. Achaal, M. Adda, M. Berger, H. Ibrahim, and A. Awde, "Study of smart grid cyber-security, examining architectures, communication networks, cyber-attacks, countermeasure techniques, and challenges," *Cybersecurity*, vol. 7, no. 1, p. 10, May 2024.

[2] T. Adamczyk, "Application of the Huber and Hampel M-estimation in real estate value modeling," *Geomat. Environ. Eng.*, vol. 11, no. 1, pp. 15–23, Jan. 2017.

[3] A. Adepetu, E. Rezaei, D. Lizotte, and S. Keshav, "Critiquing time-of-use pricing in Ontario," in *2013 IEEE International Conference on Smart Grid Communications (SmartGridComm)*, Vancouver, BC, Canada, Dec. 2013, pp. 223–228.

[4] B. Ahi and M. Haeri., "Linear active disturbance rejection control from the practical aspects," *IEEE ASME Trans. Mechatron.*, vol. 23, no. 6, pp. 2909–2919, Sept. 2018.

[5] M. J. M. Al Essa, "Home energy management of thermostatically controlled loads and photovoltaic-battery systems," *Energy*, vol. 176, pp. 742–752, June 2019.

[6] A. Al Mamun, M. Sohel, N. Mohammad, M. S. H. Sunny, D. R. Dipta, and E. Hossain, "A comprehensive review of the load forecasting techniques using single and hybrid predictive models," *IEEE Access*, vol. 8, pp. 134 911–134 939, July 2020.

[7] M. S. Alam, F. S. Al-Ismail, A. Salem, and M. A. Abido, "High-level penetration of renewable energy sources into grid utility: Challenges and solutions," *IEEE Access*, vol. 8, pp. 190 277–190 299, Oct. 2020.

[8] I. Alotaibi, M. A. Abido, M. Khalid, and A. V. Savkin, "A comprehensive review of recent advances in smart grids: A sustainable future with renewable energy resources," *Energies*, vol. 13, no. 23, p. 6269, Nov. 2020.

[9] B. D. O. Anderson, "Controller design: moving from theory to practice," *IEEE Contr. Syst. Mag.*, vol. 13, no. 4, pp. 16–25, Aug. 1993.

[10] M. Annunziato and B. Alfio, "A Fokker–Planck control framework for multidimensional stochastic processes," *J. Comput. Appl. Math.*, vol. 237, no. 1, pp. 487–507, Jan. 2013.

[11] A. Aoun, M. Ghandour, A. Ilinca, and H. Ibrahim, "Demand-side management," in *Hybrid Renewable Energy Systems and Microgrids*, E. Kabalci, Ed. London, UK: Academic Press, 2020, pp. 463–490.

[12] L. Ardito, G. Procaccianti, G. Menga, and M. Morisio, "Smart grid technologies in Europe: An overview," *Energies*, vol. 6, no. 1, pp. 251–281, Jan. 2013.

[13] J. Auriol, K. A. Morris, and F. Di Meglio, "Late-lumping backstepping control of partial differential equations," *Automatica*, vol. 100, pp. 247–259, Jan. 2018.

[14] P. Bacher and H. Madsen, "Identifying suitable models for the heat dynamics of buildings," *Energy Build.*, vol. 43, no. 7, pp. 1511–1522, July 2011.

[15] M. S. Bakare, A. Abdulkarim, M. Zeeshan, and A. N. Shuaibu, "A comprehensive overview on demand side energy management towards smart grids: challenges, solutions, and future direction," *Energy Informatics*, vol. 6, no. 1, p. 4, Mar. 2023.

[16] S. Banik, M. Rogers, S. M. Mahajan, C. M. Emeghara, T. Banik, and R. Craven, "Survey on vulnerability testing in the smart grid," *IEEE Access*, vol. 12, pp. 119 146–119 173, Aug. 2024.

[17] Y.-Q. Bao, M. Hu, Y.-Y. Hong, P.-P. Chen, J.-Q. Ju, and G. Ma, "Accuracy analysis and improvement of the state-queuing model for the thermostatically controlled loads," *IET Gener. Transm. Distrib.*, vol. 11, no. 5, pp. 1303–1310, Jan. 2017.

[18] Y.-Q. Bao, Z.-L. Yao, and X.-H. Wu, "Thermal parameters estimation of air conditioners based on reduced order equivalent thermal parameters model," *Int. J. Electr. Power Energy Syst.*, vol. 151, p. 109149, Sept. 2023.

[19] Y. Bao, P. Chen, M. Hu, and X. Zhu, "Control parameter optimization of thermostatically controlled loads using a modified state-queuing model," *CSEE J. Power Energy Syst.*, vol. 6, no. 2, pp. 394–401, May 2019.

[20] S. Bashash and H. K. Fathy, "Modeling and control insights into demand-side energy management through setpoint control of thermostatic loads," in *Proceedings of the 2011 American control conference*, San Francisco, CA, USA, Aug. 2011, pp. 4546–4553.

[21] ——, "Modeling and control of aggregate air conditioning loads for robust renewable power management," *IEEE Trans. Control Syst. Technol.*, vol. 21, no. 4, pp. 1318–1327, July 2013.

[22] V. Bogachev, G. Da Prato, and M. Röckner, "Existence and uniqueness of solutions for Fokker–Planck equations on Hilbert spaces," *J. Evol. Equ.*, vol. 10, pp. 487–509, Mar. 2010.

[23] W. Briggs, L. Cochran, B. Gillett, and E. Schulz, *Calculus: Early Transcendentals*, 3rd ed. Boston, USA: Pearson Education, 2011.

[24] D. S. Callaway, "Tapping the energy storage potential in electric loads to deliver load following and regulation, with application to wind energy," *Energy Conv. Manag.*, vol. 50, no. 5, pp. 1389–1400, May 2009.

[25] R. P. Canale and S. C. Chapra, *Numerical Methods for Engineers*. New York, NY, USA: McGraw-Hill Education, 2015.

[26] S. Chakraborty, R. Verzijlbergh, and Z. Lukszo, "Reduction of price volatility using thermostatically controlled loads in local electricity markets," in *2020 IEEE PES Innovative Smart Grid Technologies Europe (ISGT-Europe)*, The Hague, Netherlands, Oct. 2020, pp. 76–80.

[27] D. P. Chassin, K. Schneider, and C. Gerkensmeyer, "Gridlab-d: An open-source power systems modeling and simulation environment," in *2008 IEEE/PES Transmission and Distribution Conference and Exposition*, Chicago, IL, USA, May 2008, pp. 1–5.

[28] G. S. Chawda, A. G. Shaik, M. Shaik, S. Padmanaban, J. B. Holm-Nielsen, O. P. Mahela, and P. Kaliannan, "Comprehensive review on detection and classification of power quality disturbances in utility grid with renewable energy penetration," *IEEE Access*, vol. 8, pp. 146 807–146 830, Aug. 2020.

[29] X. Chen, J. Wang, J. Xie, S. Xu, K. Yu, and L. Gan, "Demand response potential evaluation for residential air conditioning loads," *IET Gener. Transm. Distrib.*, vol. 12, no. 19, pp. 4260–4268, Sept. 2018.

[30] Y. Chen, K.-W. Lao, D. Qi, H. Hui, S. Yang, Y. Yan, and Y. Zheng, "Distributed self-triggered control for frequency restoration and active power sharing in islanded microgrids," *IEEE Trans. Industr. Inform.*, vol. 19, no. 10, Oct. 2023.

[31] Y. Chen, C. Li, D. Qi, Z. Li, Z. Wang, and J. Zhang, "Distributed event-triggered secondary control for islanded microgrids with proper trigger condition checking period," *IEEE Trans. on Smart Grid*, vol. 13, no. 2, pp. 837–848, Mar. 2022.

[32] Z. Chen, J. Shi, Z. Song, W. Yang, and Z. Zhang, "Genetic algorithm based temperature-queuing method for aggregated IAC load control," *Energies*, vol. 15, no. 2, p. 535, Jan. 2022.

[33] L.-M. Cheng and Y.-Q. Bao, "A day-ahead scheduling of large-scale thermostatically controlled loads model considering second-order equivalent thermal parameters model," *IEEE Access*, vol. 8, pp. 102 321–102 334, June 2020.

[34] B. J. Claessens, D. Vanhoudt, J. Desmedt, and F. Ruelens, "Model-free control of thermostatically controlled loads connected to a district heating network," *Energy Build.*, vol. 159, pp. 1–10, Jan. 2018.

[35] B. J. Claessens, P. Vrancx, and F. Ruelens, "Convolutional neural networks for automatic state-time feature extraction in reinforcement learning applied to residential load control," *IEEE Trans. Smart Grid*, vol. 9, no. 4, pp. 3259–3269, Nov. 2016.

[36] A. Coffman, A. Bušić, and P. Barooah, "A unified framework for coordination of thermostatically controlled loads," *Automatica*, vol. 152, p. 111002, June 2023.

[37] F. Conte, M. Crosa Di Vergagni, S. Massucco, F. Silvestro, E. Ciapessoni, and D. Cirio, "Performance analysis of frequency regulation services provided by aggregates of domestic thermostatically controlled loads," *Int. J. Electr. Power Energy Syst.*, vol. 131, p. 107050, Oct. 2021.

[38] S. C'ordova, C. A. Ca nizares, A. Lorca, and D. E. Olivares, "Aggregate modeling of thermostatically controlled loads for microgrid energy management systems," *IEEE Trans. Smart Grid*, vol. 14, no. 6, pp. 4169–4181, Mar. 2023.

[39] W. Cui, Y. Ding, H. Hui, Z. Lin, P. Du, Y. Song, and C. Shao, "Evaluation and sequential dispatch of operating reserve provided by air conditioners considering lead–lag rebound effect," *IEEE Trans. Power Syst.*, vol. 33, no. 6, pp. 6935–6950, June 2018.

[40] W. Cui, W. Tan, D. Li, and Y. Wang, "Tuning of linear active disturbance rejection controllers based on step response curves," *IEEE Access*, vol. 8, pp. 180 869–180 882, Oct. 2020.

[41] D. De Menezes, D. M. Prata, A. R. Secchi, and J. C. Pinto, "A review on robust M-estimators for regression analysis," *Comput. Chem. Eng.*, vol. 147, p. 107254, Apr. 2021.

[42] A. De Paola, V. Trovato, D. Angeli, and G. Strbac, "A mean field game approach for distributed control of thermostatic loads acting in simultaneous energy-frequency response markets," *IEEE Trans. Smart Grid*, vol. 10, no. 6, pp. 5987–5999, Jan. 2019.

[43] G. Dileep, "A survey on smart grid technologies and applications," *Renew. Energy*, vol. 146, pp. 2589–2625, Feb. 2020.

[44] S. Dorahaki, R. Dashti, and H. R. Shaker, "Optimal outage management model considering emergency demand response programs for a smart distribution system," *Applied Sciences*, vol. 10, no. 21, p. 7406, Oct. 2020.

[45] P. Dueñas, T. Leung, M. Gil, and J. Reneses, "Gas–electricity coordination in competitive markets under renewable energy uncertainty," *IEEE Trans. Power Syst.*, vol. 30, no. 1, pp. 123–131, May 2014.

[46] Eur. Technol. Platform, "Smart grids-strategic deployment document for Europe's electricity networks of the future," Apr. 2010. [Online]. Available: http://kigeit.org.pl/FTP/PRCIP/Literatura/020_SmartGrids_ETP_SDD_FINAL_APRIL2010.pdf

[47] L. C. Evans, *Partial Differential Equations*. Providence, RI, USA: American Mathematical Society, 2022, vol. 19.

[48] R. Fareh, S. Khadraoui, M. Y. Abdallah, M. Baziyad, and M. Bettayeb, "Active disturbance rejection control for robotic systems: A review," *Mechatronics*, vol. 80, p. 102671, Dec. 2021.

[49] M. Farhadi-Kangarlu, E. Babaei, and F. Blaabjerg, "A comprehensive review of dynamic voltage restorers," *Int. J. Electr. Power Energy Syst.*, vol. 92, pp. 136–155, May 2017.

[50] M. Franceschelli, A. Pilloni, and A. Gasparri, "Multi-agent coordination of thermostatically controlled loads by smart power sockets for electric demand side management," *IEEE Trans. Control Syst. Technol.*, vol. 29, no. 2, pp. 731–743, Mar. 2020.

[51] Z. Gao, "Scaling and bandwidth-parameterization based controller tuning," in *2003 American Control Conference*, vol. 4, Denver, CO, USA, Nov. 2003, pp. 989–4.

[52] X. Ge, Q.-L. Han, L. Ding, Y.-L. Wang, and X.-M. Zhang, "Dynamic event-triggered distributed coordination control and its applications: A survey of trends and techniques," *IEEE Trans. Syst., Man, Cybern. Syst.*, vol. 50, no. 9, pp. 3112–3125, July 2020.

[53] C. W. Gellings, *The Smart Grid: Enabling Energy Efficiency and Demand Response*. London, England: Taylor & Francis, 2020.

[54] A. Ghaffari, S. Moura, and M. Krstić, "Modeling, control, and stability analysis of heterogeneous thermostatically controlled load populations using partial differential equations," *J. Dyn. Syst. Meas. Control*, vol. 137, no. 10, p. 101009, July 2015.

[55] M. Ghanavati and A. Chakravarthy, "Demand-side energy management by use of a design-then-approximate controller for aggregated thermostatic loads," *IEEE Trans. Control Syst. Technol.*, vol. 26, no. 4, pp. 1439–1448, July 2017.

[56] A. Girard, "Dynamic triggering mechanisms for event-triggered control," *IEEE Trans. Automat. Contr.*, vol. 60, no. 7, pp. 1992–1997, Nov. 2014.

[57] A. A. Godbole, J. P. Kolhe, and S. E. Talole, "Performance analysis of generalized extended state observer in tackling sinusoidal disturbances," *IEEE Trans. Control Syst. Technol.*, vol. 21, no. 6, pp. 2212–2223, Dec. 2012.

[58] X. Gong, E. Castillo-Guerra, J. L. Cardenas-Barrera, B. Cao, S. A. Saleh, and L. Chang, "Robust hierarchical control mechanism for aggregated thermostatically controlled loads," *IEEE Trans. Smart Grid*, vol. 12, no. 1, pp. 453–467, July 2020.

[59] A. Gopstein, C. Nguyen, C. O'Fallon, N. Hastings, and D. A. Wollman, "Nist framework and roadmap for smart grid interoperability standards, release 4.0," Feb. 2021. [Online]. Available: https://tsapps.nist.gov/publication/get_pdf.cfm?pub_id=931882

[60] D. Y. Goswami and F. Kreith, *Energy Efficiency and Renewable Energy Handbook*, 2nd ed. Boca Raton, FL, USA: CRC press, 2015.

[61] I. Griva, S. G. Nash, and A. Sofer, *Linear and Nonlinear Optimization*, 2nd ed. Philadelphia, PA, USA: SIAM, 2009.

[62] Z. Gu, P. Shi, and D. Yue, "An adaptive event-triggering scheme for networked interconnected control system with stochastic uncertainty," *Int. J. Robust Nonlinear Control*, vol. 27, no. 2, pp. 236–251, Jan. 2017.

[63] B.-Z. Guo and Z.-L. Zhao, *Active Disturbance Rejection Control for Nonlinear Systems: An Introduction.* Singapore, Singapore: John Wiley & Sons, 2016.

[64] Z. Guo, W. Wei, L. Chen, Z. Y. Dong, and S. Mei, "Impact of energy storage on renewable energy utilization: A geometric description," *IEEE Trans. Sustain. Energy*, vol. 12, no. 2, pp. 874–885, Sept. 2020.

[65] W. M. Haddad, S. G. Nersesov, and L. Du, "Finite-time stability for time-varying nonlinear dynamical systems," in *2008 American control conference*, Seattle, WA, USA, Aug. 2008, pp. 4135–4139.

[66] H. T. Haider, O. H. See, and W. Elmenreich, "A review of residential demand response of smart grid," *Renew. Sust. Energ. Rev.*, vol. 59, pp. 166–178, June 2016.

[67] J. Han, "From PID to active disturbance rejection control," *IEEE Trans. Ind. Electron.*, vol. 56, no. 3, pp. 900–906, Feb. 2009.

[68] H. Hao, B. M. Sanandaji, K. Poolla, and T. L. Vincent, "Aggregate flexibility of thermostatically controlled loads," *IEEE Trans. Power Syst.*, vol. 30, no. 1, pp. 189–198, June 2014.

[69] H. Harb, N. Boyanov, L. Hernandez, R. Streblow, and D. M"uller, "Development and validation of grey-box models for forecasting the thermal response of occupied buildings," *Energy Build.*, vol. 117, pp. 199–207, Apr. 2016.

[70] T. He, Z. Wu, D. Li, and J. Wang, "A tuning method of active disturbance rejection control for a class of high-order processes," *IEEE Trans. Ind. Electron.*, vol. 67, no. 4, pp. 3191–3201, Apr. 2019.

[71] W. H. Heemels, M. Donkers, and A. R. Teel, "Periodic event-triggered control for linear systems," *IEEE Trans. Autom. Control*, vol. 58, no. 4, pp. 847–861, Apr. 2012.

[72] W. Heemels, K. H. Johansson, and P. Tabuada, "Event-triggered and self-triggered control," in *Encyclopedia of Systems and Control*, Cham, Switzerland, Aug. 2021, pp. 724–730.

[73] G. Herbst, "Practical active disturbance rejection control: Bumpless transfer, rate limitation, and incremental algorithm," *IEEE Trans. Ind. Electron.*, vol. 63, no. 3, pp. 1754–1762, Nov. 2015.

[74] K. Hinkelman, S. Huang, J. Wang, J. Lian, and W. Zuo, "Enhancing the implementation of a first-order equivalent thermal parameter model to enable accurate and robust building thermal response prediction," in *Proceeding of the 16th Conference of International Building Performance Simulation Association (Building Simulation 2019)*, Rome, Italy, Sept. 2019, pp. 1859–1865.

[75] J. Hong, H. Hui, H. Zhang, N. Dai, and Y. Song, "Distributed control of large-scale inverter air conditioners for providing operating reserve based on consensus with nonlinear protocol," *IEEE Internet Things J.*, vol. 9, no. 17, pp. 15 847–15 857, Feb. 2022.

[76] Y. Hong, Z.-P. Jiang, and G. Feng, "Finite-time input-to-state stability and applications to finite-time control design," *SIAM J. Control Optim.*, vol. 48, no. 7, pp. 4395–4418, Jan. 2010.

[77] J. Hu, J. Cao, M. Z. Chen, J. Yu, J. Yao, S. Yang, and T. Yong, "Load following of multiple heterogeneous TCL aggregators by centralized control," *IEEE Trans. Power Syst.*, vol. 32, no. 4, pp. 3157–3167, Oct. 2016.

[78] J. Hu, J. Cao, T. Yong, J. M. Guerrero, M. Z. Chen, and Y. Li, "Demand response load following of source and load systems," *IEEE Trans. Control Syst. Technol.*, vol. 25, no. 5, pp. 1586–1598, Oct. 2016.

[79] X. Hu, B. Wang, S. Yang, T. Short, and L. Zhou, "A closed-loop control strategy for air conditioning loads to participate in demand response," *Energies*, vol. 8, no. 8, pp. 8650–8681, Aug. 2015.

[80] Y. Hua, Q. Xie, L. Zheng, J. Cui, L. Shao, and W. Hu, "Coordinated voltage control strategy by optimizing the limited regulation capacity of air conditioners," *Energies*, vol. 15, no. 9, p. 3225, Apr. 2022.

[81] HydroQuebec, "2024 Electricity Rates," April 2024. [Online]. Available: https://www.hydroquebec.com/data/documents-donnees/pdf/electricity-rates.pdf

[82] S. Iacovella, F. Ruelens, P. Vingerhoets, B. Claessens, and G. Deconinck, "Cluster control of heterogeneous thermostatically controlled loads using tracer devices," *IEEE Trans. Smart Grid*, vol. 8, no. 2, pp. 528–536, Oct. 2015.

[83] IEA, "Technology roadmap–smart grids–analysis," Apr. 2011. [Online]. Available: https://www.iea.org/reports/technology-roadmap-smart-grids

[84] IEA, "World energy investment 2024," June 2024. [Online]. Available: https://www.iea.org/reports/world-energy-investment-2024

[85] M. Jamali, H. R. Baghaee, M. S. Sadabadi, G. B. Gharehpetian, and A. Anvari Moghaddam, "Distributed cooperative event-triggered control of cyber-physical AC microgrids subject to denial-of-service attacks," *IEEE Trans. Smart Grid*, pp. 1–12, Mar. 2023.

[86] V. Jenkins, "Regulation no. 347/2013 on guidelines for Trans-European energy infrastructure: The provisions on permit granting and public participation and their implementation in the UK," *Env'tl Law Rev.*, vol. 17, no. 1, pp. 44–54, 2015.

[87] Z.-P. Jiang, I. M. Mareels, and Y. Wang, "A Lyapunov formulation of the nonlinear small-gain theorem for interconnected ISS systems," *Automatica*, vol. 32, no. 8, pp. 1211–1215, Aug. 1996.

[88] H. J. Jo, I. S. Kim, and D. H. Lee, "Efficient and privacy-preserving metering protocols for smart grid systems," *IEEE Trans. Smart Grid*, vol. 7, no. 3, pp. 1732–1742, July 2015.

[89] L. Kang, L. Liu, Q. An, J. Yang, J. Zhao, H. Jia, and D. Wang, "The equivalent thermal parameter model and simulation of air conditioner system in demand response programs," *Energy Procedia*, vol. 61, pp. 2004–2007, Jan. 2015.

[90] E. C. Kara, M. Bergés, and G. Hug, "Impact of disturbances on modeling of thermostatically controlled loads for demand response," *IEEE Trans. Smart Grid*, vol. 6, no. 5, pp. 2560–2568, Mar. 2015.

[91] C. M. Kellett, "A compendium of comparison function results," *Mathematics of Control, Signals, and Systems*, vol. 26, pp. 339–374, Mar. 2014.

[92] H. K. Khalil, *Nonlinear Control*, 3rd ed. New York, USA: New York: Pearson, 2015.

[93] K. J. Kircher, A. O. Aderibole, L. K. Norford, and S. B. Leeb, "Distributed peak shaving for small aggregations of cyclic loads," *IEEE Trans. Power Deliv.*, vol. 37, no. 5, pp. 4315–4325, Feb. 2022.

[94] X. Kong, B. Sun, J. Zhang, S. Li, and Q. Yang, "Power retailer air-conditioning load aggregation operation control method and demand response," *IEEE Access*, vol. 8, pp. 112 041–112 056, May 2020.

[95] M. Lakeridou, M. Ucci, A. Marmot, and I. Ridley, "The potential of increasing cooling set-points in air-conditioned offices in the UK," *Applied Energy*, vol. 94, pp. 338–348, June 2012.

[96] C. Le Bris and P. L. Lions, "Renormalized solutions of some transport equations with partially $W^{1,1}$ velocities and applications," in *Annali di Matematica pura ed applicata*, Firenze, Italy, 2004, vol. 183, pp. 97–130.

[97] ——, "Existence and uniqueness of solutions to Fokker–Planck type equations with irregular coefficients," *Commun. Partial Differ. Equ.*, vol. 33, no. 7, pp. 1272–1317, Aug. 2008.

[98] M. Lemmon, "Event-triggered feedback in control, estimation, and optimization," in *Networked Control Systems*, London, UK, Oct. 2010, pp. 293–358.

[99] J. Lévine, *Analysis and Control of Nonlinear Systems: A Flatness-based Approach*. Berlin, Germany: Springer-Verlag, 2009.

[100] J. Li, L. Zhang, S. Li, Q. Mao, and Y. Mao, "Active disturbance rejection control for piezoelectric smart structures: A review," *Machines*, vol. 11, no. 2, p. 174, Jan. 2023.

[101] L. Li, M. Dong, D. Song, J. Yang, and Q. Wang, "Distributed and real-time economic dispatch strategy for an islanded microgrid with fair participation of thermostatically controlled loads," *Energy*, vol. 261, p. 125294, Dec. 2022.

[102] Y. Li, Z. O'Neill, L. Zhang, J. Chen, P. Im, and J. DeGraw, "Grey-box modeling and application for building energy simulations–a critical review," *Renew. Sustain. Energy Rev.*, vol. 146, p. 111174, Aug. 2021.

[103] J. Lian, H. Ren, Y. Sun, and D. J. Hammerstrom, "Performance evaluation for transactive energy systems using double-auction market," *IEEE Trans. Power Syst.*, vol. 34, no. 5, pp. 4128–4137, Sept. 2019.

[104] D. Liberzon, *Calculus of Variations and Optimal Control Theory: A concise introduction*. Princeton, NJ, USA: Princeton University Press, 2011.

[105] M. Liserre, M. A. Perez, M. Langwasser, C. A. Rojas, and Z. Zhou, "Unlocking the hidden capacity of the electrical grid through smart transformer and smart transmission," *Proc. of the IEEE*, vol. 111, no. 4, pp. 421–437, Apr. 2023.

[106] C. Liu, X. Wang, Y. Ren, X. Wang, and J. Zhang, "A novel distributed secondary control of heterogeneous virtual synchronous generators via event-triggered communication," *IEEE Trans. Smart Grid*, vol. 13, no. 6, pp. 4174–4189, Nov. 2022.

[107] H. Liu, H. Xie, H. Luo, J. Qi, H. H. Goh, and S. Rahman, "Optimal strategy for participation of commercial HVAC systems in frequency regulation," *IEEE Internet Things J.*, vol. 8, no. 23, pp. 17 100–17 110, Apr. 2021.

[108] M. Liu and Y. Shi, "Model predictive control of aggregated heterogeneous second-order thermostatically controlled loads for ancillary services," *IEEE Trans. Power Syst.*, vol. 31, no. 3, pp. 1963–1971, May 2016.

[109] M. Liu, Y. Shi, and X. Liu, "Distributed MPC of aggregated heterogeneous thermostatically controlled loads in smart grid," *IEEE Trans. Ind. Electron.*, vol. 63, no. 2, pp. 1120–1129, Oct. 2015.

[110] Y. Liu, H. Li, R. Lu, Z. Zuo, and X. Li, "An overview of finite/fixed-time control and its application in engineering systems," *IEEE CAA J. Autom. Sinica*, vol. 9, no. 12, pp. 2106–2120, Jan. 2022.

[111] Y. Liu and Y. C. Senior, "Decentralized resilient finite-time-control for large-scale power systems via dynamic triggering against deception attacks," *IEEE Trans. Smart Grid*, pp. 1–11, Feb. 2023.

[112] J. M. P. S. Lizarraga and A. Picallo-Perez, *Exergy Analysis and Thermoeconomics of Buildings*. Butterworth-Heinemann, 2020.

[113] T. Logenthiran, D. Srinivasan, and T. Z. Shun, "Demand side management in smart grid using heuristic optimization," *IEEE Trans. Smart Grid*, vol. 3, no. 3, pp. 1244–1252, June 2012.

[114] F. Lopez-Ramirez, D. Efimov, A. Polyakov, and W. Perruquetti, "Finite-time and fixed-time input-to-state stability: Explicit and implicit approaches," *Syst. Control. Lett.*, vol. 144, p. 104775, Oct. 2020.

[115] N. Lu, "An evaluation of the HVAC load potential for providing load balancing service," *IEEE Trans. Smart Grid*, vol. 3, no. 3, pp. 1263–1270, Mar. 2012.

[116] N. Lu and D. P. Chassin, "A state-queueing model of thermostatically controlled appliances," *IEEE Trans. Power Syst.*, vol. 19, no. 3, pp. 1666–1673, Aug. 2004.

[117] N. Lu, D. P. Chassin, and S. E. Widergren, "Modeling uncertainties in aggregated thermostatically controlled loads using a state queueing model," *IEEE Trans. Power Syst.*, vol. 20, no. 2, pp. 725–733, May 2005.

[118] N. Lu and Y. Zhang, "Design considerations of a centralized load controller using thermostatically controlled appliances for continuous regulation reserves," *IEEE Trans. Smart Grid*, vol. 4, no. 2, pp. 914–921, Dec. 2012.

[119] Y. Luo, H. Yuan, Z. Hu, D. Yang, and H. Zhang, "Optimal scheduling of micro-energy grid based on pareto frontier under uncertainty and pollutant emissions," *IEEE Trans. Smart Grid*, vol. 15, no. 1, pp. 368–380, May 2023.

[120] K. Ma, P. Liu, J. Yang, and X. Guan, *Control and Communication for Demand Response with Thermostatically Controlled Loads*. Singapore, Singapore: Springer Nature, Dec. 2022.

[121] K. Ma, C. Yuan, X. Xu, J. Yang, and Z. Liu, "Optimising regulation of aggregated thermostatically controlled loads based on multi-swarm PSO," *IET Gener. Transm. Distrib.*, vol. 12, no. 10, pp. 2340–2346, Mar. 2018.

[122] N. Mahdavi, J. H. Braslavsky, and C. Perfumo, "Mapping the effect of ambient temperature on the power demand of populations of air conditioners," *IEEE Trans. Smart Grid*, vol. 9, no. 3, pp. 1540–1550, July 2016.

[123] N. Mahdavi, J. H. Braslavsky, M. M. Seron, and S. R. West, "Model predictive control of distributed air-conditioning loads to compensate fluctuations in solar power," *IEEE Trans. Smart Grid*, vol. 8, no. 6, pp. 3055–3065, June 2017.

[124] N. Mahdavi and J. H. Braslavsky, "Modelling and control of ensembles of variable-speed air conditioning loads for demand response," *IEEE Trans. Smart Grid*, vol. 11, no. 5, pp. 4249–4260, May 2020.

[125] P. Mair and R. Wilcox, "Robust statistical methods in R using the WRS2 package," *Behav. Res. Methods*, vol. 52, pp. 464–488, Apr. 2020.

[126] R. Malhame and C.-Y. Chong, "Electric load model synthesis by diffusion approximation of a high-order hybrid-state stochastic system," *IEEE Trans. Automat. Contr.*, vol. 30, no. 9, pp. 854–860, Sept. 1985.

[127] L. Marko, J.-F. Mennemann, L. Jadachowski, W. Kemmetmüller, and A. Kugi, "Early- and late-lumping observer designs for long hydraulic pipelines: Application to pumped-storage power plants," *Int. J. Robust Nonlinear Control*, vol. 28, no. 7, pp. 2759–2779, Jan. 2018.

[128] R. A. Maronna, R. D. Martin, V. J. Yohai, and M. Salibián-Barrera, *Robust Statistics: Theory and Methods (with R)*, 2nd ed. Hoboken, NJ, USA: John Wiley & Sons, 2019.

[129] J. L. Mathieu, M. Kamgarpour, J. Lygeros, G. Andersson, and D. S. Callaway, "Arbitraging intraday wholesale energy market prices with aggregations of thermostatic loads," *IEEE Trans. Power Syst.*, vol. 30, no. 2, pp. 763–772, July 2014.

[130] J. L. Mathieu, M. Kamgarpour, J. Lygeros, and D. S. Callaway, "Energy arbitrage with thermostatically controlled loads," in *2013 European Control Conference (ECC)*, Zurich, Switzerland, Dec. 2013, pp. 2519–2526.

[131] J. L. Mathieu, S. Koch, and D. S. Callaway, "State estimation and control of electric loads to manage real-time energy imbalance," *IEEE Trans. Power Syst.*, vol. 28, no. 1, pp. 430–440, July 2012.

[132] J. L. Mathieu, M. G. Vayá, and G. Andersson, "Uncertainty in the flexibility of aggregations of demand response resources," in *IECON 2013-39th Annual Conference of the IEEE Industrial Electronics Society*, Vienna, Austria, Jan. 2014, pp. 8052–8057.

[133] J. L. Mathieu, G. Verbic, T. Morstyn, M. Almassalkhi, K. Baker, J. Braslavsky, K. Bruninx, Y. Dvorkin, G. S. Ledva, N. Mahdavi, *et al.*, "A new definition and research agenda for demand response in the distributed energy resource era," *IEEE Transactions on Energy Markets, Policy and Regulation*, 2025.

[134] L. G. Meegahapola, S. Bu, D. P. Wadduwage, C. Y. Chung, and X. Yu, "Review on oscillatory stability in power grids with renewable energy sources: Monitoring, analysis, and control using synchrophasor technology," *IEEE Trans. Ind. Electron.*, vol. 68, no. 1, pp. 519–531, Jan. 2020.

[135] F. Y. Melhem, O. Grunder, Z. Hammoudan, and N. Moubayed, "Energy management in electrical smart grid environment using robust optimization algorithm," *IEEE Trans. Ind. Appl.*, vol. 54, no. 3, pp. 2714–2726, Feb. 2018.

[136] W. Mendieta and C. A. Cañizares, "Primary frequency control in isolated microgrids using thermostatically controllable loads," *IEEE Trans. Smart Grid*, vol. 12, no. 1, pp. 93–105, July 2020.

[137] T. Meurer, *Control of higher-dimensional PDEs: Flatness and backstepping designs*. Berlin, Germany: Springer, Aug. 2012.

[138] A. Mironchenko, *Input-to-State Stability: Theory and Applications*. Cham, Switzerland: Springer, Apr. 2023.

[139] M. Miskowicz, *Event-Based Control and Signal Processing*, 1st ed. Boca Raton, FL, USA: CRC press, 2018.

[140] S. Misra and S. Bera, *Smart Grid Technology: A Cloud Computing and Data Management Approach*. New York, NY, USA: Cambridge University Press, 2018.

[141] N. Mlilo, J. Brown, and T. Ahfock, "Impact of intermittent renewable energy generation penetration on the power system networks–a review," *Technol. Econ. Smart Grids Sustain. Energy*, vol. 6, no. 1, p. 25, Dec. 2021.

[142] A. Molina-Garcia, M. Kessler, J. A. Fuentes, and E. Gómez-Lázaro, "Probabilistic characterization of thermostatically controlled loads to model the impact of demand response programs," *IEEE Trans. Power Syst.*, vol. 26, no. 1, pp. 241–251, May 2010.

[143] K. Morris and W. Levine, "Control of systems governed by partial differential equations," in *The Control Systems Handbook*, 2nd ed. Boca Raton, FL, USA: CRC Press, 2011, ch. 67, pp. 671–681.

[144] S. Moura, J. Bendtsen, and V. Ruiz, "Observer design for boundary coupled PDEs: Application to thermostatically controlled loads in smart grids," in *52nd IEEE Conference on Decision and Control*, Florence, Italy, 10-13 Dec. 2013, pp. 6286–6291.

[145] ——, "Parameter identification of aggregated thermostatically controlled loads for smart grids using PDE techniques," *Int. J. Control*, vol. 87, no. 7, pp. 1373–1386, May 2014.

[146] S. Moura, V. Ruiz, and J. Bendsten, "Modeling heterogeneous populations of thermostatically controlled loads using diffusion-advection PDEs," in *Dynamic Systems and Control Conference*, vol. 2, Palo Alto, CA, USA, Oct. 2013, p. V002T23A001.

[147] D. Muyizere, L. K. Letting, and B. B. Munyazikwiye, "Effects of communication signal delay on the power grid: A review," *Electronics*, vol. 11, no. 6, p. 874, Mar. 2022.

[148] M. S. Nazir and I. A. Hiskens, "Noise and parameter heterogeneity in aggregate models of thermostatically controlled loads," *IFAC-PapersOnLine*, vol. 50, no. 1, pp. 8888–8894, July 2017.

[149] ——, "A dynamical systems approach to modeling and analysis of transactive energy coordination," *IEEE Trans. Power Syst.*, vol. 34, no. 5, pp. 4060–4070, Sept. 2018.

[150] S. A. Nugroho, I. M. Granitsas, J. L. Mathieu, and I. A. Hiskens, "Aggregate modeling and non-disruptive control of residential air conditioning systems with two-zone cooling capacity," in *2022 American Control Conference (ACC)*, Atlanta, GA, USA, Sept. 2022, pp. 4668–4675.

[151] N. K. Nwaobia, P. E. Ohenhen, C. N. Nwasike, J. O. Gidiagba, and E. C. Ani, "Energy dynamics in the developing world: Current state and future prospects in the context of technological advancements," *i-TECH MAG*, vol. 5, pp. 58–66, 2023.

[152] E. Nyholm, S. Puranik, E. Mata, M. Odenberger, and F. Johnsson, "Demand response potential of electrical space heating in Swedish single-family dwellings," *Build. Environ.*, vol. 96, pp. 270–282, Feb. 2016.

[153] M. Ourahou, W. Ayrir, B. E. Hassouni, and A. Haddi, "Review on smart grid control and reliability in presence of renewable energies: Challenges and prospects," *Math. Comput. Simul.*, vol. 167, pp. 19–31, Jan. 2020.

[154] K. Pal and V. Harish, "Modeling and simulation of thermostatically controlled loads for power system regulation," in *International Conference on Hydro and Renewable Energy*, Roorkee, India, Oct. 2022, pp. 111–123.

[155] P. Palensky and D. Dietrich, "Demand side management: Demand response, intelligent energy systems, and smart loads," *IEEE Trans. Ind. Inform.*, vol. 7, no. 3, pp. 381–388, June 2011.

[156] S. Panda, S. Mohanty, P. K. Rout, and B. K. Sahu, "A conceptual review on transformation of micro-grid to virtual power plant: Issues, modeling, solutions, and future prospects," *Int. J. Energy Res.*, vol. 46, no. 6, pp. 7021–7054, Jan. 2022.

[157] I. Patrao, E. Figueres, G. Garcerá, and R. González-Medina, "Microgrid architectures for low voltage distributed generation," *Renew. Sustain. Energy Rev.*, vol. 43, pp. 415–424, Mar. 2015.

[158] C. Perfumo, J. H. Braslavsky, and J. K. Ward, "Model-based estimation of energy savings in load control events for thermostatically controlled loads," *IEEE Trans. Smart Grid*, vol. 5, no. 3, pp. 1410–1420, Apr. 2014.

[159] C. Perfumo, E. Kofman, J. H. Braslavsky, and J. K. Ward, "Load management: Model-based control of aggregate power for populations of thermostatically controlled loads," *Energy Convers. Manage.*, vol. 55, pp. 36–48, Mar. 2012.

[160] R. Postoyan, P. Tabuada, D. Nešić, and A. Anta, "A framework for the event-triggered stabilization of nonlinear systems," *IEEE Trans. Automat. Contr.*, vol. 60, no. 4, pp. 982–996, Oct. 2014.

[161] S. A. Pourmousavi, S. N. Patrick, and M. H. Nehrir, "Real-time demand response through aggregate electric water heaters for load shifting and balancing wind generation," *IEEE Trans. Smart Grid*, vol. 5, no. 2, pp. 769–778, Mar. 2014.

[162] S. Raab, H. Habbi, and A. Maidi, "Late-lumping fuzzy boundary geometric control of nonlinear partial differential systems," *Int. J. Robust Nonlinear Control*, vol. 30, no. 16, pp. 6473–6501, Aug. 2020.

[163] A. Radaideh, U. Vaidya, and V. Ajjarapu, "Sequential set-point control for heterogeneous thermostatically controlled loads through an extended Markov chain abstraction," *IEEE Trans. Smart Grid*, vol. 10, no. 1, pp. 116–127, July 2017.

[164] A.-M. H. Radaideh Ashraf, Al-Quraan Ayman and Z. Albataineh, "Rolling horizon control architecture for distributed agents of thermostatically controlled loads enabling long-term grid-level ancillary services," *Int J. Electr. Power Energy Syst.*, vol. 127, p. 106630, May 2021.

[165] S. K. Rathor and D. Saxena, "Energy management system for smart grid: An overview and key issues," *Int. J. Energy Res.*, vol. 44, no. 6, pp. 4067–4109, Jan. 2020.

[166] A. Raza, M. Noor-ul Amin, A. Ayari-Akkari, M. Nabi, and M. Usman Aslam, "A redescending M-estimator approach for outlier-resilient modeling," *Sci. Rep.*, vol. 14, no. 1, p. 7131, Mar. 2024.

[167] M. A. Robdera, *A Concise Approach to Mathematical Analysis*. London, UK: Springer London, 2011.

[168] F. Ruelens, B. J. Claessens, S. Vandael, S. Iacovella, P. Vingerhoets, and R. Belmans, "Demand response of a heterogeneous cluster of electric water heaters using batch reinforcement learning," in *2014 Power Systems Computation Conference*, Wroclaw, Poland, Aug. 2014, pp. 1–7.

[169] N. Ruiz, I. Cobelo, and J. Oyarzabal, "A direct load control model for virtual power plant management," *IEEE Trans. Power Syst.*, vol. 24, no. 2, pp. 959–966, May 2009.

[170] R. F. Rupp, N. G. Vásquez, and R. Lamberts, "A review of human thermal comfort in the built environment," *Energy Build.*, vol. 105, pp. 178–205, Oct. 2015.

[171] B. M. Sanandaji, H. Hao, and K. Poolla, "Fast regulation service provision via aggregation of thermostatically controlled loads," in *2014 47th Hawaii International Conference on System Sciences*, Waikoloa, HI, USA, Mar. 2014, pp. 2388–2397.

[172] B. M. Sanandaji, T. L. Vincent, and K. Poolla, "Ramping rate flexibility of residential HVAC loads," *IEEE Trans. Sustain. Energy*, vol. 7, no. 2, pp. 865–874, Dec. 2015.

[173] P. Siano, "Demand response and smart grids–A survey," *Renew. Sust. Energ. Rev.*, vol. 30, pp. 461–478, Feb. 2014.

[174] J.-J. E. Slotine, W. Li, *et al.*, *Applied Nonlinear Control*. Englewood Cliffs, NJ, USA: Prentice hall, 1991.

[175] F. M. Solinas, L. Bottaccioli, E. Guelpa, V. Verda, and E. Patti, "Peak shaving in district heating exploiting reinforcement learning and agent-based modelling," *Eng. Appl. Artif. Intell.*, vol. 102, p. 104235, June 2021.

[176] R. C. Sonderegger, "Dynamic models of house heating based on equivalent thermal parameters," Ph.D. dissertation, Princeton University, Princeton, NJ, USA, Dec. 1978.

[177] M. Song, G. Ciwei, J. Yang, Y. Liu, and G. Cui, "Novel aggregate control model of air conditioning loads for fast regulation service," *IET Gener. Transm. Distrib.*, vol. 11, no. 17, pp. 4391–4401, Nov. 2017.

[178] M. Song, C. Gao, M. Shahidehpour, Z. Li, J. Yang, and H. Yan, "State space modeling and control of aggregated TCLs for regulation services in power grids," *IEEE Trans. Smart Grid*, vol. 10, no. 4, pp. 4095–4106, June 2018.

[179] M. Song and W. Sun, "Applications of thermostatically controlled loads for demand response with the proliferation of variable renewable energy," *Front. Energy*, vol. 16, no. 1, pp. 64–73, Mar. 2021.

[180] E. D. Sontag *et al.*, "Smooth stabilization implies coprime factorization," *IEEE Trans. Automat. Contr.*, vol. 34, no. 4, pp. 435–443, Aug. 1989.

[181] E. D. Sontag and Y. Wang, "On characterizations of input-to-state stability with respect to compact sets," in *IFAC Nonlinear Control Systems Design 1995*, Tahoe City, CA, USA, June 1995, pp. 203–208.

[182] B. Sorensen, *Energy Intermittency*, 1st ed. Boca Raton, FL, USA: CRC Press, 2018.

[183] D. Soudbakhsh, A. M. Annaswamy, Y. Wang, S. L. Brunton, J. Gaudio, H. Hussain, D. Vrabie, J. Drgona, and D. Filev, "Data-driven control: Theory and applications," in *2023 American Control Conference (ACC)*, San Diego, CA, USA, Sept. 2022, pp. 1922–1939.

[184] S. E. Z. Soudjani and A. Abate, "Aggregation and control of populations of thermostatically controlled loads by formal abstractions," *IEEE Trans. Control Syst. Technol.*, vol. 23, no. 3, pp. 975–990, Oct. 2014.

[185] J. Su, H. Zhang, C.-K. Wong, L. Yu, and Z. Tan, "Hierarchical control of inverter air conditioners for frequency regulation service of islanded microgrids with fair power participation," *IEEE Trans. Smart Grid*, vol. 15, no. 5, pp. 4602–4617, Mar. 2024.

[186] P. Tabuada, "Event-triggered real-time scheduling of stabilizing control tasks," *IEEE Trans. Automat. Contr.*, vol. 52, no. 9, pp. 1680–1685, Sept. 2007.

[187] W. Tang and P. Daoutidis, "Data-driven control: Overview and perspectives," in *2022 American control conference (ACC)*, Atlanta, GA, USA, Sept. 2022, pp. 1048–1064.

[188] V. Telukunta, J. Pradhan, A. Agrawal, M. Singh, and S. G. Srivani, "Protection challenges under bulk penetration of renewable energy resources in power systems: A review," *CSEE J. Power Energy Syst.*, vol. 3, no. 4, pp. 365–379, Dec. 2017.

[189] W. J. Terrell, *Stability and Stabilization: An Introduction*. Princeton, NJ, USA: Princeton University Press, 2009.

[190] P. Thepparat, D. Retzmann, E. Ogée, and M. Wiesinger, "Smart transmission system by HVDC and FACTS," in *2013 IEEE Grenoble Conference*, Grenoble, France, June 2013, pp. 1–6.

[191] S. H. Tindemans and G. Strbac, "Low-complexity decentralized algorithm for aggregate load control of thermostatic loads," *IEEE Trans. Ind. Appl.*, vol. 57, no. 1, pp. 987–998, Oct. 2020.

[192] S. H. Tindemans, V. Trovato, and G. Strbac, "Decentralized control of thermostatic loads for flexible demand response," *IEEE Trans. Control Syst. Technol.*, vol. 23, no. 5, pp. 1685–1700, Jan. 2015.

[193] L. C. Totu, R. Wisniewski, and J. Leth, "Demand response of a TCL population using switching-rate actuation," *IEEE Trans. Control Syst. Technol.*, vol. 25, no. 5, pp. 1537–1551, Oct. 2016.

[194] K. Ullah, A. Basit, Z. Ullah, S. Aslam, and H. Herodotou, "Automatic generation control strategies in conventional and modern power systems: A comprehensive overview," *Energies*, vol. 14, no. 9, p. 2376, Apr. 2021.

[195] U.S. DOE, "2020 smart grid system report," Jan. 2020. [Online]. Available: https://www.energy.gov/sites/default/files/2022-05/2020%20Smart%20Grid%20System%20Report_0.pdf

[196] J. S. Vardakas, N. Zorba, and C. V. Verikoukis, "A survey on demand response programs in smart grids: Pricing methods and optimization algorithms," *IEEE Commun. Surv. Tutor.*, vol. 17, no. 1, pp. 152–178, July 2015.

[197] P. Verma and C. Chakraborty, "Load redistribution attacks against smart grids-models, impacts, and defense: A review," *IEEE Trans. Ind. Inform.*, vol. 20, no. 8, pp. 10 192–10 208, 2024.

[198] C. H. Wai, M. Beaudin, H. Zareipour, A. Schellenberg, and N. Lu, "Cooling devices in demand response: A comparison of control methods," *IEEE Trans. Smart Grid*, vol. 6, no. 1, pp. 249–260, Oct. 2014.

[199] G. Wang, Z. Li, and F. Wang, "Enhanced sufficient battery model for aggregate flexibility of thermostatically controlled loads considering coupling constraints," *IEEE Trans. Sustain. Energy*, vol. 12, no. 4, pp. 2493–2496, Oct. 2021.

[200] E. Webborn, "Natural heterogeneity prevents synchronization of fridges with deterministic frequency control," *IEEE Access*, vol. 7, pp. 130 206–130 214, June 2019.

[201] R. R. Wilcox, *Introduction to Robust Estimation and Hypothesis Testing*, 3rd ed. New York, NY, USA: Academic Press, Dec. 2011.

[202] J. Wu and X. Guan, "Coordinated multi-microgrids optimal control algorithm for smart distribution management system," *IEEE Trans. Smart Grid*, vol. 4, no. 4, pp. 2174–2181, Nov. 2013.

[203] Z.-H. Wu, H.-C. Zhou, B.-Z. Guo, and F. Deng, "Review and new theoretical perspectives on active disturbance rejection control for uncertain finite-dimensional and infinite-dimensional systems," *Nonlinear Dynamics*, vol. 101, no. 2, pp. 935–959, July 2020.

[204] K. Xie, H. Hui, and Y. Ding, "Review of modeling and control strategy of thermostatically controlled loads for virtual energy storage system," *Prot. Control Mod. Power Syst.*, vol. 4, no. 4, pp. 1–13, Oct. 2019.

[205] L. Xing, C. Wen, Z. Liu, H. Su, and J. Cai, "Event-triggered adaptive control for a class of uncertain nonlinear systems," *IEEE Trans. Automat. Contr.*, vol. 62, no. 4, pp. 2071–2076, July 2016.

[206] H. Xu, L. Cheng, N. Qi, and X. Zhou, "Peak shaving potential analysis of distributed load virtual power plants," *Energy Rep.*, vol. 6, pp. 515–525, Dec. 2020.

[207] L. Xu, S. Zhuo, J. Liu, S. Jin, Y. Huangfu, and F. Gao, "Advancement of active disturbance rejection control and its applications in power electronics," *IEEE Trans. Ind. Appl.*, vol. 60, no. 1, pp. 1680–1694, Sept. 2023.

[208] X. Yang and Y. Huang, "Capabilities of extended state observer for estimating uncertainties," in *2009 American control conference*, St. Louis, MO, USA, July 2009, pp. 3700–3705.

[209] Y. Yu, L. Quan, Z. Mi, J. Lu, S. Chang, and Y. Yuan, "Improved model predictive control with prescribed performance for aggregated thermostatically controlled loads," *J. Mod. Power Syst. Clean Energy*, vol. 10, no. 2, pp. 430–439, June 2021.

[210] Z.-W. Yu, L. Ding, Z.-M. Kong, Z.-W. Liu, P. Hu, and Y. Xiao, "A distributed coordinated framework with fair comfort level sharing for inverter air conditioner in auxiliary services," *IEEE Trans. Smart Grid*, vol. 15, no. 3, pp. 2776–2790, May 2024.

[211] G. Yuan and H. Duan, "Robust control for UAV close formation using LADRC via sine-powered pigeon-inspired optimization," *Drones*, vol. 7, no. 4, p. 238, Mar. 2023.

[212] Y. Zeng, R. Zhang, D. Wang, Y. Mu, and H. Jia, "A regional power grid operation and planning method considering renewable energy generation and load control," *Applied Energy*, vol. 237, pp. 304–313, Mar. 2019.

[213] D. Zhang, S. Li, M. Sun, and Z. O'Neill, "An optimal and learning-based demand response and home energy management system," *IEEE Trans. Smart Grid*, vol. 7, no. 4, pp. 1790–1801, Apr. 2016.

[214] H. Zhang, E. Arens, and W. Pasut, "Air temperature thresholds for indoor comfort and perceived air quality," *Build. Res. Inf.*, vol. 39, no. 2, pp. 134–144, Mar. 2011.

[215] W. Zhang, J. Lian, C. Y. Chang, and K. Kalsi, "Aggregated modeling and control of air conditioning loads for demand response," *IEEE Trans. Power Syst.*, vol. 28, no. 4, pp. 4655–4664, July 2013.

[216] W. Zhang, K. Kalsi, J. Fuller, M. Elizondo, and D. Chassin, "Aggregate model for heterogeneous thermostatically controlled loads with demand response," in *2012 IEEE Power and Energy Society General Meeting*, San Diego, CA, USA, July 2012, pp. 1–8.

[217] X.-M. Zhang, Q.-L. Han, and B.-L. Zhang, "An overview and deep investigation on sampled-data-based event-triggered control and filtering for networked systems," *IEEE Trans. Ind. Inform.*, vol. 13, no. 1, pp. 4–16, Sept. 2016.

[218] Z. Zhang, C. Dou, D. Yue, Y. Zhang, B. Zhang, and Z. Zhang, "Event-triggered hybrid voltage regulation with required BESS sizing in high-PV-penetration networks," *IEEE Trans. Smart Grid*, vol. 13, no. 4, pp. 2614–2626, July 2022.

[219] Z. Zhang, J. Zheng, and G. Zhu, "Event-triggered power tracking control of heterogeneous TCL populations," *IEEE Trans. Smart Grid*, vol. 15, no. 4, pp. 3601–3612, Jan. 2024.

[220] ——, "Power tracking control of heterogeneous populations of thermostatically controlled loads with partially measured states," *IEEE Access*, vol. 12, pp. 57 674–57 687, Apr. 2024.

[221] L. Zhao and W. Zhang, "A unified stochastic hybrid system approach to aggregate modeling of responsive loads," *IEEE Trans. Automat. Contr.*, vol. 63, no. 12, pp. 4250–4263, Feb. 2018.

[222] L. Zhao, W. Zhang, H. Hao, and K. Kalsi, "A geometric approach to aggregate flexibility modeling of thermostatically controlled loads," *IEEE Trans. Power Syst.*, vol. 32, no. 6, pp. 4721–4731, Feb. 2017.

[223] J. Zheng, G. Laparra, G. Zhu, and M. Li, "Aggregate power control of heterogeneous TCL populations governed by Fokker–Planck equations," *IEEE Trans. Control Syst. Technol.*, vol. 28, no. 5, pp. 1915–1927, Sept. 2020.

[224] J. Zheng, G. Zhu, and M. Li, "A PDE-based aggregate power tracking control of heterogeneous tcl populations," in *Handbook of Smart Energy Systems*, M. Fathi, E. Zio, and P. M. Pardalos, Eds. Cham, Switzerland: Springer, Jan. 2023, pp. 47–76.

[225] Q. Zheng, L. Q. Gao, and Z. Gao, "On validation of extended state observer through analysis and experimentation," *J. Dyn. Sys., Meas., Control.*, vol. 134, no. 2, p. 024505, Jan. 2012.

[226] Q. Zheng and Z. Gao, "Active disturbance rejection control: some recent experimental and industrial case studies," *Control Theory Technol.*, vol. 16, pp. 301–313, Nov. 2018.

[227] Q. Zheng, L. Q. Gaol, and Z. Gao, "On stability analysis of active disturbance rejection control for nonlinear time-varying plants with unknown dynamics," in *2007 46th IEEE conference on decision and control*, New Orleans, USA, Dec. 2007, pp. 3501–3506.

[228] Z. Zheng, S. Wang, W. Li, and X. Luo, "A consensus-based distributed temperature priority control of air conditioner clusters for voltage regulation in distribution networks," *IEEE Trans. Smart Grid*, vol. 14, no. 1, pp. 290–301, June 2022.

[229] R. Zhou, C. Fu, and W. Tan, "Implementation of linear controllers via active disturbance rejection control structure," *IEEE Trans. Ind. Electron.*, vol. 68, no. 7, pp. 6217–6226, May 2020.

[230] X. Zhou, M. Sang, M. Bao, S. Wang, W. Cui, C. Ye, and Y. Ding, "Exploiting integrated demand response for operating reserve provision considering rebound effects," *IEEE Access*, vol. 10, pp. 15 151–15 162, Jan. 2022.

[231] Z. Zhu, Y. Xia, and M. Fu, "Attitude stabilization of rigid spacecraft with finite-time convergence," *Int. J. Robust Nonlinear Control*, vol. 21, no. 6, pp. 686–702, Feb. 2011.

[232] W. Zhuo, A. V. Savkin, and K. Meng, "Decentralized optimal control of a microgrid with solar PV, BESS and thermostatically controlled loads," *Energies*, vol. 12, no. 11, p. 2111, Mar. 2019.

APPENDIX A SUPPLYMENTARY MATERIALS FOR CHAPTER 6

Due to page limitations, the computation of the error dynamics and some proofs are not included in the original journal article in Chapter 6. This appendix is to provide the details of the related mathematical development.

Calculating the tracking error dynamics

The Leibniz integral rule for multidimensional integrals

The Leibniz integral rule for higher dimensions (LIR-higher) can be expressed as follows:

$$\frac{\mathrm{d}}{\mathrm{d}t}\int_{D(t)} F(\mathbf{x},t)\,\mathrm{d}V = \int_{D(t)} \frac{\partial}{\partial t}F(\mathbf{x},t)\,\mathrm{d}V + \int_{\partial D(t)} F(\mathbf{x},t)(\mathbf{v}_b\cdot n)\,\mathrm{d}S,$$

where $F(\mathbf{x},t)$ can be tensor-, vector- or scalar-valued, $D(t)$ and $\partial D(t)$ are a time-varying connected region and its boundary respectively, $\mathbf{v}_b$ denotes the Eulerian velocity of the region, n is the outward unit normal vector of the surface element.

Computing the derivative of $e(t)$ for second-order populations

To compute the derivative of $e(t)$, based on the mathematical expression for $y(t)$ in (6.14), we decompose the computation process into the following three steps.
Step 1: Compute $\frac{\mathrm{d}}{\mathrm{d}t}\int_{\underline{x}}^{\overline{x}}\int_{-\infty}^{+\infty} f_{1b}(x_a(t),x_m(t),t)\mathrm{d}x_m\mathrm{d}x_a$.

$$\begin{aligned}
&\frac{\mathrm{d}}{\mathrm{d}t}\int_{\underline{x}}^{\overline{x}}\int_{-\infty}^{+\infty} f_{1b}(x_a(t),x_m(t),t)\mathrm{d}x_m\mathrm{d}x_a\\
=&u(t)\int_{-\infty}^{+\infty} f_{1b}|_{\overline{x}}\mathrm{d}x_m - u(t)\int_{-\infty}^{+\infty} f_{1b}|_{\underline{x}}\mathrm{d}x_m + \int_{\underline{x}}^{\overline{x}}\int_{-\infty}^{+\infty}\frac{\partial}{\partial t}f_{1b}\mathrm{d}x_m\mathrm{d}x_a &\text{(A.1a)}\\
=&u(t)\int_{-\infty}^{+\infty} f_{1b}|_{\overline{x}}\mathrm{d}x_m + \int_{\underline{x}}^{\overline{x}}\int_{-\infty}^{+\infty}\frac{\partial}{\partial t}f_{1b}\mathrm{d}x_m\mathrm{d}x_a &\text{(A.1b)}\\
=&u(t)\int_{-\infty}^{+\infty} f_{1b}|_{\overline{x}}\mathrm{d}x_m + \int_{\underline{x}}^{\overline{x}}\int_{-\infty}^{+\infty}[-\frac{\partial}{\partial x_a}((\alpha_1-u)f_{1b})\\
&-\frac{\partial}{\partial x_m}((\alpha_1-u)f_{1b}) + \frac{\sigma^2}{2}\frac{\partial^2}{\partial x_a^2}f_{1b} + \frac{\sigma^2}{2}\frac{\partial^2}{\partial x_m^2}f_{1b}]\mathrm{d}x_m\mathrm{d}x_a &\text{(A.1c)}\\
=&u(t)\int_{-\infty}^{+\infty} f_{1b}|_{\overline{x}}\mathrm{d}x_m - \int_{-\infty}^{+\infty}((\alpha_1-u)f_{1b})|_{\underline{x}}^{\overline{x}}\mathrm{d}x_m + 0
\end{aligned}$$

$$+\frac{\sigma^2}{2}\int_{-\infty}^{+\infty}(\frac{\partial}{\partial x_a}f_{1b})|_{\underline{x}^+}^{\overline{x}^-}\mathrm{d}x_m+0 \tag{A.1d}$$
$$=2u(t)\int_{-\infty}^{+\infty}f_{1b}|_{\overline{x}}\mathrm{d}x_m-\int_{-\infty}^{+\infty}(\alpha_1 f_{1b})|_{\overline{x}}\mathrm{d}x_m+\frac{\sigma^2}{2}\int_{-\infty}^{+\infty}(\frac{\partial}{\partial x_a}f_{1b})|_{\overline{x}^-}\mathrm{d}x_m$$
$$-\frac{\sigma^2}{2}\int_{-\infty}^{+\infty}(\frac{\partial}{\partial x_a}f_{1b})|_{\underline{x}^+}\mathrm{d}x_m$$

Note that in (A.1), for simplicity, we use the notations $f_{1b}|_{\overline{x}} := f_{1b}(\overline{x}, x_m(t), t)$, and $f_{1b}|_{\underline{x}} := f_{1b}(\underline{x}, x_m(t), t)$. Equation (A.1a) is derived based on Leibniz integral rule for higher dimensions (LIR-higher), shown in Appendix A. Specifically, in (A.1), the region is $D(t) := [\underline{x}, \overline{x}] \times \mathbb{R}$. Let $\partial D_1, \partial D_2$ be the left and right boundaries of $D(t)$ respectively. For these boundaries, the outward unit normal vector are $(-1, 0)$ and $(1, 0)$ respectively. Moreover, for $\partial D_1, \partial D_2$, the Eulerian velocity both are $(u(t), 0)$. Therefore, with LIR-higher, we have:

$$\frac{\mathrm{d}}{\mathrm{d}t}\int_{\underline{x}}^{\overline{x}}\int_{-\infty}^{+\infty}f_{1b}(x_a(t), x_m(t), t)\mathrm{d}x_m\mathrm{d}x_a$$
$$=\int_{\underline{x}}^{\overline{x}}\int_{-\infty}^{+\infty}\frac{\partial}{\partial t}f_{1b}\mathrm{d}x_m\mathrm{d}x_a+\int_{\partial D_1}f_{1b}(-u(t))\,\mathrm{d}S+\int_{\partial D_2}f_{1b}u(t)\,\mathrm{d}S$$
$$=\int_{\underline{x}}^{\overline{x}}\int_{-\infty}^{+\infty}\frac{\partial}{\partial t}f_{1b}\mathrm{d}x_m\mathrm{d}x_a-u(t)\int_{\partial D_1}f_{1b}\,\mathrm{d}S+u(t)\int_{\partial D_2}f_{1b}\,\mathrm{d}S$$
$$=\int_{\underline{x}}^{\overline{x}}\int_{-\infty}^{+\infty}\frac{\partial}{\partial t}f_{1b}\mathrm{d}x_m\mathrm{d}x_a-u(t)\int_{-\infty}^{+\infty}f_{1b}|_{\underline{x}}\mathrm{d}x_m+u(t)\int_{-\infty}^{+\infty}f_{1b}|_{\overline{x}}\mathrm{d}x_m.$$

Equation (A.1b) is obtained by the absorbing condition (6.10). Then, the PDE dynamics in (6.8c) is substituted in (A.1c). As $f_{1b}(x, t) \in C^{2,1}$ and the integral in the domain $[\underline{x}, \overline{x}] \times \mathbb{R}$ is finite, Fubini's theorem is valid. Combining with the boundary conditions for the mass in (6.11), the result in (A.1d) is obtained. By using the absorbing condition (6.10), the final step is derived.

Step 2: Compute $\frac{\mathrm{d}}{\mathrm{d}t}\int_{\overline{x}}^{+\infty}\int_{-\infty}^{+\infty}f_{1c}(x_a(t), x_m(t), t)\mathrm{d}x_m\mathrm{d}x_a$.

$$\frac{\mathrm{d}}{\mathrm{d}t}\int_{\overline{x}}^{+\infty}\int_{-\infty}^{+\infty}f_{1c}(x_a(t), x_m(t), t)\mathrm{d}x_m\mathrm{d}x_a$$
$$=-u(t)\int_{-\infty}^{+\infty}f_{1c}|_{\overline{x}}\mathrm{d}x_m+\int_{\overline{x}}^{+\infty}\int_{-\infty}^{+\infty}\frac{\partial}{\partial t}f_{1c}\mathrm{d}x_m\mathrm{d}x_a \tag{A.2a}$$
(LIR-higher, see Appendix A)
$$=-u(t)\int_{-\infty}^{+\infty}f_{1c}|_{\overline{x}}\mathrm{d}x_m+\int_{\overline{x}}^{+\infty}\int_{-\infty}^{+\infty}[-\frac{\partial}{\partial x_a}((\alpha_1-u(t))f_{1c})$$
$$-\frac{\partial}{\partial x_m}((\alpha_1-u(t))f_{1c})+\frac{\sigma^2}{2}\frac{\partial^2}{\partial x_a^2}f_{1c}+\frac{\sigma^2}{2}\frac{\partial^2}{\partial x_m^2}f_{1c}]\mathrm{d}x_m\mathrm{d}x_a \tag{A.2b}$$

(substitute PDE (6.8d))

$$\begin{aligned}
&= - u(t) \int_{-\infty}^{+\infty} f_{1c}|_{\overline{x}} \mathrm{d}x_m - \int_{-\infty}^{+\infty} ((\alpha_1 - u(t)) f_{1c})|_{\overline{x}}^{+\infty} \mathrm{d}x_m \\
&\quad + 0 + \frac{\sigma^2}{2} \int_{-\infty}^{+\infty} (\frac{\partial}{\partial x_a} f_{1c})|_{\overline{x}^+}^{+\infty} \mathrm{d}x_m + 0 \qquad \text{(A.2c)}
\end{aligned}$$

(Fubini, mass natural condition (6.11)

$$\begin{aligned}
&= - u(t) \int_{-\infty}^{+\infty} f_{1c}|_{\overline{x}} \mathrm{d}x_m - 0 + \int_{-\infty}^{+\infty} ((\alpha_1 - u(t)) f_{1c})|_{\overline{x}} \mathrm{d}x_m + 0 \\
&\quad - \frac{\sigma^2}{2} \int_{-\infty}^{+\infty} (\frac{\partial}{\partial x_a} f_{1c})|_{\overline{x}^+} \mathrm{d}x_m \qquad \text{(A.2d)}
\end{aligned}$$

(air natural condition (6.11))

$$= - 2u(t) \int_{-\infty}^{+\infty} f_{1c}|_{\overline{x}} \mathrm{d}x_m + \int_{-\infty}^{+\infty} (\alpha_1 f_{1c})|_{\overline{x}} \mathrm{d}x_m - \frac{\sigma^2}{2} \int_{-\infty}^{+\infty} (\frac{\partial}{\partial x_a} f_{1c})|_{\overline{x}^+} \mathrm{d}x_m$$

The computation with LIR-higher is similar as that in (A.1), and it shows that

$$\begin{aligned}
&\frac{\mathrm{d}}{\mathrm{d}t} \int_{\overline{x}}^{+\infty} \int_{-\infty}^{+\infty} f_{1c}(x_a(t), x_m(t), t) \mathrm{d}x_m \mathrm{d}x_a \\
&\qquad = \int_{\overline{x}}^{+\infty} \int_{-\infty}^{+\infty} \frac{\partial}{\partial t} f_{1c} \mathrm{d}x_m \mathrm{d}x_a - u(t) \int_{-\infty}^{+\infty} f_{1c}|_{\overline{x}} \mathrm{d}x_m.
\end{aligned}$$

Step 3: Compute $\frac{\mathrm{d}}{\mathrm{d}t} \int_{-\infty}^{\underline{x}} \int_{-\infty}^{+\infty} f_{0a}(x_a(t), x_m(t), t) \mathrm{d}x_m \mathrm{d}x_a$.

$$\begin{aligned}
&\frac{\mathrm{d}}{\mathrm{d}t} \int_{-\infty}^{\underline{x}} \int_{-\infty}^{+\infty} f_{0a}(x_a(t), x_m(t), t) \mathrm{d}x_m \mathrm{d}x_a \\
=&u(t) \int_{-\infty}^{+\infty} f_{0a}|_{\underline{x}} \mathrm{d}x_m + \int_{-\infty}^{\underline{x}} \int_{-\infty}^{+\infty} \frac{\partial}{\partial t} f_{0a}(x_a(t), x_m(t), t) \mathrm{d}x_m \mathrm{d}x_a \qquad \text{(A.3a)}
\end{aligned}$$

(LIR-higher)

$$\begin{aligned}
=&u(t) \int_{-\infty}^{+\infty} f_{0a}|_{\underline{x}} \mathrm{d}x_m + \int_{-\infty}^{\underline{x}} \int_{-\infty}^{+\infty} [-\frac{\partial}{\partial x_a}((\alpha_0 - u(t)) f_{0a}) \\
&- \frac{\partial}{\partial x_m}((\alpha_0 - u(t)) f_{0a}) + \frac{\sigma^2}{2} \frac{\partial^2}{\partial x_a^2} f_{0a} + \frac{\sigma^2}{2} \frac{\partial^2}{\partial x_m^2} f_{0a}] \mathrm{d}x_m \mathrm{d}x_a
\end{aligned}$$

(substitute PDE)

$$\begin{aligned}
=&u(t) \int_{-\infty}^{+\infty} f_{0a}|_{\underline{x}} \mathrm{d}x_m - \int_{-\infty}^{+\infty} ((\alpha_0 - u(t)) f_{0a})|_{-\infty}^{\underline{x}^-} \mathrm{d}x_m \\
&+ 0 + \frac{\sigma^2}{2} \int_{-\infty}^{+\infty} (\frac{\partial}{\partial x_a} f_{0a})|_{-\infty}^{\underline{x}^-} \mathrm{d}x_m + 0 \qquad \text{(A.3b)}
\end{aligned}$$

(Fubini, mass natural condition (6.11))

$$=u(t) \int_{-\infty}^{+\infty} f_{0a}|_{\underline{x}} \mathrm{d}x_m - \int_{-\infty}^{+\infty} ((\alpha_0 - u(t)) f_{0a})|_{\underline{x}} + \frac{\sigma^2}{2} \int_{-\infty}^{+\infty} (\frac{\partial}{\partial x_a} f_{0a})|_{\underline{x}^-} \mathrm{d}x_m \qquad \text{(A.3c)}$$

(air natural condition(6.11))

$$=2u(t)\int_{-\infty}^{+\infty} f_{0a}|_{\underline{x}}\mathrm{d}x_m - \int_{-\infty}^{+\infty}(\alpha_0 f_{0a})|_{\underline{x}} + \frac{\sigma^2}{2}\int_{-\infty}^{+\infty}(\frac{\partial}{\partial x_a}f_{0a})|_{\underline{x}^-}\mathrm{d}x_m$$

The LIR-higher is similarly used in (A.3), and we have

$$\frac{\mathrm{d}}{\mathrm{d}t}\int_{-\infty}^{\underline{x}}\int_{-\infty}^{+\infty} f_{0a}(x_a(t),x_m(t),t)\mathrm{d}x_m\mathrm{d}x_a = \int_{-\infty}^{\underline{x}}\int_{-\infty}^{+\infty}\frac{\partial}{\partial t}f_{0a}\mathrm{d}x_m\mathrm{d}x_a + u(t)\int_{-\infty}^{+\infty} f_{0a}|_{\underline{x}}\mathrm{d}x_m.$$

Summing the equations in (A.1), (A.2), (A.3), and using the continuity condition in (6.12) and the flux conservation condition in (6.9), the derivative of $y(t)$ can be written as:

$$\begin{aligned}
\dot{y}(t) =& -2\frac{P}{\eta}u(t)(\int_{-\infty}^{+\infty} f_{1c}|_{\overline{x}}\mathrm{d}x_m + \int_{-\infty}^{+\infty} f_{0a}|_{\underline{x}}\mathrm{d}x_m)\\
&+\frac{P}{\eta}\int_{-\infty}^{+\infty}(\alpha_1 f_{1c})|_{\overline{x}}\mathrm{d}x_m + \frac{P}{\eta}\int_{-\infty}^{+\infty}(\alpha_0 f_{0a})|_{\underline{x}}\mathrm{d}x_m\\
&+\frac{P\sigma^2}{2\eta}\int_{-\infty}^{+\infty}(\frac{\partial}{\partial x_a}f_{1b})|_{\overline{x}^-}\mathrm{d}x_m - \frac{P\sigma^2}{2\eta}\int_{-\infty}^{+\infty}(\frac{\partial}{\partial x_a}f_{1b})|_{\underline{x}^+}\mathrm{d}x_m\\
&-2\cdot\frac{P\sigma^2}{2\eta}\int_{-\infty}^{+\infty}(\frac{\partial}{\partial x_a}f_{1c})|_{\overline{x}^+}\mathrm{d}x_m - \frac{P\sigma^2}{2\eta}\frac{\partial}{\partial x_a}\int_{-\infty}^{+\infty} f_{0a}|_{\underline{x}^-}\mathrm{d}x_m\\
=& -2\frac{P}{\eta}u(t)(\int_{-\infty}^{+\infty} f_{1c}|_{\overline{x}}\mathrm{d}x_m + \int_{-\infty}^{+\infty} f_{0a}|_{\underline{x}}\mathrm{d}x_m)\\
&+\frac{P}{\eta}\int_{-\infty}^{+\infty}(\alpha_1 f_{1c})|_{\overline{x}}\mathrm{d}x_m + \frac{P}{\eta}\int_{-\infty}^{+\infty}(\alpha_0 f_{0a})|_{\underline{x}}\mathrm{d}x_m\\
&-\frac{P\sigma^2}{2\eta}\int_{-\infty}^{+\infty}(\frac{\partial}{\partial x_a}f_{1c})|_{\overline{x}^+}\mathrm{d}x_m - \frac{P\sigma^2}{2\eta}\int_{-\infty}^{+\infty}(\frac{\partial}{\partial x_a}f_{0b})|_{\overline{x}^-}\mathrm{d}x_m\\
&-\frac{P\sigma^2}{2\eta}\int_{-\infty}^{+\infty}(\frac{\partial}{\partial x_a}f_{1b})|_{\underline{x}^+}\mathrm{d}x_m - \frac{P\sigma^2}{2\eta}\int_{-\infty}^{+\infty}(\frac{\partial}{\partial x_a}f_{0a})|_{\underline{x}^-}\mathrm{d}x_m
\end{aligned}$$

Thus,

$$\begin{aligned}
\dot{e}(t) =& \dot{y}_d(t) + 2\frac{P}{\eta}u(t)(\int_{-\infty}^{+\infty} f_{1c}|_{\overline{x}}\mathrm{d}x_m + \int_{-\infty}^{+\infty} f_{0a}|_{\underline{x}}\mathrm{d}x_m)\\
&-\frac{P}{\eta}\int_{-\infty}^{+\infty}(\alpha_1 f_{1c})|_{\overline{x}}\mathrm{d}x_m - \frac{P}{\eta}\int_{-\infty}^{+\infty}(\alpha_0 f_{0a})|_{\underline{x}}\mathrm{d}x_m\\
&+\frac{P\sigma^2}{2\eta}\int_{-\infty}^{+\infty}(\frac{\partial}{\partial x_a}f_{1c})|_{\overline{x}^+}\mathrm{d}x_m + \frac{P\sigma^2}{2\eta}\int_{-\infty}^{+\infty}(\frac{\partial}{\partial x_a}f_{0b})|_{\overline{x}^-}\mathrm{d}x_m\\
&+\frac{P\sigma^2}{2\eta}\int_{-\infty}^{+\infty}(\frac{\partial}{\partial x_a}f_{1b})|_{\underline{x}^+}\mathrm{d}x_m + \frac{P\sigma^2}{2\eta}\int_{-\infty}^{+\infty}(\frac{\partial}{\partial x_a}f_{0a})|_{\underline{x}^-}\mathrm{d}x_m
\end{aligned}$$

A well-defined denominator of the second-order controller

Maximum principle for unbounded region

In this section, strong parabolic maximum principle, see [47], is generalized to unbounded regions with vanishing boundary values. More specifically, define $\Omega_T := \Omega_a \times (t_0, T]$, $\Gamma_T := \overline{\Omega_T} \backslash \Omega_T$ and suppose $f_{0a}(x_a^0, x_m^0, T_0)$ attains a non-positive minimum m_f in Ω_T, then $f_{0a}(x_a, x_m, t) \equiv 0, \forall (x_a, x_m, t) \in \Omega_{T_0}$. Here, we take $f_{0a}(x_a, x_m, t)$ as an example. For other functions $f_{0b}(x_a, x_m, t)$, $f_{1b}(x_a, x_m, t)$, $f_{1c}(x_a, x_m, t)$, the conclusion holds following a similar reasoning process.

Note that $f_{0a}(x_a, x_m, t)$ vanishes at the infinities, then $\forall \epsilon > 0$, there exist G_a, G_m such that

$$(x_a^0, x_m^0) \in (-G_a, \underline{x}) \times (-G_m, G_m) =: \Omega_0,$$

and

$$|f_{0a}(x_a, x_m, T_0)| < \epsilon, \forall (x_a, x_m) \in \Omega_a \backslash \overline{\Omega_0}. \tag{A.4}$$

By the strong maximum principle for the bounded region $\Omega_0 \times (t_0, T]$, $f_{0a}(x_a, x_m, t) \equiv m_f, \forall (x_a, x_m, t) \in \Omega_0 \times (t_0, T_0]$. By the inequality in (A.4) and the continuity of $f_{0a}(x_a, x_m, t)$ in Ω_a, it follows that $|m_f| \leq \epsilon$. Letting $\epsilon \to 0$, then $m_f = 0$. Thus,

$$f_{0a}(x_a, x_m, t) = m_f \equiv 0, \quad \forall (x_a, x_m, t) \in \Omega_0 \times (t_0, T_0].$$

Since (x_a^0, x_m^0) is arbitrary, $f_{0a}(x_a, x_m, t) \equiv 0$ holds in all the region Ω_{T_0}.

Non-negativity of the solutions

Take $f_{0a}(x_a, x_m, t)$ as an example, and try to prove that $f_{0a}(x_a, x_m, t) \geq 0, \forall (x_a, x_m) \in \overline{\Omega_a}, t \in (t_0, T]$. For other functions $f_{0b}(x_a, x_m, t)$,$f_{1b}(x_a, x_m, t)$ and $f_{1c}(x_a, x_m, t)$, the conclusion holds following a similar reasoning process.

Proof. (proof by contradiction). Suppose the minimum value of $f_{0a}(x_a, x_m, t)$ achieves at (x_a^0, x_m^0, T_0), $T_0 \in (t_0, T]$ and satisfies $m_f := f_{0a}(x_a^0, x_m^0, T_0) < 0$.

Case 1: $(x_a^0, x_m^0) \in \Omega_a$, i.e. $f_{0a}(x_a, x_m, t)$ attains a non-positive minimum in the interior of Ω_a. Then by the strong parabolic maximum principle (shown in the following subsection), $f_{0a}(x_a, x_m, t) \equiv 0$ in Ω_{T_0}. This contradicts the initial condition that $f_{0a}(x_a, x_m, t_0) > 0$ in proposition 6.10. *Case 2:* $x_a^0 = \underline{x}$, i.e. $f_{0a}(x_a, x_m, t)$ attains a non-positive minimum on the boundary of Ω_a. Then, it follows that $\dfrac{\partial}{\partial t} f_{0a}(\underline{x}^-, x_m^0, T_0) \leq 0$. Now consider the region

$\Omega_b \times (t_0, T_0]$. Similar to the arguments in the first case, $f_{0b}(x_a, x_m, t)$ attains its minimum value on the boundary $x = \overline{x}$ or $x = \underline{x}$. Note that $f_{0b}(\overline{x}, x_m, t) = 0$ always holds by the absorbing boundary condition in (6.10), thus, $f_{0b}(x_a, x_m, t)$ also attains its minimum on $x = \underline{x}$. Note that $f_{0a}(\underline{x}, x_m, t) = f_{0b}(\underline{x}, x_m, t)$ always holds by the continuity condition in (6.12), thus, $f_{0b}(\underline{x}^+, x_m^0, T_0)$ is also the minimum value in $\Omega_b \times (t_0, T_0]$. Hence, $\frac{\partial}{\partial t} f_{0b}(\underline{x}^+, x_m^0, T_0) \geq 0$. Then, by the flux conservation condition in (6.9), it follows that

$$\frac{\partial}{\partial x_a} f_{1b}(\underline{x}^+, x_m(t), t) = \frac{\partial}{\partial x_a} f_{0a}(\underline{x}^-, x_m(t), t) - \frac{\partial}{\partial x_a} f_{0b}(\underline{x}^+, x_m(t), t) \leq 0,$$

which contradicts the absorbing condition in (6.10).

Therefore, $f_{0a}(x_a^0, x_m^0, T_0) \geq 0$ always holds, i.e. $f_{0a}(x_a, x_m, t)$ is always non-negative for all $(x_a, x_m) \in \overline{\Omega_a}, t \in (t_0, T]$. □

Well-defined denominator of the controller

Proposition A.1. *Suppose $f_{0a}(x_a, x_m, t_0)$, $f_{0b}(x_a, x_m, t_0)$, $f_{1b}(x_a, x_m, t_0)$, and $f_{1c}(x_a, x_m, t_0)$ are all $C^{2,1}$ functions and have uniformly continuous 2nd-order partial derivatives on bounded subsets in each region. Furthermore, assume that $\forall x_m \in \mathbb{R}$, $f_{0a}(x_a, x_m, t_0)$, $f_{0b}(x_a, x_m, t_0)$, $f_{1b}(x_a, x_m, t_0)$, and $f_{1c}(x_a, x_m, t_0)$ are strictly positive, except $f_{0b}(\overline{x}, x_m, t_0) = 0$, $f_{1b}(\underline{x}, x_m, t_0) = 0$ at t_0. And finally, suppose that they also satisfy the boundary conditions in* (6.9), (6.10), (6.11), (6.12), *and the probability conservation property in* (6.13). *Then, the denominator in the controller* (6.20) *will always be positive in $[t_0, T], 0 \leq t_0 < T < \infty$.*

Proof. (prove by contradiction) Suppose there exists some $T_0 \in (t_0, T]$ such that the denominator is zero, i.e.

$$\int_{-\infty}^{+\infty} f_{0a}(\underline{x}, x_m, T_0) \mathrm{d}x_m + \int_{-\infty}^{+\infty} f_{1c}(\overline{x}, x_m, T_0) \mathrm{d}x_m = 0. \tag{A.5}$$

It is shown that the probability density functions (PDFs) are always non-negative, i.e.

$$f_{0a}(x_a, x_m, t) \geq 0, f_{1c}(x_a, x_m, t) \geq 0, \quad \forall (x_a, x_m, t) \in \mathbb{R} \times \mathbb{R} \times [t_0, T].$$

This fact is validated in the Section A or the readers can refer to [10]. Together with (A.5), it follows that:

$$f_{0a}(\underline{x}, x_m, T_0) = 0, \forall x_m \in \mathbb{R},$$
$$f_{1c}(\overline{x}, x_m, T_0) = 0, \forall x_m \in \mathbb{R}.$$

Therefore,

$$\frac{\partial}{\partial x_a} f_{0a}(\underline{x}^-, x_m, T_0) \leq 0, \frac{\partial}{\partial x_a} f_{0b}(\underline{x}^+, x_m, T_0) \geq 0.$$
$$\frac{\partial}{\partial x_a} f_{1c}(\overline{x}^-, x_m, T_0) \leq 0, \frac{\partial}{\partial x_a} f_{1b}(\overline{x}^+, x_m, T_0) \geq 0.$$

Based on the flux conservation condition in (6.9), it follows that

$$\frac{\partial}{\partial x_a} f_{1b}(\underline{x}^+, x_m(t), t) = \frac{\partial}{\partial x_a} f_{0a}(\underline{x}^-, x_m(t), t) - \frac{\partial}{\partial x_a} f_{0b}(\underline{x}^+, x_m(t), t) \leq 0,$$
$$\frac{\partial}{\partial x_a} f_{0b}(\overline{x}^-, x_m(t), t) = \frac{\partial}{\partial x_a} f_{1c}(\overline{x}^+, x_m(t), t) - \frac{\partial}{\partial x_a} f_{1b}(\overline{x}^-, x_m(t), t) \leq 0,$$

which contradicts the absorbing condition in (6.10). Hence, the denominator in the control scheme (6.20) will never be zero. □